

NMR Spectroscopic Investigations on Copper-Catalyzed Reactions and Zintl Anions

Dissertation

zur Erlangung des Doktorgrades der Naturwissenschaften

(Dr. rer. nat.)

an der Fakultät für Chemie und Pharmazie

der Universität Regensburg



vorgelegt von

Carina Koch

aus Kempten (Allgäu)

April 2015

Die vorliegende Dissertation beruht auf Arbeiten, die zwischen Dezember 2011 und April 2015 am Arbeitskreis von Frau Professor Dr. Ruth M. Gschwind am Institut für Organische Chemie der Universität Regensburg durchgeführt wurden.

Promotionsgesuch eingereicht am:

22.04.2015

Die Arbeit wurde angeleitet von:

Prof. Dr. Ruth M. Gschwind

Promotionsausschuss:

Vorsitzender:

PD Dr. Sabine Amslinger

1. Gutachter:

Prof. Dr. Ruth M. Gschwind

2. Gutachter:

Prof. Dr. Nikolaus Korber

3. Prüfer:

Prof. Dr. Manfred Scheer

SMILE!

It confuses people.

Für mein Patenkind Leni

An dieser Stelle möchte ich mich bei allen bedanken, die zum Gelingen dieser Arbeit beigetragen haben. Meinen besonderen Dank möchte ich meiner Doktormutter Frau Prof. Dr. Ruth M. Gschwind an dieser Stelle aussprechen, zum einen für die interessante und anspruchsvolle Themenstellung und das Vertrauen in meine Arbeit, zum anderen für alles was ich über die Arbeit hinaus von ihr in den letzten Jahren gelernt habe.

Herrn Prof. Dr. Nikolaus Korber danke ich für die Übernahme des Zweitgutachtens und für die Freiheiten bei der Bearbeitung der Kooperationsprojekte.

Bei Herrn Prof. Dr. Manfred Scheer und Frau PD Dr. Sabine Amslinger möchte ich mich für die Ausübung des Amtes als Prüfer bzw. als Vorsitzende recht herzlich bedanken.

Meinen Kooperationspartnern auf dem Gebiet der Zintlphasen, Franziska Fendt, Stefanie Gärtner und Ute Friedrich möchte ich für die erfolgreiche Zusammenarbeit und die konstruktiven Diskussionen danken. Den Nachfolgern Corinna Lorenz und Florian Hastreiter danke ich für das große Interesse und wünsche ihnen viel Erfolg und weiterhin tolle Ergebnisse bei ihrer Forschung.

Bei Herrn Prof. Dr. Burkhard Luy möchte ich mich für die Zurverfügungstellung des xyBEBOP Pulses bedanken.

Georgii Kachkovskiy und Thomas Rawner vom Arbeitskreis Prof. Dr. Oliver Reiser danke ich für die Zusammenarbeit auf dem Gebiet der kupferkatalysierten Photoreaktionen.

Den Forschungspraktikanten Florian Hastreiter, Efrain Reyes-Rodriguez, Tobias Burger und dem Bacheloranden Jakob Asenbauer danke ich für ihre Mitarbeit und ihr Engagement.

Einen besonderen Dank möchte ich an meine aktuellen und ehemaligen Kollegen aussprechen, die mir nicht nur mit hilfreichen Ratschlägen zur Seite standen, sondern auch meinen Arbeitsalltag durch so manches Grillen, Kaffeetrinken, Feierabendbier, Landkreisläufe oder andere witzige Aktionen bereichert haben. Vielen Dank euch allen! Dr. Katrin Schober, Dr. Markus Schmid, Dr. Matthias Fleischman, Dr. Diana Drettwan, Dr. Evelyn Hartmann, Nils Sorgenfrei, Michael Haindl, Michael Hammer, Hanna Bartling, Florian Hastreiter, Julian Greindl, Andreas Seegerer, Peter Braun, Thomas Hausler, Dr. Johnny Hioe, Dr. Fabio Morana, Dr. Maxime Melikian und Dr. Polyssena Renzi, sowie den „Adoptivkindern“ Franziska Fendt und Veronika Kropf. Dr. Maria Neumeier und Dr. Felicitas von Rekowski danke ich zudem für die konstruktive Zusammenarbeit an Teilprojekten dieser Arbeit. Dem Nachwuchs Kerstin Rothermel und Patrick Nitschke, viel Erfolg und Durchhaltevermögen.

Ich danke Nikola Kastner-Pustet und den Mitarbeitern der NMR-Abteilung, Dr. Ilya Shenderovich, Fritz Kastner, Annette Schramm, Georgine Stühler, sowie unserer Sekretärin Ulrike Weck für ihre stets freundliche Hilfe und Unterstützung in technischen und bürokratischen Fragen.

Ein großes Dankeschön geht an meine „Ladies“ und allen Freunden für die nötige Ablenkung außerhalb der Universität.

Meinem Freund Andi danke ich für seine große Unterstützung und sein Verständnis während der letzten Monate.

Vor allem aber gilt mein Dank meiner Familie. Meinen Eltern, die immer wieder beweisen, dass ich mich auf ihren Rückhalt verlassen kann und die mich stets unterstützen, sowie meiner Oma und meiner Schwester mit ihrer Familie.

Vielen Dank!

**NMR Spectroscopic Investigations on
Copper-Catalyzed Reactions
and Zintl Anions**

Contents

1	Introduction and Outline.....	5
1.1	Asymmetric Copper Catalyzed Synthesis.....	5
1.2	The Solvation and Transformation Chemistry of Zintl Ions in Liquid Ammonia	6
2	Overview of NMR Spectroscopic Aspects in Copper-Catalyzed Asymmetric Synthesis.....	9
2.1	Introduction	10
2.2	Copper Complexes with Phosphoramidite Ligands.....	12
2.2.1	Precatalytic Copper Complexes	13
2.2.2	Phosphoramidite Trialkylaluminum Interactions	18
2.3	Copper Complexes with TADDOL-based Thiolate Ligands.....	19
2.4	Copper Complexes with Ferrocenyl-Based Ligands	20
2.4.1	Structural Studies of Asymmetric Conjugate Addition Reactions	21
2.4.2	Structural Studies of Asymmetric Allylic Alkylation	25
2.5	Conclusion.....	26
2.6	References	28
3	NMR Spectroscopic Investigations on Mechanistic Steps of Copper Catalyzed Reactions.....	31
3.1	Abstract	32
3.2	Manuscript.....	33
3.2.1	Introduction	33
3.2.2	Results and Discussion.....	35
3.2.3	Conclusion.....	46
3.3	Supporting Information	47
3.3.1	Additional NMR Spectra and Information	47
3.3.2	Experimental Part.....	57
3.4	Additional Findings	60
3.4.1	Introduction	60
3.4.2	Investigation on the Transmetalation Step with ZnMe_2	60
3.4.3	Interactions between Structural Moieties of the Ligand $\text{L}^{(SS)}$ and ZnMe_2	63
3.4.4	Investigation on the Structure of a Transmetalation Intermediate with MeLi	67
3.4.5	Investigation on a $\text{Cu(I)}-\pi$ -Intermediate / Cu(III) -Intermediate – Addition of ^{15}N -tosyl imine to the Precatalytic Complex	73
3.4.6	Mechanistic Studies on a Trifluoromethylsulfochlorination of Non-activated Alkenes by Copper Complexes in a Photoredox Catalyzed Process	78
3.4.7	Experimental Part for the Additional Findings.....	88
3.5	References	91
4	Relief for Heteronuclear NMR Spectroscopy by using a Broadband Pulse (xyBEBOP Pulse)	95
4.1	Abstract	96
4.2	Manuscript.....	96
4.2.1	Introduction	96
4.2.2	Results and Discussion.....	97
4.2.3	Conclusion.....	105

4.3	Supporting Information	106
4.3.1	Overview of Recording Times	106
4.3.2	Comparison of Integrals and Line Widths of a Further Sample	106
4.3.3	Excitation Profile of the xyBEBOP Pulse	107
4.3.4	Sinc Shaped Excitation Profile of a 90° Hard Pulse	109
4.3.5	NMR Data Collection and Processing	110
4.4	References	111
5	Detection and Transformation of Highly Charged Zintl Anions	113
5.1	Abstract	114
5.2	Manuscript	114
5.2.1	Introduction	114
5.2.2	Results and Discussion	116
5.2.3	Conclusion	120
5.3	Supporting Information	121
5.3.1	Synthesis	121
5.3.2	Phase Determination and NMR data	122
5.4	Additional Findings	129
5.4.1	Reaction of Sn_4^{4-} in Liquid Ammonia: The formation of $\text{Rb}_6[(\eta^2\text{-Sn}_4)\text{Zn}(\eta^3\text{-Sn}_4)] \cdot 5\text{NH}_3$	129
5.5	References	138
6	Investigations on the Solvation and Transformation Chemistry of Zintl Anions in Liquid Ammonia	141
6.1	Abstract	142
6.2	Manuscript	142
6.2.1	Introduction	142
6.2.2	Results and Discussion	144
6.2.3	Conclusion	151
6.3	Supporting Information	152
6.3.1	Solid State Phases	152
6.3.2	Sample Preparation	155
6.3.3	NMR Data	156
6.4	Additional Findings	158
6.4.1	Synthesis of Heteroatomic Zintl Anions in Liquid Ammonia – the New Highly Charged $[\text{Sn}_4\text{Bi}_4]^{4-}$ and Fully Ordered $[\text{Sn}_2\text{Bi}_2]^{2-}$	158
6.4.1	Supporting Information	164
6.5	References	167
7	NMR Spectroscopic Investigations on the Solvation of Alkali Salts (^{87}Rb, ^{23}Na, ^7Li) in Liquid Ammonia	171
7.1	Abstract	172
7.2	Introduction	172
7.3	Results and Discussion	173
7.3.1	RbX ($\text{X} = \text{F}, \text{Cl}, \text{Br}$) in Liquid Ammonia at Various Temperatures	173
7.3.2	Influence of Additives on the Solvation of RbCl in Liquid Ammonia	177
7.3.3	RbCl in Organic Solvents and Enhancement of Solvation by Chelating Additives	180
7.3.4	Investigations on Alkali Salts of ^{23}Na and ^7Li	182

7.4	Conclusion.....	186
7.5	Supporting Information	187
7.5.1	Further ⁸⁷ Rb NMR Spectra.....	187
7.5.2	Experimental Part.....	191
7.5.3	NMR Data Collection and Processing.....	192
7.6	References	194
8	Summary and Outlook	195
9	Zusammenfassung.....	199
10	Appendix.....	203
10.1	Curriculum Vitae	203
10.2	Publications and Conferences.....	204

1 Introduction and Outline

1.1 Asymmetric Copper Catalyzed Synthesis

During the last decades, the request for chiral compounds is strongly increasing, e.g. for biological active compounds like agrochemicals or for the synthesis of chiral pharmaceutical compounds. The huge importance of transition-metal catalysis in the field of stereoselective synthesis is underlined by the Nobel Prizes in 2001, 2005 and 2010. Thereby, chiral ligands are applied to reach high regio-, diastereo- and enantio-selectivities. A big library of chiral ligands is available, one special group represents the monodentate phosphoramidite ligands, which were entitled by Feringa as “privileged ligands” (*Angew. Chem. Int. Ed.* **2011**, 49, 2486), owing to their low costs, compatibility to functional groups and high synthetic availability, in comparison to classical bidentate ligands such as DIOP and BINAP derivatives. The use of phosphoramidite ligands in copper-catalyzed asymmetric conjugated addition reactions leads to almost complete conversion and *ee*-values up to > 99 %. The number of publications containing the words ‘enantioselective’ and ‘copper’ is tremendously increasing during the last decades. Owing to this success the application of Cu complexes is nowadays also strongly increasing in the field of photo-catalyzed reactions.

For structural and mechanistic investigations of copper catalyzed reactions in solution the NMR spectroscopy is the method of choice. But despite the widely use of Cu complexes in asymmetric synthesis, an insight to these famous reactions is very limited and mainly performed on organocuprates. The reason for this might be that the investigations are very challenging. On the one hand copper complexes have the tendency to aggregate and form supramolecular structures in solution. On the other hand the high quadrupole moment of $^{63/65}\text{Cu}$ combined with the electric field gradient of asymmetric complexes leads to a strong line broadening of neighboring atoms and hampers the magnetization transfers over copper. These difficulties for the detection of intermediates might be one reason for the lack of detailed structural and mechanistic studies. In former extensive NMR spectroscopic investigations of our group it was possible to determine the structure of the precatalytic complex in solution under reaction conditions, where the dimeric copper complex shows a trigonal/tetrahedral coordination on copper.

In chapter 2, an overview of the NMR spectroscopic aspects of copper catalyzed asymmetric synthesis is presented. In the very few detailed structural investigations, the

focus of the three most prominent studies was on the structures of the precatalytic copper complexes with phosphoramidite, TADDOL-based and ferrocenyl-based ligands, while with the latter-mentioned until then the only study about structures of the transmetalation intermediates occurring in the reaction with Grignard reagents was performed. This chapter is published as a contribution to “Copper-Catalyzed Asymmetric Synthesis” edited by Alexakis, Krause and Woodward.

In chapter 3, the mechanistic and structural study on the outstanding copper-catalyzed conjugate addition reaction of organozinc reagents to α,β -unsaturated substrates using phosphoramidite ligands is presented. Thereby, for the first time a direct experimental proof of a transmetalation intermediate in asymmetric copper-catalyzed addition reactions is presented. Therefore, the use of special combinations of ^1H , ^{31}P HMBC spectra were applied to detect species beyond the detection limit of ^1H and ^{31}P spectra. The access for the structural characterization of the intermediates was given by utilizing samples with enantiopure and enantiomeric ligand mixtures. Furthermore, occurring interactions between the organozinc reagent and the phosphoramidite ligand, as well as the potential preorganization of an α,β -unsaturated substrate by the precatalytic complex were examined. The investigations were extended to mechanistic studies on Cu complexes with dap ligands in a photoredox reaction.

1.2 The Solvation and Transformation Chemistry of Zintl Ions in Liquid Ammonia

The reduction of elemental lead with sodium in liquid ammonia by Joannis in 1891, and his detection of Pb_9^{4-} anions in such green solutions was the basis for the chemistry of homoatomic group 14 and 15 cluster. Zintl phases, named after the German chemist Eduard Zintl, who was able to identify the compositions of various Zintl anions by potentiometric titration methods in the 1930s, are binary alloys formed by the reaction of alkali metals or alkaline earth metals with metals or metalloids of group 13 to 16. By dissolving those solids in appropriate solvents, they become available as reactants and building blocks in solution chemistry. Corbett *et al.* showed that the availability of these anions in solution can be highly improved by the use of chelating [2.2.2]-cryptand. However, besides direct NMR spectroscopic investigations by Rudolph in ethylene diamine on Sn_9^{4-} , the solvation chemistry of Zintl anions is so far not well investigated. But a deeper understanding of the dissolution, transformation and degradation processes

might provide the possibility of rational syntheses of functionalized Zintl clusters and opens an approach to the design of new materials.

Therefore, in the second part of this work the focus is on the facilitation of heteronuclear NMR spectroscopy and on the solvation processes of Zintl anions and alkali metals in liquid ammonia.

For heteronuclear spins that exhibit a large chemical shift range NMR spectroscopic investigations are often very time-consuming as a block wise measurement of the spectra is necessary owing to the poor offset performance of hard pulses. Even if they provide an excellent inversion profile the high peak pulse amplitude makes these hard pulses unsuitable for applications over a broad bandwidth. In chapter 4, the application of a broadband pulse on samples of stannides is presented. The validation studies on integrals, line widths and coupling constants in comparison to a 90° hard pulse showed reliability of this pulse over a chemical shift range of 1000 kHz and will improve future NMR spectroscopic investigations by an extreme saving of time and the simultaneous observation of several species even if they are showing a huge chemical shift range.

In chapter 5, the detection of the for a long-time elusive highly charged Zintl anions Sn_4^{4-} and Si_4^{4-} in liquid ammonia is presented. The stabilization of these polyanions was possible by using chelating [2.2.2]-cryptand. Furthermore, the observation of NH_2^- revealed that the protons of the solvent molecule are responsible for the oxidation of the highly charged anions. With this knowledge at hand, it was for the first time possible to perform a reaction of the highly charged Sn_4^{4-} cluster with ZnPh_2 to a homoleptic complex.

In chapter 6, the solvation and transformation processes of Zintl cluster in liquid ammonia were investigated. Thereby, it was shown, that the stability of the highly charged anions is not exclusively based on the enhanced solubility by the [2.2.2]-cryptand but also on the oxidation property of the solvent which is reduced by the separation of the cations from the solvent. Furthermore, the detection of heteroatomic Zintl anions in solution by ^{119}Sn NMR spectra is presented.

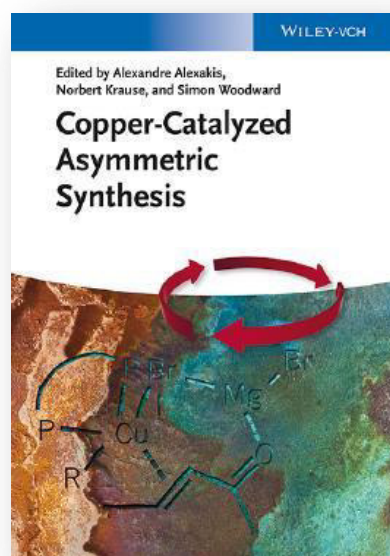
After realizing that the cation is non-innocent for the destabilization of Zintl anions in liquid ammonia, as direct cation-ammonia contacts enhance the oxidation properties of the solvent, in chapter 7, the investigations were focused on alkali halide salts in liquid ammonia and the influence of chelating additives. As for rubidium salts contact ion pairs

and solvent separated ion pairs were stabilized side by side in solution, the investigation was also focused on further alkali salts, various organic solvents and temperature effects.

2 Overview of NMR Spectroscopic Aspects in Copper-Catalyzed Asymmetric Synthesis

Book chapter

„*NMR Spectroscopic Aspects*”*



This chapter was prepared in close collaboration with Felicitas von Rekowski.
Chapter 2.2 and 2.3 were written by Felicitas von Rekowski.

*Felicitas von Rekowski, Carina Koch, Ruth M. Gschwind

NMR Spectroscopic Aspects in Copper-Catalyzed Asymmetric Synthesis
Edited by Alexandre Alexakis, Norbert Krause and Simon Woodward
Wiley-VCH Verlag GmbH & Co. KGaA., 1st edition published 2014

© 2014 Wiley-VCH Verlag GmbH & Co. KGaA. Reproduced with permission.

2.1 Introduction

The NMR spectroscopic investigation of copper complexes in solution is a challenging area of research. Owing to the different magnetic properties of Cu(I)/(III) and Cu(II) systems, varying spectroscopic methods are necessary for the elucidation of their structures. For paramagnetic Cu(II) complexes electron spin resonance (ESR) spectroscopy is applied, while for diamagnetic Cu(I)/(III) complexes high resolution NMR spectroscopy is the method of choice.^[1]

Though the two NMR spectroscopic active Cu isotopes ($^{63/65}\text{Cu}$) have a quite high natural abundance and gyromagnetic ratios similar to ^{13}C , the scope of $^{63/65}\text{Cu}$ NMR spectroscopy is limited by their high quadrupole moment.^[2] Owing to this magnetic property of copper, it is only possible to detect a copper signal if very small electric field gradients are present at the copper nucleus, which occurs mainly in highly symmetric complexes with a tetrahedral coordination on Cu.^[3-4] In such symmetric complexes it is possible to get structural information about the π -acceptor properties of the ligand, the complex geometry or ligand exchange processes. The π -acceptor properties of copper bound ligands or vice versa the electron-donating effects of copper to these ligands can be measured by ^{63}Cu NMR. This is possible, because the ^{63}Cu chemical shifts are mainly determined by the back-donation of electrons of the copper d orbitals to the ligands.^[5-6] Information on the symmetry of the complex and also ligand exchange processes are obtainable from the linewidths of the ^{63}Cu signal and its temperature dependency. In contrast the $^{63/65}\text{Cu}$ signals of complexes with reduced symmetry appear extremely broad or even undetectable owing to fast relaxation processes. The synthetically relevant copper complexes are normally less symmetrical and therefore to the best of our knowledge direct $^{63/65}\text{Cu}$ spectroscopy have not been used for the structure elucidation in asymmetric copper catalyzed reactions. Therefore, NMR structural investigations are limited to NMR active nuclei of the ligands or substituents. In addition, common structural properties of copper complexes are challenging features for NMR spectroscopists. For example, copper complexes are known to tend to self-aggregation, resulting in dimeric, oligomeric or polymeric supramolecular complexes, which hampers the application of classical NMR spectroscopic methods. Additionally, in such partially highly symmetric complexes ligand exchange processes exist, which could either be intramolecular between the ligands themselves, or intermolecular between different complex species, leading to averaged sets of signals. Furthermore, often very similar ^1H chemical shifts occur for the

free ligands and their complexes. From synthetic and spectroscopic studies, it is known, that these complex structures are very sensitive toward the solvent, salt effects and the ligand used. Owing to this sensitivity, it is difficult to propose a general structural model for all reactions; thereby the structure among various experimental conditions has to be examined separately. All these structural properties of the copper complexes are limitations for the applicability of the classical NMR spectroscopic approach for small molecules, especially for the structure elucidation of the precatalytic complexes in copper-catalyzed reactions. Moreover, for such sensitive structural equilibria as known for the copper complexes, the structures in solution are not necessarily identical with the crystal structures. Therefore, a structure determination in solution, including aggregation numbers and aggregate size, is necessary for each of these variable systems.^[1] Despite all these limitations, it is possible to get some insight into the structures of copper complexes especially with a combination of classical NMR spectroscopic methods and diffusion-ordered spectroscopy (DOSY).^[1, 7]

Owing to the spectroscopic properties of copper and the difficulties in the investigation of copper complexes, only few studies dealing with structure elucidation are known. Investigations concerning the mechanism or catalytic cycle are often based on organocuprates as model system, which are the best investigated copper systems so far. However, these systems are already described in several reviews^[1, 8-13] and therefore are not addressed. In this chapter we concentrate on NMR spectroscopic investigations of Cu complexes used in enantioselective catalysis. We selected exemplarily three prominent NMR spectroscopic investigations out of the few available studies dealing with the structure elucidation of the catalytically active species or the precatalytic complexes. Firstly, we report about a catalytic system consisting of phosphoramidite ligands and a copper(I) salt. On the one hand, this study represents the most extensive investigation on the precatalytic system, on the other hand the use of a monodentate class of ligands is described. Furthermore, the structural NMR spectroscopic approach is presented. For this system, a binuclear mixed trigonal/tetrahedral complex structure was identified as new structural motif for the precatalytic complexes. Next, a study using TADDOL-based ($\alpha,\alpha,\alpha',\alpha'$ -tetraaryl-2,2-dimethyl-1,3-dioxolane-4,5-dimethanol) thiolate ligands in combination with CuCl is presented. There is the first study performed on the basis of DOSY and in contrast to the phosphoramidite ligands, a bidentate class of ligands was used. With this system, a tetranuclear complex structure was identified as active catalyst.

In this case, the normally bidentate TADDOL-derived ligands act as monodentate ligands. At least the application of ferrocenyl-based ligands in the copper-catalyzed conjugate addition (CA) reaction with Grignard reagents is described. With this system the first detailed transmetalation study until now has been presented and in contrast to the other studies, which combine mainly NMR spectroscopy and X-Ray analysis, a variety of analytical methods was used. In this study, a mononuclear complex structure was identified as the active transmetalation intermediate. In addition, a brief insight into the structures of the asymmetric allylic alkylation (AAA) with ferrocenyl-based ligands and Grignard reagents is given. Beside these three structure elucidations, further investigations were also done by ESR spectroscopy,^[14] theoretically calculations,^[15] kinetic studies with an early observation of nonlinear effects^[16] on further classes of ligands.^[17-18] But a comprehensive coverage of all these methods is beyond the scope of this chapter.

2.2 Copper Complexes with Phosphoramidite Ligands

The enantioselective C—C-bond formation is one of the most important reaction types among the large number of organic transformations. A very powerful method for this reaction is the asymmetric copper-catalyzed conjugate addition (ACA) reaction. The advantages of this reaction are the high compatibility with many functional groups, low costs of the copper salts and excellent regio- and enantioselectivities. Recent efforts enable to enlarge the scope of substrates and nucleophiles, in order to increase the synthetic application for more complex molecules, such as biologically active and natural compounds (for recent reviews see [19-22]). The phosphoramidite ligands are a very powerful class of ligands, not only in the ACA, but also for many other reactions,^[23] because they are a low-priced and easily accessible class of ligands, enabling high yields and *ee* values. Their electronic properties can be controlled by different substituents on the oxygen or nitrogen atom, therefore a fine-tuning for specific catalytic applications is possible. Furthermore, the chiral diol or amine moiety can be used as source for stereodiscrimination of the desired catalytic system, such as matched or mismatched effects.^[23] In contrast to the broad application range of the ACA in synthesis, structural and mechanistic information on the copper complexes and their intermediates is very rare,^[24-26] although these information is an essential prerequisites for further development on this types of reactions.^[19, 21, 23] Therefore this chapter provides a literature survey of known NMR studies dealing with this topic.

2.2.1 Precatalytic Copper Complexes

Structure Determination

The first and very important step of each structural investigation is to select a system among the synthetically applied ones, which is suitable for NMR spectroscopic investigation. In synthetic applications, Cu(I) and Cu(II) salts are appropriate copper sources, because the Cu(II) salts are completely reduced during the reaction by the organometallic reagent.^[14] In contrast to synthesis, only Cu(I) salts are suitable for NMR spectroscopic investigation of the precatalytic system, because Cu(II) is paramagnetic and no reducing agent is present in the precatalytic system. A further prerequisite for successful structure elucidation are sharp and well-separated signals of the examined system.

In 2006, Zhang and Gschwind^[27] were able to identify a binuclear Cu(I) complex with mixed trigonal/tetrahedral stereochemistry as new structural motif for the precatalytic copper complex **C2** (Figure 2.1a).

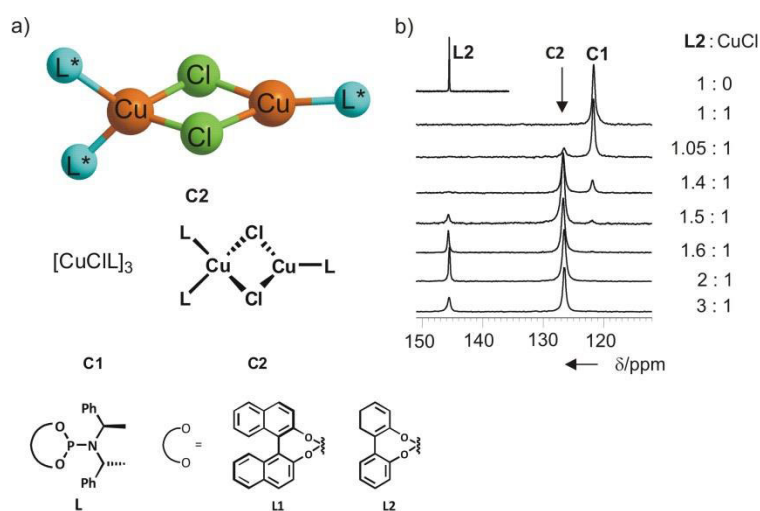


Figure 2.1: a) Schematic drawing of the binuclear copper complex **C2** with mixed trigonal/tetrahedral coordination site on copper and of the 1:1 complex **C1**^[28] and the highly selective phosphoramidite ligands **L1** and **L2**; b) ^{31}P NMR spectra of **L2** and mixtures with CuCl at varying ratios in CDCl_3 at 220 K.^[27]

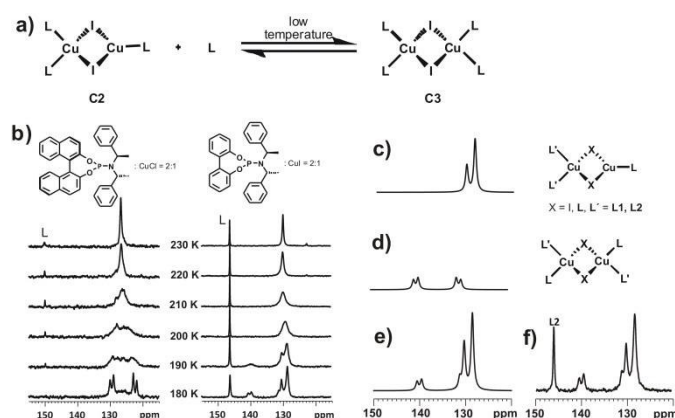
For this study, **L1** and **L2** were selected (see Figure 2.1a), because they give high selectivities and represent the binaphthol- and biphenol-based ligands introduced by Feringa and Alexakis.^[16, 29] They were spectroscopically investigated with different copper salts, ligand-to-salt ratios and solvents.^[27-28] As described above, sufficient signal distribution is necessary, here about 20 ppm for free ligand and complexes, which was obtained in dichloromethane with a ligand-to-salt ratio of 2:1,^[27] corresponding well to

synthetic applications.^[16, 30-31] Also in chloroform, it is possible to receive relatively sharp, separated signals for complexes **C1** and **C2** at 230 K. For **C2**, only one averaged ³¹P signal is observed for all three ligands, because of a fast ligand exchange within the complex at 230 K. Using other solvents such as tetrahydrofuran (THF) or toluene in combination with CuCl, broad signals occur, which indicate the existence of further complexes beside **C1** and **C2** and higher aggregates.^[27] By variation of the ligand-to-salt ratio, it was possible to determine how many ligands are involved in the complex structures of **C1** and **C2**; furthermore the amount of each was controllable (schematic drawings shown in Figure 2.1a). In Figure 2.1b, the ³¹P NMR spectra of **L2** and CuCl at varying ratios in CDCl₃ at 220 K are shown. For a 1:1 ratio or lower, only **C1** occurs, while at ratios higher than 1.05:1, the signal intensity for **C2** starts to increase, while the signal for **C1** decreases. At ratios higher than 1.5:1 mainly **C2** and an increasing amount of free ligand as well as a small amount of **C1** is observed, indicating a 1.5:1 ratio of ligand to copper salt in **C2**. Unfortunately, no proton chemical shift differences were observed for nearly all proton signals of the free ligand and the complexes. Therefore, the classical NMR spectroscopic approach is not applicable and it is necessary to switch to further NMR methods, like DOSY, which provides further information about the molecular size of the complexes. Although the signals in the ³¹P NMR spectra are well separated it is not possible to measure ³¹P DOSY spectra, because of the rapid relaxation of the phosphorous atoms in the copper complexes; so ¹H DOSY experiments were performed. But the problem is that due to the chemical shift overlap of **C1**, **C2** and free ligand only diffusion coefficients with contributions of all three species can be measured. The solution of this problem is to take advantage of the effect of dynamic NMR at temperatures close to the synthetic application. There, the difference in the internal dynamic processes within the ligand and the complexes – especially **C2** – are big enough to cause different linewidths of the methine signals. By choosing a suitable pulse sequence, it is possible to separate the methine signal of **C2** by eliminating the exchange broadened signals of free ligand and **C1** through a T₂ filter (here the longish convection compensating pulse sequence of Müller and Jerschow).^[1, 27] Thus, it was possible to determine, that in the precatalytic complex three ligands are involved. In combination with the 1.5:1 ratio it was possible to identify a binuclear mixed trigonal/tetrahedral structure for **C2**.

Because of the known sensitivity towards salt effects, the dependency of the precatalytic complex structure on the used salt was also addressed in the elucidation. Therefore, Gschwind *et al.* tested four different Cu(I) salts (CuX, X = Cl, Br, I, TC (2-thiophenecarboxylate)). In all cases, the binuclear mixed trigonal/tetrahedral structure could be identified as basic structural motif and therefore it is not an exclusive effect of chloride.^[28]

Temperature Dependence

Since temperature plays a crucial role for high *ee* values, as well as for the reaction yield in copper catalyzed reactions,^[24, 32-36] it is essential to get an insight into temperature-dependent interconversion mechanisms of the complexes. For that reason, Gschwind *et al.* carried out low-temperature NMR spectroscopic investigations. Reducing the temperature decelerates the exchange processes. At low-temperatures, two ³¹P signals are expected for the two different kinds of ligands in **C2**, which would allow confirming the structure of **C2** by classical NMR methods. In Scheme 2.1b the temperature-dependent ³¹P NMR spectra of **L1**:CuCl and **L2**:CuI, each in a 2:1 ratio, are shown. At 180 K, it was possible to identify a further complex structure **C3**, which arises from the addition of free ligand **L** to **C2** (Scheme 2.1a). Furthermore, the low-temperature ³¹P NMR spectra shows an AA'BB' scalar coupling pattern for **C3**, which is typical for slightly distorted L₂Cu fragments. In a ³¹P, ³¹P COSY (correlation spectroscopy) spectra, the observed coupling pattern was confirmed as the result of scalar coupling between the two ligands. The existence of two L₂CuX units in the dimeric complex **C3** was shown by DOSY experiments. Beside the signal for **C3**, a signal splitting for **C2** at 180 K in a 2:1 ratio can be observed, which represents a slow intraligand exchange on the NMR timescale for the two different ligand groups in the mixed trigonal/tetrahedral precatalytic complex structure at low temperatures. In order to confirm the existence of these two complexes, the ³¹P NMR spectra of **C2** and **C3** have been simulated (Scheme 2.1c,d), superimposed (Scheme 2.1e) and compared with the experimental spectrum at 180 K (Scheme 2.1f).^[37] Thus the temperature-dependent conversion of **C2** into **C3** was observed. As expected, the low-temperature structures in solution approximate the solid-state structure. However at reaction temperature exclusively **C2** exists, which is in good agreement with the crucial role of the temperature on the outcome of the reaction.^[24,32-36]



Scheme 2.1: a) Intermolecular interaction between **C2** and **L** generating **C3** at low temperatures; b) ^{31}P NMR spectra of **L1**:CuCl (left) and **L2**:CuI (right) in a 2:1 ratio at varying temperatures in CD_2Cl_2 . Simulated ^{31}P NMR spectra of binuclear copper complexes with c) mixed trigonal/tetrahedral and d) tetrahedral coordination on copper e) superposition of c) and d) for comparison with f) experimental spectra of **L2**:CuI (2:1) in CD_2Cl_2 at 180 K.^[37]

The presented NMR study describes the first direct experimental proof for the precatalytic complex structure **C2**, which was previously only identified by DOSY NMR measurements.^[37] In a density functional theory (DFT) study by Woodward, investigating the reaction mechanism of the ACA, a mononuclear copper complex was detected as ground state of the transmetalation intermediate using a phosphoramidite ligand, copper(I) salt, and ZnMe_2 . Interestingly, after the addition of a dienone a binuclear copper complex was identified as the energetically most accessible, which enables the postulation of a possible favored reaction pathway.^[15] This binuclear complex structure is essentially identical with the determined structure of the Gschwind group.

Ligand-Specific Aggregation Trends

The temperature-dependent interconversion of copper complexes described above raised the question, as to whether this structure variation is mediated by the general properties of the phosphoramidites as ligands or whether it is a particular effect of the copper complexes due to their high structural variability. Therefore, a temperature-dependent aggregation study of different phosphoramidite ligands and their transition metal complexes was performed (Figure 2.2). The ligands **L1** and **L2** were selected to represent the binaphthol- and biphenol-based ligand families introduced by Feringa and Alexakis.^[16, 29] For the investigation of the influence of steric effects and rotary motion on the catalysis, the smaller ligand **L3** was the ligand of choice. In order to check the influence of different transition metals and coordination spheres in terms of complex structures and stoichiometries, transition metal complexes bearing different copper, palladium and iridium salts were tested.

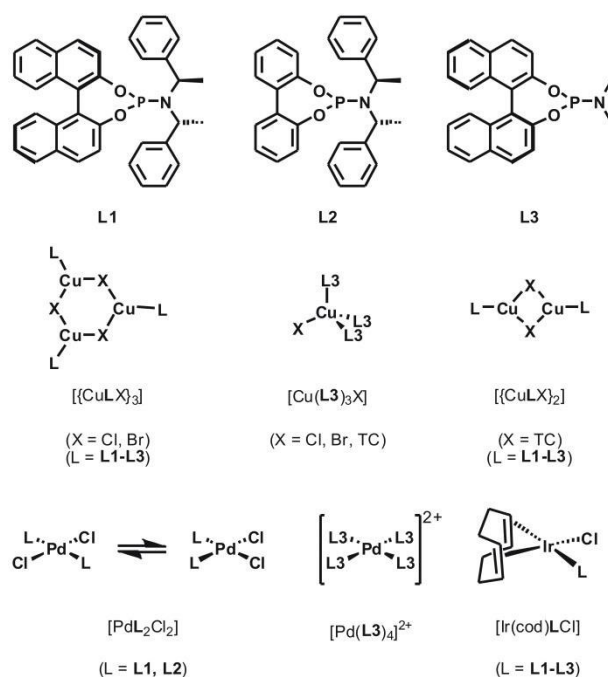


Figure 2.2: Phosphoramidite ligands **L1-L3** and different transition metal complexes investigated concerning their aggregation trends (TC, 2-thiophenecarboxylate; cod, 1,5-cyclooctadiene).^[38]

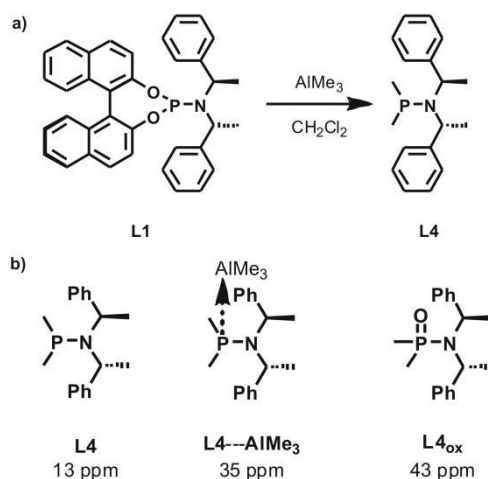
The method of choice to gain an insight into the aggregation behavior of all these systems was to use temperature-dependent 1H DOSY NMR spectra and to calculate the viscosity- and temperature-corrected diffusion coefficients. For all ligands and complexes used in this study baseline-separated specific signals were used for the DOSY analysis. Therefore, out of the whole series of copper complexes only $[CuLX]_n$, $[Cu(L3)_3X]$ and two $[Cu_2L_3X_2]$ were appropriate for this study. First the aggregation trends of the free ligands were determined. At 270 K, all three ligands exist as monomers and all of them show threshold temperatures, where aggregation starts. As expected the individual threshold temperatures and the slopes of the aggregation curves depend on the ligand structures.^[38]

Interestingly, the aggregation trends of all transition metal complexes with the highly stereoselective ligands **L1** and **L2** show a behavior very similar to that of the corresponding free ligands. This was found to be independent of the transition metal used, the complex structure, or the complex stoichiometry. Only in the case of the smaller ligand **L3**, which shows only moderate *ee* values in catalytic application, significant different aggregation trends were observed. In conclusion a fast and simple 1H DOSY NMR screening method was presented on the example of phosphoramidite ligands to predict the aggregation behavior of ligands and their transition metal complexes. Furthermore, this offers a great opportunity to apply a fast and simple method for the

optimization of catalytic reaction conditions – especially temperature - via ^1H DOSY NMR spectroscopy.^[38] This shows that, in case of the highly stereoselective phosphoramidite ligands, the aggregation trend of the copper complexes as well as other transition metal complexes is mainly influenced by the ligand properties.

2.2.2 Phosphoramidite Trialkylaluminum Interactions

The first step in the proposed mechanism of the ACA is the transmetalation step, where an alkyl or aryl moiety from the organometallic reagent is transferred to the precatalytic complex.^[28] The spectroscopic proof for such a transmetalation product is very difficult to achieve. The only extensive example for a detected transmetalation product via NMR spectroscopy is published by Feringa with ferrocenyl-based ligands in the addition reaction of Grignard reagents (Section 2.4.1).^[25] For the ACA with phosphoramidite ligands, no transmetalation studies having been published until now, potential organometallic reagents are ZnR_2 and AlR_3 . The only NMR spectroscopic study about interactions of phosphoramidite ligands with AlMe_3 was published by Alexakis *et al.* in 2006 with dichloromethane as solvent.^[39] After the addition of AlMe_3 , the ligand signal for **L1** disappears in the ^{31}P NMR spectra and a new signal at 35 ppm appears. The workup of the mixture and purification via column chromatography provides two substances, which could be identified as 1,1'-bi-2-naphtol (BINOL) and oxidized aminophosphine ligand **L4_{ox}**, so the signal at 35 ppm is the result of a complexation of diaminophosphine ligand **L4** by AlMe_3 (Scheme 2.2).^[39]

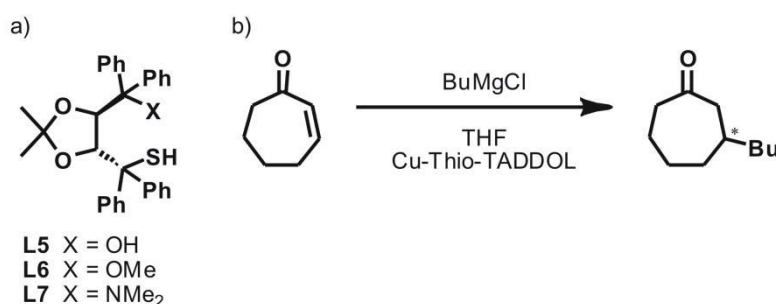


Scheme 2.2: a) Reaction between **L1** and AlMe_3 yielding **L4**; b) ^{31}P NMR chemical shifts of aminophosphine **L4**, complexation of aminophosphine by AlMe_3 **L4---AlMe₃** and oxidized aminophosphine **L4_{ox}**.

The modification of the phosphoramidite ligands is also visible in toluene, but is not observed in coordinating solvents, like THF or diethyl ether.^[39] With other transmetalation reagents, e. g. ZnR_2 these ligand transformation reaction was also not observed.

2.3 Copper Complexes with TADDOL-based Thiolate Ligands

The first NMR-based study, to our knowledge, about structure elucidation of precatalytic copper complexes in enantioselective catalysis was published in 2000 by the groups of Pregosin and Seebach. The 1,4-addition reaction of Grignard reagents to enones with a combination of CuCl and the TADDOL-based thiolate ligands **L5-L7** as catalysts was selected as model system (Scheme 2.3).^[7]



Scheme 2.3: a) TADDOL-based thiolate ligands **L5-L7**; b) copper catalyzed conjugate addition of BuMgCl to cycloheptenone (TADDOL = $\alpha,\alpha,\alpha',\alpha'$ -tetraaryl-2,2-dimethyl-1,3-dioxolane-4,5-dimethanol).^[7]

Modest positive nonlinear effects suggested that more than one ligand (and perhaps several metals) might be involved in the catalysis.^[40-42] In accordance with this result, the crystal structure of **C4** showed a tetranuclear complex structure. What is surprising is that in this crystal structure, the normally bidentate^[43] thiolate ligand acts as a monodentate ligand in which the oxygen atom of the hydroxyl group is not complexed. In order to investigate whether these structural features are also present in solution NMR spectroscopic investigations, especially ^1H DOSY and nuclear overhauser effect spectroscopy (NOESY) experiments were performed on the copper complexes with the thiolate ligands **L5-L7**. With diffusion NMR measurements, it was possible to confirm the tetranuclear complex structure also in solution. In addition, the ^1H low field shift of the hydroxyl proton (about 8.7 ppm) proved the monodentate coordination of **L5** in solution. For the complexes **C5** and **C6**, similar results were accessible via NMR studies (Figure 2.3).^[7]

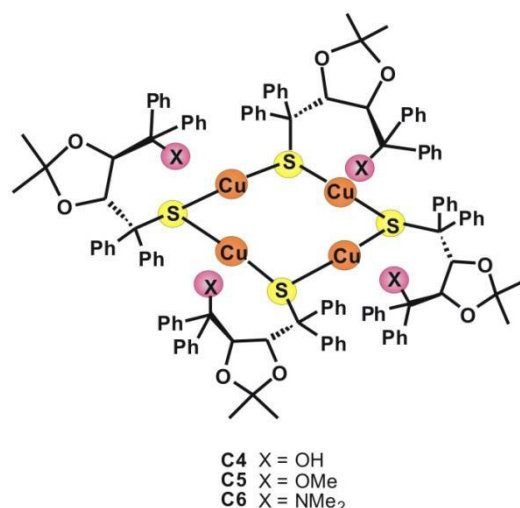
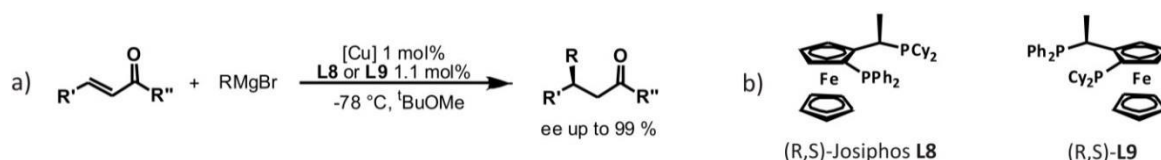


Figure 2.3: Schematic presentation of the tetranuclear copper thiolate complexes **C4-C6**.^[7]

In order to prepare further model systems related to the copper chemistry in the copper-catalyzed 1,4-addition reactions of Grignard reagents, the complexes **C4-C6** were treated with an excess of *tert*-butylisocyanide in THF-*d*8, which was assumed as additional donor ligand in order to get the corresponding isocyanide complexes. With diffusion NMR measurements, it was possible to confirm the tetranuclear complex structure of these systems also in solution, that is, no deaggregation to mononuclear species of **C4-C6** occurs, even in presence of additional donor ligands. In the ¹H, ¹H NOESY spectra, various cross-peaks were observed for the basic ligands, suggesting different structures of the complexes based on the ligand used and so the structural differences generate other chiral environments on the copper atom. With this, a hint for the stereoselective inversion was perceived.^[1, 7] In conclusion, Pregosin and Seebach were able to identify a tetranuclear copper thiolate complex, which uses an unprecedented monodentate complexation mode, in solution, as well as in solid state. Furthermore, they present the first example for an application of diffusion measurements for the determination of aggregation behavior of organocopper complexes in solution.^[7]

2.4 Copper Complexes with Ferrocenyl-Based Ligands

Another prominent example of the structure elucidation of catalytically active copper complexes and their intermediates is an extensive study of Feringa and coworkers,^[25] regarding the mechanism of the ACA reaction of Grignard reagents to α,β -unsaturated carbonyl compounds. In this study, they selected the ferrocenyl-based ligands **L8** and **L9** (Scheme 2.4b) which are known to catalyze the ACA of Grignard reagents to α,β -unsaturated enones with high yields and enantioselectivities (Scheme 2.4a).^[44]

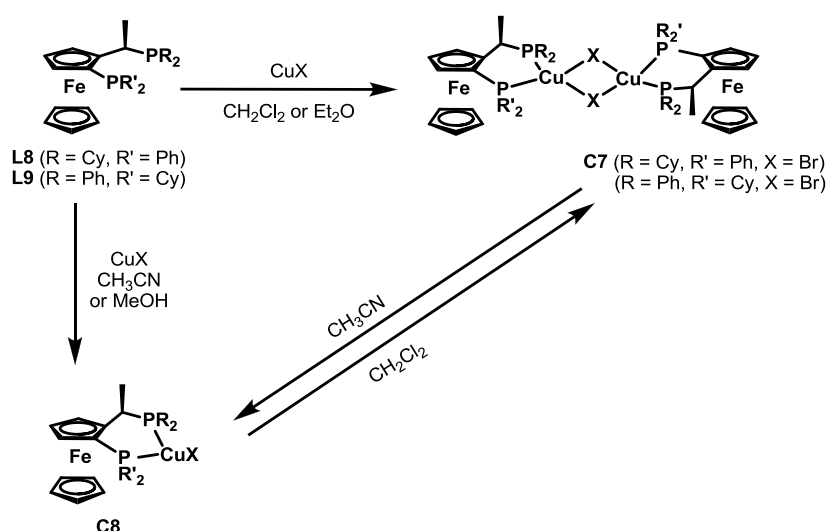


Scheme 2.4: a) Enantioselective conjugate addition reaction of Grignard reagents to acyclic α,β -unsaturated enones; b) ferrocenyl-based ligands **L8** and **L9**.^[25]

2.4.1 Structural Studies of Asymmetric Conjugate Addition Reactions

Precatalytic Copper Complexes

The precatalytic complexes were identified either as mononuclear (**C8**) or binuclear (**C7**) complex by X-ray diffraction analysis (Scheme 2.5).^[25, 45]



Scheme 2.5: Formation of the precatalytic, solvent-dependent, copper complexes **C7** and **C8** (CuX ; X = Cl, Br, I).^[25]

Owing to the fact that the structures in solution may differ from these crystal structures, Feringa and coworkers investigated the existence of the precatalytic structures also in solution. Because the ^1H and ^{31}P NMR spectra of the mononuclear and the binuclear complexes are nearly identical, classical NMR spectroscopic methods could not be applied for their differentiation. Compared to the above described phosphoramidite copper complexes, this is a second example of indistinguishable signals in the ^1H spectrum of the precatalytic complexes. Owing to this fact no ^1H DOSY measurements^[1, 7, 27-28, 38] would be possible, because this requires a specific, baseline-separated signal in the corresponding 1D spectrum. Feringa and coworkers^[25] surmounted this problem using a combination of ESI-MS, IR spectroscopy and electrochemical studies, to examine the behavior of the complexes by changes of the solvent. They were able to show that the solvent-dependent equilibrium between the mono- and binuclear complex structures **C8**

and **C7** (Scheme 2.5) also exists in solution. In particular, electrochemical studies confirmed the existence of a binuclear halide-bridged copper complex **C7** in CH_2Cl_2 , which is the thermodynamically most favored complex in halogenated solvents. In addition, this voltammetry investigation showed that the electron density on the copper(I) centers in several binuclear complexes varies despite a high structural similarity. Interestingly, these differences are caused by the ligand involved, and do not depend on the bridging halide.^[25] This study reveals that severe signal overlap preventing the application of DOSY experiments, can be circumvented by the use of elaborated combinations of various analytical methods.

Transmetalation Intermediates with Grignard Reagents

Transmetalation Studies by NMR. As first step in the copper catalyzed 1,4-addition, transmetalation between the organometallic reagent and the copper complex is postulated. For this generally assumed transmetalation intermediate, some hypothetical structures have been proposed for the enantioselective CA^[16, 31] and a number of studies about non chiral transmetalated copper salts are known.^[10, 46-52] Experimental reports about the transmetalated intermediate species under catalytic conditions are very rare and, to our knowledge, only two reports have been published so far. In a very short report about the addition of ZnEt_2 to copper complexes with a chiral diphosphate ligand, an extremely large upfield shift in the ^{31}P spectrum was detected and attributed to an Et-Cu transmetalation intermediate.^[53] The second report of Feringa about the transmetalation intermediates in the ACA of Grignard reagents to α,β -unsaturated carbonyl compounds is very detailed and interestingly there very small ^{31}P chemical shift differences between the precatalytic and the transmetalated species were found.^[25] Owing to the fact that reliable structural information about the transmetalation intermediates is very important for mechanistic understanding, the study of the transmetalation intermediates that occur is explained in detail. However, we would like to remind the known sensitivity of copper-catalyzed reactions to variation in the ligand structures, copper salts, solvents, temperatures and organometallic reagents. Thus, it might not be possible to propose one general mechanism and one common transmetalation intermediate for all copper-catalyzed reactions.

Feringa and coworkers were able to elucidate the structure of the transmetalation complex on the basis of classical 1D NMR spectroscopic experiments, such as changes of the ^1H and ^{31}P chemical shifts, scalar coupling pattern, and integrals upon the variation of

reaction parameters. The reactive intermediate species was then identified by connecting the appearance of different compounds with known reactivities.

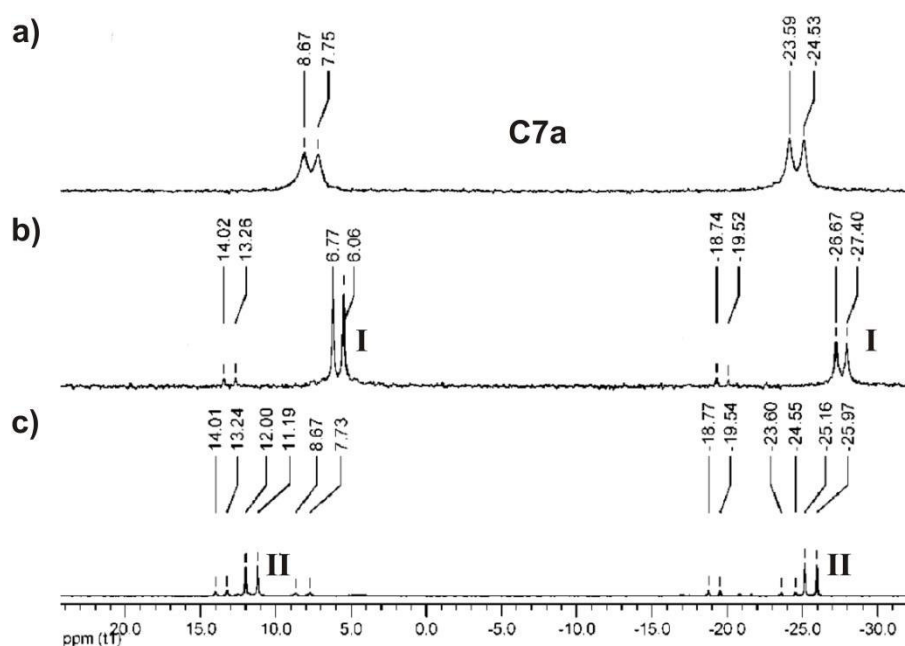
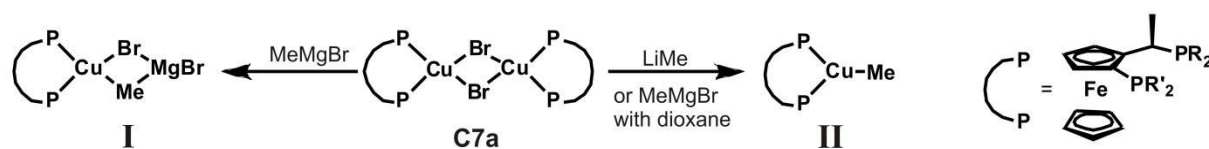


Figure 2.4: ^{31}P NMR spectra in CD_2Cl_2 at 213 K: a) complex **C7a**; b) complex **C7a** with 3 equiv. of MeMgBr ; c) complex **C7a** with 3 equiv. of MeMgBr followed by addition of 3 equiv. of dioxane. (Reprinted with permission from Ref. [25]. Copyright 2006 American Chemical Society.

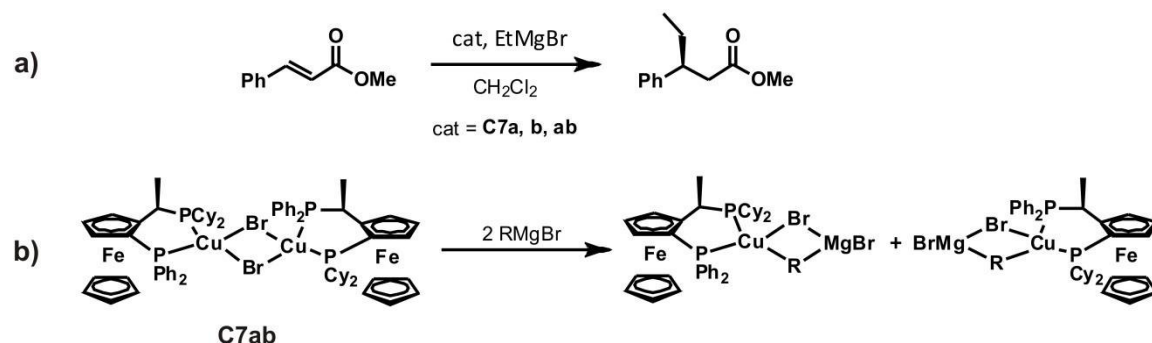


Scheme 2.6. Transmetalated complexes **I** and **II**, after the addition of organometallic reagents or dioxane to the precatalytic complex **C7a**.^[25]

Upon addition of an excess of MeMgBr to the precatalytic complex **C7a**, a main new species appeared in the ^{31}P spectrum (see **I** in Figure 2.4b). The chemical shift values and the integral ratio of the corresponding new methyl signal in the ^1H spectrum indicated a transmetalated species with a ratio of one methyl group at the copper per ligand attached. To test whether MgBr_2 is part of this intermediate, dioxane, which is known to coordinate strongly to MgBr_2 and removes it from the solution, was added (Figure 2.4c). As a result, it drives the Schlenk equilibrium towards the formation of R_2Mg . Under these conditions, a new transmetalated species **II** is detected (Figure 2.4c). The identical intermediate can be created upon addition of MeLi with and without crown ether. This set of experiments allows to assign species **I** to a transmetalated intermediate with MgBr_2 attached, whereas in **II**, MgBr_2 or LiBr is not part of the intermediate (see Scheme 2.6 for structures).

Next, Feringa and coworkers performed stoichiometric addition reactions with **I** and **II** to identify the catalytically active species. The outcome of these reactions and subsequent studies of the solvent and salt dependence of the intermediate and the synthetic outcome are all in agreement “that species **I** rather than species **II** is essential to obtain high levels of regio- and enantioselectivity in the catalytic CA of Grignard reagents to unsaturated carbonyl compounds.”^[25] With this experimental setup, the composition of **I** was clearly defined. However it remained to be clarified whether **I** was a mono- or a binuclear copper complex.

Kinetic Studies. Additional evidence for the mononuclearity of the catalytically active species was obtained by kinetic studies. Therefore, the catalytic activity of heterocomplex **C7ab** compared with that of the homocomplexes **C7a** and **C7b**, in the CA of EtMgBr to methyl cinnamate was determined (Scheme 2.7a).

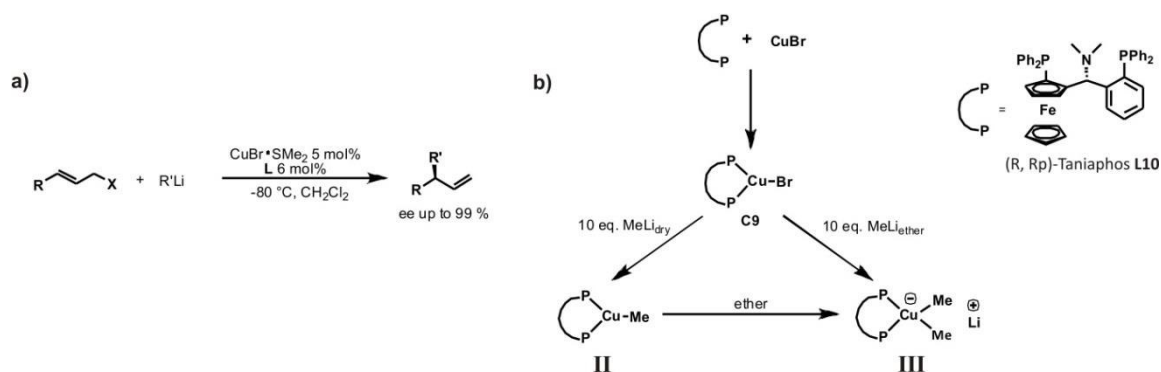


Scheme 2.7: a) Analyzed reaction in the kinetic study; b) dissociation of the heterocomplex **C7ab**.^[25]

For the reaction performed with the homodimeric precatalyst **C7a**, a low yield (4 %) was reached; in contrast, for **C7b**, a high conversion of 69 % was observed (**C7a** and **C7b**, see Scheme 2.5). The heterocomplex **C7ab** was then applied as precatalytic complex in an identical reaction, resulting in halved conversion (32 %) corresponding to the reaction with **C7b**. In accordance, double the amount of the precatalyst **C7ab** resulted in the same yield compared with **C7b** (65 %). Thus, the catalytically active species could be identified to be the mononuclear complex **I** (Scheme 2.6).

2.4.2 Structural Studies of Asymmetric Allylic Alkylation

In 2011, Feringa *et al.*^[54] developed the first AAA of allylic halides with high yields and enantioselectivities, despite the high reactivity of the organolithium compounds (Scheme 2.8a). Moreover, they performed a further NMR spectroscopic study, dealing with this reaction. In contrast to other organometallic reagents (ZnR_2 , AlR_3 , RMgX), in the case of organolithium compounds, further structural information can be collected using the NMR active nuclei $^6/7\text{Li}$. On the basis of the above described experience, 1D NMR spectra were used to identify the precatalytic complex **C9** and complex **II** as transmetalated species in solution. Thereby, an incorporation of lithium ions can be excluded directly by $^6/7\text{Li}$ NMR spectra.^[54]



Scheme 2.8: a) Asymmetric allylic alkylation reaction with organolithium reagents ($\text{X} = \text{Br}, \text{Cl}$); b) By NMR spectroscopy identified structures: precatalytic complex **C9** and the transmetalated species **II** and **III** in CD_2Cl_2 at 200 K.^[54]

The chemical shifts in the ^1H , ^{31}P and $^6/7\text{Li}$ NMR spectra were used to identify the complex structures present in solution. Thereby, the spectra of different combinations of copper salts, solvents, and quantities of MeLi over a range of temperatures were analyzed. The investigation on the influence of ethereal solvents on the structure in the reaction mixture was also relevant. In the presence of Et_2O , a drastic decrease in yield and enantioselectivity is observed (for instance, if Et_2O is used as cosolvent e.g. to delute $n\text{-BuLi}$).^[54] When MeLi without Et_2O was added, complex **II** was observed exclusively in the ^{31}P spectrum. In contrast, by adding Et_2O subsequently to this reaction mixture or using MeLi containing Et_2O , the occurrence of complex **III** was observed (Scheme 2.8). Hence, it is concluded that complex **II** is responsible for the unique activity and selectivity in the copper-catalyzed allylic alkylation with organolithium reagents. A further proof for the postulated structure of species **II** was the absence of a peak in the $^6/7\text{Li}$ NMR spectra, when complex **II** is prepared exclusively. This shows that there is no lithium ion incorporated in this structure.^[54]

This study clearly shows the problem mentioned earlier, that is, the structures of the transmetalation intermediates differ significantly, depending on the respective reaction. In the present case, the use of MeLi instead of a Grignard reagent and a small change of the ligand structure are responsible for the formation of species **II** during the transmetalation step, which was found to be the less reactive species in the above describe reaction with Grignard reagents. Great care is recommended for proposing a general transmetalation intermediate, as each reaction has to be investigated separately.

2.5 Conclusion

In conclusion, this chapter provides a literature survey of the performed NMR spectroscopic investigations dealing with the elucidation of ACA and AAA reactions. This research area is a quite challenging field, owing to the magnetic properties of copper (e.g., high quadrupole moment). Out of the few studies concerning the mechanism elucidation, three prominent examples were selected and presented here in detail. For phosphoramidite copper complexes, Gschwind *et al.* were able to identify a binuclear Cu(I) complex with a mixed trigonal/tetrahedral stereochemistry as new structural motif for the precatalytic complex structure by diffusion NMR measurements (DOSY) and they confirmed this structure also by classical NMR methods. This structural motif is independent of the halide used, but can be interconverted into other complex structures dependent on the temperature. For the investigation of the origin of the structure variations, a fast and simple ^1H DOSY NMR screening method was developed on the example of phosphoramidite ligands to predict the aggregation behavior of ligands and their transition metal complexes. For transition metal complexes with highly stereoselective phosphoramidite ligands, aggregation trends were determined, which are mainly dependent on the ligand properties. With TADDOL-based ligands, Pregosin and Seebach identified a tetranuclear thiolate complex with an unprecedented monodentate complexation mode both in the solid state and in solution. This was the first study applying NMR diffusion measurements for the determination of aggregation trends of organocopper complexes. Although various organometallic reagents (RMgX , ZnR_2 , AlR_3) have been already introduced to synthetic applications, only one extensive NMR spectroscopic investigation concerning the proposed transmetalation intermediates was published by Feringa for the ACA of Grignard reagents with ferrocenyl-based ligands. By combination of various analytical methods (NMR spectroscopic, electrochemical and kinetic investigations, X-ray diffraction), they were able to identify equilibrium between

mono- and binuclear precatalytic complexes, depending on the solvent properties. In synthetically applied solvents, the binuclear structure is present. Upon the addition of an excess of MeMgBr, one major new species could be identified. On the basis of chemical shift values, integral ratios, and variation of the reaction conditions, it was possible to determine that the transmetalation intermediate obtained attached one methyl group at the copper per ligand and include MgBr₂. The mononuclearity of this intermediate was confirmed by kinetic studies. Also the transmetalation intermediate structures in the AAA with a ferrocenyl-based ligand and CuBr as catalyst and MeLi as transmetalation reagent were investigated by Feringa; for this reaction, they assigned a diphosphine copper monoalkyl species, without included lithium, as the active one.

In summary, from the very few detailed structural studies in solution, it is still difficult to conclude a structural trend and for that purpose a lot more of research will be required. However, some common trends and deviations are already visible. Under experimental conditions, all precatalytic complexes known so far in ACA are not mononuclear, but dimer, tetramer, or mixed aggregates. Thus, self-aggregation of precatalytic copper complexes has to be considered as important property also in catalytically active enantioselective systems. For the transmetalation intermediates, interestingly the structural outcome of the two studies with a bidentate ferrocenyl-based ligand shows the identical monomethylation of the copper complexes. However the transmetalation intermediates differ in the inclusion or exclusion of the metal atom of the transmetalation reagent. This is a strong reminder to the sensitivity of copper reactions and also of their intermediates to the reaction conditions used. Therefore, in case of copper-catalyzed enantioselective reactions, great care has to be taken to transfer structural information from one system to another without structural studies in solution, and, most probably, more than one mechanistic pathway is possible in enantioselective copper-catalyzed reactions.

2.6 References

- [1] R. M. Gschwind, *Chem. Rev.* **2008**, *108*, 3029-3053.
- [2] R. K. Harris, E. D. Becker, S. M. C. d. Menezes, R. Goodfellow, P. Granger, *Pure Appl. Chem.* **2001**, *73*, 1795-1818.
- [3] P. Kroneck, J. Kodweiss, O. Lutz, A. Nolle., D. Zepf, *Z. Naturforsch., Teil A* **1982**, *37A*, 186-190.
- [4] T. Gärtner, R. M. Gschwind, *The Chemistry of Organocopper Compounds*, John Wiley & Sons Ltd., **2009**.
- [5] M. Kujime, T. Kurahashi, M. Tomura, H. Fujii, *Inorg. Chem.* **2006**, *46*, 541-551.
- [6] H. Nakatsuji, K. Kand, K. Endo, T. Yonezawa, *J. Am. Chem. Soc.* **1984**, *106*, 4653-4660.
- [7] A. Pichota, P. S. Pregosin, M. Valentini, M. Wörle, D. Seebach, *Angew. Chem. Int. Ed.* **2000**, *39*, 153-156.
- [8] N. Yoshikai, E. Nakamura, *Chem. Rev.* **2011**, *112*, 2339-2372.
- [9] E. Nakamura, S. Mori, *Angew. Chem. Int. Ed.* **2000**, *39*, 3750-3771.
- [10] S. Woodward, *Chem. Soc. Rev.* **2000**, *29*, 393-401.
- [11] B. H. Lipshutz, S. Sengupta, *Organic Reactions*, Wiley-VCH, **1992**.
- [12] E. Nakamura, *Modern Organocopper Chemistry*, Wiley-VCH, **2002**.
- [13] B. L. Feringa, *Modern Organocopper Chemistry*, Wiley-VCH, Weinheim, **2002**.
- [14] T. Pfretzschner, L. Kleemann, B. Janza, K. Harms, T. Schrader, *Chem. Eur. J.* **2004**, *10*, 6048-6057.
- [15] M. Welker, S. Woodward, L. F. Veiros, M. J. Calhorda, *Chem. Eur. J.* **2010**, *16*, 5620-5629.
- [16] L. A. Arnold, R. Imbos, A. Mandoli, A. H. M. d. Vries, R. Naasz, B. L. Feringa, *Tetrahedron* **2000**, *56*, 2865-2878.
- [17] K. Nakano, Y. Bessho, M. Kitamura, *Chem. Lett.* **2004**, *32*, 224-225.
- [18] E. Gallo, F. Ragaini, L. Bilello, S. Cenini, C. Gennari, U. Piarulli, *J. Organomet. Chem.* **2004**, *689*, 2169-2176.
- [19] A. Alexakis, J. E. Bäckvall, N. Krause, O. Pàmies, M. Diéguez, *Chem. Rev.* **2008**, *108*, 2796-2823.
- [20] S. R. Harutyunyan, T. den Hartog, K. Geurts, A. J. Minnaard, B. L. Feringa, *Chem. Rev.* **2008**, *108*, 2824-2852.
- [21] T. Jeraphagnon, M. G. Pizzuti, A. J. Minnaard, B. L. Feringa, *Chem. Soc. Rev.* **2009**, *38*, 1039-1075.
- [22] J. Christoffers, G. Koripelly, A. Rosiak, M. Rössle, *Synthesis* **2007**, *9*, 1279-1300.
- [23] J. F. Teichert, B. L. Feringa, *Angew. Chem. Int. Ed.* **2010**, *49*, 2486-2528.
- [24] N. Krause, *Modern Organocopper Chemistry*, Wiley-VCH, Weinheim, **2002**.

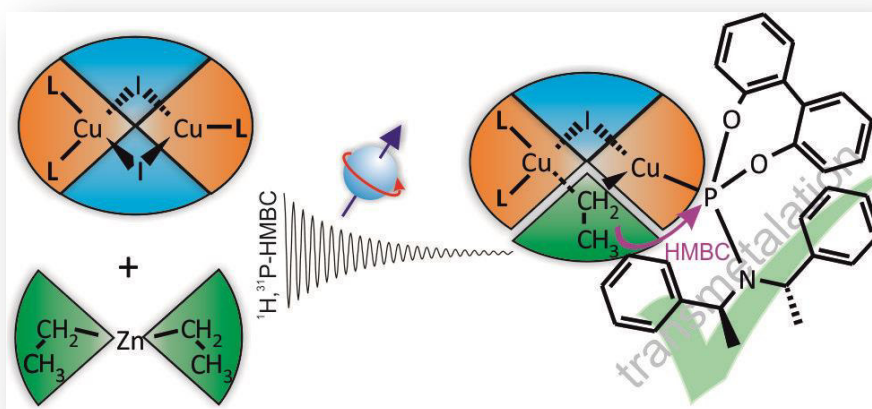
- [25] S. R. Harutyunyan, F. López, W. R. Browne, A. Correa, D. Pena, R. Badorrey, A. Meetsma, A. J. Minnaard, B. L. Feringa, *J. Am. Chem. Soc.* **2006**, *128*, 9103-9118.
- [26] M. D. Murphy, C. A. Ogle, S. H. Bertz, *Chem. Comm.* **2005**, 854-856.
- [27] H. Zhang, R. M. Gschwind, *Angew. Chem. Int. Ed.* **2006**, *45*, 6391-6394.
- [28] H. Zhang, R. M. Gschwind, *Chem. Eur. J.* **2007**, *13*, 6691-6700.
- [29] A. Alexakis, S. Rosset, J. Allamand, S. March, F. Guillen, C. Benhaim, *Synlett* **2001**, *9*, 1375-1378.
- [30] A. H. M. d. Vries, A. Meetsma, B. L. Feringa, *Angew. Chem. Int. Ed.* **1996**, *35*, 2374-2376.
- [31] A. Alexakis, C. Benhaim, S. Rosset, M. Human, *J. Am. Chem. Soc.* **2002**, *124*, 5262-5263.
- [32] A. Alexakis, C. Benhaim, *Org. Lett.* **2000**, *2*, 2579-2581.
- [33] H. Malda, A. W. v. Zijl, L. A. Arnold, B. L. Feringa, *Org. Lett.* **2001**, *3*, 1169-1171.
- [34] D. Pena, F. López, S. R. Harutyunyan, A. J. Minnaard, B. L. Feringa, *Chem. Comm.* **2004**, 1836-1837.
- [35] W. Zhang, C.-J. Wang, W. Gao, X. Zhang, *Tetrahedron Lett.* **2005**, *46*, 6087-6090.
- [36] A. H. Hoyveda, A. W. Hird, M. Kacprzynski, *Chem. Comm.* **2004**, 1779-1785.
- [37] K. Schober, H. Zhang, R. M. Gschwind, *J. Am. Chem. Soc.* **2008**, *130*, 12310-12317.
- [38] K. Schober, E. Hartmann, H. Zhang, R. M. Gschwind, *Angew. Chem. Int. Ed.* **2010**, *49*, 2794-2797.
- [39] C. Bournaud, C. Falciola, T. Lecourt, S. Rosset, A. Alexakis, L. Micouin, *Org. Lett.* **2006**, *8*, 3581-3584.
- [40] D. Guillaneux, S.-H. Zhao, O. Samuel, D. Rainford, H. B. Kagan, *J. Am. Chem. Soc.* **1994**, *116*, 9430-9439.
- [41] M. Reggelin, *Nach. Chem. Tech. Lab.* **1997**, *45*, 392-396.
- [42] C. Girard, H. B. Kagan, *Angew. Chem. Int. Ed.* **1998**, *37*, 2922-2959.
- [43] D. Seebach, A. K. Beck, A. Heckel, *Angew. Chem. Int. Ed.* **2001**, *40*, 92-138.
- [44] F. López, S. R. Harutyunyan, A. J. Minnaard, B. L. Feringa, *J. Am. Chem. Soc.* **2004**, *126*, 12784-12785.
- [45] F. López, S. R. Harutyunyan, A. Meetsma, A. J. Minnaard, B. L. Feringa, *Angew. Chem. Int. Ed.* **2005**, *44*, 2752-2756.
- [46] B. Christenson, T. Olsson, C. Ullenius, *Tetrahedron* **1989**, *45*, 523-534.
- [47] S. H. Bertz, R. A. Smith, *J. Am. Chem. Soc.* **1989**, *111*, 8276-8277.
- [48] S. H. Bertz, M. K. Carlin, D. A. Deadwyler, M. Murphy, C. A. Ogle, P. H. A. Seagle, *J. Am. Chem. Soc.* **2002**, *124*, 13650-13651.
- [49] N. Krause, R. Wagner, A. Gerold, *J. Am. Chem. Soc.* **1994**, *116*, 381-382.

- [50] K. Nilsson, C. Ullenius, N. Krause, *J. Am. Chem. Soc.* **1996**, *118*, 4194-4195.
- [51] A. Alexakis, A. Commercon, C. Coulentianos, J. F. Normant, *Pure Appl. Chem.* **1983**, *55*, 1759-1766.
- [52] B. H. Lipshutz, C. Hackmann, *J. Org. Chem.* **1994**, *59*, 7437-7444.
- [53] M. Yan, L.-W. Yang, K.-Y. Wong, A. S. C. Chan, *Chem. Comm.* **1999**, 11-12.
- [54] M. Pérez, M. Fañanás-Mastral, P. H. Bos, A. Rudolph, S. R. Harutyunyan, B. L. Feringa, *Nat. Chem.* **2011**, *3*, 377-381.

3 NMR Spectroscopic Investigations on Mechanistic Steps of Copper Catalyzed Reactions

Full Paper

*„The Elusive Transmetalation Intermediate in Copper-Catalyzed Conjugate Additions: Direct NMR Detection of an Ethyl Group Attached to a Binuclear Phosphoramidite Copper Complex”**



This project was performed in close collaboration with Felicitas von Rekowski. NMR spectroscopic investigations of ZnEt_2 were performed by Felicitas von Rekowski and those of ZnPh_2 by Katrin Schober.

*Felicitas von Rekowski, Carina Koch and Ruth M. Gschwind
J. Am. Chem. Soc. **2014**, *136*, 11389-11395.

DOI: 10.1021/ja504577t

Reproduced with permission from *J. Am. Chem. Soc.* **2014**, *136*, 11389-11395.
© 2014 American Chemical Society.

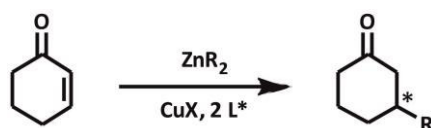
3.1 Abstract

Copper-catalyzed asymmetric conjugate addition reactions are a very powerful and widely applied method for the enantioselective carbon-carbon bond formation. However, the structural and mechanistic insight into these famous reactions has been very limited so far. In this article, the first direct experimental detection of transmetalation intermediates in copper-catalyzed reactions is presented. Special combinations of ^1H , ^{31}P HMBC spectra allow for the identification of complexes with chemical bonds between the alkyl groups and the copper complexes. For the structural characterization of these transmetalation intermediates, a special approach is applied, in which samples using enantiopure ligands are compared with others using enantiomeric mixtures of ligands. It is experimentally proven, for the first time, that the dimeric copper complex structure is retained upon transmetalation, providing an intermediate with mixed trigonal/tetrahedral coordination on the copper atoms. In addition, monomeric intermediates with one ligand, but no intermediates with two ligands, are detected. These experimental results in combination with the well-known optimal ligand-to-copper ratio of 2:1 in synthetic applications, allow us to propose that a binuclear transmetalation intermediate is the reactive species in copper-catalyzed asymmetric conjugate addition reactions. This first direct experimental insight into the structure of the transmetalation intermediate is expected to support the mechanistic and theoretical understanding of this important class of reactions and to enable their further synthetic development. In addition, the special NMR approach presented here for the identification and characterization of intermediates below to the detection limit of ^1H spectra can be applied also to other classes of catalyzes.

3.2 Manuscript

3.2.1 Introduction

The copper-catalyzed asymmetric conjugate addition (ACA) reaction is one of the most powerful methods for enantioselective carbon-carbon bond formation in organic synthesis (Scheme 3.1), which often combines excellent regio- and stereoselectivities, high compatibility with many functional groups, and low costs of the copper salts (for recent reviews, see [1–4]). In this active research area, recent efforts considerably enlarged the scope of substrates and nucleophiles, which allowing numerous syntheses of complex chiral organic compounds, including, e.g., biologically active and natural compounds.^[1–7] However, despite the great synthetic success of the ACA reaction, structural and mechanistic studies focused on the copper complexes and their reaction intermediates are very rare. Therefore, more structural information about the reaction intermediates and the enantiodiscriminating steps were claimed to be an essential prerequisite for the further development of this important class of reactions.^[1,4,8]



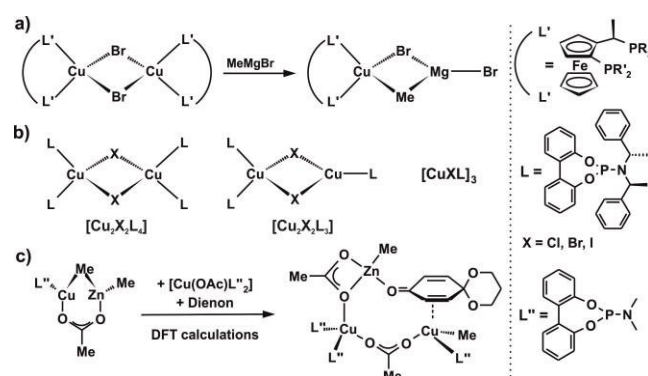
Scheme 3.1: General reaction scheme for ACA reactions.

To our knowledge, the only in-depth experimental study of transmetalation intermediates in copper-mediated ACA reactions known so far was done by Feringa *et al.* using a combination of copper complexes with chiral bidentate ferrocenyl-based diphosphine ligands and Grignard reagents.^[9] In that brilliant study, a binuclear, halide-bridged diphosphine copper complex was reported as a precatalyst based on e.g., on the basis of ^{31}P NMR spectroscopic, electrochemical and kinetic investigations (Scheme 3.2a). After performing several sophisticated indirect experimental studies, Feringa reasoned that the dimeric copper precatalyst breaks up via transmetalation with the Grignard reagent and forms a bimetallic complex, which is mononuclear in copper (Scheme 3.2a).^[9] This mixed metallic composition of the complex proposed by Feringa agrees perfectly with the core element of the famous intermetallic Knochel cuprates, e.g., $\text{FGRCu}(\text{CN})\text{ZnI}$.^[10]

In our NMR studies of copper complexes with monodentate phosphoramidite ligands, similar binuclear copper complexes were found as basic structural motif of the thermodynamic ground state of precatalysts with highly stereoselective ligands.^[11–13]

However, in solution, a binuclear copper complex with mixed trigonal/tetrahedral stereochemistry (see $[\text{Cu}_2\text{X}_2\text{L}_3]$ in Scheme 3.2b) was identified as the main species. At temperatures below 200 K, self-aggregation of the phosphoramidite ligands starts,^[14] and intermolecular interactions between free ligand and $[\text{Cu}_2\text{X}_2\text{L}_3]$ induce the formation of the binuclear complex $[\text{Cu}_2\text{X}_2\text{L}_4]$, corroborating the known crystal structures.^[9,15] Recently, a density functional theory (DFT) study of the reaction mechanism of ACA reactions with monodentate phosphoramidite ligands corroborated both studies.^[16] Monomeric zinc cuprates were identified as the lowest energy transmetalation complexes accessible from simplified phosphoramidite ligands, $\text{Cu}(\text{OAc})$ and ZnMe_2 , (Scheme 3.2c left).ⁱ

However, starting from this monomeric zinc cuprate, reasonable energetic pathways were accessible only for π -complexes derived from the binuclear structure with mixed trigonal/tetrahedral stereochemistry (Scheme 3.2c right).^[16]



Scheme 3.2: Proposed structures of precatalysts and transmetalation intermediates: a) Monomerization and formation of a bimetallic transmetalation complex upon addition of MeMgBr ,^[9] b) Interconversion/coexistence of phosphoramidite copper complexes $[\text{Cu}_2\text{X}_2\text{L}_4]$, $[\text{Cu}_2\text{X}_2\text{L}_3]$, and $[\text{CuXL}]_3$ with $[\text{Cu}_2\text{X}_2\text{L}_3]$ as proposed precatalyst of the ACA reaction,^[11] c) Monomeric in Cu, but bimetallic transmetalation intermediate and a π -complex, which essentially agrees with $[\text{Cu}_2\text{X}_2\text{L}_3]$ calculated theoretically.^[16]

The transmetalation of an organic moiety from ZnR_2 , RMgX , or AlR_3 reagents is a commonly accepted step in mechanistic schemes of ACA reactions.^[1,3,4,8] However, to the best of our knowledge, a direct experimental detection of a transmetalated intermediate has been elusive so far, and no information about the structure or even the stoichiometry of transmetalation complexes with ZnR_2 or AlR_3 is available.^[1,4]

Therefore, we present in this paper an NMR spectroscopic investigation of the transmetalation reaction between phosphoramidite copper precatalyst $[\text{Cu}_2\text{X}_2\text{L}_3]$ and

ⁱ The change from the monodentate Br to the bidentate OAc is in accordance with the by-one-reduced number of ligands in the transmetalation complex.

diethylzinc. For the first time, direct experimental evidence of a transmetalation intermediate in the ACA reaction is presented. In addition, for the first time, a transmetalation complex that is binuclear in copper is detected, which essentially retains the structure of the precatalytic complex $[\text{Cu}_2\text{X}_2\text{L}_3]$. Apart from this binuclear transmetalation complex, also several mononuclear copper transmetalation complexes were detected.

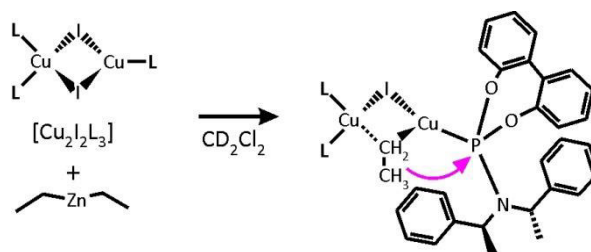
3.2.2 Results and Discussion

For the NMR spectroscopic investigation of transmetalated phosphoramidite copper complexes, a 2:1 ratio of the highly enantioselective phosphoramidite ligand **L** and CuI in CD_2Cl_2 was chosen (see Scheme 3.3). Previous investigations^[11] and low temperature studies^[12] showed that this model system reveals the best ^{31}P chemical shift dispersion at 180 K and the broadest temperature range for the exclusive existence of $[\text{Cu}_2\text{X}_2\text{L}_3]$. Furthermore, in CD_2Cl_2 , narrow line widths were observed for the complex species.^[13] From the variety of organometallic reagents, ZnEt_2 as well as ZnMe_2 and ZnPh_2 were selected to cover a broader spectrum of transmetalation reagents. ZnEt_2 is broadly used in synthetic applications, providing high yields and enantioselectivities.^[1] The methyl groups in ZnMe_2 should stabilize the transmetalation intermediate, due to their lower reactivity,^[17,18] and phenyl groups are assumed to be more readily transferred than alkyl groups.^[17,19–22] However, for ZnMe_2 and ZnPh_2 , only non-specific interactions with the copper complexes were detected (see the supporting information). Therefore, in the following, only investigations with ZnEt_2 are discussed.

In synthetic applications, a high excess of ZnEt_2 with regard to the copper complex is applied (60-70 eq).^[23] In order to increase the signal-to-noise ratio (S/N) and to enable the detection of upstream intermediates, here a reduced excess of ZnEt_2 is used (4-20 eq compared to $[\text{Cu}_2\text{X}_2\text{L}_3]$). With commercially available solutions of ZnEt_2 in toluene, the spectral quality was too bad to detect any transmetalation intermediates. Therefore, neat ZnEt_2 in CD_2Cl_2 was used (for spectra and details see the supporting information). Investigations in a temperature range of 170-250 K showed that both the highest signal intensities and the highest number of intermediate species were detected at 170 and 180 K. Therefore, in the following, the low-temperature spectra (170-180 K) are discussed.

After addition of ZnEt_2 to the copper complex, neither in the ^1H nor in the ^{31}P NMR spectra could any signals of transmetalated species be detected. Therefore, $^1\text{H}^{31}\text{P}$

heteronuclear multiple-bond correlation (HMBC) spectra were recorded, which allow for magnetization transfers via multibond scalar couplings ${}^nJ_{\text{H,P}}$, and additionally act as a spectroscopic filter for free ZnEt_2 .^[24] By removing the huge signals of free ZnEt_2 (up to 20 equivalents), the dynamic range of the NMR spectrometer can be increased, and so the sensitivity of the resulting ${}^1\text{H}$, ${}^{31}\text{P}$ HMBC spectra to transmetalation complexes is much higher than in classical one-dimensional (1D) ${}^1\text{H}$ or ${}^{31}\text{P}$ NMR spectra. In case of the transmetalation intermediate expected here (see Scheme 3.3 for the example of $[\text{Cu}_2\text{X}_2\text{L}_3]$), a magnetization transfer of the protons of the ethyl group via copper to the phosphorous atom of a ligand should become possible. Similar to the classical ${}^nJ_{\text{H,P}}$ scalar coupling transfers within a ligand, such a magnetization transfer across copper would then be visible as cross signal in a ${}^1\text{H}$, ${}^{31}\text{P}$ HMBC spectrum.



Scheme 3.3: Proposed transmetalation step of ZnEt_2 to $[\text{Cu}_2\text{I}_2\text{L}_3]$. In the case in which an ethyl group and a phosphoramidite ligand are both bound to one copper atom, a ${}^1\text{H}$, ${}^{31}\text{P}$ HMBC cross peak between those moieties (see purple arrow) should indicate a transmetalation intermediate.ⁱⁱ

${}^1\text{H}$ ${}^{31}\text{P}$ HMBC spectroscopy was already successfully applied in investigations of palladium-catalyzed Negishi coupling reactions.^[25] However, in contrast to the palladium complexes used in the previous study, the transfer of magnetization via copper is much more difficult.^[26] The high quadrupole moment of ${}^{63/65}\text{Cu}$ provides an efficient relaxation pathway for magnetization, leading to short relaxation times and broad line widths of the nuclei directly coordinated to the copper atom (see, e.g., the ${}^{31}\text{P}$ line width of $[\text{Cu}_2\text{I}_2\text{L}_3]$ versus **L** in the supporting information, Figure 3.4). Therefore, especially in complexes with relevant electric field gradients, i.e., with P-, N-, or S-ligands, and structures deviating from a highly symmetrical coordination, scalar couplings across copper are

ⁱⁱ For the sake of clarity, in Scheme 3.3 only one magnetization transfer possibility is shown. In principle, magnetization transfers to two chemically nonequivalent phosphorous moieties are expected in these transmetalation intermediates. However, in none of our 2D ${}^1\text{H}$, ${}^{31}\text{P}$ HMBC spectra did we detect a doubling in the ${}^{31}\text{P}$ dimension. This can have several reasons: first and easiest, chemical shift overlap in the intermediate; second, the dependence of the ${}^3J_{\text{H,P}}$ on the dihedral angles potentially different in tetrahedral or trigonal planar copper coordinations; third, the different electric field gradients of the two copper centers leading to different degrees of partial decoupling or total decoupling; and fourth, combinations of the second and the third factors. We have no chance to separate the different possibilities; furthermore, they do not affect the conclusion of the experiments. Therefore, the simplification shown in Scheme 3.3 is used.

usually not detectable.^[26] As a result, successful experimental magnetization transfers via copper have only been reported for a few examples, e.g., in ^1H , ^{13}C HMBC spectra of ^{13}C -labelled organocuprates,^[27] in ^1H , ^{31}P HMBC spectra of $\text{Me}_3\text{Cu}(\text{PPh})_2\text{Li}$,^[28] or ^{31}P , ^{31}P COSY spectra of complexes $[\text{Cu}_2\text{X}_2\text{L}_2]$ ($\text{X} = \text{Cl}, \text{Br}; \text{L} = \text{L}$).^[8,11] In the present study, the ^1H , ^{31}P HMBC pulse sequence should eliminate the signals of free ZnEt_2 (see above); thus, even extremely small amounts of intermediates can be detected. In addition, 1D versions of HMBC spectra are superior in sensitivity compared to two-dimensional (2D) versions. Therefore, first a 1D ^1H , ^{31}P HMBC pulse sequence was applied (see Figure 3.1a and for details see the supporting information).

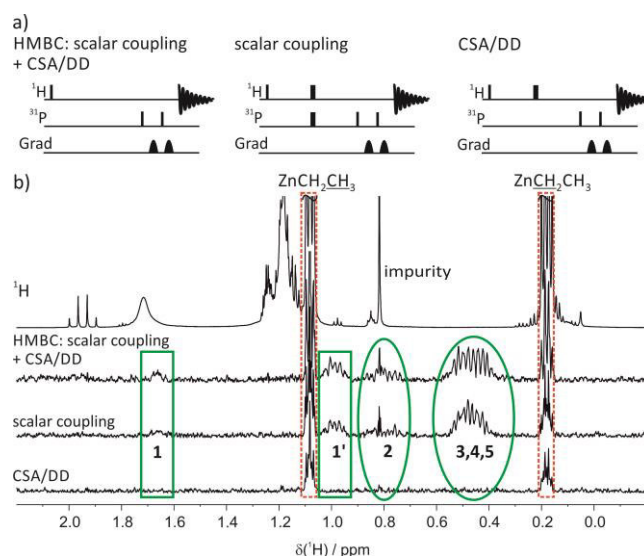


Figure 3.1: a) Pulse sequences of the 1D ^1H , ^{31}P HMBC spectra, allowing for magnetization transfers via scalar coupling and ^1H CSA/ ^{31}P DD relaxation interference (CSA/DD) as well as modified versions canceling CSA/DD or scalar coupling (for description see text, and for experimental details see the supporting information), b) Comparison of the ^1H NMR and 1D ^1H , ^{31}P HMBC spectra of 2 eq $\text{L}^{(\text{SS})}$, 1 eq CuI and 7 eq ZnEt_2 at 230 K in CD_2Cl_2 . Green ellipses and boxes indicate transfers via scalar couplings; red dashed boxes represent non-specific interactions.

Indeed, despite all obstacles associated with copper complexes, we were able to detect very small cross signals between ethyl groups and ^{31}P species under transmetalation conditions (see Figure 3.1b, trace two; each signal in the 1D ^1H , ^{31}P HMBC corresponds to a magnetization transfer between ^1H and ^{31}P). In these 1D ^1H , ^{31}P HMBC spectra and later also in the 2D ^1H , ^{31}P HMBC spectra (see Figure 3.2 and the supporting information), two types of signals can be observed. First signals (cross peaks) indicating the chemical shifts of free ZnEt_2 and free ligand or precatalytic complex (see red dashed boxes in Figure 3.1b). Such a retention of the chemical shift is implausible for real transmetalation intermediates^[9] and most probably caused by non-specific interactions in aggregates without specific structures. Second are new signals detectable neither in ^1H nor in ^{31}P NMR spectra, which correspond to new species (green boxes and ellipses in

Figure 3.1b). Due to the similar signal intensities of both kinds of signals, it was necessary to find a spectroscopic method to differentiate between non-specific aggregates and structurally defined intermediates providing scalar coupling transfers. Within the two-spin approach, it is well-known among NMR spectroscopists that not only scalar coupling but also relaxation interference (also called cross correlated relaxation) between ^1H chemical shift anisotropy (CSA) and ^1H – ^{31}P dipolar interactions (DD) can contribute to the polarization transfer in HMBC spectra.^[29–35] The ^1H CSA/ ^1H – ^{31}P DD relaxation interference can be manipulated by 180° pulses in a different way than scalar coupling, and as a result ^1H CSA/ ^1H – ^{31}P DD relaxation interference can be separated from polarization transfer via scalar couplings.^[33–37] This concept was already successfully applied in investigations of H-bond networks of acylguanidin complexes and flavoproteins,^[33–35] but to our knowledge it has not been applied to organometallic compounds or transition metal complexes so far. Thus, two further 1D ^1H , ^{31}P HMBC pulse sequences were measured with one or two additional 180° pulses on ^{31}P and ^1H (see Figure 3.1a and Figure 3.14 for spectroscopic details). In the spectrum with one 180° pulse, the scalar coupling transfer is eliminated; in that with two 180° pulses, the ^1H CSA/ ^1H – ^{31}P DD relaxation interference is canceled.ⁱⁱⁱ

Figure 3.1b compares of the ^1H NMR spectrum and the three different 1D ^1H , ^{31}P HMBC spectra. Significantly, all signals without chemical shift changes in the ^1H and ^{31}P dimension show signals in all three types of HMBC spectra (see red dashed boxes in Figure 3.1b, and for further examples the supporting information), indicating non-specific aggregates. In contrast, all signals with chemical shift changes show high contributions of scalar coupling transfers and small or no signals originating from ^1H CSA/ ^1H – ^{31}P DD relaxation interference (see green boxes and ellipses in Figure 3.1b), which is typical for complexes or structures with well-defined chemical bonds allowing for scalar coupling transfers. This correlation of chemical shift changes and transfer pathways show that, also for transition metal complexes and organometallic substances,

ⁱⁱⁱ In two-spin systems, a clear separation between scalar coupling and CSA/DD relaxation interference is possible by the described method. In three-spin systems (e.g., scalar coupled diastereotopic CH_2 and ^{31}P as in our system), a separation between scalar coupling and ^1H , ^1H DD/ ^1H , ^{31}P DD relaxation interference is not possible with the HMBC versions shown in Figure 3.1a. With the given transfer delay of 14.3 ms in principle small contributions of ^1H , ^1H DD/ ^1H , ^{31}P DD relaxation interference cannot be excluded (*J. Chem. Phys.* **1993**, 98, 6062). However, more complicated pulse sequences are required to separate further ^1H , ^1H DD/ ^1H , ^{31}P DD relaxation interference in three-spin systems from scalar coupling (*J. Magn. Reson. A* **1996**, 118, 64; *J. Chem. Phys.* **1993**, 98, 6062), which are not applicable to our system, given the extremely low S/N of the HMBC peaks at optimized experimental conditions.

extremely small signals originating from well-defined intermediates can be separated from those of non-specific aggregates present in the bulk phase with this method.

Next the intermediate signals originating from EtCuL and EtZnL structural arrangements were separated. For this purpose, mixtures of ZnEt₂ and free ligand without copper salt were investigated by HMBC spectroscopy. Several samples with concentration ratios of ZnEt₂ to L between 3:1 and 8:1 showed only signal 1', with scalar coupling contributions, beside non-specific interactions (see the supporting information Figure 3.6a-d) in the 1D ¹H, ³¹P HMBC spectra. In none of the 2D ¹H, ³¹P HMBC spectra were cross signals of 1' detected (see the supporting information Figure 3.6e and Figure 3.2c and d); therefore, the structure of 1' was not further investigated. Samples with free ligand and ZnMe₂ or ZnPh₂ without copper salt showed cross peaks of RZnL moieties in ¹H, ³¹P HMBC spectra that were not detectable after addition of copper salt (see the supporting information Figure 3.7a and b and ref [38]). These experiments show that, in general, RCuL are preferentially formed relative to RZnL structural arrangements. In the case of ZnEt₂, only signal 1' represents an EtZnL or EtL species, but the other signals (signals 1-5) appear only in the presence of copper salt. Therefore, in the following, EtZnL structures are not further discussed. Signal 1 was assigned to a ligand with the ethyl group directly bound to the phosphorous atom, providing classical ³J_{H,P} scalar couplings (for details see the supporting information, section "Identification of side products in CuI samples").

Signals 2-5 (green ellipses in Figure 3.1b) show the two characteristics expected for transmetalation intermediates: scalar coupling transfer between the ethyl group and the phosphorous of the ligand, and presence only under transmetalation conditions. However, due to the extremely low S/N of these signals, the further structural characterization of these intermediates can only rely on chemical shift analyses and on combinations of ¹H, ³¹P HMBC spectra.

The signals of the transmetalation intermediates, 2-5, could be also detected in the 2D ¹H, ³¹P HMBC spectra (see Figure 3.2c and d). Their ¹H chemical shift range of 0.80-0.30 ppm is in agreement with a CH₂ group transmetalated to a neutral Cu(I) complex. CH₂ of negatively charged cuprates show upfield-shifted δ(¹H) signals (for Et₂CuLi•LiI and Et₂CuLi•LiCN, -0.53 and -0.54 ppm, respectively^[39]), whereas ethyl groups bound to Cu(III) show low-field-shifted signals (e.g., Me₃EtCuLi, 0.54 ppm;^[40] Me₂EtCuPMe₃, 1.89 ppm; Me₂EtCuP(OMe)₃, 2.07 ppm; and Me₂EtCu(PPh₃), 2.31 ppm^[41]). In the ³¹P

dimension, all four signals of the transmetalation intermediates are upfield shifted compared to those of the precatalytic copper complex by 2.9-7.4 ppm. This is in agreement with the upfield shifts observed for transmetalation intermediates of Grignard reagents and ferrocenyl-based diphosphine copper complexes (1.8 and 3.1 ppm).^[9] Thus, to our knowledge, the presented ^1H , ^{31}P HMBC data provide the first direct experimental proof for transmetalation intermediates of copper complexes. The low-field shifts of the ^1H and the upfield shifts of the ^{31}P resonances of the transmetalation intermediates relative to free ZnEt_2 and the precatalytic copper complex corroborate previous results of Bertz and Feringa.^[9,28]

Next the structure of these transmetalation intermediates was addressed. In principle, several structures of transmetalation intermediates are feasible that are either mono- or dimeric in copper and contain one, two, or three ligands (one ethyl group as well as varying amounts of ZnEt_2 or ZnEtI ; see Figure 3.2a). Using DFT calculations, simplified phosphoramidite ligands, $\text{Cu}(\text{OAc})$, and ZnMe_2 , Woodward and co-workers identified the monomeric zinc cuprate **A** as lowest energy structure for transmetalation intermediates.^[16] Furthermore, species **A** and **C** were proposed for monomeric transmetalation intermediates with Grignard reagents described by Feringa and co-workers.^[9] Monomeric transmetalation intermediates with two ligands, **D**, were proposed in several reaction mechanisms due to the typical ligand-to-copper ratio of 2:1.^[4,7,23] For the dimeric transmetalation intermediates with three ligands, the corresponding structures are **E-G**.

To address the structure under the prerequisite that exclusively ^1H , ^{31}P HMBC spectra can be used, a special approach has to be applied. In principle, information about the number of ligands can be gained by comparing ^1H , ^{31}P HMBC spectra of transmetalation intermediates with enantiopure phosphoramidite ligands (**L**) and such with the spectra of equal amounts of enantiomeric phosphoramidite ligands (50 % **L**^(SS), 50 % **L**^(RR)). Intermediates with one ligand are not affected by the use of the enantiomeric mixture of the phosphoramidite ligands, because complexes with one ligand form only enantiomers, which are not distinguishable by NMR spectroscopy (for a graphical representation, see Figure 3.2b). As a result, all complexes with one ligand appear with the same integral in both samples. In contrast, species with two or three ligands are expected to appear with reduced signal integrals of the enantiopure intermediates, because **L** is known to form both homo and hetero complexes.^[42,43]

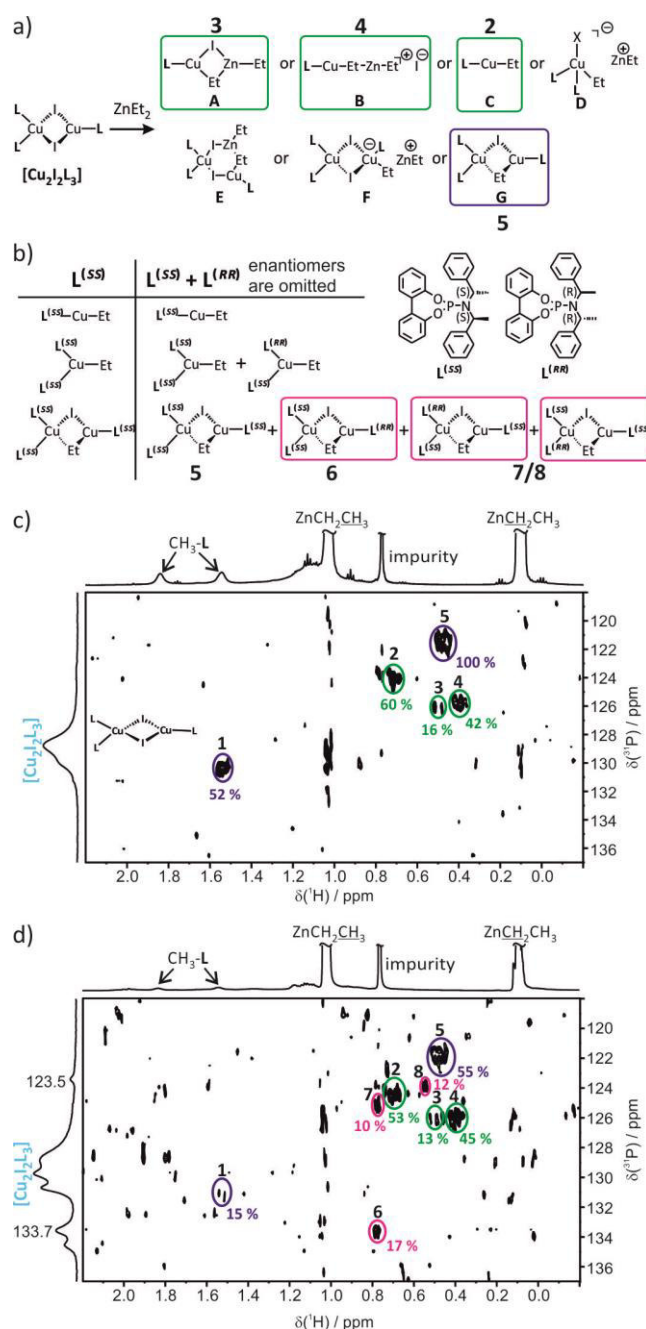


Figure 3.2: a) Possible monomeric (A–D) and dimeric (E–G) transmetalation intermediates after the addition of ZnEt_2 to the precatalyst $[\text{Cu}_2\text{I}_2\text{L}_3]$. The numbers indicate the signals ultimately assigned to these structures; b) signal distribution of the transmetalation intermediates with enantiopure ligands ($\text{L}^{(SS)}$) and an enantiomeric mixture ($\text{L}^{(SS)} + \text{L}^{(RR)}$), including signal assignment; c) section of the 2D ^1H , ^{31}P HMBC spectrum with 2 eq $\text{L}^{(SS)}$, 1 eq CuI and 14.7 eq ZnEt_2 at 170 K in CD_2Cl_2 ; d) corresponding section of the 2D ^1H , ^{31}P HMBC spectra with 1 eq $\text{L}^{(SS)}$, 1 eq $\text{L}^{(RR)}$, 1 eq CuI and 14.5 eq ZnEt_2 at 170 K in CD_2Cl_2 . The signal integrals given are referenced to signal 5 of the enantiopure sample. The integrals of signals 2–4 (green) are nearly identical in both spectra indicating monomeric complexes with one ligand. In contrast, signal 5 (blue) diminishes and signals 6–8 arise in the enantiomeric mixture (pink), indicating a complex with three ligands. For structure assignment see panels a and b and the text. (The reason for the reduction of signal 1 is explained in the supporting information, section “Identification of side products in CuI samples”).

In addition, new signals should arise due to formation of diastereomers with mixed ligand arrangements. For monomeric transmetalation intermediates with two ligands, one reduced signal and one new signal are expected; for dimeric structures with three ligands a pattern of one reduced and three new signals is expected (see Figure 3.2b).^{iv} In Figure 3.2 the 2D ^1H , ^{31}P HMBC spectra of the complexes with enantiopure ligands $\text{L}^{(SS)}$ (Figure 3.2c) and with the enantiomeric mixture of $\text{L}^{(SS)}$ and $\text{L}^{(RR)}$ (Figure 3.2d) are presented after addition of ZnEt_2 . Indeed, three classes of signals are seen in the spectrum of the enantiomeric ligand mixture. Signals 2-4 (green) show similar integrals within the experimental error. This indicates monomeric species with one ligand for complexes 2-4. In contrast, signal 5 (blue) shows around half the integral. In addition, three new signals, 6-8 (pink), appear in the enantiomeric mixture. This pattern fits exactly to a dimeric structure with three ligands (see Figure 3.2b). Furthermore, the integrals of these four intermediates 5-8 sum up to 94 %, which is strong evidence that all of these four intermediates in the enantiomeric mixture indeed originate from intermediate 5 in the enantiopure sample (see also discussion above). The integral distribution of signals 5-8 shows that the diastereomers have energetically deviating interligand interactions, because the assumption of identical interligand interactions for $\text{L}^{(SS)}\text{L}^{(SS)}$ and $\text{L}^{(SS)}\text{L}^{(RR)}$ would lead to a statistical distribution of 25 % for all four diastereomers (for details, see the supporting information). This is in agreement with previous and ongoing investigations of non-covalent interligand interactions in phosphoramidite palladium and copper complexes, which show distinct preferences for special ligand combinations^[42–44] and quite pronounced interligand interactions.^[14,42–44] Such significant interaction preferences directly lead to non-statistical distributions as observed here. Signal 5, appearing over statistically at 55 %, indicates a preference for interactions between enantiopure ligands (see Figure 3.2d). This is also visible on a lower level in the integrals of signals 6-8, at 17 %, 12 % and 10 %, showing lower values for mixed ligand arrangements at the copper fragment with two ligands (see Figure 3.2b).

^{iv} At first glance, the approach to integrate magnitude calculated HMBC spectra to gain information about the amount of species in solution seems quite strange, because within one molecule the HMBC cross peaks are only modulated by the size of the $^nJ_{\text{H,P}}$. Here, the approach is different. By using enantiomeric mixtures of ligands the structures of the enantiopure complexes (represented by the cross signals using only one enantiopure ligand; see Figure 3.2c) are not affected. As a result the size of the $^nJ_{\text{H,P}}$ scalar couplings remain constant within enantiomeric complexes and changes in the integral indicate variations in the amount. In diastereomeric complexes (see below) the different structural orientations can induce deviating $^nJ_{\text{H,P}}$ scalar couplings. As a result the sum of integrals of these diastereomers can deviate from 100 %.

To sum up, signals 2-4 are assigned to monomeric species with one ligand. The signal and integral pattern of signals 5-8 indicate a dimeric transmetalation intermediate with three ligands, i.e., experimental evidence for the retention of the binuclear complex structure upon transmetalation with mixed trigonal/tetrahedral coordination on the copper atoms. Monomeric intermediates with two ligands are not detected.

Next the structures of the transmetalation intermediates 2–8 were refined to assign the intermediates 2–8 to the structures **A–C** and **E–G** (see Figure 3.2a and b). Since a selective chelation of zinc versus copper is very difficult, the involvement of ZnI units was addressed by varying the amount of ZnI₂. For this purpose, 12 eq of ZnI₂ was added to a sample of 2 eq **L**^(SS), 1 eq CuI and 7.7 eq ZnEt₂ (for spectra see the supporting information). The Schlenk equilibria of ZnEt₂ and ZnI₂ is known to lie well to the side of ZnEtI.^[45] Thus, only signals of the complexes with ZnI moieties should become stronger, whereas those of the complexes without ZnI moieties should decrease.^v In the resulting ¹H, ³¹P HMBC spectrum, only signal 3 of a monomeric complex remained. Thus, signal 3 represents the only structure with a ZnI unit directly incorporated in the complex, and was assigned to the monomeric species **A**. Signals 2 and 4 are also associated with monomeric species (see above) but without ZnI units. They show significant differences in their proton chemical shifts, as expected for species with a ZnEt unit (upfield shift of the CH₂ group) and without. Therefore, signal 4 is assigned to **B** and signal 2 to **C**. The addition of ZnI₂ also shows that no ZnI moiety is incorporated in the complex of signal 5, which excludes structure **E**. The involvement of a halogen bridge was proven by further investigations with CuCl as copper salt. For CuI and CuCl, no identical signals of transmetalation intermediates were observed in the 2D ¹H, ³¹P HMBC spectra (for details see the supporting information). This indicated the existence of a halogen bridge in the dimeric transmetalation complex. In addition, samples with CuCl and high amounts of ZnEt₂ showed cuprate-like structures with distinct upfield-shifted signals (for details see the supporting information). This pronounced chemical shift difference excludes two ethyl groups bound to one copper atom in the transmetalation intermediates discussed here. The remaining differentiation between structures **F** and **G** for signal 5 can be solved by the trends of the transmetalation intermediates dependent on the equivalents of ZnEt₂ added (see Figure 3.3). Analysis of the monomeric transmetalation intermediates with one ligand shows that **A** and **B**, containing ZnEt units, are preferentially formed at lower

^v This trend was corroborated by the addition of high amounts of ZnEt₂, enhancing the complementary signals without ZnI moieties (see Figure 3.3).

amounts of ZnEt_2 , whereas the “final” transmetalation intermediate **C**, without a ZnEtI unit, accumulates at higher amounts of ZnEt_2 . Due to the fact that in this investigation we used a significantly reduced excess of ZnEt_2 compared to synthetic application (see above), in synthesis the preference of **C** is expected to be even more pronounced. Assuming similar trends for the formation of dimeric transmetalation intermediates, as indicated by similar intensity trends of signals 2 and 5, signal 5 can be assigned to the “final” transmetalation intermediate **G**, without ZnEt unit. Considering the results described above, further structural characteristics of **G** one ethyl and one iodine bridge and retention of the mixed trigonal/tetrahedral coordination on the copper atoms. This structural assignment is corroborated by the number (three) of the newly appearing signals 6–8 in the enantiomeric mixture as well as by their integral pattern, representing the three possible diastereomers of **G** with mixed ligand arrangements and indicating a preference for homoligand interactions.

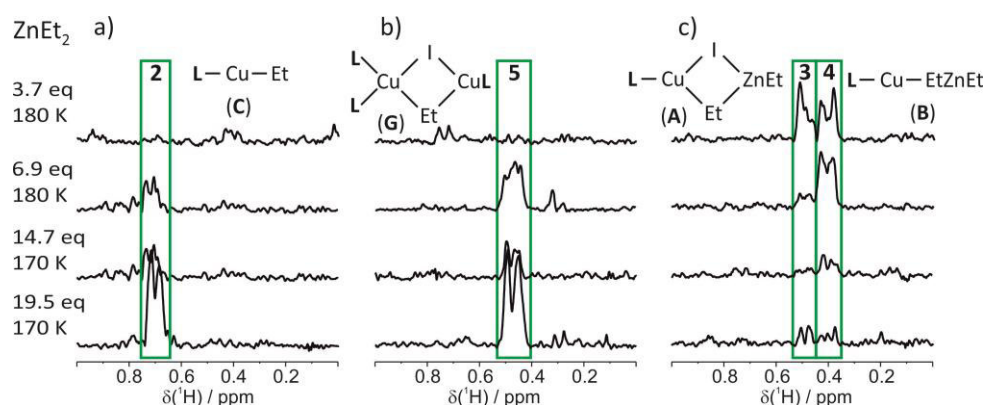


Figure 3.3: Formation trends of transmetalation intermediates with 2 eq of **L**, 1 eq CuI , and an increasing excess of ZnEt_2 (typical synthetic conditions about 60 eq ZnEt_2) at 170 and 180 K in CD_2Cl_2 . The 1D rows are taken from the 2D ^1H , ^{31}P HMBC spectra at the ^{31}P chemical shifts of the respective intermediates, reveal intermediates 3 and 4 as precursors, and 2 and 5 as final intermediates.

The existence of monomeric transmetalation intermediates with one ligand coordinated to copper is in agreement with the results of Feringa and co-workers, who found exclusively monomeric transmetalation intermediates with one ligand with Grignard reagents.^[9] The structures proposed in this study are similar to **A** and **C** observed here. Monomeric intermediates with CuL_2 fragments, as often proposed in reaction mechanisms, were not detected in our study nor previously by Feringa. Furthermore, here for the first time, a transmetalation intermediate with a binuclear structure with mixed trigonal/tetrahedral coordination on the copper atoms is experimentally detected, which provides both an open coordination place for the enone

and plenty of ligand interactions for high stereoselectivities (see studies on palladium phosphoramidite complexes for interaction schemes of phosphoramidite ligands).^[42,43] Now, the question remains whether the monomeric **C** or the binuclear **G** is the reactive transmetalation intermediate, since both are detected in similar amounts. So far, there is no direct experimental proof, but there are strong indirect arguments. The most substantial argument for the binuclear complex **G** as reactive species is the well-known ligand-to-copper ratio of 2:1 in synthetic applications. At ligand-to-copper ratios of 2:1, stabilizing optimally the binuclear complex with the mixed trigonal/tetrahedral coordination on copper,^[12] highly enantioselective reactions can be performed.^[1,8,23] At ligand-to-copper ratios of 1:1, stabilizing optimally the monomeric complex **C** with only one ligand, considerably reduced enantioselectivities are obtained. Considering **G** as reactive species, at first glance the high enantioselectivities in the presence of nearly equal amounts of **G** and **C** are puzzling. At this point, Woodward's DFT calculations give an explanation, because in that theoretical study, starting from monomeric transmetalation intermediates only, suitable energetic pathways were found for dimeric copper complexes with mixed trigonal/tetrahedral coordination.^[16]

3.2.3 Conclusion

In summary, the first direct experimental detection of transmetalation intermediates in asymmetric copper-catalyzed addition reactions is presented, using phosphoramidite copper complexes $[\text{Cu}_2\text{X}_2\text{L}_3]$ and an excess of ZnEt_2 . The transmetalation intermediates, which are below the detection limit in one-dimensional ^1H and ^{31}P spectra, were identified by using a special set of 1D $^1\text{H}, ^{31}\text{P}$ HMBC spectra separating complexes with ethyl groups chemically bound from those with non-specific interactions. For the structure characterization, again a special approach was applied using samples with enantiopure ligands and samples with mixtures of enantiomeric ligands. This and experiments with CuCl , ZnI_2 , and varying amounts of ZnEt_2 revealed two main transmetalation intermediates: one with one ethyl group and one ligand as well as, for the first time, a binuclear intermediate with three ligands, one ethyl group and a mixed trigonal/tetrahedral coordination on the copper atoms. Intermediates with two ligands were not observed. The well-known optimal ligand-to-copper ratio of 2:1, in combination with theoretical calculations proposing feasible reaction pathways only for binuclear complexes, and the experimental study presented here reveal retention of the binuclear copper complex with mixed trigonal/tetrahedral coordination in the reactive transmetalation intermediate. This first direct experimental insight into the structure of transmetalation intermediates is expected to aid the mechanistic understanding and the further synthetic development of the copper-catalyzed asymmetric conjugate addition reaction and related methods. In addition, the special NMR approach presented here to identify and characterize the structure of reaction intermediates below the detection limit of ^1H and ^{31}P spectra can be also applied to other catalytic system.

3.3 Supporting Information

3.3.1 Additional NMR Spectra and Information

Solvent influence on the spectra quality

The solvent used for the solution of ZnEt_2 has a big influence on the spectral resolution. In the ^1H NMR spectra of ZnEt_2 dissolved in different solvents, and the associated complex spectra it becomes obvious that spectral resolution is explicitly better, if no further solvent is present than the deuterated one (here CD_2Cl_2 , data not shown). All in all the spectra are slightly shifted, depending on the used solvent, while the shift of free ZnEt_2 in CD_2Cl_2 is not as big as in the toluene solution, which is based on shielding effects of the solvents. Furthermore the commercially acquired solution contains more impurities, as the freshly prepared one. A more substantial influence is observed in the 2D ^1H , ^{31}P HMBC spectra. In a sample with about commercially available 10 eq ZnEt_2 (toluene) solution (Figure Figure 3.4) it is not possible to detect any cross signals of transmetalation intermediates, in contrast in a sample with 6.5 eq ZnEt_2 in pure CD_2Cl_2 (Figure 3.6) detection of cross signals for transmetalated ethyl groups (red box) is possible.

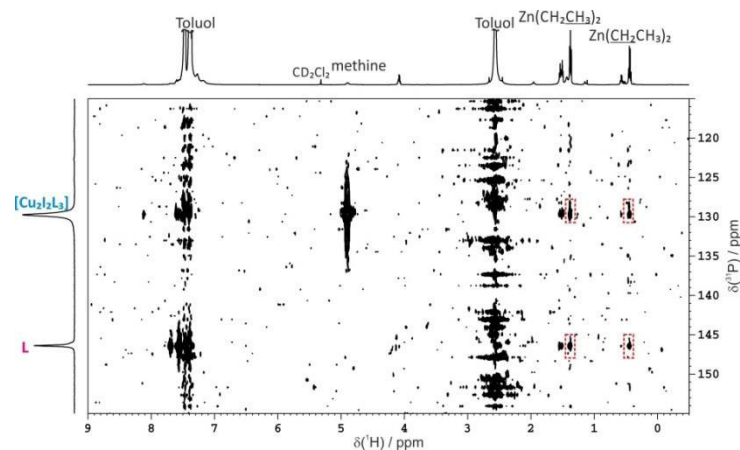


Figure 3.4: 2D ^1H , ^{31}P HMBC spectrum of 2 eq $\text{L}^{(SS)}$, 1 eq CuI and 10 eq ZnEt_2 (1M in toluene) at 230 K in CD_2Cl_2 . The red dashed boxes represent non-specific interactions between ZnEt_2 and $[\text{Cu}_2\text{I}_2\text{L}_3]$ or free ligand, respectively.

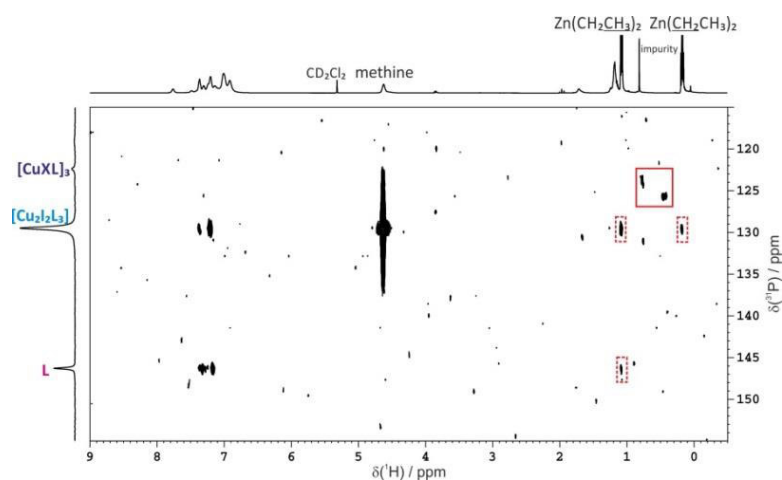


Figure 3.5: 2D ^1H , ^{31}P HMBC spectra of a sample with 2 eq $\text{L}^{(\text{SS})}$ and 1 eq CuI with 6.5 eq ZnEt_2 (circa 2M in CD_2Cl_2) at 230 K in CD_2Cl_2 . The red boxes represent new appearing signals for transmetalation intermediates, whereas the red dashed boxes represent non-specific interactions between ZnEt_2 and $[\text{Cu}_2\text{I}_2\text{L}_3]$ or L .

The red dashed boxes represent non-specific interactions. The assignment as non-specific interactions is based on further investigations using ZnMe_2 as organometallic reagent. Therefore ZnMe_2 was used as commercially available 2M solution in toluene. In the 1D ^1H , ^{31}P HMBC spectra (Figure 3.4a and c) for the differentiation of magnetization transfer, either via scalar coupling or via cross correlation (combination of chemical shift anisotropy and dipolar interaction) in both spectra a signal occurs at the chemical shifts of residual toluene (7.24, 7.15 and 2.34 ppm) therefore no clear identification of the transfer pathway is possible. Such a signal without clear assignment to one transfer pathway also occurs at -0.59 ppm, the chemical shift value of free ZnMe_2 . We assume that signals occurring in spectra for both magnetization transfer pathways belong to non-specific interactions, based on strong π,π - or CH,π -interactions. From investigations with ZnEt_2 we knew, that a distinct amount of ZnEt_2 is needed before such interactions occur. In contrast for ZnMe_2 these interactions already occur with one equivalent. We assume that these non-specific interactions have no influence on the reaction, as the species remain (obvious by no changes in the chemical shift values).

Interactions between $\text{L}^{(\text{SS})}$ and ZnR_2

To identify intermediate signals occurring from RZnL species samples of $\text{L}^{(\text{SS})}$ and ZnR_2 ($\text{R} = \text{Me}, \text{Et}, \text{Ph}$) reagents were prepared without copper salt, in order to differentiate them from RCuL species they were also investigated by ^1H , ^{31}P HMBC spectra. In none of the spectra comparable signals to the transmetalation intermediates were detected. RZnL species detected with ZnMe_2 (see Figure 3.7) and ZnPh_2 ^[38] are

vanishing after addition of copper iodide. Whereas, with ZnEt_2 , only an EtZnL or EtL species $1'$ was observed. Therefore these species are not expected to be formed in the considered reaction.

With ZnEt_2 signal $1'$ is observed at 0.95 ppm with scalar coupling contributions (see light green box in Figure 3.6a-d), which is not observed in the corresponding 2D $^1\text{H}, ^{31}\text{P}$ HMBC spectra (see Figure 3.6e), but also in the 1D $^1\text{H}, ^{31}\text{P}$ HMBC spectra of a copper containing sample (see Figure 3.1). Therefore species $1'$ can be assigned to an EtZnL and EtL species, respectively. The red dashed boxes highlight non-specific interactions.

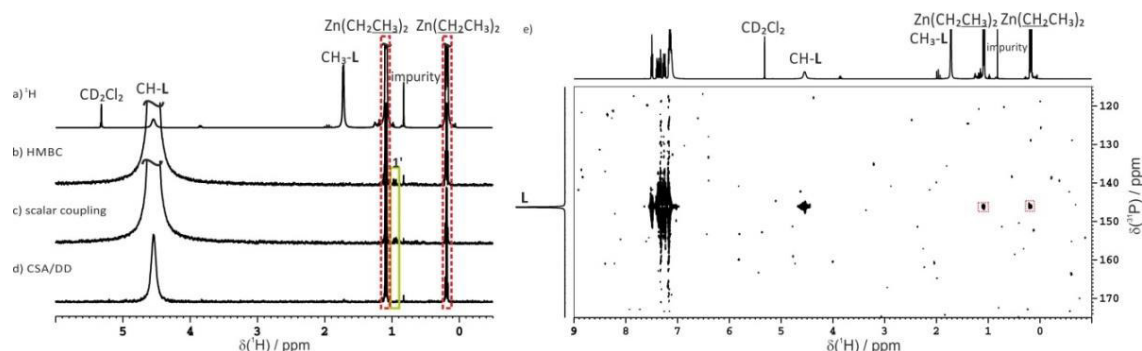


Figure 3.6: Comparison of the ^1H NMR spectrum (a) and the 1D $^1\text{H}, ^{31}\text{P}$ HMBC spectra with both pathways (b), scalar coupling (c) and CSA/DD (d) of 1 eq $\text{L}^{(\text{SS})}$ and 2.3 eq ZnEt_2 at 230 K in CD_2Cl_2 and the corresponding 2D $^1\text{H}, ^{31}\text{P}$ HMBC spectra (e).

Also investigations with ZnMe_2 and free ligand showed that some MeZnL species appear in the region of 1.0-2.0 ppm (see purple box in Figure 3.7a and b) in both the 1D and 2D $^1\text{H}, ^{31}\text{P}$ HMBC spectra, showing scalar coupling contributions. These signals disappear after the addition of CuI (see Figure 3.7c and d). This reversibility shows that the formation of such MeZnL species is not preferred in the presence of copper salts and therefore RZnL species are not discussed further.

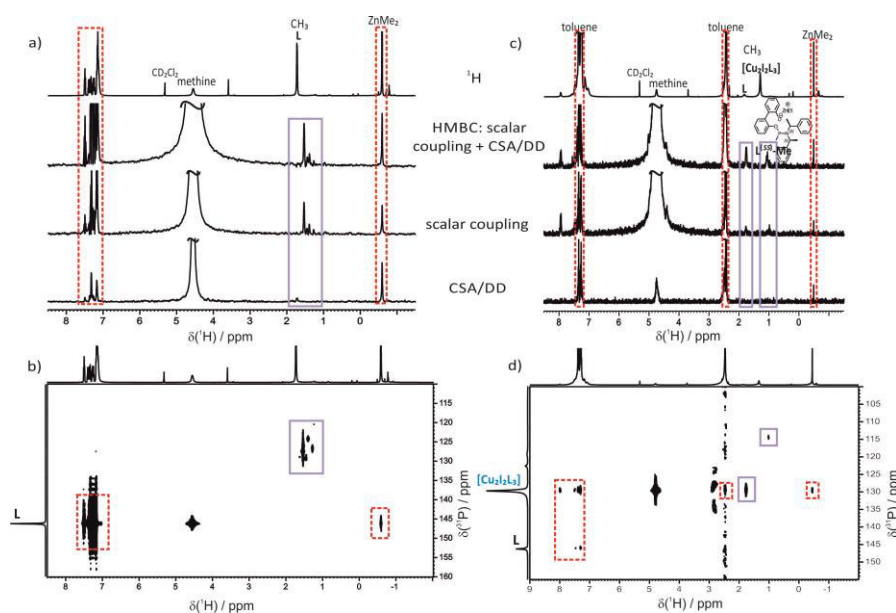


Figure 3.7: 1D and 2D ^1H , ^{31}P HMBC spectra of 1 eq $\text{L}^{(S,S)}$ and 1 eq ZnMe_2 without (a, b) and with (c, d) 2 eq CuI in CD_2Cl_2 at 230 K.

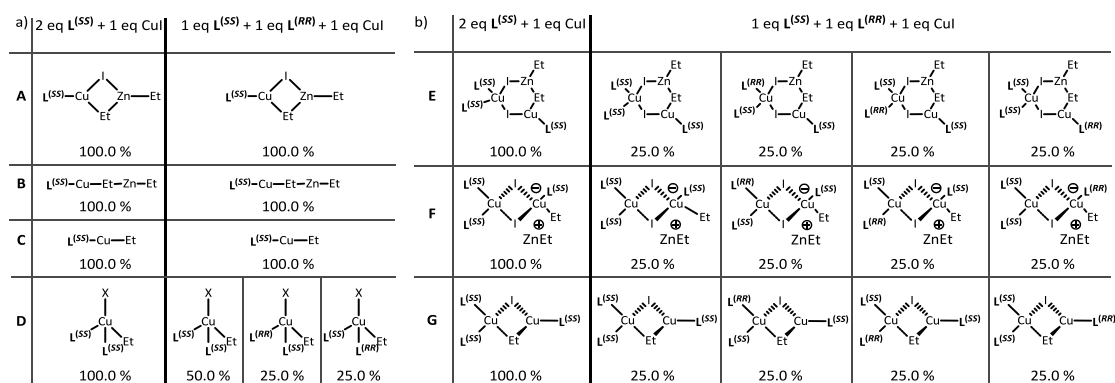
Nevertheless, the 1D and 2D ^1H , ^{31}P HMBC spectra with CuI show also signals in the region of 1.0-2.0 ppm apart from non-specific interactions (red dashed boxes). The two signals at 1.76 and 1.06 ppm (light purple boxes in Figure 3.7c and d) show scalar coupling contributions. The first one corresponds to the methyl group in the amine side chain of the free ligand, while the latter was identified as a ligand side product, in which one half of the biphenol backbone is cleaved and a methyl group is directly bound to the phosphorous atom. The assignment of the signal at 1.06 ppm to $\text{L}^{(SS)}\text{-Me}$ was made by some further experiments and literature known values. The evidence for a scalar coupling is supplied in the 1D ^1H , ^{31}P HMBC spectra, so the methyl group is directly bound to the phosphorous atom with a phosphorous chemical shift of 114.4 ppm. The ^1H chemical shift value of PMe_3 lies with 0.97 ppm in a comparable ppm range. For a ligand with a completely cleaved biphenol backbone and two methyl groups bound to the phosphorous atom the literature known ppm values are 13 ppm and 43 ppm, respectively, if the phosphorous atom is oxidized, and can therefore be excluded.^[46] Further experiments with P(Ph)_3 as representative reagent showed after the addition of ZnMe_2 several species with ^1H chemical shifts in the region of 1.0-2.0 ppm and ^{31}P chemical shifts in the region of 110.0-95.0 ppm (means $\Delta\delta(^{31}\text{P}) = (-16)-(-31)$ ppm) of the initial value, that matches to the values of $\text{L}^{(SS)}\text{-Me}$ in comparison to $\text{L}^{(SS)}$. As no comparable signals are received with PPh_3 we can conclude that an oxygen atom must still be bound to the phosphorous atom (data not shown; for detailed information of this investigation see the

additional findings). As described above, in experiments with $\mathbf{L}^{(SS)}$ and ZnMe_2 without CuI this signals are not detected, but several signals with a comparable shift deviation are observed (see Figure 3.7a and b). In sum the observed signal at a ^1H chemical shift of 1.06 ppm and a ^{31}P chemical shift of 114.4 ppm belongs to a ligand $\mathbf{L}^{(SS)}\text{-Me}$ which is incorporated to a copper complex, has one P-O-bond of the biphenol backbone cleaved and a methyl group directly bound the phosphorous atom (as drawn in Figure 3.7c).

The results with ZnMe_2 enabling a transfer of the structural assignment to spectra with ZnEt_2 . Signal 1 was proposed to correspond to the methyl group of $\mathbf{L}^{(SS)}\text{-Et}$ (see Scheme 3.5), as the $^3J_{\text{H,P}}$ coupling is stronger than the $^2J_{\text{H,P}}$ coupling, hence the latter is not observed. Furthermore the ligand must be incorporated into a complex as the signal does not arise in spectra with $\mathbf{L}^{(SS)}$ and ZnEt_2 (see Figure 3.6) and the signal intensity decreases in these spectra if an enantiomeric mixture of the ligands is used (see Figure 3.2).

Additional findings with CuI as copper salt

Possible ligand distribution in the proposed transmetalation intermediates. The special approach of using enantiopure and enantiomeric mixtures of the phosphoramidite ligands for complex formation was used in order to differentiate between species with different numbers of ligands coordinated. Scheme 3.4 represents the possible diastereomers accessible with the enantiomeric mixture and the statistical ligand distribution of the species for monomeric (**A–D**) and dimeric (**E–G**) structures. Therefore species with one ligand coordinated to the copper atom, are not affected and appear with the same integral. In contrast for species with two or three ligands, diastereomeric structures with mixed ligand arrangement are possible and therefore the signal integral is reduced. A differentiation thereby is only possible by new appearing signals in the enantiomeric mixture. For dimeric species **D** one or two new signals appear, while for the dimeric species **E–G** three new signals are expected, each with 25 % probability. The coordination of more than three ligands in the dimeric transmetalation intermediate would induce a more sophisticated signal pattern, but was not detected and therefore not taken into further account.



Scheme 3.4: Possible diastereomeric structures and statistical structure distribution in % given below each structure for the enantiopure and enantiomeric mixture of phosphoramidite ligand for complex formation for a) monomeric (A–D, charge is omitted for structures B and D) and b) dimeric (E–G) transmetalation intermediates.

Addition of ZnI_2 . In order to determine if a zinc iodine unit is part of the structure of the transmetalation species a ZnI_2 solution in CD_2Cl_2 was added (12 eq) to a sample of 2 eq $L^{(SS)}$, 1 eq CuI and 7.7 eq $ZnEt_2$ in order to force the equilibrium towards incorporation of zinc iodine units. Signal 3 is the only remaining signal after addition, therefore we assume that signal 3 is the only structure with a zinc iodine unit incorporated and was assigned to species **A**. All other signals disappeared with additional ZnI_2 and therefore we can assume that those species have no zinc iodine unit incorporated.

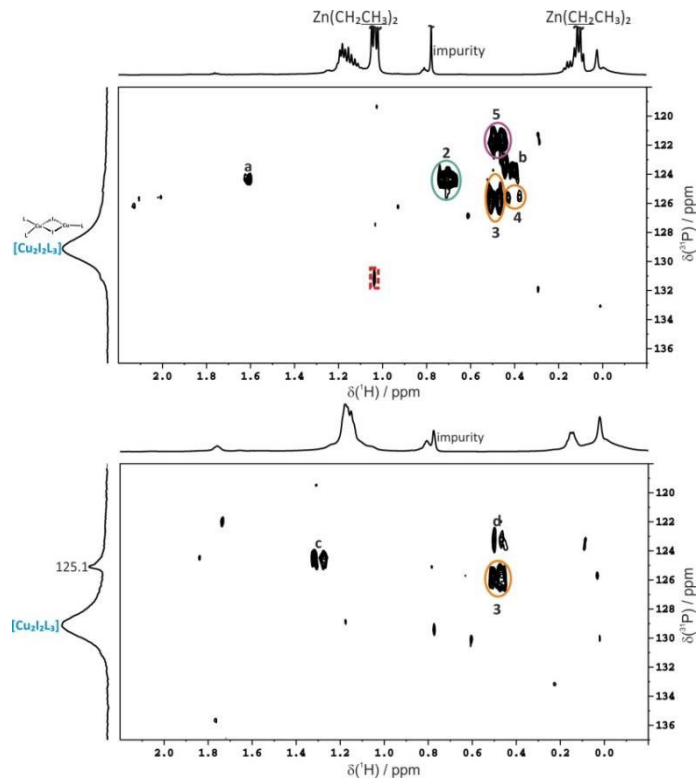
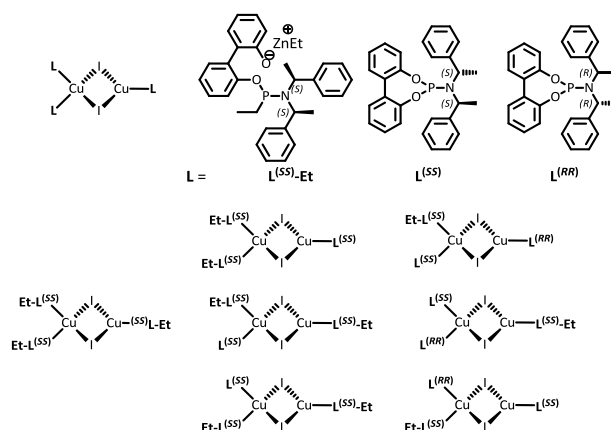


Figure 3.8: 2D 1H , ^{31}P HMBC spectra of 2 eq $L^{(SS)}$, 1 eq CuI and 7.7 eq $ZnEt_2$ before (top) and after (below) addition of 12 eq ZnI_2 solution (in CD_2Cl_2) at 180 K in CD_2Cl_2 . After addition of the zinc salt solution only signal 3 remains and two new signals c and d appear.

Identification of side products in CuI samples. In contrast signal 1, observed in the 2D ^1H , ^{31}P HMBC spectra of 2 eq $\text{L}^{(SS)}$, 1 eq CuI with 7 or 15 eq ZnEt_2 (see Figure 3.2), does not appear in the copper free sample. However, it was assigned to a copper complex with a ligand derivative, which has one half of the biphenol backbone opened and substituted by an ethyl group. This assignment to decomposed ligand is in analogy to the above described investigations with ZnMe_2 (see Figure 3.7). The missing of the signal in the copper free sample and the reduction of the signal integral in the enantiomeric mixture sample (see Figure 3.2) supports the assumption of complex formation with decomposed ligand $\text{L}^{(SS)}\text{-Et}$. With additional $\text{L}^{(SS)}\text{-Et}$ present in solution also mixed ligand arrangement with phosphoramidite ligands are possible, not only for $[\text{Cu}_2\text{I}_2\text{L}_3]$ but also for dimeric transmetalation intermediates **E-G**. Therefore Scheme 3.5 presents the possible ligand arrangements in $[\text{Cu}_2\text{I}_2\text{L}_3]$.



Scheme 3.5: Possible ligand arrangements for $[\text{Cu}_2\text{I}_2\text{L}_3]$ with decomposed ligand $\text{L}^{(SS)}\text{-Et}$ and the two enantiomeric forms of phosphoramidite ligand $\text{L}^{(SS)}$ and $\text{L}^{(RR)}$. These ligand arrangements are also possible for dimeric transmetalation intermediates, resulting in reduced signal integrals.

Investigation with CuCl as copper salt

To investigate the salt influence on the transmetalation intermediates investigations with CuCl were performed. This salt was chosen due to high *ee*-values and excellent conversions,^[23] furthermore the existence of complex species is tunable by the used ligand to salt ratio.^[11] Indeed several signals were observed in the 2D ^1H , ^{31}P HMBC spectra in a comparable shift range with those detected for transmetalation intermediates with CuI (see Figure 3.9 and 3.10). Furthermore it seems plausible to assume that no identical transmetalation intermediates are formed, due to the missing of identical signals for both copper salt samples.

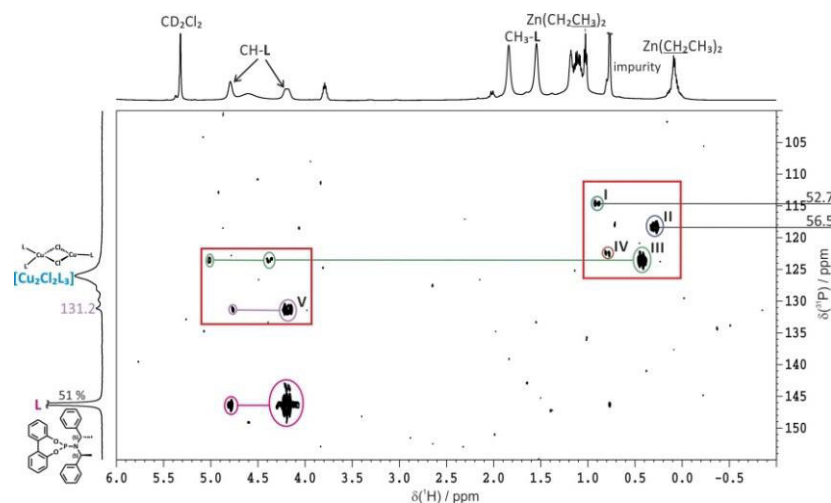


Figure 3.9: 2D ^1H , ^{31}P HMBC spectra of 2 eq $\text{L}^{(\text{SS})}$, 1 eq CuCl and 1 eq ZnEt_2 at 170 K in CD_2Cl_2 . The red boxes highlight new arising signals I-V after the addition of ZnEt_2 . The low temperature splitting of the methine signals is detected for free ligand $\text{L}^{(\text{SS})}$ (pink, 146.2 ppm), signal V (light purple, 131.2 ppm) and signal III (green, 123.5 ppm). The signals between 0.20 and 1.00 ppm are in agreement with the expected peak range of transmetalated ethyl groups.^[39–41] Signals I and II are folded back; therefore the correct phosphorous chemical shifts are indicated. The percentage in the ^{31}P NMR spectra refers to the ligand distribution in the range of 160.0 to 100.0 ppm.

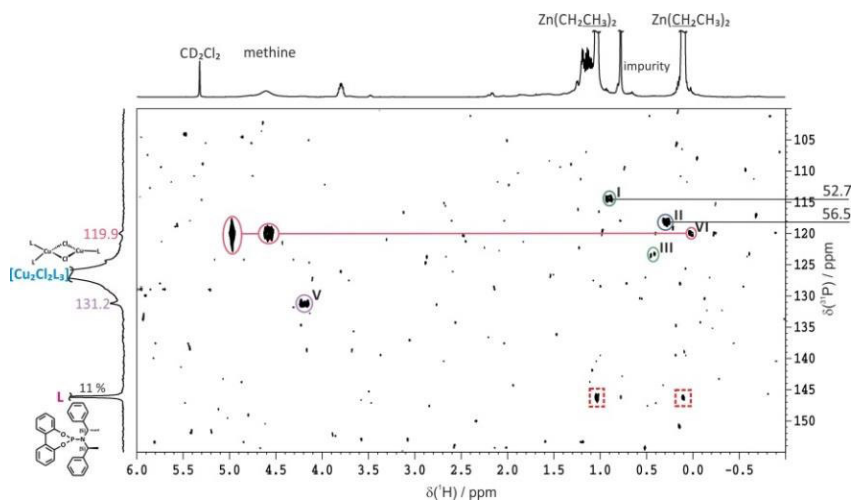


Figure 3.10: 2D ^1H , ^{31}P HMBC spectra of 2 eq $\text{L}^{(\text{SS})}$, 1 eq CuCl and 10 eq ZnEt_2 at 180 K in CD_2Cl_2 . Signals I-III and V were already detected with a smaller amount of ZnEt_2 . Signal VI arises only with the higher amount of ZnEt_2 at a phosphorous chemical shift of 119.9 ppm, where a new signal arises in the ^{31}P NMR spectrum (light rose). Furthermore for 119.9 ppm signal splitting of the methine groups is detected. Non-specific interactions occur between free ligand and ZnEt_2 (red dashed boxes). Signals I and II are folded back; therefore the correct phosphorous chemical shift is indicated. The percentage in the ^{31}P NMR refers to the ligand distribution in the range of 160.0 to 100.0 ppm.

Obviously the amount of free ligand and ZnEt_2 present in the sample has an influence on the appearance of the species. With small amounts of ZnEt_2 in combination with high amounts of free ligand signals I-V appear, while with increasing amounts of ZnEt_2 and decreasing amounts of free ligand a further signal VI appears. In the 1D ^1H , ^{31}P HMBC spectra for signals III and VI scalar coupling signals were detected (see Figure 3.11)

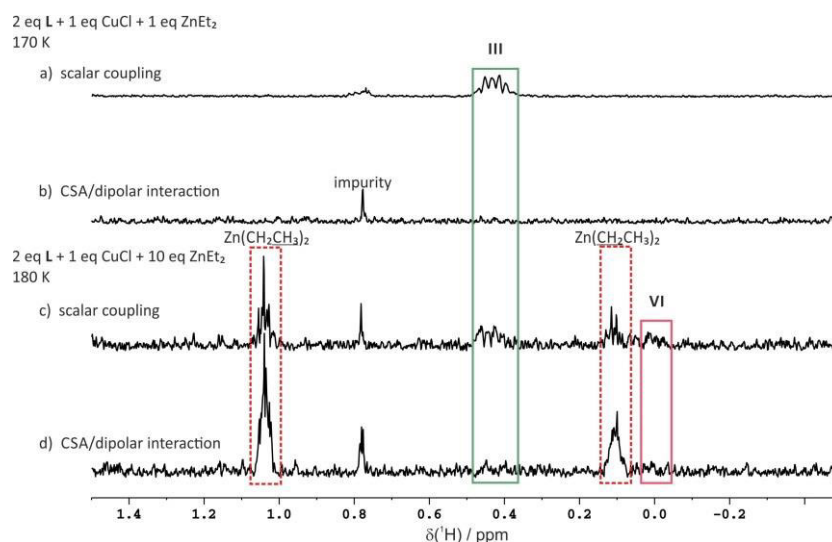


Figure 3.11: 1D ^1H , ^{31}P HMBC spectra of 2 eq $\text{L}^{(SS)}$, 1 eq CuCl and 1 eq ZnEt_2 with magnetization transfer via scalar coupling (a) and cross correlation (b) at 170 K and of 2 eq $\text{L}^{(SS)}$, 1 eq CuCl and 10 eq ZnEt_2 via scalar coupling (c) and cross correlation (d) at 180 K in CD_2Cl_2 . With 1 eq ZnEt_2 no non-specific interactions to ZnEt_2 (dashed red boxes) were detected. In both samples a scalar coupling signal for signal III of the corresponding 2D spectra is detectable (0.43 ppm). In the second sample, with higher amounts of ZnEt_2 , also scalar coupling is visible for signal VI (0.03 ppm). For signals I and II spectra with scalar coupling signals are presented below.

proving the transfer of an ethyl group. In order to get better spectral resolution a small spectral window (60 ppm) was chosen; therefore signals I and II are folded back as the spectrometer has no digital filter in the indirect dimension. These signals were assigned to diethylaminophosphine ligand copper complexes. The chemical shift values (52.7 and 56.6 ppm) are in agreement with a downfieldshift for the more electron rich dialkylaminophosphine ligands ($\delta(^{31}\text{P})$ for diethylaminophosphine ligand: 40.1 ppm in C_6D_6 ^[47]) upon complex formation. The contrary effect to phosphoarmidite ligands (complexes appear upfield shifted) is based on different electronic properties of the phosphorous atom.

In the 1D ^1H , ^{31}P HMBC spectra for detection of magnetization transfer via scalar coupling of a 1:1 enantiomeric mixture of $\text{L}^{(SS)}$ and $\text{L}^{(RR)}$ with 1 eq CuCl and 11 eq ZnEt_2 signals appear at 0.91 and 0.30 ppm, corresponding to the diethylaminophosphine ligand complexes (signals I and II respectively). Furthermore a signal appears at 0.43 ppm for signal III of the 2D ^1H , ^{31}P HMBC spectrum. Obviously the intensity of the signals

depends on the processing parameters used. As window function an e-function was chosen with varying line broadening (LB), for a LB of 1.0 the signals are hardly visible, with increased LB growing signal intensity is observed, while the best resolution is obtained with a LB of 2.0.

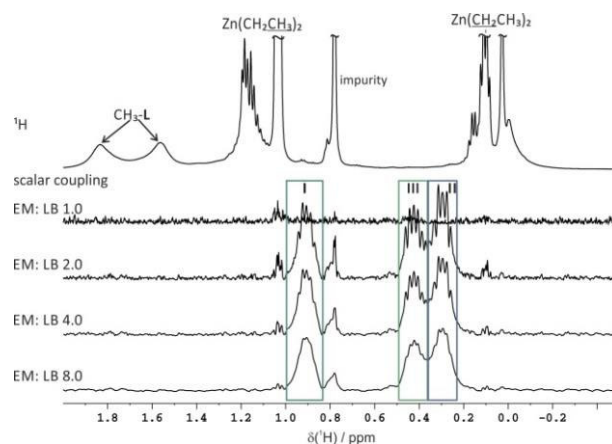


Figure 3.12: ^1H NMR spectrum and the 1D ^1H , ^{31}P HMBC spectrum for magnetization transfer via scalar coupling of 1 eq $\text{L}^{(SS)}$, 1 eq $\text{L}^{(RR)}$, 1 eq CuI and 11 eq ZnEt_2 with different processing parameters.

In the 2D ^1H , ^{31}P HMBC spectra of the enantiomeric mixture (1:1 $\text{L}^{(SS)}:\text{L}^{(RR)}$) apart from signals I-IV a new signal VII arises (data not shown), which is supposed to be a species with at least two ligands in a mixed coordination of the ligand enantiomers. In order to force the equilibrium towards structures with a zinc chloride unit incorporated a ZnCl_2 solution was added, providing significant changes in the ^{31}P NMR spectrum, thereby $[\text{Cu}_2\text{I}_2\text{L}_3]$ is almost completely decomposed and ligand is released. In the 2D ^1H , ^{31}P HMBC spectra signals I and II seems to be unaffected, while signal III decreases and IV and VII vanishes totally, in contrast a new signal VIII appears, which was assigned to the free diethylaminophosphine ligand (data not shown).

In accordance with the CuI investigations a sample with a 1:1 ligand to salt ratio was prepared. In Figure 3.13 the 2D ^1H , ^{31}P HMBC spectrum after addition of 33 eq ZnEt_2 at 200 K is presented. Therein signal III is not detected, a probable explanation therefore is that the corresponding structure involves a CuL_2 fragment. Apart from signal VI a new signal IX appears. The ^1H chemical shift of VI and the further signal pattern enables the assignment to a cuprate like species. Signal IX was assigned to a ligand side product, in which the amine side chain is substituted by an ethyl group, due to the missing of cross signals to methine protons of the amine side chain. The signal with $\delta(^{31}\text{P})$ 131.3 ppm (purple) is in agreement with the phosphorous chemical shift of signal V and was assigned as ligand derivative with a P-OEt group and intact amine side chain, due to

existing signal splitting in low temperature spectra for the methine protons, based on reduced rotation of the C-N bond and very similar chemical shifts of the methine groups to that of the free ligand.

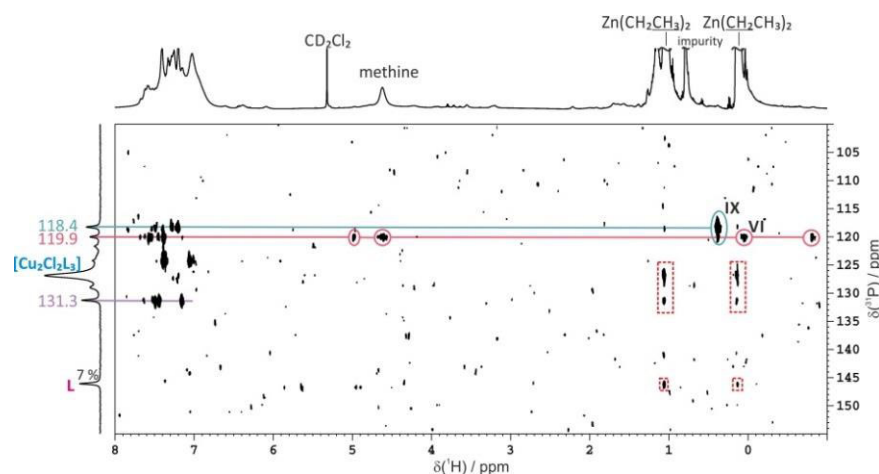


Figure 3.13: 2D ^1H , ^{31}P HMBC spectra of 1 eq $\text{L}^{(\text{SS})}$, 1 eq CuCl and 33 eq ZnEt_2 after three weeks at 200 K in CD_2Cl_2 . Signal VI was already detected in a sample with a 2:1 ligand to salt ratio with 11 eq of ZnEt_2 , while signal IX appears as a new signal in the 1:1 mixture. Due to the excess of ZnEt_2 non-specific interactions occur to free ligand $\text{L}^{(\text{SS})}$, $[\text{Cu}_2\text{Cl}_2\text{L}_3]$ and to the signal at 131.3 ppm (red dashed boxes).

3.3.2 Experimental Part

General considerations

All sample preparations were performed under standard Schlenk technique under argon atmosphere and in dry solvents. CD_2Cl_2 was purchased by Deutero GmbH (99.6 %), dried with CaH_2 and was freshly distilled before use. The phosphoramidite ligands were either prepared according to reported protocols^[48] or purchased by ABCR. Copper iodide was used as commercially available from Sigma Aldrich (99.999 %). Copper chloride was used as commercially available from Alfa Aesar (97 %). The solutions of the dialkylzinc reagents were freshly prepared in deuterated solvents (diethyl- and dimethylzinc in CD_2Cl_2). ZnEt_2 was purchased by Sigma-Aldrich (≥ 95 %) and used without further purification. ZnMe_2 was purchased either by ABCR (95 %) or as 2M solution in toluene by Sigma-Aldrich and used without further purification. ZnPh_2 was used as commercially available from Strem Chemicals or it was used as synthesized by Dipl.-Chem. Fabian Mutzbauer (AK Korber).^[49] The synthesis of ZnPh_2 was performed from a reaction of ZnCl_2 and PhLi in Et_2O at 0 °C. ZnPh_2 was purified via distillation at 120 °C under vacuum (5×10^{-2} mbar) and obtained as pure white solid. ZnCl_2 was recrystallized from 1,4-dioxane and dried before use. PhLi was synthesized from PhBr

and Li in Et₂O under reflux. All manipulations with ZnPh₂ were performed in a glove box under argon atmosphere and exclusion of daylight. In the commercially available source of ZnPh₂ traces of benzene were detected. Investigations were performed in CD₂Cl₂.

Sample preparation

Preparation of the phosphoramidite copper complexes. An argon flushed Schlenk tube equipped with magnetic stirring bar and septum was charged with 2 eq **L** (0.036 mmol, 15.81 mg) and 1 eq copper iodide (0.018 mmol, 3.43 mg) or copper chloride (0.018 mmol, 1.78 mg), freshly distilled solvent CD₂Cl₂ (0.6 ml) was added and the mixture stirred for 1-2 h at room temperature until a clear solution was obtained. Subsequently the samples were transferred to an argon flushed NMR tube. The samples were stored at -85 °C.

Preparation of the phosphoarmidite copper complexes – MRx samples. To the freshly prepared phosphoramidite copper complex solution the corresponding amount of freshly prepared ZnEt₂ or ZnMe₂ solution was added at room temperature.

ZnPh₂: Complex preparation as describe above. A second argon flushed Schlenk tube with magnetic stirring bar and septum was charged with ZnPh₂ (0.09 mmol, 22.04 mg; 5-fold excess to CuI, 10-fold excess to [Cu₂X₂L₃]) and CD₂Cl₂ (0.4 mL). After stirring for 2 h, the cloudy solution of ZnPh₂ was transferred to the solution of the phosphoramidite copper complexes. A slightly exothermic reaction was observed upon by the condensation of CD₂Cl₂ at the upper part of the Schlenk tube. The mixture was stirred for 25 min and transferred into an argon flushed NMR tube.

NMR data collection and processing

NMR spectra were recorded on a Bruker Avance DRX 600 (600.13 MHz) spectrometer equipped with a 5 mm broadband triple resonance z-gradient probe (maximum gradient strength 53.5 Gauss/cm). The temperature for all low temperature measurements were controlled by a BVTE 3000 unit. The ¹H chemical shifts were referenced to the residual solvent signal of CD₂Cl₂ (5.32 ppm), for the ³¹P chemical shifts the Ξ value of an external standard was applied. NMR data were processed and evaluated with Bruker Topspin 3.1/3.2.

2D ¹H,³¹P HMBC spectra: pulse program = inv4gplrndqf, relaxation delay = 6 s, mixing time = 0.05 s, NS = 128, DS = 8, TD = 16k F2 and 64 F1.

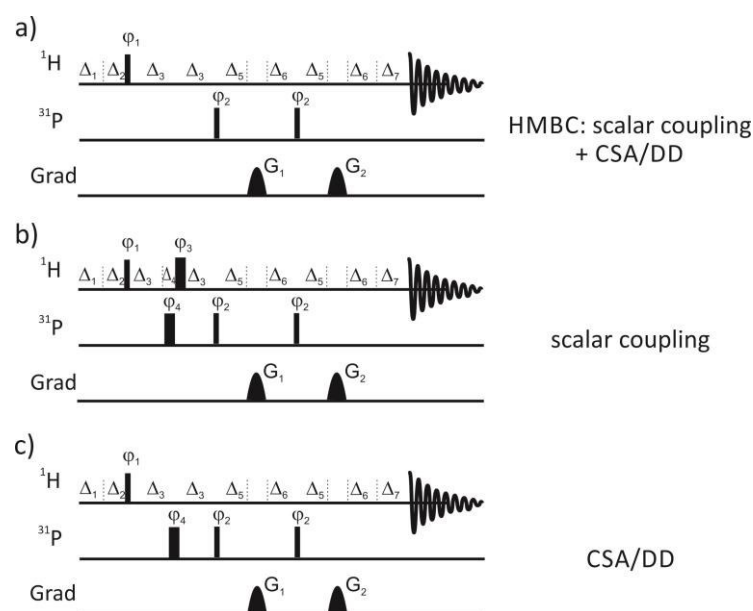


Figure 3.14: Pulse schemes of the 1D ^1H , ^{31}P HMBC allowing a) for the magnetization transfer via scalar coupling and CSA/DD; b) scalar coupling; and c) CSA/DD. The narrow and wide black bars indicate nonselective 90° and 180° pulses, respectively. The shaped black bar indicates a Gaussian cascade.

1D ^1H , ^{31}P HMBC spectra (see Figure 3.14 for pulse sequences): Narrow and wide black bars indicate nonselective 90° and 180° pulses, respectively. The shaped black bar indicates a Gaussian cascade for selective inversion of the aromatic region. $P1 = P2/2 = 8.79 \mu\text{s}$; $P3 = P4/2 = 22 \mu\text{s}$. Initial delay durations: $\Delta_1 = 6 \text{ s}$; $\Delta_2 = 50 \mu\text{s}$; $\Delta_3 = 7.13333 \text{ ms}$; $\Delta_4 = 0.1321 \text{ ms}$; $\Delta_5 = 3 \mu\text{s}$; $\Delta_6 = \Delta_7 = 20 \mu\text{s}$. Phase cycling: $\phi_1 = 2(x), 2(-x)$; $\phi_2 = x, -x$; $\phi_3 = 4(x), 4(-x)$; $\phi_4 = x$; $\phi_{\text{recx}} = x, -x, -x, x, -x, x, x, -x$. z-axis PFGs: $G_1 = (1 \text{ ms}, 40 \text{ G/cm})$, $G_2 = (1 \text{ ms}, -23.8 \text{ G/cm})$.

3.4 Additional Findings

3.4.1 Introduction

For the above described investigations on the proof of a transmetalation intermediate in ACA reactions besides ZnEt_2 ,^[50] also ZnMe_2 and ZnPh_2 ^[38] were used as transmetalation reagents. ZnMe_2 showed, beside non-specific interactions, various side products. Thus, further analyses of interactions between structural moieties of the ligand and dimethyl zinc were performed, by using representative reagents. Since no proof for a transmetalation intermediate with dimethyl zinc was found, MeLi was used for stabilizing the transmetalation intermediate with a methyl group transmetalated on the copper complex. Additionally, the structure of this intermediate was investigated by removing the Li^+ ion from the active system by a chelating agent. Furthermore, the investigation involved the analysis of the second step of the reaction, where an α,β -unsaturated carbonyl compound is added to the solution. Besides the generally used 2-cyclohexenone,^[51] here a ^{15}N labeled N-tosyl imine was used for considering the preorganization of the precatalytic complex or the free ligand $\text{L}^{(SS)}$, respectively.

All these experiments were performed for getting a better inside into the structures, interactions and chemical processes that are occurring in this prominent reaction.

A further study concentrates on the trifluoromethylsulfochlorination of non-activated alkenes by a copper-catalyzed photoredox reaction. Thus, the first step of this reaction was investigated NMR spectroscopically with a LED based NMR illumination device.

3.4.2 Investigation on the Transmetalation Step with ZnMe_2

For the NMR spectroscopic investigations with ZnMe_2 we used commercially available solutions of 1.2 M or 2.0 M ZnMe_2 in toluene. During the investigations of the differentiation between the scalar coupling and the CSA/dipol interactions, we observed a signal for toluene in both selective 1D ^1H , ^{31}P HMBC spectra (see Figure 3.7c and d). As a scalar coupling is incongruous between toluene and complex $[\text{Cu}_2\text{X}_2\text{L}_3]$ or L , respectively, we realized that these HMBC spectra are so sensitive that they are recording also non-specific interactions which are most probably based on strong π,π - or CH,π -interactions or are simple artefacts. Those non-specific interactions were observed for the

first time in spectra with $\text{ZnMe}_2(\text{tol.})$ and subsequently were transferred to the spectra with ZnEt_2 and ZnPh_2 for the assignment and interpretation of various signals in those spectra.

The signal of ZnMe_2 ($\delta(^1\text{H}) = -0.59$ ppm), also showed signals in both 1D $^1\text{H}, ^{31}\text{P}$ HMBC spectra, for scalar couplings and for CSA/dipolar interaction, respectively (see Figure 3.7c and d). First this was supposed to be the signal for the transmetalated species, however, according to the before described signal of toluene, it can be said, that here non-specific interactions were observed as well. This is supported by no change of the ^1H and ^{31}P chemical shifts, as it would be expected for a methyl group that is transferred from zinc to copper and a different geometry of the ligands in the copper complex. On the bottom line, compared to ZnEt_2 , no signal for a transmetalated group was found with ZnMe_2 and ZnPh_2 , respectively. In order to get more insight into this system, experiments to stabilize the predicted species and thus a facilitation of the analysis of the structure, were performed with MeLi (see below).

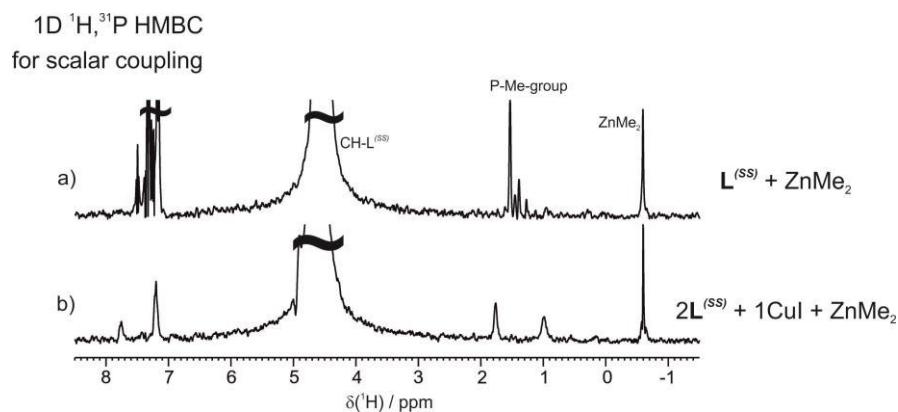
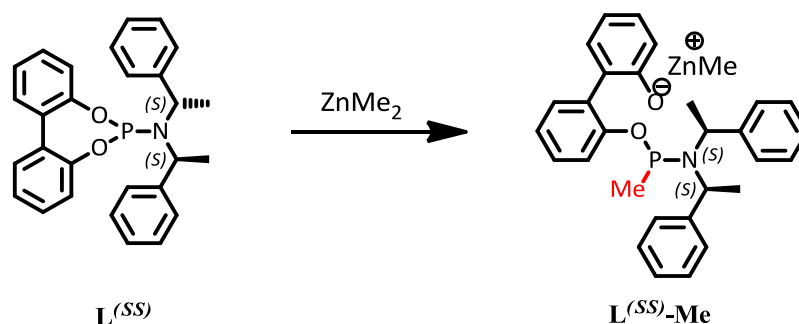


Figure 3.15: 1D $^1\text{H}, ^{31}\text{P}$ HMBC spectra with scalar coupling of a) $\text{L}^{(\text{SS})}$ and CuI with ZnMe_2 and b) $\text{L}^{(\text{SS})}$ with ZnMe_2 ; in CD_2Cl_2 at 230 K.

As the big solvent signal of toluene might cover smaller signals, for further analysis neat ZnMe_2 (2 M, dissolved in CD_2Cl_2) was used, as it was also described above for ZnEt_2 (Supporting Information 3.3.4). Without the huge solvent signal, the resolution of smaller signals was improved, thus a detailed investigation of these intermediates was possible. Thereby, in 1D and 2D $^1\text{H}, ^{31}\text{P}$ HMBC spectra of $\text{L}^{(\text{SS})}$ or $[\text{Cu}_2\text{X}_2\text{L}_3]$ with ZnMe_2 , respectively, several species with a scalar coupling between ^1H and ^{31}P in the range of 2-1 ppm were detected (see Figure 3.7 and 3.15). Those signals were not in the range that would be expected for transmetalation intermediates, which should occur at higher field (for CuMe $\delta(^1\text{H}) = -0.22$ ppm).^[52] In particular, the spectra of the ligand $\text{L}^{(\text{SS})}$ and ZnMe_2 without copper salt (see Figure 3.7a and c, and 3.15a) showed signals with a scalar coupling between ^1H and ^{31}P at $\delta(^1\text{H}) = 1.7\text{-}1.2$ ppm with $\delta(^{31}\text{P}) = 130\text{-}120$ ppm. In the

spectra with the copper complex $[\text{Cu}_2\text{I}_2\text{L}_3]$ and ZnMe_2 two signals with a scalar coupling occurred (see Figure 3.7b and d, and 3.15b), namely at $\delta(^1\text{H}) = 0.99$ ppm and $\delta(^{31}\text{P}) = 114.3$ ppm and a signal at $\delta(^1\text{H}) = 1.76$ ppm and $\delta(^{31}\text{P}) = 70$ or 10 ppm (as this signal is folded in the 2D $^1\text{H}, ^{31}\text{P}$ HMBC spectrum, the ^{31}P chemical shift value is estimated). The signal at $\delta(^1\text{H}) = 1.76$ ppm is not identified until now, but all other signals belong to a species with a methyl group, that is directly bound to the phosphorous atom, and the biphenol backbone is halve-cleaved at one O-P bond (see Scheme 3.6). Investigations on the interactions of the ligand $\text{L}^{(SS)}$ and ZnMe_2 are the basis of this suggestion, (see below). The multitude of signals in the spectrum without copper salt, is traced back to different geometries and coordination of the methyl group. The same structure is proposed for the signal at $\delta(^1\text{H}) = 0.99$ ppm, that occurs with copper salt, here the broadening of the signal, indicates that the halve-cleaved ligand is coordinated to the copper complex. The upfield shift in the ^{31}P spectrum matches well with the described structure, as it is literature-known that a complete cleavage of the biphenol backbone and an addition of two methyl groups results in $\delta(^1\text{H}) = 1.62$ ppm and $\delta(^{31}\text{P}) = 13$ ppm or $\delta(^1\text{H}) = 7.5$ ppm and $\delta(^{31}\text{P}) = 42.8$ ppm if the phosphorous atom is oxidized.^[46]



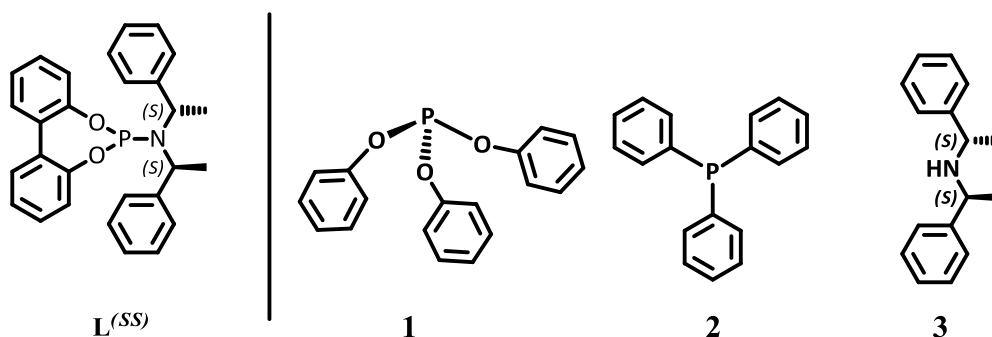
Scheme 3.6: Postulated process between $\text{L}^{(SS)}$ and ZnMe_2 . The methyl group is added to the phosphorous atom of the ligand, while one O-P bond is cleaved.

In summary, the studies of the ACA reaction with commercially available ZnMe_2 dissolved in non-deuterated toluene revealed for the first time the appearance of non-specific interactions in the 1D and 2D $^1\text{H}, ^{31}\text{P}$ HMBC spectra of this system. This identification prevented a misinterpretation of signals for potential transmetalation intermediates, also for investigations with ZnEt_2 and ZnPh_2 . Furthermore, new signals that revealed a scalar coupling between the ligand and a methyl group were observed, which are monitoring a reaction of the ligand with ZnMe_2 . Those observations helped to interpret various signals in the spectra with ZnEt_2 . Unfortunately, with ZnMe_2 it was not possible to detect a transmetalation intermediate, which might be explained by a very low

amount of the intermediate or the building of a different species, compared to ZnEt_2 . As it is known from the synthetic application, lower yields and less enantioselectivity are observed with ZnMe_2 in comparison to ZnEt_2 , which might be an explanation for the different behavior in the NMR spectroscopic investigation. Therefore, studies with MeLi were performed (see below), to get an idea about the structure and the chemical shifts of the potential transmetalation intermediate.

3.4.3 Interactions between Structural Moieties of the Ligand $\text{L}^{(SS)}$ and ZnMe_2

If ZnMe_2 is added to $\text{L}^{(SS)}$ or the precatalytic system, new signals with a scalar coupling, appeared in the 1D ^1H , ^{31}P HMBC spectra. Owing to the chemical shift region ($\delta(^1\text{H}) = 2.00\text{--}1.00$ ppm) it was excluded that these signals derived from transmetalated species, but rather from an interaction between $\text{L}^{(SS)}$ and ZnMe_2 . Even if these interactions were not expected to be important for the transmetalation process, they might be crucial for the design of new ligands and to get a deeper understanding of the mechanism of the copper catalyzed ACA reaction. For a detailed investigation on the interaction between an organozinc reagent and the phosphoramidite ligand, different structural moieties of the ligand $\text{L}^{(SS)}$ (see Scheme 3.7, **1**, **2** and **3**) were combined with ZnMe_2 .



Scheme 3.7: Structures of $\text{L}^{(SS)}$, and the used reagents that represent structural moieties of the ligand for the investigation of its interactions with ZnMe_2 ; $\text{P}(\text{OPh})_3$ (**1**), PPh_3 (**2**) and the amine side chain of $\text{L}^{(SS)}$ (**3**).

Scheme 3.7 shows the reagents that were chosen as model systems for the determination of these interactions. $\text{P}(\text{OPh})_3$ (**1**) was used, owing to a comparable binding structure like the biphenol backbone of $\text{L}^{(SS)}$, namely with P-O-Ar bonds. PPh_3 (**2**) should indicate in comparison to **1**, whether the oxygen is involved in the interactions or not. To examine the influence of the nitrogen atom, the amine side chain (**3**) of ligand $\text{L}^{(SS)}$, without any oxygen or phosphorous atom, was applied.

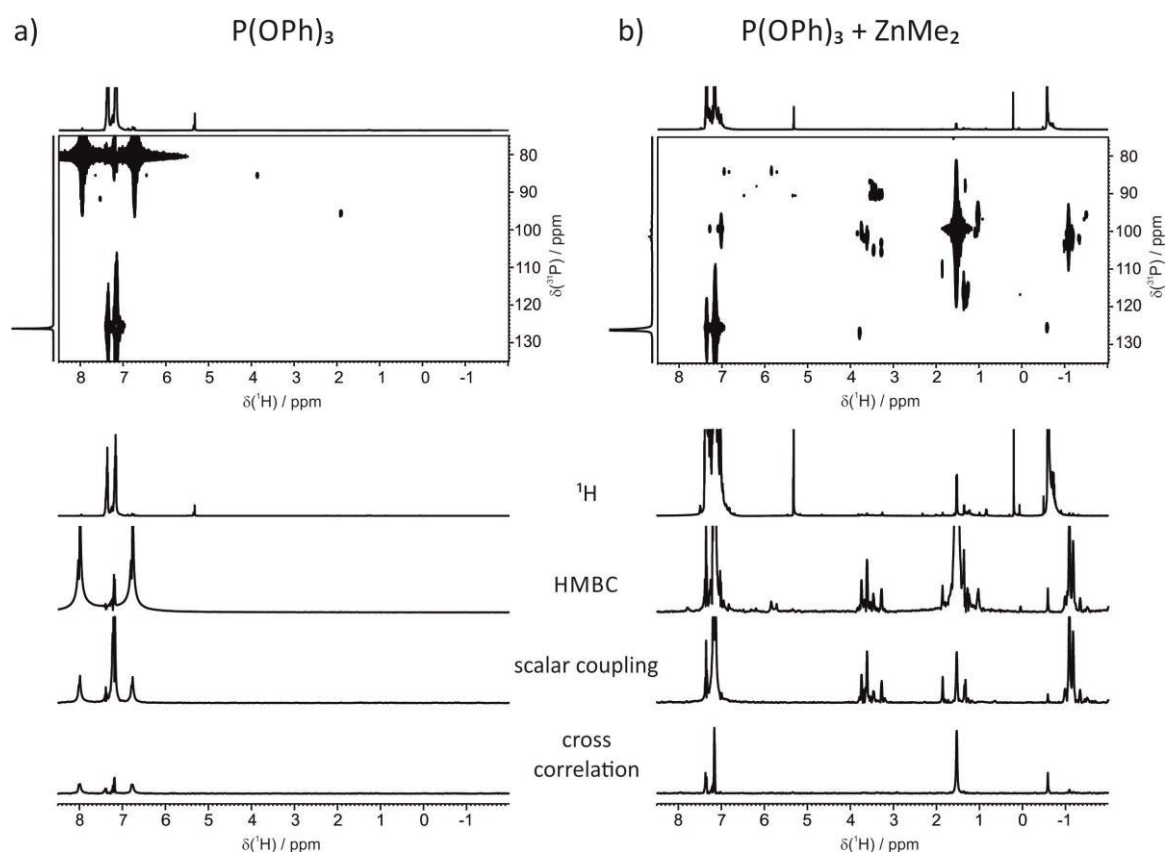


Figure 3.16: 2D (top) and 1D (below) ^1H , ^{31}P HMBC spectra of P(OPh)_3 (**1**) a) before and b) after the addition of ZnMe_2 (neat) in CD_2Cl_2 at 230 K.

Figure 3.16b shows new signals in the 2D and 1D ^1H , ^{31}P HMBC spectra after the addition of ZnMe_2 to **1**. Most of them show scalar couplings in the 1D ^1H , ^{31}P HMBC spectra (Figure 3.16b, below). Signals with a $\Delta\delta(^1\text{H}) = 2.00\text{--}1.00$ ppm are similar compared to the corresponding spectra with free and complexed phosphoramidite ligand (see Figure 3.7 and 3.15). This chemical shift range is known for species, that have a methyl group directly bound to the phosphorous atom (for PMe_3 $\delta(^1\text{H}) = 0.97$ ppm).^[61] The most pronounced cross signal occurs at $\delta(^1\text{H}) = 1.53$ to $\delta(^{31}\text{P}) = 99.4$ ppm, besides this signal further smaller signals occur, which might originate from different coordination of zinc-clusters. The same explanation is given for the multitude of signals between $\delta(^1\text{H}) = 4.00\text{--}3.00$ ppm, those species are expected to contain a P-OMe group (for P(OMe)_3 $\delta(^1\text{H}) = 3.39$ ppm).^[61] Species that arose upfield shifted to ZnMe_2 ($\delta(^1\text{H}) = -0.59$ ppm) are most probably P-Zn-Me groups.

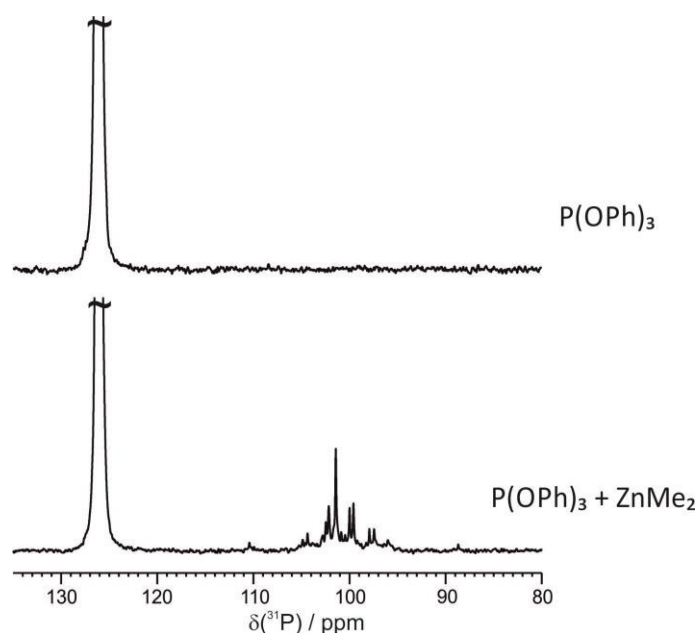


Figure 3.17: ^{31}P NMR spectra of P(OPh)_3 (**1**) before (top) and after (below) the addition of ZnMe_2 at 230 K in CD_2Cl_2 .

In the ^{31}P NMR spectrum the species with a Me-P bond occurred in a range of $\delta(^{31}\text{P}) = 111.0\text{--}94.0$ ppm (Figure 3.17, below), assigned by the 2D $^1\text{H}, ^{31}\text{P}$ HMBC spectrum. Thus, they showed the same upfield shift like the species observed with $\text{L}^{(\text{SS})}$. Therefore, it was supposed that one O-Me group was exchanged by a methyl group, which supported the idea, that only one O-P bond of the back bone of the ligand was split off (see Scheme 3.6 and explanation in chapter 3.4.2). In comparison with the signals observed there, the amount of the appearing species was so high with P(OPh)_3 , that besides the cross signals in the 2D $^1\text{H}, ^{31}\text{P}$ HMBC spectrum, also in the ^{31}P NMR spectrum the species were observable (Figure 3.17, below). This means, that these species were more stable than the observed side products with the phosphoramidite ligand.

For PPh_3 (**2**) no comparable cross peaks or signals in the 1D spectra, like it was observed with $\text{L}^{(\text{SS})}$ or **1**, were detected (spectra not shown). Hence, it was proven that rather the oxygen atom, than the aromatic moieties, led to the observation of the side products.

The examination of the mixture of amine side chain **3** and ZnMe_2 , showed a downfield shift of all protons of **3** the ^1H NMR spectrum, which was accompanied by a strong upfield shift ($\Delta\delta(^1\text{H}) = -0.2$ ppm) of the methyl group of ZnMe_2 (spectra not shown). Those shifts were expected if the zinc atom is coordinated to the nitrogen atom. However, none of these signals was observed in the spectra with phosphoramidite ligand, and therefore, an interaction between the zinc atom and the nitrogen atom of the ligand can be excluded.

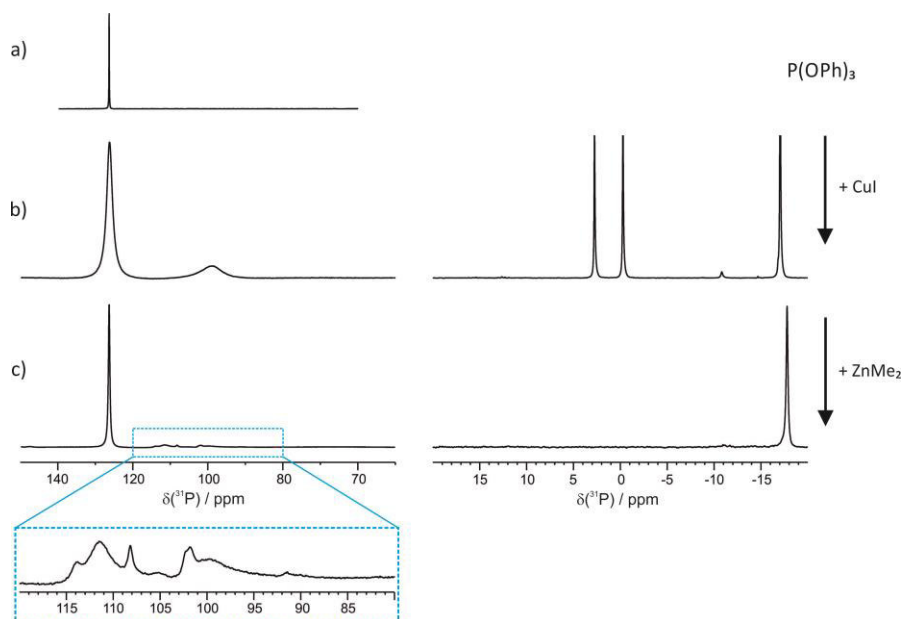


Figure 3.18: ^{31}P NMR spectra of P(OPh)_3 at 230 K in CD_2Cl_2 a) before and b) after addition of CuI , c) with CuI and ZnMe_2 and enlargement of spectra c) (blue box).

Since P(OPh)_3 seems to be a good representative, as structural moiety that is responsible for interactions between the phosphoramidite ligand and an organozinc reagent, the behavior of P(OPh)_3 during the complexation with a copper salt, and moreover, the following transmetalation step, was investigated. Therefore CuI was added to P(OPh)_3 , which resulted in a broad signal at $\delta(^{31}\text{P}) = 98.9$ ppm (Figure 3.18b), and thus showed a comparable complex to $[\text{Cu}_2\text{X}_2\text{L}_3]$ ($\Delta\delta(^{31}\text{P}) = -16$ ppm, between $\text{L}^{(\text{SS})}$ and $[\text{Cu}_2\text{X}_2\text{L}_3]$). When ZnMe_2 was added to this complex, this signal vanished accompanied with the arising of various new signals in a chemical shift range of $\delta(^{31}\text{P}) = 115.0$ – 90.0 ppm (Figure 3.18c). This multitude of signals was assigned to the occurrence of various different complex structures which were not investigated in detail.

Although **1** shows similar interactions as the phosphoramidite ligand, no transmetalated species was found in the 2D ^1H , ^{31}P HMBC spectra of P(OPh)_3 with CuI (Figure 3.19b). Moreover species with a Me-P bond in the range of $\delta(^1\text{H}) = 2.00$ – 1.00 ppm were not observed. Therefore, P(OPh)_3 enabled to elucidate the interactions and the formed intermediates between the ligand $\text{L}^{(\text{SS})}$ and ZnMe_2 , but did not provide a hint for a transmetalated species.

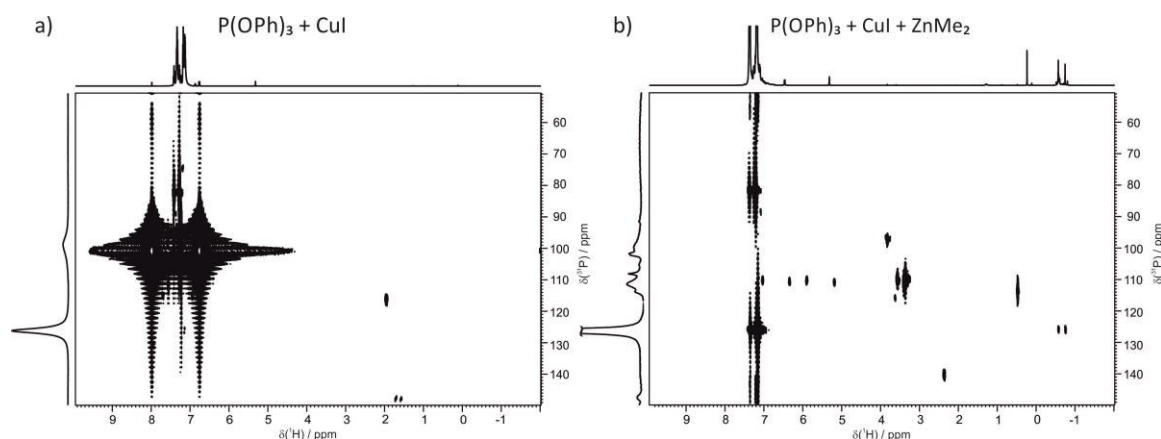


Figure 3.19: 2D ^1H , ^{31}P HMBC spectra of P(OPh)_3 and CuI a) before and b) after addition of ZnMe_2 at 230 K in CD_2Cl_2 , no transmetalated species is found.

In summary, the investigation on the interaction between the structural moieties of the phosphoramidite ligand $\text{L}^{(\text{SS})}$ and ZnMe_2 determined, that for the interaction with organozinc reagents the oxygen atom of the backbone is of high importance. Exclusively with P(OPh)_3 signals with similar proton chemical shifts were detected, compared to the system with ligand $\text{L}^{(\text{SS})}$. While with PPh_3 no interactions were observed, the amine side chain moiety showed a different interaction as it was observed for the system with the phosphoramidite ligand $\text{L}^{(\text{SS})}$, and therefore, for the ligand $\text{L}^{(\text{SS})}$ a coordination of the zinc reagent via the nitrogen atom is excluded. This study was very important for the identification of occurring species in the NMR spectra of the investigation on a transmetalation intermediate with ZnEt_2 ^[50] and ZnMe_2 . Therefore, they helped to assign signals occurring from a ligand with a halved-cleaved biphenol backbone and a methyl or ethyl group bound to the phosphorous atom of the ligand, respectively (see Scheme 3.6).

3.4.4 Investigation on the Structure of a Transmetalation Intermediate with MeLi

Since no signal in the 1D and 2D NMR spectra was found for a transmetalation intermediate with ZnMe_2 (see above), it was tried to prepare the proposed species (Scheme 3.8) by the more reactive organometallic reagent MeLi (1.6 M in Et_2O). In this way, it might be prepared in a larger and more stable amount, and therefore, an NMR spectroscopic detection would be possible. The gained information could help to optimize the parameters used for the NMR spectroscopic investigations with ZnMe_2 and furthermore facilitates the finding of the elusive species.

As no chelating additive is known with a higher affinity to complex zinc prior to copper, a further benefit of MeLi is that the structure of the transmetalation intermediate can be investigated more precisely, meaning, if the Li^+ ion is incorporated in the structure

or not. This could be done by the addition of 12-crown-4 as it was done in a sophisticated study of transmetalation intermediates with Grignard reagents by Feringa *et al.*^[9]

Spectra with an excess of MeLi, compared to complex $[\text{Cu}_2\text{I}_2\text{L}_3]$, show exclusively the formation of $\text{LiCuMe}_2\cdot\text{LiI}$ (see Figure 3.22), therefore, for the studies on the transmetalation intermediate with MeLi were performed with a substoichiometric amount with regard to the precatalytic complex $[\text{Cu}_2\text{I}_2\text{L}_3]$.



Scheme 3.8: Proposed transmetalated species, which is expected to be formed after the addition of an organometallic reagent to the precatalytic complex $[\text{Cu}_2\text{X}_2\text{L}_3]$ ($\text{X} = \text{Cl}, \text{Br}, \text{I}$).^[11]

The investigations with MeLi were performed in CD_2Cl_2 , for the comparability to the measurements with ZnR_2 ($\text{R} = \text{Et}, \text{Me}, \text{Ph}$). Since MeLi reacts with CH_2Cl_2 to a chlorocarbene (ClHC),^[53] the sample preparation was done at 170 K. Under these conditions, it was possible to suppress this side reaction. Also the NMR spectroscopic studies were exclusively performed at temperatures from 180 to 230 K, owing to the above mentioned circumstance.

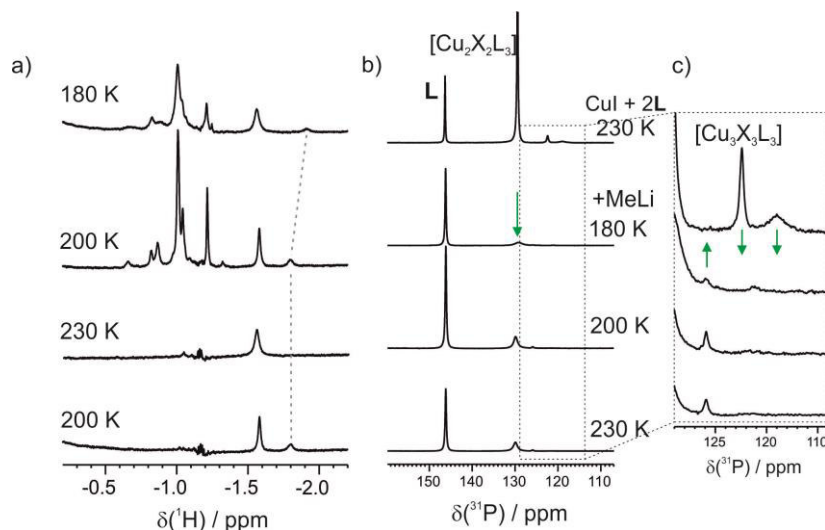


Figure 3.20: 1 eq CuI and 2 eq **L** with MeLi (substoichiometric) in CD_2Cl_2 at various temperatures; a) ^1H NMR spectra, several cuprates species are observed, the best resolution is observed at 200 K; b) ^{31}P NMR spectra (on the top without MeLi) show a new species after the addition of MeLi and the vanish of the precatalytic complex and other copper complexes; c) enlarged section of b).

In the ^1H NMR spectra of a substoichiometric amount MeLi with CuI and **L** (2:1), several new species occurred in the range of $\delta(^1\text{H}) = -0.62$ to -1.83 ppm (Figure 3.20a), which can be mostly assigned to some cuprate species. Those species were only stable at

temperatures up to 200 K. Measurements at 230 K showed a vanishing of these signals, only the signal at $\delta(^1\text{H}) = -1.58$ ppm was observable at all temperatures. Besides the signal at $\delta(^1\text{H}) = -1.80$ ppm (at 200 K) (and -1.92 ppm at 180 K, owing to the temperature shift), the formation of these species was not reversible after a repeated cooling to 200 K. The ^{31}P NMR spectra showed after the addition of MeLi a strong decreased amount of the precatalytic complex $[\text{Cu}_2\text{I}_2\text{L}_3]$ ($\delta(^{31}\text{P}) = 129.5$ ppm), the vanishing of $[\text{Cu}_3\text{X}_3\text{L}_3]$ at $\delta(^{31}\text{P}) = 122.4$ ppm and a not structurally defined complex at $\delta(^{31}\text{P}) = 119.0$ ppm. While at the same time, the integral of the free ligand was increased and a new signal at $\delta(^{31}\text{P}) = 125.9$ ppm appeared. This new signal showed a cross signal in the 2D $^1\text{H}, ^{31}\text{P}$ HMBC spectra to the signals at $\delta(^1\text{H}) = -1.80$ ppm (at 200 K, red) or $\delta(^1\text{H}) = -0.99$ ppm (at 180 K, blue), respectively (Figure 3.21a and c).

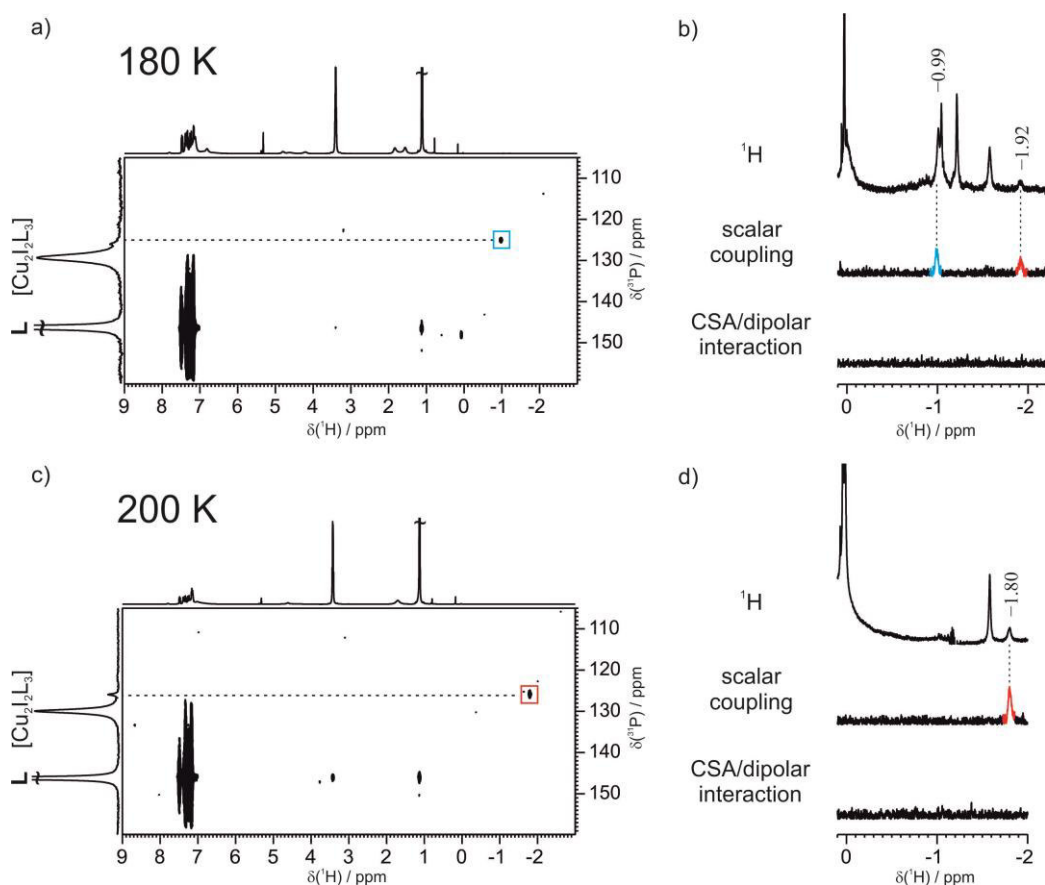


Figure 3.21: 1 eq CuI, 2 eq L and a substoichiometric amount of MeLi in CD_2Cl_2 : a) and c) 2D $^1\text{H}, ^{31}\text{P}$ HMBC spectra, b) and d) ^1H (top) and the 1D $^1\text{H}, ^{31}\text{P}$ HMBC spectra for scalar coupling (middle) and CSA/dipolar interaction (below); at a) and b) 180 K and c) and d) 200 K. Potential transmetalation intermediates with a scalar coupling between ^1H and ^{31}P are observed, colored in blue and red.

Having a closer look at the binding character between the ^1H atoms of MeLi and the ^{31}P atom of the ligand, the 1D $^1\text{H}, ^{31}\text{P}$ HMBC spectra pointed out, that both observed

signals showed scalar couplings and no CSA/dipolar interaction was detected (Figure 3.21 b and d). The reason for observing at 180 K and 200 K different cross signals in the 2D ^1H , ^{31}P HMBC spectrum ($\delta(^1\text{H}) = -0.99$ ppm (blue) and $\delta(^1\text{H}) = -1.80$ ppm (red), respectively), might be explained by the low concentration of these species, as it is observed in the corresponding ^1H NMR spectra, thus the signals are near the detection limit. If both species can be observed at 200 K in the 1D and 2D ^1H , ^{31}P HMBC spectra is not clear as the spectrum in Figure 3.21c was detected after the warming to 230 K and subsequent cooling to 200 K. So the species might have been in solution before. The ^1H spectrum at 200 K before the warming to 230 K showed a signal at $\delta(^1\text{H}) = -0.99$ ppm (Figure 3.20a, second spectrum), which confirms this suggestion. However, both signals were considered as potential transmetalation intermediates, as they fulfilled the expected characteristics. Namely, they showed a scalar coupling between ^1H and ^{31}P , and their ^1H chemical shift values were in a region expected for a methyl group that is bound to a copper atom. Furthermore, they showed a new signal in the ^{31}P NMR spectra, which is upfield shifted compared to the averaged signal of the precatalytic complex $[\text{Cu}_2\text{I}_2\text{L}_3]$ ($\Delta\delta = -3.6$ ppm). This is in agreement with the results obtained with ZnEt_2 ($\Delta\delta = -2.9$ - -7.4 ppm)^[50] and transmetalation studies of Grignard reagents and ferrocenyl-based diphosphine copper complexes ($\Delta\delta = -1.8$ and -3.1 ppm).^[9]

Next, the role of the lithium atom on the structure of these potential transmetalation intermediates was taken into account. By adding 12-crown-4 to the solution the Li^+ ion would be removed from the coordination sphere of the copper complex. If it is involved into the structure, this would be observed either by a shift or the disappearance of the corresponding signal.^[9] The ^1H and 1D ^1H , ^{31}P HMBC spectra showed, that the signal at $\delta(^1\text{H}) = -1.92$ ppm (at 180 K) did not change after the addition of an excess of 12-crown-4 and still showed a scalar coupling between ^1H and ^{31}P (data not shown). This means, that the proposed transmetalation intermediate has no lithium atom involved in the first coordination sphere. Unfortunately, the signal at $\delta(^1\text{H}) = -0.99$ ppm seemed to be very unstable and it was not possible to reproduce it, so no statement about the structure of this species can be given. But we assume that the structure of this species can not differ much from the other transmetalated species, as they showed the same ^{31}P chemical shift value. A further detailed investigation with enantiomeric and enantiopure ligand combinations, as it was described in the main part of this chapter, was not performed, as the two with MeLi observed transmetalation intermediates were so far not detected with ZnMe_2 .

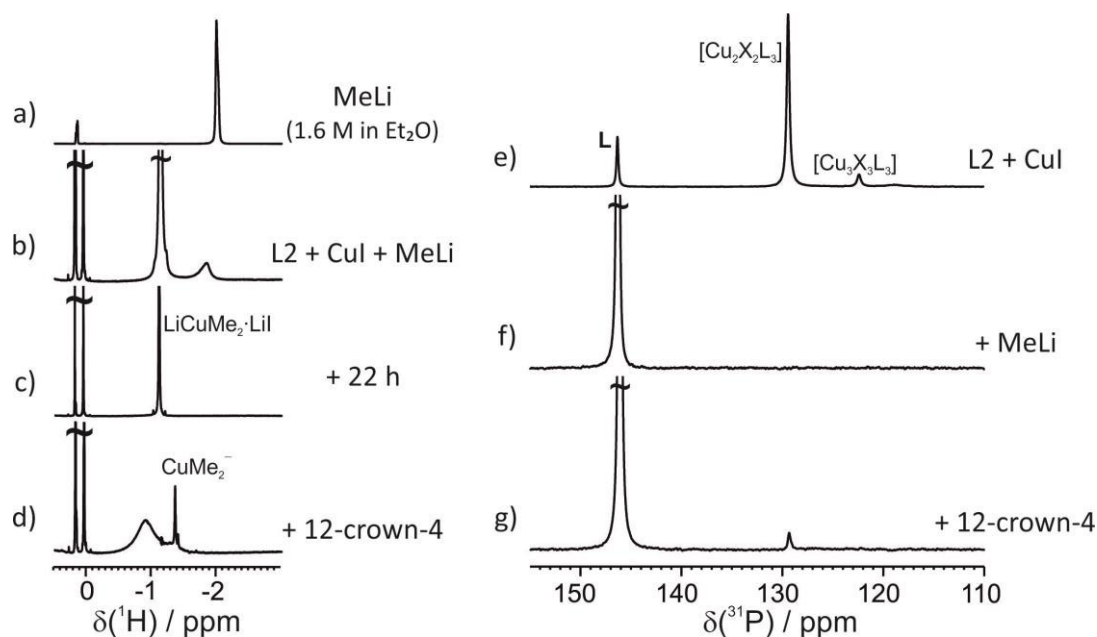


Figure 3.22: ^1H and ^{31}P NMR spectra of a) MeLi (1.6 M in Et_2O); b) 1 eq CuI and 2 eq **L**; b) and f) after the addition of MeLi (excess); c) after 22 hours; d) and g) after the addition of 12-crown-4 (excess) in CD_2Cl_2 at 230 K. The copper complex $[\text{Cu}_2\text{I}_2\text{L}_3]$ is split up after the addition of MeLi, while $\text{LiCuMe}_2\cdot\text{LiI}$ is formed, by adding 12-crown-4 the copper complex $[\text{Cu}_2\text{I}_2\text{L}_3]$ is formed back while CuMe_2^- arises.

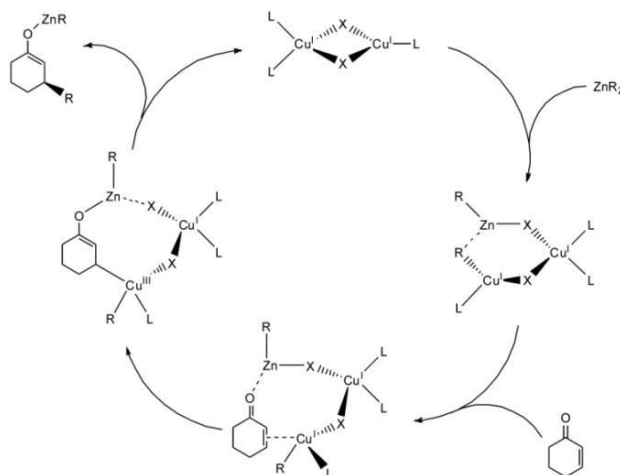
The signals of the potential transmetalation intermediate were only observed by using a substoichiometric amount of the organometallic reagent. With an excess of MeLi the precatalytic complex $[\text{Cu}_2\text{I}_2\text{L}_3]$ is split up, accompanied by the formation of $\text{LiCuMe}_2\cdot\text{LiI}$ ($\delta(^1\text{H}) = -1.13$ ppm, see Figure 3.22c) and the release of free ligand **L** (see Figure 3.22f), as it was visible by the integrals of the signals in the ^1H and ^{31}P spectra. The formation of $\text{LiCuMe}_2\cdot\text{LiI}$, by the reaction of 2 equivalents of MeLi with CuI, is well-known and investigated NMR spectroscopically.^[54] Here the reaction seemed to be hampered, owing to the low temperature, which was observable in Figure 3.22b. The formation of $\text{LiCuMe}_2\cdot\text{LiI}$ was initially accompanied by a broadening of the signal of MeLi, which disappeared after some time (see Figure 3.22c). After the addition of 12-crown-4 to the solution, CuMe_2^- ($\delta(^1\text{H}) = -1.36$ ppm) was formed and a signal at $\delta(^1\text{H}) = -0.90$ ppm arose (see Figure 3.22d). This broad signal might belong to $\text{LiCuMe}_2\cdot\text{LiI}$ with several 12-crown-4 atoms coordinated to the Li^+ ion, which removed them from the cuprate by a slow complexation. The different coordination of the chelating reagent to the cuprate and the chemical exchange process at low temperatures might be responsible for the broadening of the signal. Within one day the broad signal decreases tremendously (data not shown), what supports this suggestion. At the same time, the copper complex $[\text{Cu}_2\text{I}_2\text{L}_3]$

was partially formed back, maybe owing to the instability of CuMe_2^- and the equilibrium was shifted to the more stable copper complex $[\text{Cu}_2\text{I}_2\text{L}_3]$.

In summary, the NMR spectroscopic investigation on the transmetalation of a methyl group from MeLi to the precatalytic complex $[\text{Cu}_2\text{X}_2\text{L}_3]$ showed two potential transmetalation intermediates. Both showed a scalar coupling in 1D $^1\text{H}, ^{31}\text{P}$ HMBC spectra, between the methyl group of MeLi and the phosphorous atom of the ligand. One species was not stable and was not possible to reproduce it, but, the structure of the more stable one was investigated in detail. Thereby, the incorporation of a Li^+ ion in the coordination sphere of the transmetalated species is excluded, as no change of the signal was observable after the addition of a chelating reagent to the solution. Further investigation with $^{6/7}\text{Li}$ NMR spectroscopy could bring more light on this system. Important for the detection of the transmetalation intermediate was the use of a substoichiometric amount of MeLi, this is contrary to the results of the transmetalation intermediate with ZnEt_2 and the synthetic application, where an excess of organozinc reagent is required. Therefore, it is not clear, if these species are transferable to the system with ZnMe_2 , as none of these species was observed until now in the corresponding NMR spectra with ZnMe_2 . The addition of 2-cyclohexenone could verify the reactivity of the observed species to an α,β -unsaturated system.

3.4.5 Investigation on a Cu(I)- π -Intermediate / Cu(III)-Intermediate – Addition of ^{15}N -tosyl imine to the Precatalytic Complex

After identifying the species and elucidating the structures of the intermediates which are appearing during the transmetalation step in the copper catalyzed ACA reaction with diethyl zinc,^[50] the next step of the proposed catalytic cycle (Scheme 3.9) is the addition of an α,β -unsaturated enone.^[11]



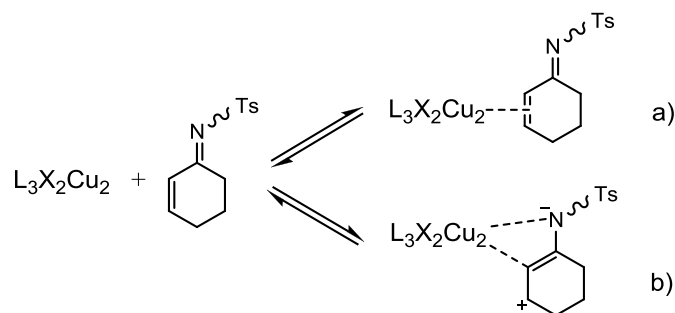
Scheme 3.9: Postulated mechanistic cycle of the copper catalyzed asymmetric conjugate 1,4-addition reaction with ZnR_2 and 2-cyclohexenone.^[11]

The α,β -unsaturated enone is proposed to be coordinated by the transmetalation intermediate by forming a π -complex, which is in the next step transformed to an enol-Cu(III)-complex. This investigation focused on the coordination and possible interactions between the complex and the α,β -unsaturated enone, to see if a preorganization of the Michael system arises and therefore getting a deeper understanding for the reason of the high enantioselectivity of the ACA reaction.

Various NMR spectroscopic investigations of olefin-copper- π -complexes are known.^[52,55–59] For these complexes strong deviating ^{13}C chemical shift values were observed for the carbon atoms of the α,β -unsaturated system, which are coordinated to copper. Most of the above mentioned investigations were performed with organocuprates, and elucidated Cu(I)- π -complexes and Cu(III)-intermediates, but to our knowledge, until today, no reaction intermediate of catalytic copper complexes was stabilized and investigated by NMR spectroscopy.

Unfortunately, the addition of 2-cyclohexenone to the precatalytic system together with ZnMe_2 resulted in an extremely fast, complete conversion.^[51] Even at low

temperatures and by using stereodemanding groups at the double bond of the carbonyl compound, it was not possible to reduce the reaction speed. Furthermore, no interaction between the precatalytic complex and 2-cyclohexenone without any transmetalation reagent was determined.^[51] Therefore, we were looking for an α,β -unsaturated system, which could be used as a model system for the investigated reaction, and which includes a sensitive sensor for monitoring even small deviations in the chemical environment of the Michael acceptor.



Scheme 3.10: Plausible intermediates between the precatalytic copper complex $[\text{Cu}_2\text{X}_2\text{L}_3]$ and *N*-tosyl imine a) a π -complex and b) an enamine.

Very recently, Zezschwitz *et al.* showed, that *N*-sulfonyl imines can also be used, as Michael acceptor in the ACA reaction with high yields and enantioselectivities.^[60] So, we decided to use ^{15}N labelled *N*-tosyl imine for this investigation.

Scheme 3.10 shows the possible interactions between the precatalytic complex $[\text{Cu}_2\text{X}_2\text{L}_3]$ and *N*-tosyl imine, which could either result in a π -complex (a) or an enamine (b). Both precoordinated structures would lead to a variation in the electronic environment of the molecule, monitored in a deviation of the chemical shifts. This deviation is more pronounced in ^{15}N spectra, than in, e.g. ^1H NMR spectra, owing to the broad chemical shift range of ^{15}N . Furthermore, the ^{15}N labeling was performed to 100 %, so in comparison to ^{13}C (as it was used for the cuprates), the sensitivity is much higher and therefore, especially the 2D spectra, can be measured much faster, which facilitates the detection of intermediates significantly. Moreover the tosyl group might strengthen this interaction, owing to π,π -interactions with the aromatic moieties of the ligand, which is well-known to form such intramolecular interactions.^[42,43]

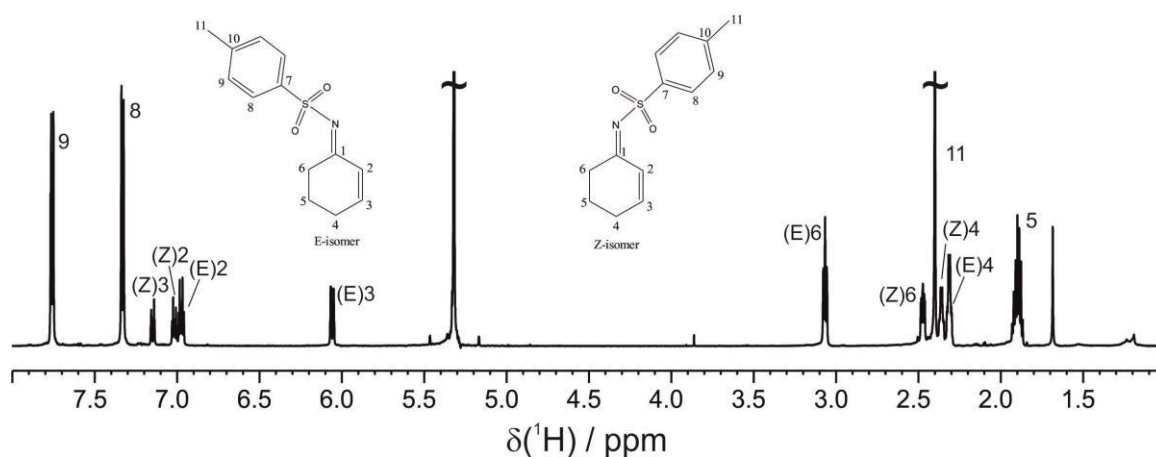


Figure 3.23: ^1H NMR spectrum of ^{15}N -tosyl imine in CD_2Cl_2 at 230 K, with assignment of the signals of the two isomers, in a ratio of 60 : 40 (E : Z).

To find out if the α,β -unsaturated imine is precoordinates by the copper catalyst $[\text{Cu}_2\text{X}_2\text{L}_3]$, different amounts of ^{15}N -tosyl imine were added to the solved precatalytic complex. Substoichiometric amounts (0.1, 0.3 and 0.8 equivalents) of the imine prevented from a fast exchange of the imine and thus from broad, averaged signals in the NMR spectra.

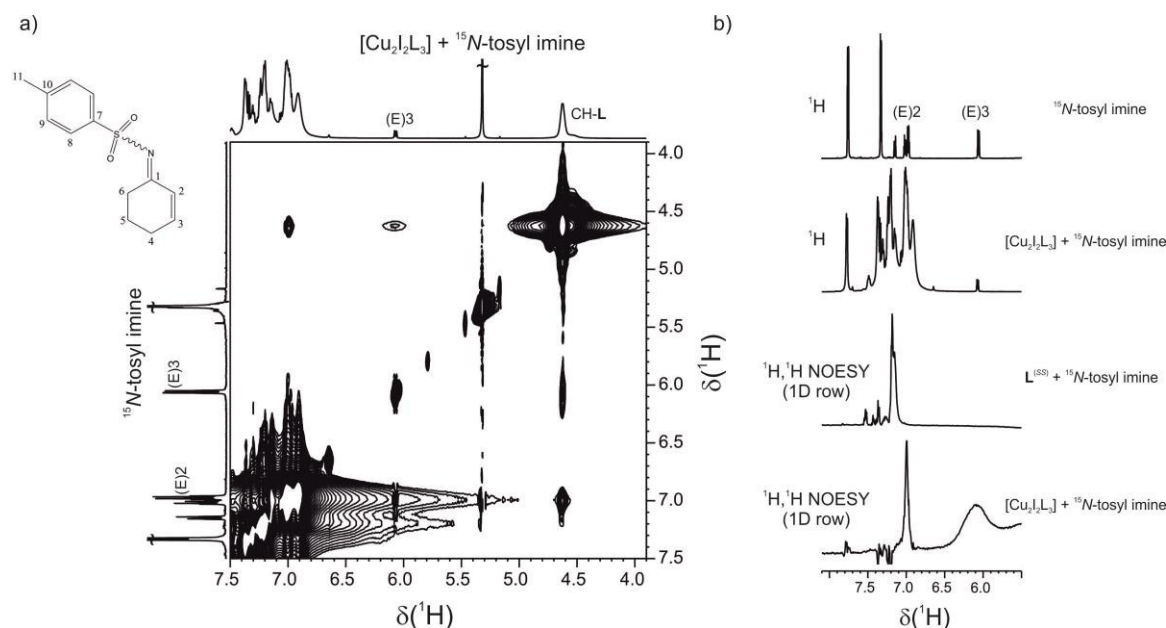


Figure 3.24: a) $^1\text{H}, ^1\text{H}$ NOESY spectrum of the interactions between $[\text{Cu}_2\text{X}_2\text{L}_3]$ and ^{15}N -tosyl imine (1:0.8) in CD_2Cl_2 at 230 K, the corresponding ^1H spectrum above, on the left axis the ^1H spectrum of the imine; on the left the numbered ^{15}N -tosyl imine; b) ^1H spectra and rows of the NOESY spectra with ^{15}N -tosyl imine without or with $[\text{Cu}_2\text{X}_2\text{L}_3]$ (1:0.8) and $\text{L}^{(\text{SS})}$ (1:0.1), respectively.

The $^1\text{H}, ^1\text{H}$ NOESY spectrum showed two cross signals that can be potentially assigned to an interaction between the protons (E)2 and (E)3 of the imine and the methine group of the ligand. (These signals were also received by using an amount of 1:0.3

(spectrum not shown), for an amount of 1:0.1 an $^1\text{H}, ^1\text{H}$ NOESY spectrum was not measured). However, for the signal to (E)2 an unambiguous assignment is not possible, as the signal is overlapped by signals of the aromatic moieties (see Figure 3.24b). To exclude an interaction between the imine and the free ligand a sample without Cu-salt was considered. Here, in the $^1\text{H}, ^1\text{H}$ NOESY spectrum no cross signal for the interaction between (E)3 and the methine group was observed (amounts 1:0.13 and 1:0.02, respectively). Even if this is a hit for a close proximity of the protons of the imine and the methine group of a ligand bound to a copper complex, it is not clear, which of the copper complexes ($[\text{Cu}_2\text{X}_2\text{L}_3]$ or $[\text{Cu}_3\text{X}_3\text{L}_3]$) is involved in this interaction as their methine groups all show equal chemical shifts. Therefore, it is unclear whether the interaction is relevant for the reaction's outcome or not.

In case these signals were showing real interactions between imine and ligand, it can be said that the E-isomer is more preferred, as for the Z-isomer no interaction was observable.

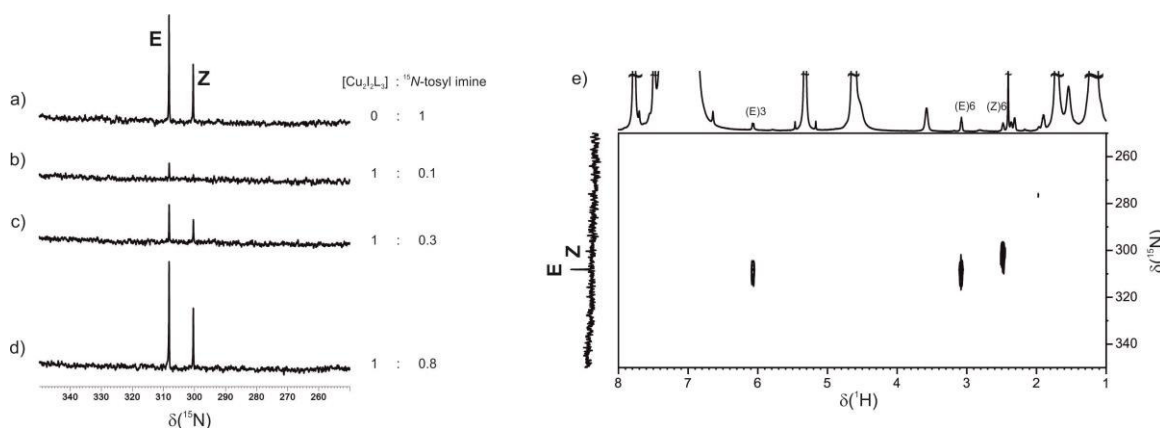


Figure 3.25: a)-d) ^{15}N NMR spectra of various amounts of $[\text{Cu}_2\text{X}_2\text{L}_3]$ to ^{15}N -tosyl imine, no chemical shift deviation for the signals of the E and Z isomer was observable as it would be expected for a coordinated species; e) $^1\text{H}, ^{15}\text{N}$ HMBC spectrum of $[\text{Cu}_2\text{X}_2\text{L}_3]$ and ^{15}N -tosyl imine (1:0.1), exclusively signals of the pure imine occurred; a)-e) in CD_2Cl_2 at 230 K.

However, no further prove for a complexation of the imine as a $\text{Cu(I)}-\pi$ -complex or enamine was found. In case of a strong binding between the imine and the ligand, as shown in Scheme 3.10, firstly a chemical shift deviation, compared to the pure imine, was expected. But this effect was not observed in any standard 1D NMR spectrum, even by varying the stoichiometry (see Figure 3.25b-c). Secondly, no new signals were obtained in the decisive spectra (data of ^1H , ^{13}C and ^{31}P NMR spectra not shown), finally a broadening of the signals was not observed as it was expected for a copper complex (signals of the E- and Z-isomers showed an unchanged line width ($\Delta\nu_{1/2} = 9\text{-}10\text{ Hz}$) in the

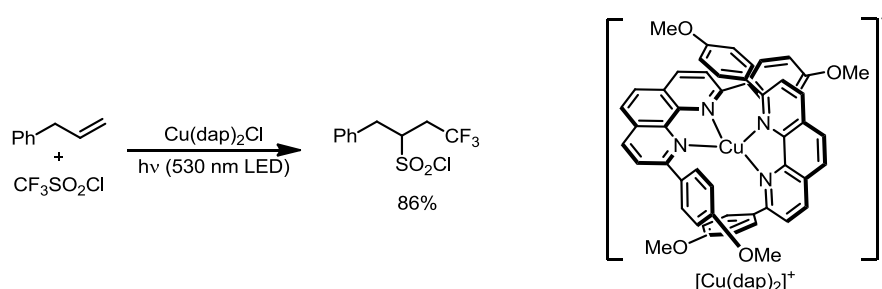
spectra of Figure 24a-d). Recently, we were able to show, that it is possible to detect even small amounts of intermediates by using the HMBC spectra as a spectroscopic filter.^[50] Unfortunately, the ^1H , ^{15}N HMBC spectrum did not contain any further signals beside the ones for the pure ^{15}N -tosyl imine, thus, no hint for a precoordinated imine was found (see Figure 3.25e).

In summary, the investigation on the copper-catalyzed ACA reaction with ZnMe_2 showed that the reaction is too fast for the NMR timescale, and led very fast to a complete conversion, furthermore, the investigation of the precoordination of 2-cyclohexenone by the precatalytic complex showed no interaction and no shifts of the signals in the ^{13}C NMR spectrum. The here presented study used a ^{15}N -tosyl imine to investigate this precoordination by using ^{15}N NMR spectra as a further access to the elusive intermediate. But it was shown that an interaction between the imine and the precatalytic complex is very doubtful. Even if there were some cross signals obtained in the ^1H , ^1H NOESY spectrum, these signals were not assigned unambiguously, and might just represent a very weak interaction. Besides these signals, no further hint for the occurrence of an intermediate was found, like the shift of the ^{15}N signals, the appearance of new signals or the broadening of the signals in the 1D NMR spectra. This result can be transferred to the α,β -unsaturated enones, owing to similarity of the structure. Therefore, it can be assumed, that the order of addition of the reagents should not be important for the enantioselective outcome of the reaction, as the stereoselective step is not occurring until both reagents, the organozinc reagent and the α,β -unsaturated system, are added to the reaction. But as mentioned above, it stays, even with well-equipped spectrometers, challenging to observe intermediates that are occurring with the precatalyst, enone and organozinc reagent. In any case, it seems like the copper catalyst is behaving different than the well-investigated cuprates.

3.4.6 Mechanistic Studies on a Trifluoromethylsulfochlorination of Non-activated Alkenes by Copper Complexes in a Photoredox Catalyzed Process^{vi}

Introduction

The use of copper-based photosensitizer in the field of organic transformation reactions is increasing during the last years, owing to their lower costs compared to iridium and ruthenium complexes and the ability to tune their excited state properties efficiently with ligand modification (for recent developments see review [61]). The understanding of the catalytic steps of such highly efficient reactions can be helpful for the development of new targeted ligands for further reagents or reactions. Therefore, often the NMR spectroscopy is the method of choice for mechanistic studies in solution. Recently, our group developed an LED based NMR illumination device,^[62] which enables the illumination of the sample in the NMR spectrometer during the measurement and therefore mechanistic studies on photo-catalyzed reactions are highly improved.

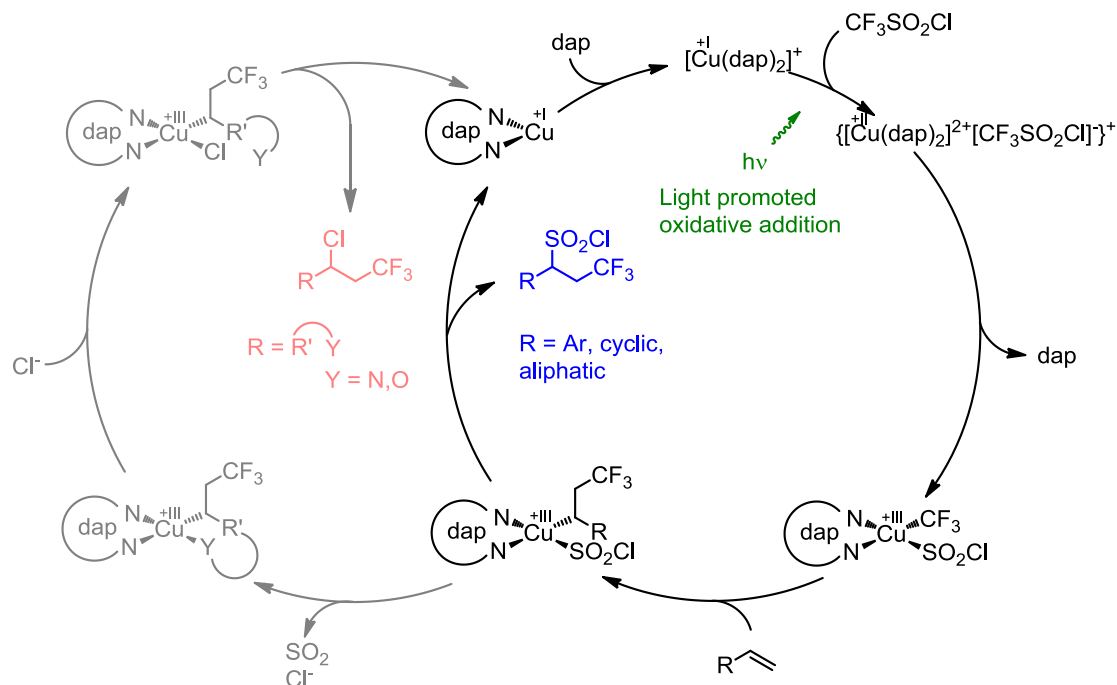


Scheme 3.11: Trifluoromethylsulfochlorination of allylbenzene by a copper-catalyzed photoredox reaction, with $[\text{Cu(dap)}_2]^+$ (on the right).

Very recently, Reiser *et al.* developed a trifluoromethylsulfochlorination of non-activated alkenes by using $[\text{Cu(dap)}_2]\text{X}$ ($\text{X} = \text{Cl}^-$, PF_6^-) as a visible-light photoredox catalyst (Scheme 3.11). The postulated mechanistic cycle (Scheme 3.12) shows after the irradiation of the copper complex the reduction of triflyl chloride (to $\text{CF}_3\text{SO}_2\text{Cl}^-$) and the oxidation of Cu^{I} to Cu^{II} , which in the second step is further oxidized to a Cu^{III} species by the release of one ligand. This Cu^{III} species is first supposed to coordinate a CF_3 and a SO_2Cl group and then to precoordinate the alkene after its addition. In the last step the product is formed, and after the addition of the dap ligand the initial Cu^{I} complex is formed back. In this reaction, the release of SO_2 seems to be suppressed and thus it is possible to transfer the SO_2Cl group to the alkene. Therefore, the elucidation of the

^{vi} This project was performed in close collaboration with the group of Prof. Dr. Oliver Reiser. I performed the NMR spectroscopic investigations. The synthesis of the dap ligand was done by Georgii Kachkovskiy and Thomas Rawner. The ^{19}F NMR spectra of $[\text{Cu(dap)}_2]\text{PF}_6$ and TfCl after six days and CuCl with TfCl (Figure 3.26d and e) were done by Georgii Kachkovskiy.

occurring steps is of great interest to understand the reasons for this special product. So far trifluoromethylations with triflyl chloride are only known with a release of SO₂ in reactions catalyzed by ruthenium catalysts or by copper catalysts with different reagents (Figure 3.11, left side).^[63]



Scheme 3.12: Postulated mechanism for the trifluoromethylsulfochlorination of non-activated alkenes with triflyl chloride via photoredox catalysis. The here presented investigations are performed on the first steps of the right side of the circle.

The here presented NMR spectroscopic investigation focused on the elucidation of the species in the first two steps of the proposed mechanism. In general, the oxidation of Cu^I to Cu^{II} is accompanied by a tremendous line broadening, owing to the paramagnetism of Cu^{II}.^[26] The release of one dap ligand could either be observed by diffusion ordered spectroscopy (DOSY), as smaller molecules show a larger diffusion coefficient or by the arising of the signals of the unbound ligand in the ¹H NMR spectra, owing to different signals for free and coordinated ligand. ¹⁹F NMR spectroscopy can be applied for the elucidation of the species with a CF₃ group, as the transfer of CF₃ from triflyl chloride to the copper complex should be observable by a new arising signal which can then be compared to a reference sample. Furthermore, with the help of the LED illumination device, all those experiments can be performed immediately after the illumination. However, owing to the high quadrupole moment of ^{63/65}Cu and an electric field gradient of the asymmetric complex, an extreme line broadening is expected, as the relaxation of

neighboring atoms is faster.^[26] Therefore, the challenge of this investigation is to find a model system which enables an NMR spectroscopic investigation of this reaction.

Results and discussion

¹⁹F NMR spectra. The fluorine atoms can be used as a sensor, as the transfer of the CF₃ group is monitored by a shift of the signal in the ¹⁹F NMR spectra. Moreover, if the CF₃ group is bound to the copper atom a line broadening is expected, owing to the quadrupole moment of copper and the electric field gradient of the asymmetric complex.^[26] Figure 3.26a shows all plausible species with a CF₃ group which might occur in solution after the addition of triflyl chloride (4) to the copper complex [Cu(dap)₂]PF₆.

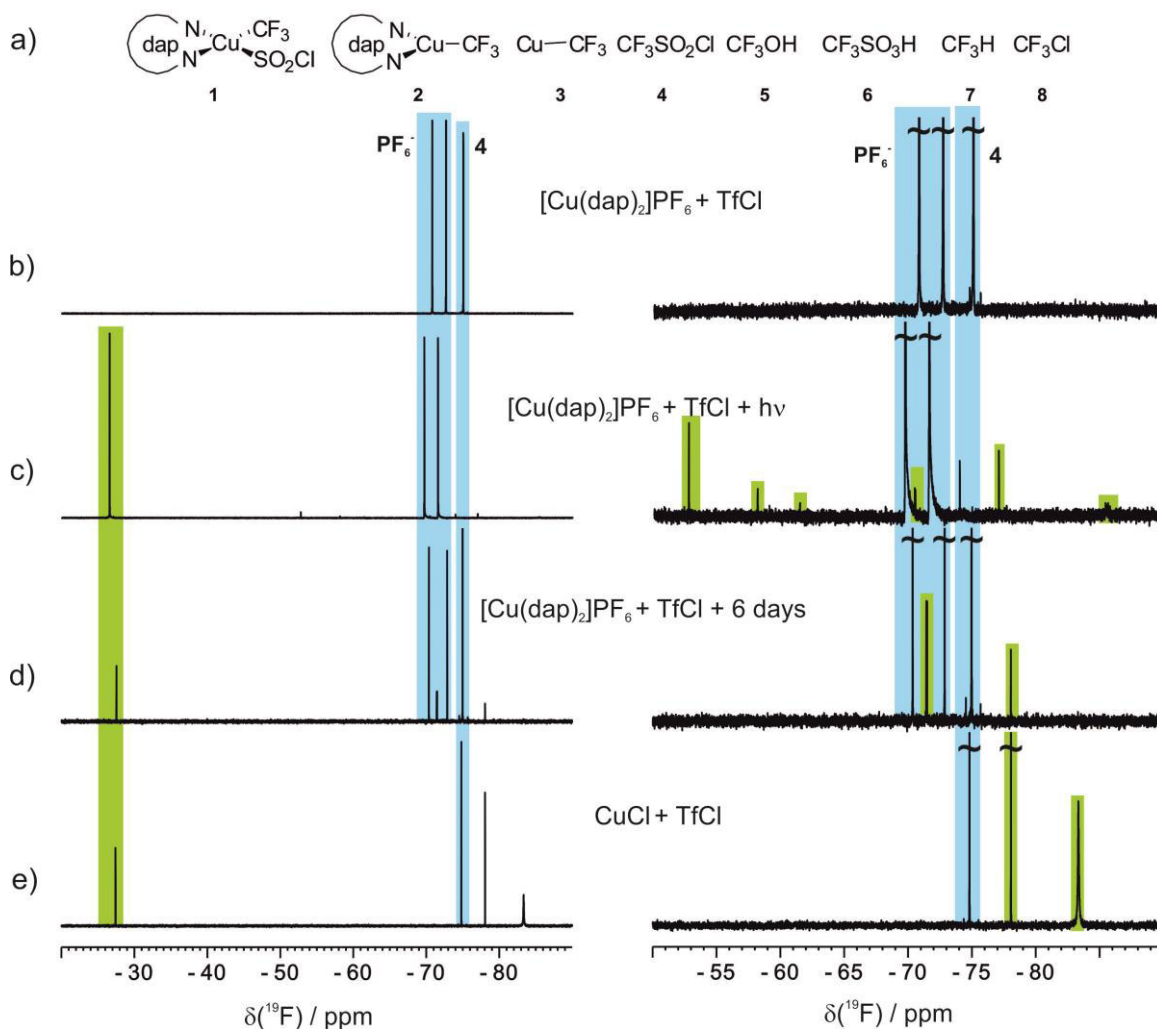


Figure 3.26: a) Plausible species which might occur in solution after the addition of TfCl to the copper complex, b)-d) [Cu(dap)₂]PF₆ with TfCl; b) after preparation, c) after illumination with 455 nm, d) after 6 days (without illumination); e) CuCl with TfCl; in acetonitrile at 300 K, b)-e) on the right fourfold enlarged section of the spectra on the left. All new arising signals are highlighted in green, the signals of PF₆⁻ and TfCl in blue.

After illuminating the sample of $[\text{Cu}(\text{dap})_2]\text{PF}_6$ with triflyl chloride (**4**) various signals appeared (Figure 3.26c, enlightened in green). The main signal arose at -26.5 ppm, accompanied by a nearly completely vanishing of **4** at -75.0 ppm. Further new signals appeared at -52.7 , -58.1 , -61.4 , -70.4 , -77.0 and -85.4 ppm (Figure 3.26c, right). If the sample is not illuminated and stored for six days, new signals appeared at -27.5 , -71.4 , -78.0 ppm (Figure 3.26d), and -137.0 ppm (data not shown), here the signal of **4** was only slightly vanishing compared to the illuminated spectrum. In the spectra of CuCl with **4** without ligands, signals at -27.4 , -78.1 and -83.4 ppm arose, again **4** is not converted completely.

The chemical shift values of the literature known complexes $[(\text{phen})_2\text{Cu}][\text{Cu}(\text{CF}_3)_2]$ and $[(\text{phen})\text{CuCF}_3]$ arise at -30.8 ppm and -22.6 ppm, respectively.^[64] Thus the signal in Figure 3.26c at -26.5 ppm was assigned either to species **1** or **2**. To differentiate between the two species, the reference spectrum of species **2** is necessary,^{vii} as the fluorine experience a different electronic environment if a SO_2Cl group is bound to the copper atom or not, hence, their signals show different chemical shift values. But the considered signal had a narrow line width ($\Delta\nu_{1/2} = 5.1$ Hz) while, a broad line width was expected for copper complexes like **1** or **2**. Furthermore, it is puzzling that the signal of **4** was nearly completely vanishing, as an excess was given to the solution. A similar signal at -27.5 ppm ($\Delta\nu_{1/2} = 2.7$ Hz) was observed without illumination after six days and also in the sample with CuCl with **4** (-27.4 ppm, $\Delta\nu_{1/2} = 2.5$ Hz). A further possible explanation is the formation of CF_3Cl (**8**) (lit: -28.1 ppm)^[65], in further experiments the addition of **8** as a reference will help to exclude this possibility. The signal of the illuminated sample (Figure 3.26c) at -70.4 ppm was also arising after six days (Figure 3.26d) at -71.4 ppm but in the later with greater amount. Species **5** (CF_3OH) was assigned to the signal at -52.7 ppm compared to the literature (lit: -54.5 ppm)^[65]. A very broad line width was observed for the signal at -85.4 ppm ($\Delta\nu_{1/2} = \sim 70\text{-}90$ Hz). Thus it was assigned to a CF_3 group which is bound to copper, also in the spectrum of CuCl with **4** a comparable signal at -83.4 ppm ($\Delta\nu_{1/2} = 25$ Hz) arose (Figure 3.26e), the two signals might belong to the same species and were assigned to CuCF_3 (**3**). The signals in Figure 3.26c, d and e, at around -78 ppm were assigned to either $\text{CF}_3\text{SO}_3\text{H}$ (**6**) (lit: -78.8 ppm)^[65] or CF_3H (**7**) (lit: -78.6 ppm)^[65], a degradation product. All other new appearing signals were not assigned

^{vii} Currently the synthesis of compound **2** is performed by Thomas Rawner (group of Prof. Dr. Oliver Reiser), but so far it was not possible to prepare this compound.

so far. The shift of TfCl from -76.2 ppm to -75.0 ppm after the addition to $[\text{Cu}(\text{dap})_2]\text{PF}_6$ hints to a reaction or interaction already before the illumination of the sample, as it was also observed in the ^1H NMR spectra (Figure 3.27b).

The species at -85.4 ppm is considered to be the most relevant one for the reaction, as it might belong to the copper complexes **1** or **2** which are assumed to be catalytic active species for the reaction. The observation of this species in spectra without the dap ligand (Figure 3.26e) is in accordance to the known reactivity without ligand. For the understanding of the mechanism it is of high importance why the SO_2Cl group is in this special reaction added to the alkene and if the coordination of copper is responsible for this effect. Further investigations will be performed for the elucidation. First experiments will be performed on the sample of CuCl as the signals at -27 ppm and -83 ppm show a high intensity. A ^{19}F , ^{13}C HSQC spectrum will show if the signals of the ^{13}C spectrum are also broadened and the corresponding chemical shift values can be compared to those of known Cuprate species. ^{19}F DOSY measurements can elucidate the size of the molecule, and thus also provides the information of the numbers of coordinated ligands on the complex. Furthermore, the reference spectrum of species **2** and of **8** will help to assign also the signal around -27 ppm.

^1H NMR spectra. Proton spectra are very often used for reaction monitoring, owing to their sensitivity and the abundance of protons in organic systems. For investigations on the above described reaction (Scheme 3.11), ^{19}F NMR spectra are the only access to monitor the transfer of the CF_3 group from triflyl chloride to the copper complex, while ^1H NMR spectra provide information about changes of the electronic environment of the ligand. For example if one dap ligand is released during the reaction, the signals of the free ligand should occur.

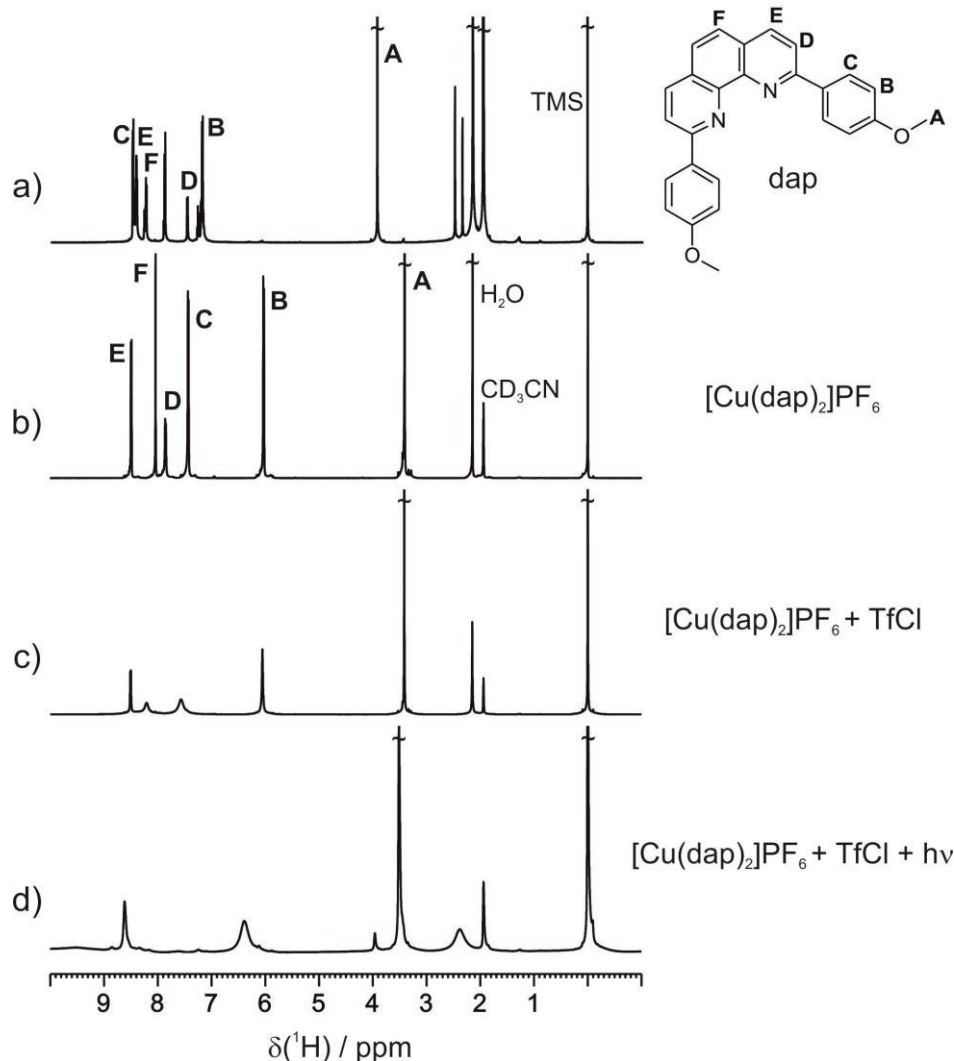


Figure 3.27: ^1H NMR spectra of a) the dap ligand and b)-c) $[\text{Cu}(\text{dap})_2]\text{PF}_6$, b) after the addition of TfCl , and c) after illumination with 455 nm; in acetonitrile at 300 K.

Figure 3.27 shows the ^1H NMR spectra of the same sample of $[\text{Cu}(\text{dap})_2]\text{PF}_6$ (a), after the addition of triflyl chloride (b) and after illumination (c). The assignment of the signals in the spectrum of Figure 3.27a was verified by a $^1\text{H}, ^1\text{H}$ COSY spectrum. After the addition of triflyl chloride to the sample especially the signals C, D and F show a decreased intensity and a line broadening, while all other signals remain as narrow as before. If the sample is illuminated, a further change in the spectrum is observable. Most conspicuous is the broadening of signals of the ligand and of H_2O at 2.15 ppm which is accompanied by a shift to 2.39 ppm.

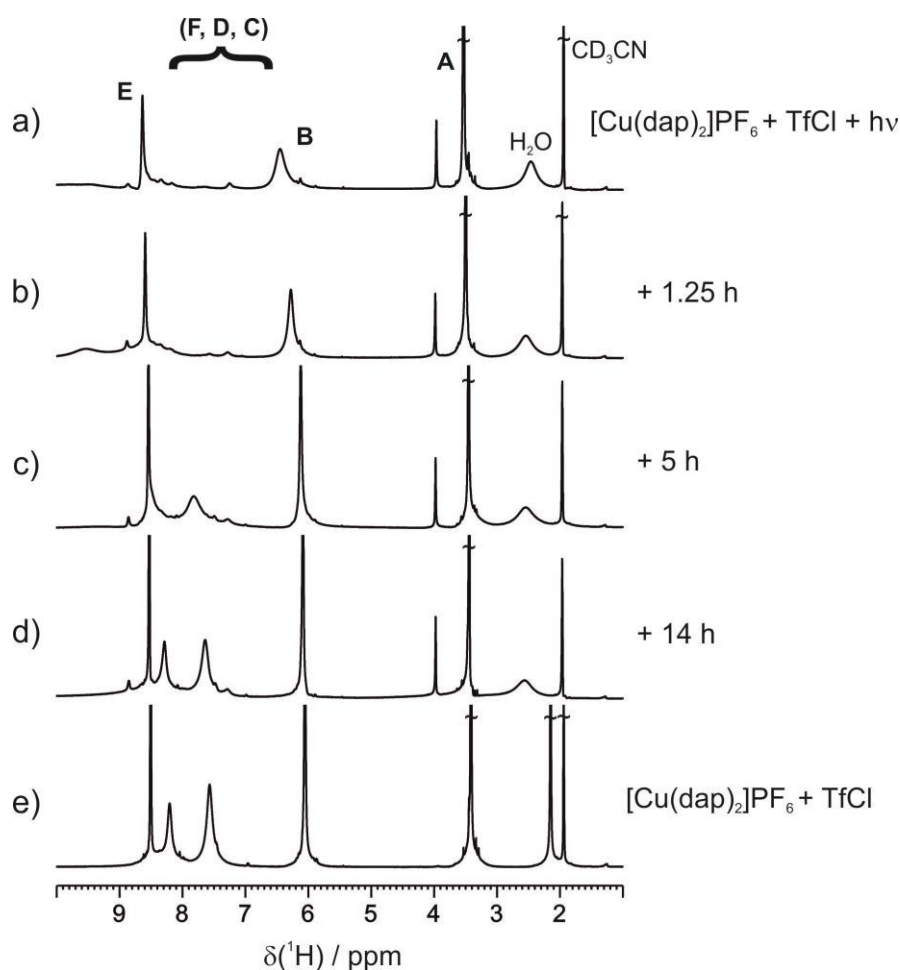


Figure 3.28: ^1H NMR spectra of $[\text{Cu}(\text{dap})_2]\text{PF}_6$ with TfCl a)-d) during illumination with 455 nm, a) directly after illumination, b) after 1.25 hours, c) after 5 hours and d) after 14 hours, e) without illumination; in acetonitrile at 300 K.

Figure 3.28 shows the kinetic of the illuminated sample. After 1.25 hours no change in comparison to the spectrum directly after the illumination was observable. While after five hours the signal of **B** occurred with a narrowed line width and it is obvious that the back reaction already started, because the signals between 9.0 and 7.0 ppm were changing. After fourteen hours the same signals compared to the spectrum before the illumination were observed. This means, that the species which arose owing to the illumination were only stable for a few hours then the initial ones were formed back.

For a splitting of the broadened signals a further examination by cooling the sample to 300, 280, 260 and 240 K was performed (data not shown). Unfortunately, $[\text{Cu}(\text{dap})_2]\text{Cl}$ was used as copper complex, which led to precipitation after the addition of triflyl chloride, which caused shim errors. However, even if the resolution of the spectrum was not very high, a splitting of the signals was not observed. Additional to all above described studies, the samples of dap ligand and of $[\text{Cu}(\text{dap})_2]\text{X}$ ($\text{X} = \text{Cl}^-$, PF_6^-) were

illuminated and examined. Thereby, no effect of the light on these systems was observable. Furthermore, dap with triflyl chloride showed no reaction (data not shown).

Without illumination already a reaction between $[\text{Cu}(\text{dap})_2]\text{PF}_6$ and triflyl chloride was taking place, monitored in the ^1H NMR spectrum by a broadening of the signals **C**, **D** and **F**, but not in the ^{19}F NMR spectra. This might be also explained by the coupling between ^{19}F and ^1H through space, as a consequence, fluorine decoupled ^1H NMR spectra ($^1\text{H}\{^{19}\text{F}\}$) are necessary for the observation of the individual species. Also ^1H , ^{19}F HOESY spectra will show if the CF_3 group is in proximity to the dap ligand of the copper complex. The illumination of the sample led to a further change of the signals. Those occurring species were stable for less than five hours, before the species which were observed before the illumination were formed back. In none of these spectra the signals of a free dap ligand were observed, which is a hint that the releasing of one ligand does not take place, as it is supposed in the mechanism. The cooling of the sample led to a precipitation, however, no splitting of the broadened signals was observable. For the repetition of this experiment it is recommended to either use $[\text{Cu}(\text{dap})_2]\text{PF}_6$ or to filter the solution before it is transferred to the NMR tube, to avoid shim errors, owing to precipitation after the addition of triflyl chloride.

^1H and ^{19}F DOSY spectra. The application of DOSY spectra on this system, would offer an access to the signal assignment in the ^{19}F spectra, whether the CF_3 group is bound to the complex, and to the question of the release of one dap ligand from the copper complex during the first steps of the mechanism, by comparing the received diffusion coefficients with the ones of the ligand or the copper complex. Furthermore, the molecular masses of the species can be estimated in this way.^[66]

Despite great efforts, so far these experiments were not successful. The reasons are one the one hand the used inlet in the NMR tube, which enables to illuminate the sample without a contact between the solution and the optical fiber, and on the other hand the illumination leads to a partial warming of the sample. Both of them cause a distortion in the diffusion of the molecules. Furthermore, the sample shows a precipitation after the addition of triflyl chloride, which results in a shim error. Moreover, DOSY measurements require baseline separated signals in the proton spectrum, but the only signal with this feature is signal **A**, all others are overlapping.

So far, the few received diffusion coefficients showed that the size of the molecule did not change during the reaction. This leads to the suggestion that either no ligand was

released or that already from the beginning only one ligand was bound to the copper atom. Even if the crystal structure shows a copper complex with two ligands, it is not uncommon for copper complexes to show a deviating structure in solution compared to the solid state.^[12,13,67] But further experiments are necessary to prove these observations.

In further investigations the ^{19}F DOSY measurements can be performed at the TBI-F probe head at the 600 MHz spectrometer, as there a better temperature control unit is available. Moreover, a further advice is to filter the solution if a precipitation is observed.

Summary and outlook

In summary, so far an elucidation of the reaction mechanism of the trifluoromethyl-sulfochlorination was not possible, as several difficulties arose during NMR spectroscopic measurements.

The addition of triflyl chloride to $[\text{Cu}(\text{dap})_2]\text{PF}_6$ showed a reaction already before the illumination, in the ^1H NMR spectrum immediately after the addition, and in the ^{19}F NMR spectrum after six days. The illuminated the sample showed a further reaction. In the ^{19}F spectrum a new signal appeared, while in the ^1H NMR spectrum a broadening of the signals was observable. The elucidation and assignment of the occurring species was so far not possible. Variable temperature measurements did not show a splitting of signals. ^1H and ^{19}F DOSY measurements failed, owing to technical problems. The few received data did not support the proposed release of one ligand, as they did not show a variation of the size of the complex.

The elucidation of the catalyzing species of this reaction will be part of future work. Therefore, the new equipment (a fluorine sensitive TBI-F probe head) of our working group will enable the ^{19}F DOSY measurements at various stable temperatures and at a higher frequency. Also, test DOSY measurements will be performed without inlet, with inlet and during illumination to recognize the source of errors. If the warming is the reason for the occurring errors in diffusion, the sample should be illuminated outside the spectrum and measured without inlet in the NMR tube. However, this method is only feasible if the occurring species are stable over a long period. Furthermore, ^{19}F , ^{13}C HSQC and ^1H , ^{19}F HOESY spectra can help to observe the ^{13}C signals and compare the broadening of these signals to those of ^{19}F , and to see whether protons of the dap ligand are in proximity to the fluorine atoms of the CF_3 group. The synthesis of species **2** is currently performed in the group of Prof. Dr. Oliver Reiser. The reference spectrum of species **2** and CF_3Cl will help to distinguish and to assign the occurring species in the ^{19}F

NMR spectra. Also the addition of CF_3Cl to the sample as an internal reference is possible, as this compound is very stable and should not interfere the measurement. As our group has experience with freons, it should be possible to handle this gaseous substance. For further examinations it is recommended to prepare the sample in a separated Schlenk tube and to filter it before it is transferred to the NMR tube, this will avoid precipitations in the NMR tube, which are leading to shim errors, owing to field inhomogeneity by small particles in solution. Our experience on the copper-catalyzed ACA reactions showed, that the variation of the used cooper salt, the temperature and the solvent helps to find a model system for NMR spectroscopic investigations. For copper complexes it is known that they are forming various complexes and aggregates in solution, but for DOSY measurements, baseline separated signals are necessary, therefore such a model system is necessary to perform these measurements, even if they are not leading to high yields and *ee*-values in synthetic procedures.^[12,13,67] Furthermore, the use of green light (530 nm) is more promising, since the blue light is mostly used in reactions with ruthenium complexes.

3.4.7 Experimental Part for the Additional Findings

Sample preparation

Preparation of the precatalytic complex $[\text{Cu}_2\text{I}_2\text{L}_3]$. A Schlenk tube equipped with magnetic stirring bar and septum was charged with 2 eq $\text{L}^{(SS)}$ (0.036 mmol, 15.81 mg) and 1 eq copper iodide (0.018 mmol, 3.43 mg), freshly distilled solvent CD_2Cl_2 (0.6 ml) was added and the mixture stirred for 2 h at room temperature until a clear solution was obtained. Subsequently the samples were transferred to an NMR tube.

Preparation of the samples for investigations with ZnMe_2 . After the preparation of the precatalytic complex or solving the ligand $\text{L}^{(SS)}$ (0.036 mmol, 15.81 mg) in CD_2Cl_2 , the required amount of ZnMe_2 (1.2 M, 2.0 M in toluene or neat 2 M in CD_2Cl_2) was given directly to the NMR tube. The NMR tube was cooled to 230 K by a freezing mixture of benzene and liquid nitrogen.

Preparation of the samples for investigations on the different ligand moieties.

$\text{P}(\text{OPh})_3$ (**1**) (0.01 mL, 0.04 mmol), PPh_3 (**2**) (10.5 mg, 0.04 mmol) or the amine side-chain (**3**) (0.01 mL, 0.04 mmol), respectively, were dissolved with ZnMe_2 (neat, 2 M in CD_2Cl_2) (0.03 mL) under argon atmosphere in 0.6 mL freshly distilled CD_2Cl_2 directly in the NMR tube.

For the experiment with Cu salt, an argon flushed Schlenk tube equipped with magnetic stirring bar and septum was charged with 2 eq $\text{P}(\text{OPh})_3$ (**1**) (0.01 mL, 0.04 mmol) and 1 eq CuI (3.42 mg, 0.02 mmol) in freshly distilled CD_2Cl_2 (0.6 mL) and stirred for 1 h at room temperature. The mixture was transferred to an argon flushed NMR tube and stored over night at -80°C . ZnMe_2 (neat, 2 M in CD_2Cl_2) (0.03 mL) was given directly to the mixture in the NMR tube.

Preparation of the samples for investigations with MeLi and 12-crown-4. After the preparation and measuring of the precatalytic complex, MeLi (1.6 M in Et_2O) was given either a substoichiometric amount or an excess directly to the NMR tube. The NMR tube is thereby cooled to 170 K by a freezing mixture of benzene and liquid nitrogen. The solution turns yellow if a substoichiometric amount is added. If an excess is added the solution turns first yellow but fast decolorize again.

To the solution an excess of 12-crown-4 is given under argon atmosphere. If a substoichiometric amount of MeLi was before added, the solution turns from colorless to yellow, otherwise it stays yellow.

Preparation of ^{15}N -tosyl imine.^{viii} The ^{15}N labelled *N*-tosyl imine was prepared after the literature known procedure.^[68] With an ratio of E : Z of 60 : 40 (lit: 62 : 38).

Table 3.1: ^1H signal assignment of *N*-tosyl imine in CD_2Cl_2 at 230 K, values in [ppm].

	2	3	4	5	6	8	9	11
E-isomer	6.98	6.06	2.31	1.90	3.07	7.33	7.76	2.40
Z-isomer	7.12	7.15	2.36		2.47			

Preparation of the samples for the investigation with ^{15}N -tosyl imine. After the preparation and measuring of the precatalytic complex $[\text{Cu}_2\text{X}_2\text{L}_3]$, 0.1, 0.2 and 0.5 eq of ^{15}N -tosyl imine were given to the sample directly in the NMR tube. The solution stays thereby clear and colorless.

Preparation of the samples for investigations on the trifluorosulfochlorination.^{ix} The copper complex $\text{Cu}(\text{dap})_2\text{X}$ ($\text{X} = \text{PF}_6$ or Cl) was prepared by solvation of CuX and dap in a 1:2 ratio in CH_3Cl and stirred it at room temperature for 30 minutes. Then the solvent was evaporated.

For the NMR spectroscopic investigations, the samples were prepared in amberized Rototec-Spintec 5 mm NMR tube 7 inch 535-PP-7 to protect the samples from unwanted exposition to light. 30.32 mg (0.03 mmol) $\text{Cu}(\text{dap})_2\text{PF}_6$ or 26.58mg (0.03 mmol) $\text{Cu}(\text{dap})_2\text{Cl}$ were solved in 0.5 mL CD_3CN directly in the NMR tube. Then, the sample was purged with argon for 1 hour and afterwards a transparent inlet inserted for the LED illumination device. For the DOSY measurements a tiny amount of TMS was given to the sample.

After the investigation of the complex, an excess of TfCl (about 0.01 mL) was given to the same sample.

^{viii} The preparation of the ^{15}N labelled *N*-tosyl imine was performed by Fabio Morana.

^{ix} The preparation of the dap ligand was performed by Georgii Kachkovskyi and Thomas Rawner (AK Reiser).

NMR data collection and processing

The NMR spectra which are presented in chapter 3.4.1-3.4.4 and 3.4.6, were recorded according to the parameters described in chapter 3.3 (Supporting Information).

The NMR spectra which are presented in chapter 3.4.5, were recorded on a Bruker Avance III HD 600 spectrometer (600.13 MHz for ^1H) equipped with a 5 mm double resonance broad band Prodigy (BBO) z-gradient probe. The temperatures for all measurements were controlled by a Bruker VTU temperature unit.

2D ^1H , ^{15}N HMBC spectra: pulse program = inv4gplrndqf, relaxation delay = 3 s, NS = 8, DS = 16, TD 4k (F2) and 128 (F1).

^1H , ^1H NOESY spectra: pulse program = noesygpqh, relaxation delay = 2 s, NS = 16, DS = 16, TD 4k (F2) and 256 (F1).

The ^1H chemical shifts were referenced to the residual solvent signal of CD_2Cl_2 (5.32 ppm), for the ^{31}P and ^{15}N chemical shifts the Ξ value of an external standard was applied. NMR data were processed and evaluated with Bruker Topspin 3.1/3.2.

The ^{19}F NMR spectra of chapter 3.4.6 were recorded either on a Bruker Avance 300 spectrometer (300.13 MHz for ^1H) equipped with a 5 mm QNP probe or on a Bruker Avance 400 spectrometer (400.13 MHz for ^1H) equipped with a 5 mm BBI probe.

3.5 References

- [1] A. Alexakis, J. E. Backvall, N. Krause, O. Pamies, M. Dieguez, *Chem. Rev.* **2008**, *108*, 2796–2823.
- [2] J. Christoffers, G. Koripelly, A. Rosiak, M. Rössle, *Synthesis (Stuttg.)* **2007**, *9*, 1279–1300.
- [3] C. Hawner, A. Alexakis, *Chem. Commun.* **2010**, *46*, 7295–7306.
- [4] T. Jerphagnon, M. G. Pizzuti, A. J. Minnaard, B. L. Feringa, *Chem. Soc. Rev.* **2009**, *38*, 1039–1075.
- [5] E. Gallo, F. Ragaini, L. Bilello, S. Cenini, C. Gennari, U. Piarulli, *J. Organomet. Chem.* **2004**, *689*, 2169–2176.
- [6] M. Shi, W. Zhang, *Adv. Synth. Catal.* **2005**, *347*, 535–540.
- [7] T. Pfretzschner, L. Kleemann, B. Janza, K. Harms, T. Schrader, *Chem. - A Eur. J.* **2004**, *10*, 6048–6057.
- [8] J. F. Teichert, B. L. Feringa, *Angew. Chem. Int. Ed.* **2010**, *49*, 2486–2528.
- [9] S. R. Harutyunyan, F. López, W. R. Browne, A. Correa, D. Peña, R. Badorrey, A. Meetsma, A. J. Minnaard, B. L. Feringa, *J. Am. Chem. Soc.* **2006**, *128*, 9103–9118.
- [10] P. Knochel, R. D. Singer, *Chem. Rev.* **1993**, *93*, 2117–2188.
- [11] H. Zhang, R. M. Gschwind, *Chem. – A Eur. J.* **2007**, *13*, 6691–6700.
- [12] K. Schober, H. Zhang, R. M. Gschwind, *J. Am. Chem. Soc.* **2008**, *45*, 12310–12317.
- [13] H. Zhang, R. M. Gschwind, *Angew. Chem. Int. Ed.* **2006**, *45*, 6391–6394.
- [14] K. Schober, E. Hartmann, H. Zhang, R. M. Gschwind, *Angew. Chem. Int. Ed.* **2010**, *49*, 2794–2797.
- [15] W.-J. Shi, L.-X. Wang, Y. Fu, S.-F. Zhu, Q.-L. Zhou, *Tetrahedron: Asymmetry* **2003**, *14*, 3867–3872.
- [16] M. Welker, S. Woodward, L. F. Veiros, M. J. Calhorda, *Chem. - A Eur. J.* **2010**, *16*, 5620–5629.
- [17] S. Woodward, in *Copper-Catalyzed Asymmetric Synth.* (Eds.: A. Alexakis, N. Krause, S. Woodward), Wiley-VCH: Weinheim, **2014**, p. 3.
- [18] K. S. Lee, M. K. Brown, A. W. Hird, A. H. Hoveyda, *J. Am. Chem. Soc.* **2006**, *128*, 7182–7184.

- [19] S. H. Bertz, G. Dabbagh, X. He, P. P. Power, *J. Am. Chem. Soc.* **1993**, *115*, 11640–11641.
- [20] J. B. Johnson, R. T. Yu, P. Fink, E. A. Bercot, R. T., *Org. Lett.* **2006**, *8*, 4307–4310.
- [21] M. Schinnerl, M. Seitz, A. Kaiser, O. Reiser, *Org. Lett.* **2001**, *3*, 4259–4262.
- [22] C. Bolm, J. P. Hildebrand, K. Muñiz, N. Hermanns, *Angew. Chem. Int. Ed.* **2001**, *40*, 3284–3308.
- [23] A. Alexakis, C. Benhaim, S. Rosset, M. Humam, *J. Am. Chem. Soc.* **2002**, *124*, 5262–5263.
- [24] J. Furrer, *J. Concept. Magn. Reson. A* **2012**, *40A*, 101–127.
- [25] T. Thaler, B. Haag, A. Gavryushin, K. Schober, E. Hartmann, R. M. Gschwind, H. Zipse, P. Mayer, P. Knochel, *Nat. Chem.* **2010**, *2*, 125–130.
- [26] R. M. Gschwind, *Chem. Rev.* **2008**, *108*, 3029–3053.
- [27] T. Gärtner, R. M. Gschwind, in *Chem. Organocopper Compd.* (Eds.: Z. Rappoport, I. Marek), Wiley-VCH, **2009**, p. 163.
- [28] S. H. Bertz, M. D. Murphy, C. A. Ogle, A. A. Thomas, *Chem. Commun.* **2010**, *46*, 1255–1256.
- [29] M. Goldman, *J. Magn. Reson.* **1984**, *60*, 437–452.
- [30] N. Tjandra, A. Szabo, A. Bax, *J. Am. Chem. Soc.* **1996**, *118*, 6986–6991.
- [31] N. Tjandra, A. Bax, *J. Am. Chem. Soc.* **1997**, *119*, 8076–8082.
- [32] M. Tessari, H. Vis, R. Boelens, R. Kaptein, G. W. Vuister, *J. Am. Chem. Soc.* **1997**, *119*, 8985–8990.
- [33] R. M. Gschwind, M. Armbrüster, I. Z. Zubrzycki, *J. Am. Chem. Soc.* **2004**, *126*, 10228–10229.
- [34] F. Löhr, S. G. Mayhew, H. Rüterjans, *J. Am. Chem. Soc.* **2000**, *122*, 9289–9295.
- [35] G. Federwisch, R. Kleinmaier, D. Drettwan, R. M. Gschwind, *J. Am. Chem. Soc.* **2008**, *130*, 16846–16847.
- [36] S. Bouguet-Bonnet, S. Leclerc, P. Mutzenhardt, D. Canet, *J. Magn. Reson.* **2005**, *173*, 29–33.
- [37] B. Brutscher, *Concept. Magn. Reson.* **2000**, *12*, 207–229.
- [38] K. Schober, PhD Thesis, University of Regensburg, Germany, **2011**.

-
- [39] S. H. Bertz, *J. Am. Chem. Soc.* **1990**, *112*, 4031–4032.
- [40] S. H. Bertz, S. Cope, D. Dorton, M. Murphy, C. A. Ogle, *Angew. Chem. Int. Ed.* **2007**, *46*, 7082–7085.
- [41] E. R. Bartholomew, S. H. Bertz, S. Cope, D. C. Dorton, M. Murphy, C. A. Ogle, *Chem. Commun.* **2008**, 1176–1177.
- [42] E. Hartmann, R. M. Gschwind, *Angew. Chem. Int. Ed.* **2013**, *52*, 2350–2354.
- [43] E. Hartmann, M. M. Hammer, R. M. Gschwind, *Chem. - A Eur. J.* **2013**, *19*, 10551–10562.
- [44] F. Hastreiter, Master Thesis, University of Regensburg, Germany, **2014**.
- [45] D. F. Evans, G. V. Fazakerley, *J. Chem. Soc. A* **1971**, 182–183.
- [46] C. Bournaud, C. Falciola, Thomas-Lecourt, S. Rosset, A. Alexakis, L. Micouin, *Org. Lett.* **2006**, *8*, 3581–3584.
- [47] D. Müller, M. Tissot, A. Alexakis, *Org. Lett.* **2011**, *13*, 3040–3043.
- [48] A. Alexakis, S. Rosset, J. Allamand, S. March, F. Guillen, C. Benhaim, *Synlett* **2001**, *2001*, 1375–1378.
- [49] F. Mutzbauer, Diploma Thesis, University of Regensburg, Germany, **2008**.
- [50] F. von Rekowski, C. Koch, R. M. Gschwind, *J. Am. Chem. Soc.* **2014**, *136*, 11389–11395.
- [51] C. Koch, Master Thesis, University of Regensburg, Germany, **2011**.
- [52] S. H. Bertz, C. M. Carlin, D. A. Deadwyler, M. D. Murphy, C. A. Ogle, P. H. Seagle, *J. Am. Chem. Soc.* **2002**, *124*, 13650–13651.
- [53] G. L. Closs, L. E. Closs, *J. Am. Chem. Soc.* **1960**, *82*, 5723–5728.
- [54] H. O. House, W. L. Respess, G. M. Whitesides, *J. Org. Chem.* **1995**, *31*, 3128–3141.
- [55] G. Hallnemo, T. Olsson, C. Ullenius, *J. Organomet. Chem.* **1985**, *282*, 133–144.
- [56] S. H. Bertz, R. A. J. Smithlc, *J. Am. Chem. Soc.* **1989**, *111*, 8276–8277.
- [57] S. H. Bertz, S. Cope, M. Murphy, C. A. Ogle, B. J. Taylor, *J. Am. Chem. Soc.* **2007**, *129*, 7208–7209.
- [58] T. Gärtner, W. Henze, R. M. Gschwind, *J. Am. Chem. Soc.* **2007**, *129*, 11362–3.
- [59] W. Henze, T. Gärtner, R. M. Gschwind, *J. Am. Chem. Soc.* **2008**, 13718–13726.
-

- [60] J. Westmeier, P. von Zezschwitz, *Chem. Commun.* **2014**, 50, 15897–15900.
- [61] S. Paria, O. Reiser, *Chem. Cat. Chem.* **2014**, 6, 2477–2483.
- [62] C. Feldmeier, H. Bartling, R. M. Gschwind, *J. Magn. Reson.* **2013**, 232, 39–44.
- [63] N. Kamigata, T. Fukushima, Y. Terakawa, M. Yoshida, H. Sawada, *J. Chem. Soc. Perkin Trans. 1* **1991**, 627–633.
- [64] H. Morimoto, T. Tsubogo, N. D. Litvinas, J. F. Hartwig, *Angew. Chem. Int. Ed.* **2011**, 50, 3793–3798.
- [65] H. J. Reich, “<http://www.chem.wisc.edu/areas/reich/handouts/nmr/> (17.04.2015),” **2012**.
- [66] C. A. Crutchfield, D. J. Harris, *J. Magn. Reson.* **2007**, 185, 179–182.
- [67] H. Zhang, R. M. Gschwind, *Chem. - A Eur. J.* **2007**, 13, 6691–6700.
- [68] S. Hirner, J. Westmeier, G. Sandra, C. H. Müller, P. von Zezschwitz, *Synlett* **2014**, 25, 1697–1700.

4 Relief for Heteronuclear NMR Spectroscopy by using a Broadband Pulse (xyBEBOP Pulse)

I performed the NMR spectroscopic measurements, the implementation of the pulse at our spectrometer and the validation studies.

The xyBEBOP pulse was developed by the group of Prof. Dr. Burkhard Luy (Karlsruhe Institute of Technology).

The samples in liquid ammonia were prepared by Ute Friedrich.

To be published.

4.1 Abstract

Heteronuclear NMR spectroscopy is a widely used tool for structure elucidation of inorganic molecules in solution. However, the monitoring of reactions like solvation, transformation or degradation processes of two or more non-stable species was so far not possible with standard NMR spectroscopic methods, if they show highly deviating chemical shift values. Now, a broadband pulse with an excitation range of 1000 kHz was developed, which allows for the simultaneous observation of all species, within this excitation range. The reliability of this pulse was tested on samples of Zintl ion cluster in liquid ammonia with ^{119}Sn NMR spectra. Additionally, the reproduction of scalar coupling constants, integrals and line widths was verified, in comparison to a conventional 90° hard pulse which has a poor offset performance. This broadband pulse provides an enormous time benefit, and therefore, it is supposed to facilitate future heteronuclear NMR spectroscopic investigations tremendously.

4.2 Manuscript

4.2.1 Introduction

In the field of inorganic chemistry, heteronuclear NMR spectroscopy is the method of choice for structure elucidation and reaction monitoring in solution. Unfortunately, various heteronuclei exhibit a large chemical shift range, e.g. approximately 2140 kHzⁱ (17000 ppm) for ^{207}Pb , 1540 kHzⁱ (12000 ppm) for ^{195}Pt , 670 kHzⁱ (3000 ppm) for ^{119}Sn and 220 kHzⁱ (900 ppm) for ^{31}P (to mention only a few).^[1] Therefore, a 90° hard pulse is technically unsuitable to excite their complete bandwidth. The reason for this is, on the one hand, the sinc function shaped excitation profile of hard pulses, which leads to a reduced or no excitation at the borders of the excitation region and also the technical restriction of the pulse length, because it cannot be set infinitely short, as it would be needed to excite those huge expanded chemical shift ranges. For that reason, often the desired spectrum is divided into several regions, which are measured block wise and recombined afterwards.^[2–5] However, this recombination method can only be applied on samples which include stable species, as species with highly deviating chemical shift values cannot be observed simultaneously. Particularly, in the case of low concentrated and non-stable samples, which e.g. react or precipitate and have a low solubility, this becomes a significant problem. Here, an enormous increase of the number of scans is

ⁱ kHz values are specified with regard to a spectrometer of 600 MHz for ^1H .

required, leading to measurement times of several hours for one 1D NMR spectrum (e.g. ^{119}Sn : 35k scans in 4 hours 50 minutes for a spectral width of 90 kHz). Hence, no appropriate monitoring of chemical processes can be made, as, owing to the time delay, species outside the considered chemical shift region cannot be detected at the same time.

Recently, a broadband pulse, named xyBEBOP pulse, with an excitation range of 1000 kHz was developed. Now the application and performance of this pulse was tested on real samples, in which extreme chemical shift differences of the species are combined with various scalar coupling pattern, line widths and integrals. As test sample, solutions of Zintl ions in liquid ammonia were selected, and investigated by ^{119}Sn NMR spectroscopy. These systems provide both, a chemical shift range of about 500 kHzⁱ (2200 ppm) and a scalar coupling pattern between the NMR active isotopes ^{119}Sn and ^{117}Sn ($^1J(^{119}\text{Sn}-^{117}\text{Sn}) = 256 - 1466 \text{ Hz}$ for homoatomic cluster),^[2,6,7] which is required for an unambiguous assignment of the cluster sizes. In addition, these samples show a low solubility, which results in extremely long measurement times, owing to the required number of scans, as already mentioned above.

Here, we show the facilitation of measuring heteronuclear NMR spectra by using the xyBEBOP pulse in comparison to a 90° hard pulse. Additional to a remarkable time benefit, the use of this broadband pulse enables a reaction monitoring for signals over the whole chemical shift range and also the signal assignment by coupling constants is possible. The results exemplarily presented in this paper for ^{119}Sn can be transferred to any NMR active nucleus.

4.2.2 Results and Discussion

Model system. For heteronuclear NMR spectroscopic studies of two or more species, which exhibit extremely deviating chemical shift values, it was so far necessary to measure the appropriate spectra block wise and recombine them afterwards, as they cannot be observed parallel with a 90° hard pulse.^[2-5] However, the prerequisite for that are stable species in solution. If this is not the case, as it is known for example for Zintl anions, where solvation, transformation and degradation processes are taking place,^[2] and furthermore the solubility of the species is very low, the assembling does not provide the real situation. Thus, even with a Prodigy BBO probe at an Avance III 600 HD spectrometer, specially equipped for heteronuclear NMR spectroscopy, there is a long time delay between the spectra, owing to an increased number of scans (e.g. ^{119}Sn : 35k scans in 4 hours 50 minutes for a spectral width of 90 kHzⁱ / 400 ppm and S/N = 20-500), which

are necessary to observe an adequate signal-to-noise ratio. At least three to four spectra are needed to scan the known chemical shift range for Zintl anions (approximately 500 kHz, 2200 ppm), so a reaction monitoring is obviously not possible with this method. Additionally, the preparation of those samples is extremely complex, costly and very difficult to reproduce exactly, therefore, all information should be gained from the same sample.

To our knowledge the only pulse, which is able to cover extremely broad excitation ranges of 1000 kHz is the xyBEBOP pulse. So, the performance of this pulse was tested on real samples, showing signals with different line widths and integrals, a whole set of different scalar couplings and partially overlapping signals. The obtained spectra were compared with those observed with a 90° hard pulse, to see whether they are completely reliable or if artefacts occur. Also the dependence of the offset of the signals to the transmitter frequency was investigated, as owing to induced phases by different phase profiles during this pulse, errors might occur.

As model system, a sample of KSnBi in liquid ammonia was used for these validation studies, which was stored for one year to exclude conversions during the measurement. Furthermore, a screening of freshly prepared samples (K₂Sn₃Bi, K₂SnBi₃, K₃SnBi in liquid ammonia) was performed. These samples fulfil all above mentioned criteria for a real sample and cannot be analyzed with a single 90° hard pulse, as they include several species, that occur at highly deviating chemical shift values.

Chemical shift range. Figure 4.1 shows the comparison of the NMR spectra using either a 90° hard pulse processed with automatic phase correction (a, each spectrum SW = 90 kHz, P1 = 13.5 µs, PL = 70 W / -18.45 -dBW) or the xyBEBOP pulse processed with magnitude calculation (b, SW = 1000 kHz, P1 = 25.0 µs, PL = 80 W / -19.03 -dBW). As expected from the excitation profile of the xyBEBOP pulse, the signals **A-D** are reproduced in the compared regions (-750 to -1850 ppm). Additionally, the broad excitation range of the xyBEBOP pulse, allows for the observation of species **E** and **F** (red ellipses; -149 and -558 ppm, respectively). As these signals arise far beyond the expected chemical shift range of stannides (-800 to -2000 ppm) those species haven not been observed in the former studies using 90° hard pulses.

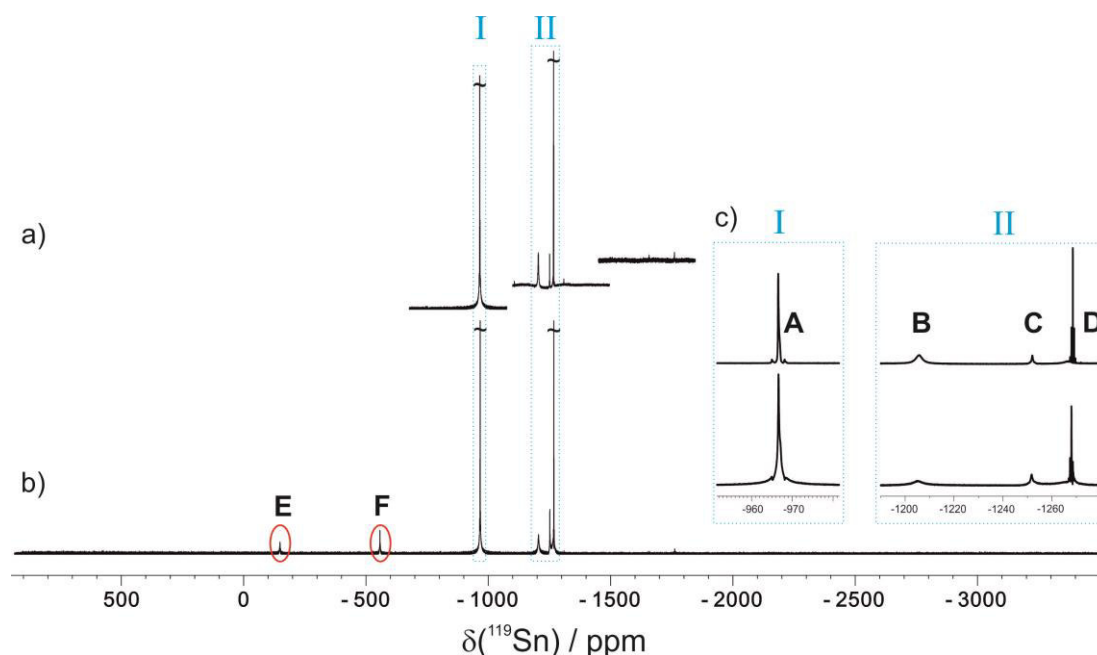


Figure 4.1: ^{119}Sn NMR spectra applying a) a 90° hard pulse (three overlapping spectra, each with a spectral width of 90 kHz, duration: 4 h 50 min); b) the xyBEBOP pulse (with a spectral width of 1000 kHz, duration: 5 h 17 min) of an one year old sample of KSnBi in liquid ammonia at 233 K; c) enlargement of the blue dotted sections I and II.

Hence, the xyBEBOP pulse is suitable for simultaneous observation of all species appearing in solution without showing any artefacts. The whole spectrum can be obtained in 5 h 17 min, while for receiving the same information with 90° hard pulses, six spectra and 29 h of measurement time would be necessary.ⁱⁱ

Next, not only the observability of the signals was investigated, but also the effect of the xyBEBOP pulse on scalar coupling constants, integrals, line widths and the offset to the transmitter frequency.

Scalar coupling constants. Often for investigations on heteronuclear cluster, the scalar coupling constants of the signals are of utmost importance. For example for stannides, the $^1J(^{119}\text{Sn}-^{117}\text{Sn})$ coupling is the only possible access for an unambiguous assignment of the cluster sizes.ⁱⁱⁱ

ⁱⁱ For analyzing a spectral range from 0 to -2150 ppm, each spectra with a spectral width of 90 kHz / 400 ppm. To exclude artefacts at the boarder of the spectra an overlap of 50 ppm is applied.

ⁱⁱⁱ In our investigations on stannides, the signals are assigned to the different cluster by their characteristic signal patten, which is different for, e.g., four and nine atomic cluster. Therefore, the isotope pattern for various cluster sizes is simulated, assuming a fluctuation of the cluster. (For detailed information, see chapter 6 of this thesis.)

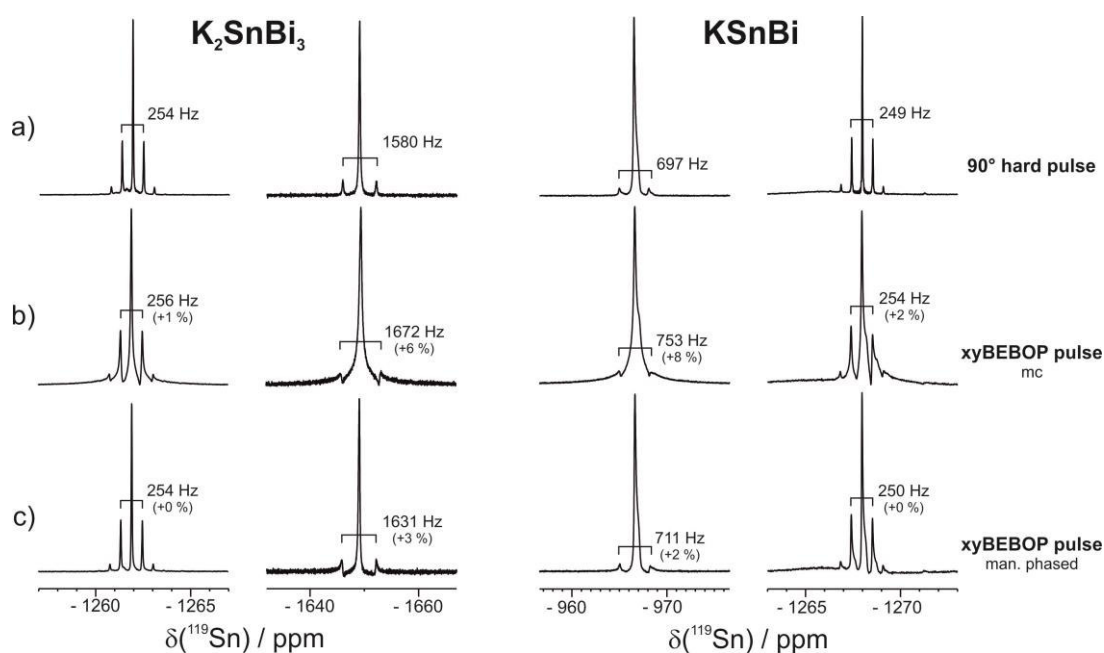


Figure 4.2: Comparison of the resolution received with a 90° hard pulse a), and the xyBEBOP pulse b) by using magnitude calculation (mc) for processing and c) manually phased signals; from samples of K_2SnBi_3 (left spectra) and $KSnBi$ (right spectra) in liquid ammonia at 233 K. In brackets the deviations with regard to the values of a).

Two different samples (K_2SnBi_3 and $KSnBi$), which are showing scalar coupling constants of various stannide cluster from 250 to 1600 Hz are investigated. Figure 4.2 shows the deviation of the coupling constants observed with a 90° hard pulse (a) and the xyBEBOP pulse, either processes with magnitude calculation (b) or by manual phasing of each signal (c). It is obvious, that small scalar coupling constants of about 250 Hz (Figure 4.2, left signal of K_2SnBi_3 and right signal of $KSnBi$) are reproduced very precisely with an error of 1 Hz, if the spectra are manually phased (c), or 5 Hz by using magnitude calculation (b), these deviations are within the experimental error.^{iv}

For larger scalar coupling constants of about 700 Hz a more pronounced deviation is obtained (Figure 4.2, left signal of $KSnBi$). The manually phased signal (c) shows a deviation of 14 Hz (2 %), which is still very precisely, while by using magnitude calculation (b) a larger deviation of 56 Hz (8 %) occurs. In the case of very large scalar coupling constants of about 1600 Hz (Figure 4.2, right signal of K_2SnBi_3) especially the absolute errors are much larger, while the error in percent is still considerably small ($\leq 6\%$). The signal processed with magnitude calculation shows a deviation of 92 Hz (6 %), this can be improved considerably to 51 Hz (3 %) by phasing the signal manually (c). Thus, the best matching results of the xyBEBOP pulse for the scalar coupling constants are

^{iv} The FID resolution (FIDRES) is 11 Hz for the 90° hard pulse and 8 Hz for xyBEBOP pulse.

received by manual phasing of each signal separately, without magnitude calculation (mc).

These deviations seem to correspond to the widths at the baseline of the signals. There, the combination of broad line widths, antiphase contributions and magnitude calculation leads to the largest deviation of 92 Hz (6 %) for the signal at -1650 ppm.

Nevertheless, a correct assignment of the cluster size is feasible, as the coupling constants are highly deviating for different cluster, e.g. for $\text{Sn}_9^{4-} {}^1J(^{119}\text{Sn}-^{117}\text{Sn}) = 254$ Hz (see Figure 4.2) and for $\text{Sn}_4^{4-} {}^1J(^{119}\text{Sn}-^{117}\text{Sn}) = 1466$ Hz.^[2] Therefore, it is not necessary to analyze the observed signals additionally with a 90° hard pulse, as all information is already gained by applying the xyBEBOP pulse. Overall, very good correlations of the scalar coupling constants with errors less or equal than 6 % are received by the xyBEBOP pulse in comparison to a 90° hard pulse. This can be even improved by applying manual phasing on the spectra, to errors of less or equal 3 %.

Integrals and line widths. Beside the chemical shift range and the coupling constants also the integrals and line widths are of great importance, if quantitative determinations are requested. Table 4.1 shows the comparison of the integrals and the line widths which are received with either a 90° hard pulse or the xyBEBOP pulse, processed with magnitude calculation (mc) or manually phased, respectively (values of a further investigated sample are listed in the Supporting Information).

Table 4.1: Comparison of the integrals and the line widths ($\Delta\nu_{1/2}$) of the signals **A-D** shown in Figure 4.1 received with a 90° hard pulse or the xyBEBOP pulse, either processed with magnitude calculation (mc) or manually phased.

	A	B	C	D
Integral^{*)}				
90° hard	1.0 (± 0.10)	1.1 (± 0.11)	0.2 (± 0.02)	0.6 (± 0.06)
xyBEBOP (mc)	0.9 (± 0.09)	0.3 (± 0.03)	0.6 (± 0.06)	
xyBEBOP (man. phased)	0.9 (± 0.09)	0.4 (± 0.04)	0.2 (± 0.02)	0.6 (± 0.06)
$\Delta\nu_{1/2}$ [Hz]				
90° hard	51	711	135	9
xyBEBOP (mc)	84	1239	251	27
xyBEBOP (man. phased)	55	672	144	18

^{*)} Integrals are listed with an error of ± 10 %, as it is commonly accepted for heteronuclei.

For signal **A** the values received with the xyBEBOP pulse (0.9), either processed with magnitude calculation or manually phased is slightly deviating from the integral of the 90° hard pulse (1.0) (Table 4.1 – Integral of **A**), but this deviation is within the experimental error. In case magnitude calculation is applied, signals **C** and **D** cannot be integrated, as they are overlapping (Table 4.1 – Integral of **C** and **D**, middle). But by phasing each of these signals separately the integrals of 0.2 and 0.6 are matching exactly with those observed with the 90° hard pulse (Table 4.1 – Integral of **C** and **D**, above and below). An exception shows the integral of signal **B**. Here the broad line width off about 700 Hz, indicates a fast transversal relaxation of species **B**, which might be too fast for the length of the used broadband pulse (1000 μ s for a spectral width of 1000 kHz), and results in greatly deviating integrals with the xyBEBOP pulse, no matter which processing method is used (Table 4.1 – Integral **B** middle and below). To circumvent this problem, a shorter pulse, e.g. with a spectral width of 500 kHz (500 μ s), can be applied.

By comparing the line widths ($\Delta\nu_{1/2}$) of species **A** to **D**, it is obvious, that the ones received by manual phasing of the signals are well-matching with those of the 90° hard pulse (see Table 4.1 - $\Delta\nu_{1/2}$, below). While the line width of the signals, that were processed by magnitude calculation show a very large deviation and therefore will not be considered for further investigations (see Table 4.1 - $\Delta\nu_{1/2}$, middle).

These data show, that in terms of integrations and for the line widths, again a manual phasing of each signal is superior to magnitude calculation. A potential drawback of the manual phase correction are artefacts induced by deviating baselines, which might be one reason for the remaining errors in Table 4.1. However, using different offsets to the transmitter frequencies, the signal can shift into regions of high phase shifts within the phase profiles during the xyBEBOP pulse, leading to large deviations of the integrals (see the Supporting Information).

Overall, these data show the reliability of the xyBEBOP pulse, which can also be used for quantitative NMR spectroscopy. Only signals with line widths as large as 700 kHz show significantly reduced integrals, owing to relaxation during the 1000 μ s long xyBEBOP pulse. Even signals with slight chemical shift overlap can be integrated, if they are phased separately.

Screening method. The NMR spectroscopy is the method of choice for structure elucidation and monitoring of transformation processes of heteronuclei species in solution. For our investigations on Zintl ions, the investigated species often show a low solubility product constants. Hence to reach the suitable concentration for NMR spectroscopic studies it might take several hours to days. As in general no protons are bound to those cluster also the help of ^1H NMR spectra to verify the concentration cannot be used. Thus, the only possible access to estimate the amount of solved species was the sample's intensity of coloration. As the sample preparation is very costly, the formation of the signals was controlled by continuously, block wise measurement of the different regions of the spectrum with a 90° hard pulse. But beside the loss of measurement time, it was not possible to control the change of the species outside the considered chemical shift range. Therefore, it was necessary to find a method to recognize very fast the sufficient amount of solved species. For these investigations mainly the reliability of the signals is of huge interest, while the integrals and the line width are of secondary importance.

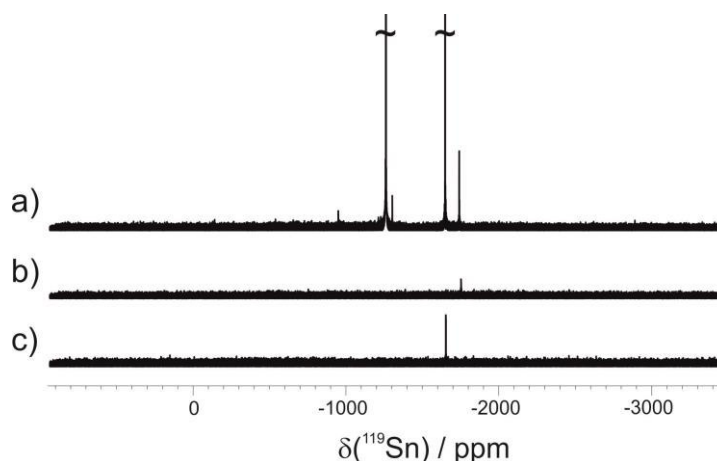


Figure 4.3: a) $\text{K}_2\text{Sn}_3\text{Bi}$, b) K_2SnBi_3 and c) K_3SnBi in liquid ammonia at 233 K. After a first screening of the samples with the xyBEBOP pulse it is obvious that sample a) contains solved species in an appropriate amount.

Figure 4.3 shows the ^{119}Sn NMR spectra of three samples, which were recorded shortly after their preparation. It is obvious, that exclusively for sample a) the solvation was proceeded sufficiently for further analysis, as for this sample various signals with a great intensity were observable. Therefore, the associated species was examined in detail in a further investigations. This was not the case for samples b) and c), those samples were stored and analyzed at a later time.

Hence, the xyBEBOP pulse provides an enormous time and cost benefit, as samples with a too low concentration of essential species are recognized very fast. Thus, the xyBEBOP pulse can be also used as fast and simple screening method.

Application to further heteronuclei (^{207}Pb , ^{29}Si , ^{13}C). The xyBEBOP broadband pulse was also applied on samples of $\text{Pb}(\text{NO}_3)_2$ and SiMe_4 to examine its behavior on further heteronuclei, which are also often relevant for investigations in the inorganic chemistry.

Figure 4.4 shows that the xyBEBOP pulse is also applicable for ^{207}Pb , ^{29}Si and ^{13}C . Here, no quantitative validation was performed, as described above for ^{119}Sn , but obviously for all those heteronuclei, the xyBEBOP pulse can be applied. Especially for ^{207}Pb , with a chemical shift range of 1500 kHz,^[1] the xyBEBOP pulse will be of high benefit for future investigations, because a chemical shift range of 1000 kHz can be observed in one spectrum. For ^{29}Si and ^{13}C the excitation range even surpasses the know chemical shift range of these nuclei.

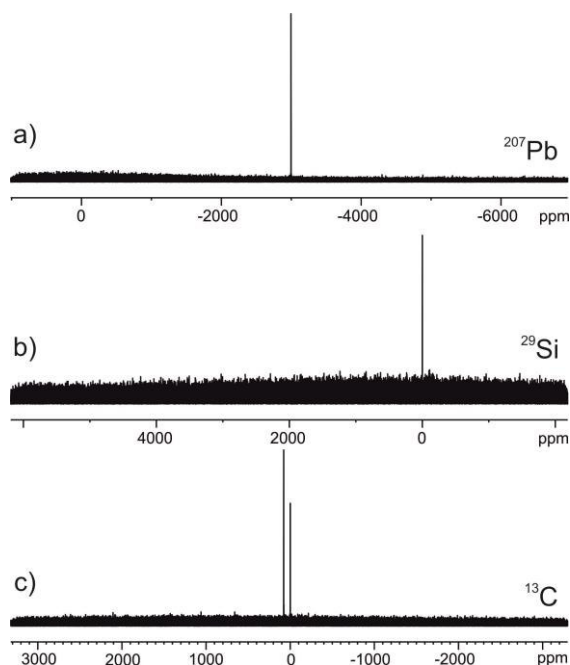


Figure 4.4: Application of the xyBEBOP pulse for a) ^{207}Pb NMR spectrum of $\text{Pb}(\text{NO}_3)_2$ in D_2O ; b) ^{29}Si NMR spectrum and c) ^{13}C NMR spectrum, of SiMe_4 in CDCl_3 at 300 K.

4.2.3 Conclusion

In conclusion, the xyBEBOP pulse is a helpful tool for heteronuclear NMR spectroscopy, which provides highly reliable results, if some restrictions are considered.

With this broadband pulse, the observation of all species occurring simultaneously in solution, even if they show strongly deviating chemical shift values, is possible without any artefacts. For receiving reliable scalar coupling constants, integrals and line widths manual phasing of each signal is recommended instead of magnitude calculation. An unexpected good reproducibility was found for the investigated coupling constants in the range of 250 to 1600 Hz. For manually phased signals a maximum deviation of only 3 % was obtained and a deviation up to 6 % if magnitude calculation was applied for processing. Therefore, the received spectra allow for unambiguous assignments (of e.g. cluster sizes) via coupling constants. For the integrals both kinds of processing provided good results. However, the advantage of manual phasing is the possibility to integrate even partially overlapped signals which is not possible by magnitude calculated spectra. A limiting factor for reliable integrals are species with a fast transversal relaxation, observable in a broad line width (in this investigation a deviation occurred for line widths of 700 Hz). In this case a shorter pulse with a length of e.g. 0.5 ms is recommended. Furthermore, a slight offset dependence is observable and should be taken into account. For obtaining precise line widths the manual phasing should be applied in any case, as with magnitude calculation strongly deviating values occurred. Additionally, it was shown that the xyBEBOP pulse can be used for sample screening.

The xyBEBOP pulse will improve future investigations on heteronuclei by a simultaneous observation of all species which are occurring in a chemical shift range of 1000 kHz by very reliable results and the tremendous saving of measurement time. A drawback is the processing of the spectra by manual phasing to receive reliable results, which can be very complex if several signals are arising in the spectrum. Furthermore, signals which are deviating from optimal values should be investigated again with a 90° hard pulse.

Besides these few restrictions, the xyBEBOP pulse leads to an enormous time benefit and facilitates investigations on solvation, transformation and degradation processes in solution. This application can be used for all NMR spectroscopic studies of heteronuclei with a broad chemical shift range, if a simultaneous observation of various species is not possible with standard experiments.

4.3 Supporting Information

4.3.1 Overview of Recording Times

Table 4.2: Illustrative list of measurement times of the investigation of KSnBi by ^{119}Sn NMR spectra (see Figure 4.1). The measuring time (t) for each 1D spectrum is approximately the same for 90° hard pulse and xyBEBOP pulse, but the sum for the whole investigation (t_{total}) is much longer, if a 90° hard pulse is applied, as it can excite only a range of 90 kHz.

	Pulse	SW [kHz]	t [hh:mm]	t_{total} [hh:mm]
a)	90°	90	4:50	14:30-29:00
b)	xyBEBOP	1 000	5:17	5:17

Table 4.2 shows the superiority in time of the broadband pulse compared to a 90° hard pulse on the example of ^{119}Sn NMR spectra of KSnBi (shown in Figure 4.1). If a spectral width (SW) of 90 kHz is chosen (a), to ensure a sufficient excitation at the borders of the spectrum (see 4.3.4 for more details about the excitation profile of the 90° hard pulse), the experiment needs to be repeated several times with variation of the transmitter frequency to cover the relevant ppm range of the Zintl anion species (about 500 kHz, 2200 ppm), resulting in an overall measuring time of 14 h 30 min to 29 h, respectively. By applying the xyBEBOP pulse, the whole chemical shift region is screened in approximately the same time needed for one single 1D spectrum with a 90° hard pulse.

4.3.2 Comparison of Integrals and Line Widths of a Further Sample

The main part of this chapter already showed that for quantitative analysis, better results are observed if each signal is phased manually, and not processed by magnitude calculation. If necessary, also the baseline correction should be performed manually. Magnitude calculation is applicable for illustration of the pulses but not for quantitative evaluation.

Table 4.3: Comparison of the integrals and the line widths ($\Delta\nu_{1/2}$) of $\text{K}_2\text{Sn}_3\text{Bi}$ (Figure 4.3a).

	-1262 ppm	-1650 ppm	-1741 ppm
Integral^{*)}			
90° hard	1.0 (± 0.10)	0.56 (± 0.06)	0.15 (± 0.02)
xyBEBOP (mc)	0.84 (± 0.08)	0.26 (± 0.03)	0.13 (± 0.01)
xyBEBOP (man. phased)	0.83 (± 0.08)	0.41 (± 0.04)	0.15 (± 0.02)
$\Delta\nu_{1/2}$ [Hz]			
90° hard	11	73	115
xyBEBOP (mc)	21	136	229
xyBEBOP (man. phased)	12	79	130

*) Integrals are listed with an error of ± 10 %, as it is commonly accepted for heteronuclei.

Table 4.3 shows the integrals and line widths of the signals observed for the sample of $\text{K}_2\text{Sn}_3\text{Bi}$ (see Figure 4.3a). Also for this sample, the values observed with different pulses show a good agreement, as long as manual phasing is applied.

4.3.3 Excitation Profile of the xyBEBOP Pulse

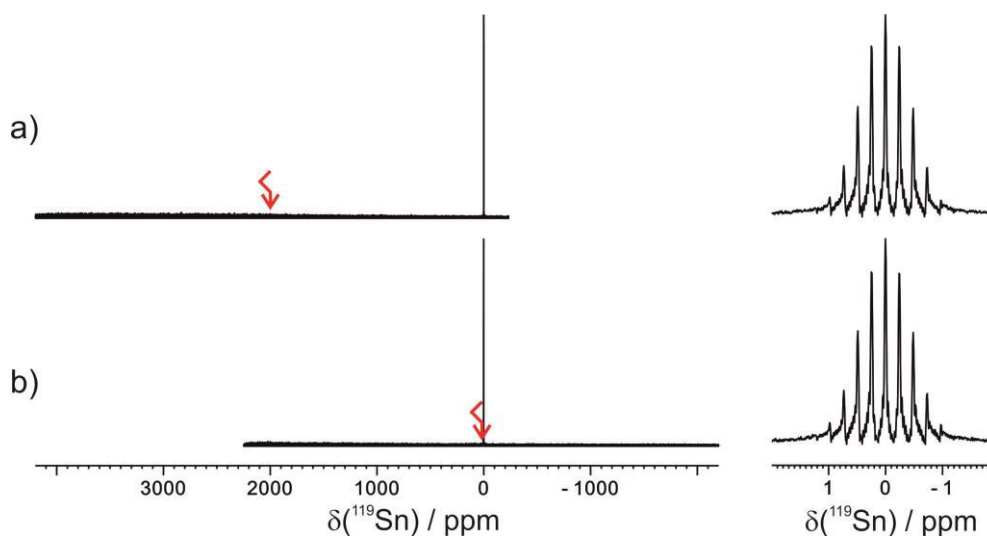


Figure 4.5: ^{119}Sn NMR spectra of SnMe_4 with a different transmitter frequency (O1P) a) 2000 ppm and b) 10 ppm. The signals show the same intensity and resolution.

Investigations with SnMe_4 as standard reagent showed that there is no influence nor in the intensity of the signal, neither in its resolution even if the transmitter frequency (O1P) is set far away from the signal, by using a xyBEBOP pulse. The situation is different in case of the intensity, by applying a 90° hard pulses (see chapter 4.3.4). Therefore two NMR spectra with deviating O1P values have been compared (Figure 4.5),

the one recorded with an O1P next to the signal at 10 ppm (b) and the other with an O1P of 2000 ppm (a) for setting the signal at the boarder of the NMR spectrum b). Their signal-to-noise ratios are also comparable with a) $S/N = 180$ and b) $S/N = 190$. For a 90° hard pulse a $S/N = 200$ was observed, which shows a good agreement.

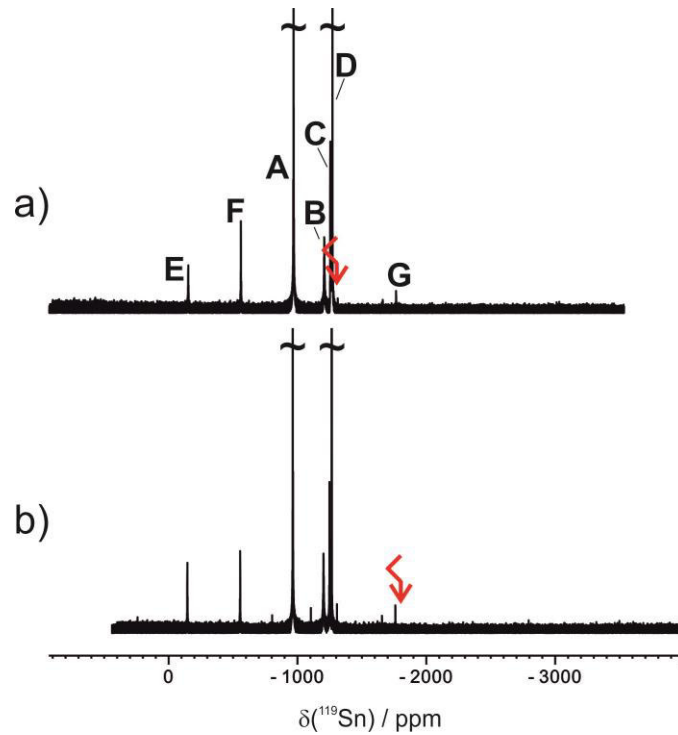


Figure 4.6: Comparison of the ^{119}Sn NMR spectra of a one year old sample of KSnBi in liquid ammonia with varying O1P a) -1300 and b) -1800 ppm.

Table 4.4: Integrals [ppm], offset values [kHz] between the transmitter frequency and the respective signal, and the line widths [Hz] of the spectra shown in Figure 4.6 processed by manual phasing.

	E	F	A	B	C	D	G
	[-148]	[-558]	[-967]	[-1206]	[-1252]	[-1269]	[-1762]
Integral^{*)} [ppm]							
a)	0.11 (± 0.01)	0.15 (± 0.02)	0.89 (± 0.09)	0.44 (± 0.04)	0.23 (± 0.02)	0.62 (± 0.06)	0.03 (± 0.00)
b)	0.11 (± 0.01)	0.12 (± 0.01)	0.78 (± 0.08)	0.50 (± 0.05)	0.25 (± 0.03)	0.33 (± 0.03)	0.03 (± 0.00)
Offset [kHz]							
a)	257.95	166.57	74.86	21.58	11.13	7.76	102.84
b)	369.47	277.70	186.26	132.75	122.59	118.87	8.13
$\Delta\nu_{1/2}$ [Hz]							
a)	149	156	55	672	144	18	~200
b)	214	133	26	698	145	10	145

*) Integrals are listed with an error of $\pm 10\%$, as it is commonly accepted for heteronuclei.

Table 4.4 shows the comparison of the integrals received by repeating the experiment shown in Figure 4.1b with a variation of the transmitter frequency (O1P). All integrals are well reproduced, even the broad signal **B** shows comparable integrals, so the reduced integral in comparison to a 90° hard pulse (Table 4.1) arises from the fast transversal relaxation as proposed above. The deviation of the integral for signal **D** can be most probably traced to the partial overlapping with signal **C** and therefore baseline error might occur. All other deviations can be explained that owing to the different transmitter frequency the signals might experience different phase profiles of the xyBEBOP pulse.

4.3.4 Sinc Shaped Excitation Profile of a 90° Hard Pulse

Owing to the sinc shaped excitation profile of a 90° hard pulse (see Figure 4.7), the excitation of some signals is less sensitive, especially at the borders of the spectra it leads to a reduced or no excitation. This depends on the offset of the signal to the transmitter frequency. If the offset is 78.4 kHz between the transmitter frequency and the signal (for ^{119}Sn $\Delta(\text{O1P} - \text{signal}) = \pm 350$ ppm) only an intensity of 5 % can be obtained. The spectra shown in this investigation as comparison to the xyBEBOP pulse were recorded with a spectral width of 90 kHz (for ^{119}Sn : SW = 400 ppm), which provides even at the boarder of the spectra a signal intensity of 68 %, as the offset between the transmitter frequency and the board of the spectrum is 44.8 kHz (200 ppm for ^{119}Sn).

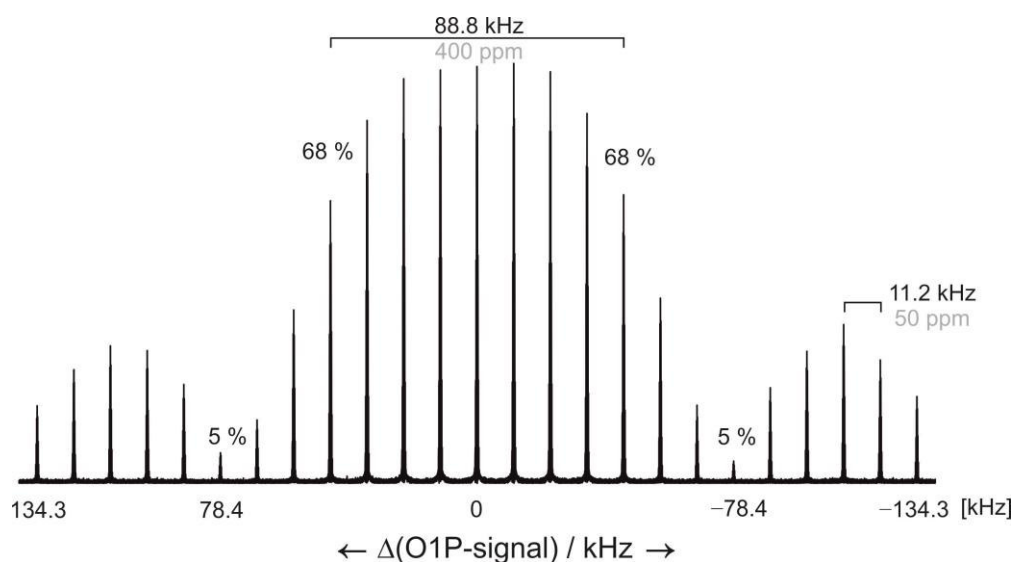


Figure 4.7: The 90° hard pulse has a sinc function shaped excitation profile. So, the signals with a greater offset to the transmitter frequency (O1P) are occurring with a reduced intensity, which is obvious by comparing the spectra with varied O1P. [ppm]-values in gray correspond to a ^{119}Sn NMR spectrum (224 MHz) of SnMe_4 in C_6D_6 in at 300 K.

Table 4.5: Remaining intensities by variation of the offset (in kHz and ppm) between the transmitter frequency and the signal, owing to the sinc shaped excitation profile of a 90° hard pulse. The values in ppm correspond to Figure 4.7, ^{119}Sn NMR spectra (224 MHz) of SnMe_4 .

$\Delta(\text{O1P} - \text{signal})$ [kHz]	$\Delta(\text{O1P} - \text{signal})$ [ppm / ^{119}Sn]	remaining intensity
0 ± 11.2	0 ± 50	100 %
± 33.6	± 150	87 %
± 44.8	± 200	68 %
± 78.4	± 350	5%

4.3.5 NMR Data Collection and Processing

The NMR spectra were recorded on a Bruker Avance III HD 600 spectrometer (600.13 MHz for ^1H ; 223.79 MHz for ^{119}Sn ; 125.55 MHz for ^{207}Pb ; 119.23 MHz for ^{29}Si ; 150.90 MHz for ^{13}C) equipped with a 5 mm double resonance broad band Prodigy (BBO) z-gradient probe. The temperatures for all measurements were controlled by a Bruker VTU temperature unit. ^{119}Sn measurements were carried out with a standard Bruker pulse program zg with $P1 = 13.5 \mu\text{s}$, $\text{PLW} = 70 \text{ W}$ / $\text{PLdB} = -18.45$ and “bulu_zg_shape” with the shaped pulse “xyBEBOP_1m_RF10kHz_BW1000kHz” $P1 = 25.0 \mu\text{s}$, $\text{PLW} = 80$ / $\text{PLdB} = -19.03$, using for both: 40k number of scans, 0 dummy scans, $\text{TD} = 16\text{k}$ ($\text{FIDRES} = 11 \text{ Hz}$; for 90° hard pulse) and 262 k ($\text{FIDRES} = 8 \text{ Hz}$; for xyBEBOP pulse) with a relaxation delay of 0.3 s. Data were processed with the Bruker software TOPSPIN 3.2 using the processing parameters $\text{SI} = 32 \text{ k}$ (for 90° hard pulse) and 524 k (for xyBEBOP pulse) and $\text{WDW} = \text{EM}$ (1-50 Hz). The chemical shifts are reported in ppm and for ^{119}Sn the Ξ value of SnMe_4 , used as external standard (300 K, 98/2 [v/v] in C_6D_6), was applied.

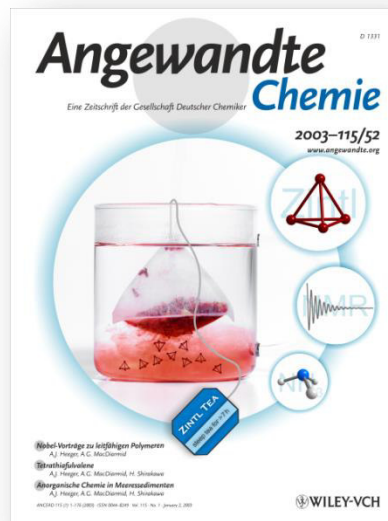
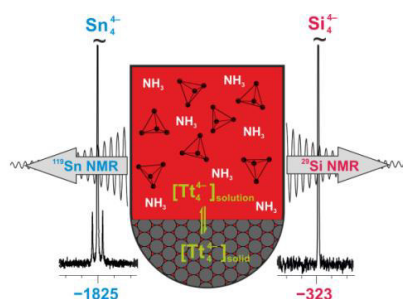
4.4 References

- [1] C. Brevard, P. Granger, *Handbook of High Resolution Multinuclear NMR*, John Wiley & Sons, **1981**.
- [2] M. Neumeier, F. Fendt, S. Gärtner, C. Koch, T. Gärtner, N. Korber, R. M. Gschwind, *Angew. Chem. Int. Ed.* **2013**, 52, 4483–4486.
- [3] U. Friedrich, M. Neumeier, C. Koch, N. Korber, *Chem. Commun.* **2012**, 48, 10544–10546.
- [4] B. Kesanli, J. Fettingner, D. R. Gardner, B. Eichhorn, *J. Am. Chem. Soc.* **2002**, 124, 4779–4786.
- [5] B. Kesanli, J. E. Halsig, P. Zavalij, J. C. Fettingner, Y.-F. Lam, B. Eichhorn, *J. Am. Chem. Soc.* **2007**, 129, 4567–4575.
- [6] R. W. Rudolph, W. L. Wilson, F. Parker, R. C. Taylor, D. C. Young, *J. Am. Chem. Soc.* **1978**, 100, 4629–4630.
- [7] B. Eichhorn, S. Kocak, in *Zintl Ions Princ. Recent Dev.* (Ed.: T.F. Fässler), Springer-Verlag, Berlin Heidelberg, Germany, **2010**.

5 Detection and Transformation of Highly Charged Zintl Anions

Communication

„Detection of the Elusive Highly Charged Zintl Ions Si_4^{4-} and Sn_4^{4-} in Liquid Ammonia by NMR Spectroscopy”*



The NMR spectroscopic investigations were performed in close collaboration with Maria Neumeier. The ^{29}Si MAS-NMR measurements were performed by Tobias Gärtner. The synthesis and the characterization of the solids as well as the sample preparation were carried out by Franziska Fendt and Stefanie Gärtner.

*Maria Neumeier, Franziska Fendt, Stefanie Gärtner, Carina Koch, Tobias Gärtner, Nikolaus Korber and Ruth M. Gschwind

Angew. Chem. Int. Ed. **2013**, 52, 4483-4486. (VIP)

Angew. Chem. Int. Ed. **2013**, 52, 4494. (Back Cover)

Angew. Chem. **2013**, 125, 4579-4582. (VIP)

Angew. Chem. **2013**, 125, 4590. (Rücktitelbild)

DOI: 10.1002/anie.201209578

© 2014 Wiley-VCH Verlag GmbH & Co. KGaA. Reproduced with permission.

In Additional Findings:

“Reaction of Sn_4^{4-} in liquid ammonia: the formation of $\text{Rb}_6[(\eta^2\text{-Sn}_4)\text{Zn}(\eta^3\text{-Sn}_4)] \cdot 5\text{NH}_3$ ”**

Franziska Fendt, Carina Koch, Stefanie Gärtner and Nikolaus Korber, *Dalton Trans.* **2013, 42, 15548-15550.

5.1 Abstract

It's detected! The existence of the prototypical Zintl ions Tt_4^{4-} (Tt = Groupe 14 element), which are isoelectronic to the P_4 molecule, used to be confined to the solid state. Recently, circumstantial evidence for a solution chemistry in liquid ammonia emerged. Direct spectroscopic observation of the dissolved anions has now been achieved. In the case of Si_4^{4-} , this is the first solution detection of any homoatomic silicide.

5.2 Manuscript

5.2.1 Introduction

The appeal of Zintl anions originates from the fact that they are molecular building blocks of main group elements that may be manipulated in solution. Apart from their intrinsic significance for the chemistry of the elements, they are promising starting materials for the development of new hybrid materials containing transition metals and main group elements.^[1] The solution chemistry of the bare clusters also offers the possibility to find new elemental modifications by oxidative coupling, as it was shown for germanium, or to create potential semiconducting amorphous or crystalline films by anodical deposition.^[2,3] The dominant characterization method for nearly all of the reported compounds and materials is so far single crystal x-ray structure analysis. In contrast, much less is known about the species that actually occur in solution. In order to better understand the complicated processes which take place when Zintl anions react with reagents, the behavior of the bare polyanions in pure solutions must first be investigated. The long range-goal of these investigations would be a better understanding of Zintl anion solutions, facilitating an increasingly rational approach to their use in chemical transformations.

Solutions of group 15 polyanions were studied intensely by Baudler *et al.*,^[4] in contrast, a systematic investigation of ligand-free group 14 polyanions in solution is still absent. Furthermore, highly reduced clusters such as Sn_4^{4-} and Pb_4^{4-} have never been detected in solution and the observation of any silicides at all remains elusive. Therefore, our studies focused on the characterization of highly reduced homoatomic group 14 polyanions in solution by using NMR spectroscopy. In former ^{119}Sn NMR studies Rudolph *et al.* reported the detection of Sn_9^{4-} . They documented a further upfield shifted signal, which was tentatively assigned to Sn_4^{2-} .^[5-7] Moreover, Eichhorn *et al.* recently

demonstrated the influence of [2.2.2]-cryptand on the Sn_9^{4-} species in solution. Their ^{119}Sn NMR studies showed that a stoichiometric excess (4.5 equivalents) of cryptand led to HSn_9^{3-} along with several different K^+ -coordinated species $\text{K}_x\text{Sn}_9^{(4-x)-}$ ($x = 0-3$).^[8] More highly reduced clusters as Sn_4^{4-} and Pb_4^{4-} , have until now only been proven to exist in solution by the circumstantial evidence of solvate crystal structures, which were obtained from direct reduction experiments in liquid ammonia.^[9] For the lighter homologues Si and Ge, the only known analogues solvate crystal structure is a functionalized tetrahedral silicide.^[10] An alternative route to access these E_4^{4-} ($\text{E} = \text{element of group 14}$) clusters would be the dissolution of the precursor phases A_4E_4 ($\text{A} = \text{alkali metal}$), but they were supposed to be completely insoluble for the lighter congeners $\text{E} = \text{Si, Ge and Sn}$.^[11] Indeed, there has not been any report on an NMR signal of a bare homoatomic polyanion of silicon in solution to date. The only ^{29}Si signal for a negatively charged silicon cluster in solution stems from the R_3Si_4^- anion, where $\text{R} = \text{SiMe}[\text{CH}(\text{SiMe}_3)_2]_2$, which was studied in toluene by Sekiguchi *et al.*^[11] However, starting from the binary phases $\text{A}_{12}\text{Si}_{17}$ with one Si_9^{4-} and two Si_4^{4-} anions per formula unit ($\text{A} = \text{K, Rb}$), Sevov *et al.* were able to show that silicides may be dissolved in liquid ammonia to yield the oxidized polyanions Si_9^{3-} , Si_9^{2-} and Si_5^{2-} in cryptand-containing solvate compounds.^[12,13] In previous recrystallization experiments of a solid starting material with the nominal composition $\text{K}_6\text{Rb}_6\text{Si}_{17}$ in liquid ammonia, we were also able to indirectly find evidence for the existence of unoxidized Si_9^{4-} in solution,^[14,15] and we also used this ternary material to form the complex ion $[\{\text{Ni}(\text{CO})_2\}_2(\mu\text{-Si}_9)_2]^{8-}$.^[16] Fässler *et al.* also succeeded in the synthesis of a functionalized silicide, $[(\text{MesCu})_2(\eta^3\text{-Si}_4)]^{4-}$, which contains Si_4 tetrahedra bonded to copper, in liquid ammonia from a similar starting material.^[10] Considering these results, the question if and which silicide species may be detected in solution became urgent.

Herein we present the first NMR signal of a bare silicide in solution. To our knowledge, the detected Si_4^{4-} signal is the most highfield shifted ^{29}Si signal of a tricoordinated Si atom in a molecular environment without the involvement of any transition-metal complex. Therefore, the upfield limit of the NMR scale of all measured ^{29}Si signals is now extended from -274.2 ppm ^[17] to -323 ppm . Furthermore, we provide the first experimental evidence that Rb_4Sn_4 is soluble in liquid ammonia and that Sn_4^{4-} can be stabilized in solution in the presence of [2.2.2]-cryptand. We also observe the oxidation of Sn_4^{4-} to Sn_9^{4-} in these solutions and, based on the detection of

NH_2^- , unambiguously identify the oxidizing agent as being protons. This knowledge about solution processes of Group 14 polyanions might provide the possibility of rational syntheses of functionalized Zintl clusters and opens an approach to material design.

5.2.2 Results and Discussion

For the study of the highly charged Sn_4^{4-} and Si_4^{4-} clusters in solution, we selected the stannide system as a starting point. With respect to the detection of stannides, a convenient NMR approach has already been established, in which ^{119}Sn is observed and the ^{117}Sn satellite pattern is used for the assignment of the cluster sizes Sn_x (for details see the Supporting Information).^[5–8] Furthermore, stannides provide higher stability towards moisture and oxidation processes as well as better solubility than the highly sensitive silicides. For the synthesis, we chose the direct reduction of elemental tin with elemental rubidium (1:1) in liquid ammonia, because this additive-free preparation method minimizes external influences on the properties and the preferred cluster sizes and allowed for the crystallization of the solvates $\text{A}_4\text{Sn}_4 \cdot 2\text{NH}_3$ ($\text{A} = \text{Rb}, \text{Cs}$) in previous studies.^[9]

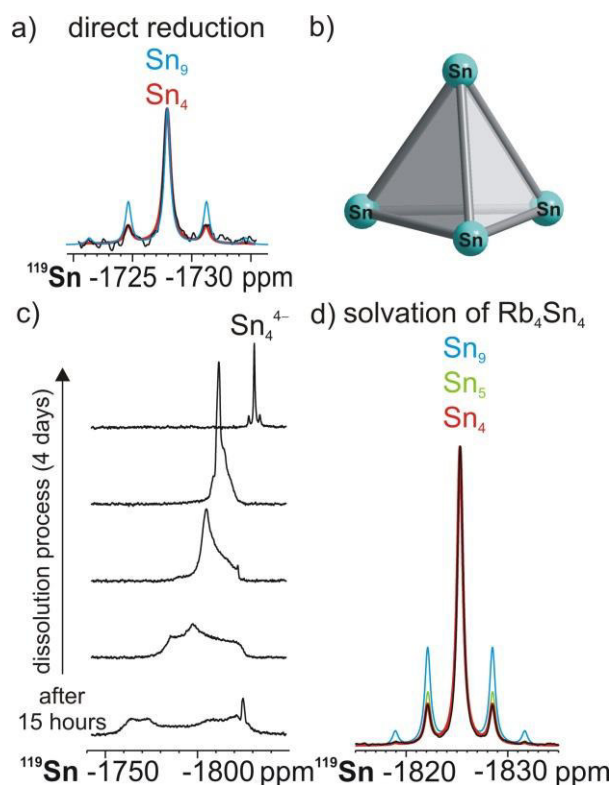


Figure 5.1: Sn_4^{4-} in liquid ammonia: a) Experimental (black) and simulated (colored) ^{119}Sn spectra of Sn_4^{4-} (195 K, 224 MHz) resulting from direct reduction; b) Sn_4^{4-} cluster present in Rb_4Sn_4 ; c) ^{119}Sn spectra showing the dissolution process of Rb_4Sn_4 in the presence of [2.2.2]-cryptand (233 K, 224 MHz); d) assignment to Sn_4^{4-} based on simulations of the ^{117}Sn satellite pattern.

With this setup, a small ^{119}Sn signal at -1727 ppm with a coupling constant of 1466 Hz and a ^{117}Sn satellite pattern of $0.13:1.00:0.12$ was observed (Figure 5.1a), despite the fact that the solubility of Sn_9^{4-} is expected to be very limited. In additive-free crystal structures, exclusively Sn_9^{4-} and Sn_4^{4-} have been observed;^[1] for A_4Sn_9 clusters (A = alkali metals) the chemical shift range as well as the scalar coupling constants in ethylenediamine (en) are well-known (-1115 – -1241 ppm; 256 – 293 Hz).^[7] The upfield shift of the detected ^{119}Sn signal at -1727 ppm indicates a higher negative charge per Sn atom than Sn_9^{4-} , and the large coupling constant of 1466 Hz hints at a smaller cluster size. Both parameters and also the ^{117}Sn satellite pattern are in accordance with the assignment to Sn_4^{4-} , but owing to the limited signal-to-noise-ratio (S/N) in the experiment with the sample prepared by direct reduction, slightly larger or smaller stannide clusters with five or three Sn atoms cannot be unambiguously excluded. Therefore, the solubility improving and stabilizing effect of [2.2.2]-cryptand^[18,19] was used for dissolution experiments on Rb_4Sn_4 in liquid ammonia. Prior to dissolution, the solid Rb_4Sn_4 was characterized by Raman spectroscopy and X-ray diffraction (see the Supporting Information), which confirmed the presence of Sn_4^{4-} as the exclusive anionic moiety (Figure 5.1b). Despite the fact that Rb_4Sn_4 has been assumed to be insoluble so far,^[1] a broad signal covering 21000 Hz appeared in the ^{119}Sn spectrum after 7.5 h of dissolution and 7.5 h of acquisition and sharpened within 4 days to a signal at -1825 ppm which shows a surprisingly high S/N of 196 (Figure 5.1c). This allowed for the unambiguous assignment to Sn_4^{4-} by simulation of the experimental ^{117}Sn satellite pattern ($0.133:1.000:0.132$; see Figure 5.1d) and shows a coupling constant (1423 Hz) that is similar to the direct reduction. The signal of Sn_4^{4-} in the presence of [2.2.2]-cryptand is significantly shifted upfield compared to the additive-free direct reduction sample ($\Delta\delta = -98$ ppm). This is in agreement with previous reports about the effect of different counterions or [2.2.2]-cryptand on the chemical shift of Sn_9^{4-} , where the degree of ion dissociation or sequestration correlates with upfield shifts.^[7,8] The larger absolute upfield shift for Sn_4^{4-} compared to Sn_9^{4-} is in accordance with the higher negative charge per Sn atom. In contrast, in dissolution experiments on Rb_4Sn_4 without [2.2.2]-cryptand, exclusively Sn_9^{4-} was detected (-1248 ppm, $J = 263$ Hz). Interestingly, the intensity of this signal grew over time and simultaneously the signal of NH_2^- appeared in the proton spectrum (see the Supporting Information). This is to our knowledge the first experimental evidence for the long standing suggestion that protons of ammonia or other solvents act as the oxidizing

agent in the oxidation of Sn_4^{4-} to Sn_9^{4-} . Thus, direct reduction experiments of elemental tin with elemental rubidium (1:1) in combination with dissolution experiments of Rb_4Sn_4 with and without [2.2.2]-cryptand not only allowed the first detection and the assignment of the highly charged cluster Sn_4^{4-} but also for the identification of ammonia as potential oxidizing agent.

Next, we focused on the detection of bare silicides in solution. To date, there is only circumstantial evidence for dissolved silicide clusters, but direct observation by ^{29}Si NMR has remained elusive. The only known NMR signals of silicides have been reported in solid state MAS-NMR studies of the binary phases ASi (A = alkali metal). Progressing from Cs to Na an upfield trend of the signals is observed in accordance with a reduced electron transfer between cluster anion and counterion.^[20,21] For Rb and K it was even possible to resolve the two crystallographic sites, which resulted in separated NMR signals for each phase (Rb: -290 , -305 ppm; K: -320 , -340 ppm). Given the tremendous intensity enhancement of Sn_4^{4-} in the dissolution experiments with [2.2.2]-cryptand compared to the direct reduction (vide supra), the cryptand-aided dissolution method was also chosen for the detection of silicides. Based on our experience with recrystallization experiments^[14,15] and conversion^[16] of silicides, a solid with the nominal composition $\text{K}_6\text{Rb}_6\text{Si}_{17}$ was used as the starting material. The $\text{A}_{12}\text{Si}_{17}$ phase (A = alkali metal) are the only silicides with known solubility. To facilitate the NMR detection in solution ^{29}Si isotope labeling was applied. For $\text{K}_6\text{Rb}_6\text{Si}_{17}$ an enrichment of 20 % ^{29}Si was chosen as a compromise between absolute signal enhancement and intensity reduction owing to ^{29}Si - ^{29}Si scalar couplings that would be expected for example for Si_9^{4-} . Prior to the solvation experiments, the characterization of the mixed cationic solid $\text{K}_6\text{Rb}_6\text{Si}_{17}$ by Raman spectroscopy showed the presence of both Si_4^{4-} and Si_9^{4-} clusters precast in the solid state (see Figure 5.2a and the Supporting Information). Deviating from that, the X-ray powder diffraction pattern showed only the presence of the binary Si_4^{4-} containing phase Rb_4Si_4 (see the Supporting Information), which was attributed to the poor crystallinity and the plural phase character of the solid starting material. In the solid state MAS-NMR of $\text{K}_6\text{Rb}_6\text{Si}_{17}$, only elemental Si and a broad signal at -311 ppm was observed (Figure 5.2b), which is exactly in between the known chemical shifts of Rb_4Si_4 and K_4Si_4 .^[20,21] Again no signal for Si_9^{4-} was detected, probably due to line-broadening effects caused by scalar coupling and the poor crystallinity of the material, which also prohibited its detection in the X-ray powder diffraction pattern. Next, $\text{K}_6\text{Rb}_6\text{Si}_{17}$ was dissolved in the presence of

cryptand in liquid ammonia, and the first ^{29}Si spectrum of the sample was started after 19 h. Unexpectedly, already after 4.5 hours of acquisition time and without further optimization of the NMR parameters, an extremely broad signal covering 180 Hz appeared in the ^{29}Si NMR spectrum, which sharpened within 11 days to a signal at -323 ppm with an extremely high signal to noise ratio of 80 (see Figure 5.2c and the Supporting Information). Therefore, this signal was assigned to a specific silicide cluster. ^{29}Si is the only NMR active isotope, and thus only the chemical shift can be used to differentiate between Si_4^{4-} and Si_9^{4-} , which are both present in the starting material. The ^{29}Si signal detected in solution has an only slightly upfield shift (-323 ppm) compared to the solid state MAS-NMR signal of Si_4^{4-} in $\text{K}_6\text{Rb}_6\text{Si}_{17}$ at -311 ppm. For Si_9^{4-} no MAS-NMR signal has been reported, and thus the exact chemical shift range is unknown. However, from the trends observed for the stannides, a lower charge per atom shifts the signal considerably downfield (Sn_4^{4-} : -1727 ppm; Sn_9^{4-} : -1248 ppm). Thus, the signal of Si_9^{4-} is expected to be in between the solid state signal of Si_4^{4-} and elemental Si. The chemical shift reported for R_3Si_4^- in solution ($\delta = -153.6$ ppm; $\text{R} = \text{SiMe}[\text{CH}(\text{SiMe}_3)_2]_2$) corroborates this trend.^[11] Furthermore, theoretical calculations suggest a higher rigidity for Si_9^{4-} than for Sn_9^{4-} ,^[15] which would result in three separated signals for Si_9^{4-} (Figure 5.2a).

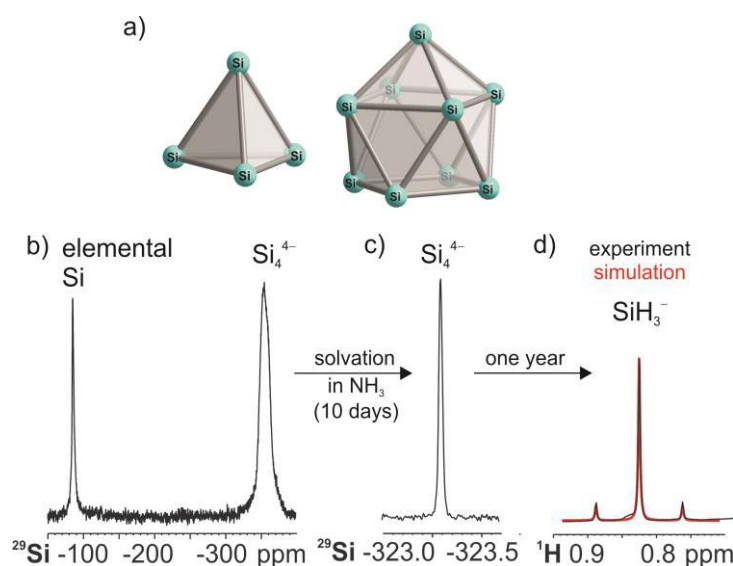


Figure 5.2: NMR detection of Si_4^{4-} in the solid state and in solution along with identification of the degradation product SiH_3^- : a) Si_4^{4-} and Si_9^{4-} clusters present in $\text{K}_6\text{Rb}_6\text{Si}_{17}$; b) ^{29}Si MAS-NMR spectrum of $\text{K}_6\text{Rb}_6\text{Si}_{17}$ with 20 % ^{29}Si labeling at RT; c) ^{29}Si NMR spectrum after dissolution of the 20% ^{29}Si labeled $\text{K}_6\text{Rb}_6\text{Si}_{17}$ in the presence of [2.2.2]-cryptand in liquid ammonia (195 K, 119 MHz); d) ^1H NMR spectrum (195 K, 600 MHz) after dissolution of the 20% ^{29}Si labeled $\text{K}_6\text{Rb}_6\text{Si}_{17}$ without [2.2.2]-cryptand in NH_3 and one year storage at 195 K including the simulation (red) of SiH_3^- .

This fact and all of the chemical shift trends for silicides and stannides known so far corroborate the assignment to Si_4^{4-} . Next, the slight upfield shift between Si_4^{4-} in solution and in the MAS-NMR spectrum is addressed. As discussed above for stannides, the dissociation of cations from Zintl anions induces upfield shifts. For the highly charged Sn_4^{4-} signal without and with cryptand separating the cations from the clusters, an upfield shift of $\Delta\delta = -98$ ppm is observed (see above). For ^{29}Si the absolute chemical shift range is significantly smaller. Thus, the upfield shift of Si_4^{4-} in solution by only 12 ppm with respect to the MAS-NMR signal fits to the ion sequestration during the dissolution process. Beyond that, Si_4^{4-} was observed to be surprisingly stable in the presence of [2.2.2]-cryptand. Even in a sample of $\text{K}_6\text{Rb}_6\text{Si}_{17}$, which was stored at 195 K for one further month and measured at an elevated temperature of 233 K, the Si_4^{4-} signal was detected in 87 % of the maximal intensity observed after 11 days at 195 K (see the Supporting Information). After an extended storage (one year) of $\text{K}_6\text{Rb}_6\text{Si}_{17}$ in liquid ammonia without [2.2.2]-cryptand, a variety of degradation products was observed in the proton spectrum (see the Supporting Information). Among these, the signal at 0.83 ppm with a $^1J_{\text{H,Si}} = 75$ Hz could be identified as SiH_3^- . The simulation considering the 20% ^{29}Si labeling (Figure 5.2d) and the coupling constant of the previously reported signal of KSiH_3 in benzene^[22] corroborate this assignment. Recently, Eichhorn *et al.* reported the protonated stannide HSn_9^{3-} in a reversible equilibrium with Sn_9^{4-} in the presence of [2.2.2]-cryptand in ethylenediamine.^[8] For the less stable silicides without the stabilizing influence of [2.2.2]-cryptand, the protonation is expected to be irreversible, resulting in the formation of SiH_3^- as final degradation product.

5.2.3 Conclusion

In summary, the detection of silicides in solution, which has been elusive for a long time, has been achieved for Si_4^{4-} . Furthermore, the elusive first NMR observation of the highly charged stannide Sn_4^{4-} is reported. Amazingly high signal intensities and stabilities were observed for both highly charged Zintl anions, Si_4^{4-} and Sn_4^{4-} , by utilizing the stabilizing effect of [2.2.2]-cryptand, and in the case of Si_4^{4-} the enhanced solubility of the mixed cationic starting material $\text{K}_6\text{Rb}_6\text{Si}_{17}$. Furthermore, by observing the generation of NH_2^- the first experimental evidence for the longstanding assumption that solvent protons act as oxidizing agent on Zintl anions is given, and in case of silicides, SiH_3^- was detected as a degradation product.

5.3 Supporting Information

5.3.1 Synthesis

General considerations

All manipulations described below were performed in a purified argon atmosphere (Glovebox) by using glass vessels dried at least four times in vacuo. [2.2.2]-cryptand was purchased from Sigma-Aldrich and used without further drying. Elemental rubidium was synthesized by the reduction of RbCl and purified by distillation. Elemental potassium was obtained from a commercial source and purified by distillation. By condensing the commercially acquired gaseous ammonia onto elemental sodium and storing this cooled Na/ammoniasolution for about three days, residual moisture traces were removed.

Solid phase synthesis of the Zintl anions (high temperature synthesis)

Rb₄Sn₄. Rb₄Sn₄ was obtained by gradually heating (60 °C/h) stoichiometric amounts of elemental rubidium (0.64 g, 7.5 mmol) and elemental tin (0.78 g, 6.6 mmol) in a Duran glass ampoule to 450 °C and holding it at this temperature for 20 h. Subsequently, the reaction mixture slowly cooled to room temperature (25 °C/h). Due to its sensitivity towards moisture and air the solid state phase was handled and stored under an argon atmosphere.

K₆Rb₆Si₁₇. K₆Rb₆Si₁₇ was synthesized by a high temperature fusion of stoichiometric amounts of the elements, where 0.294 g (7.5 mmol) potassium, 0.644 g (7.5 mmol) rubidium and 0.5 g (17.8mmol, 20% ²⁹Si) silicon were placed in a Duran glass ampoule and heated to 460 °C at a rate of 25 °C/h and held at this temperature for 72 h. Afterwards the mixture was gradually cooled down to room temperature (20 °C/h). Due to its sensitivity towards moisture and air the solid state phase was handled and stored under an argonatmosphere.

Direct reduction in liquid ammonia (low temperature synthesis)

All direct reduction experiments were carried out directly in an NMR tube. Therefore, at first 39 mg (0.46 mmol) elemental Rb and 60 mg (0.51mmol) Sn were placed into a tube and subsequently anhydrous liquid ammonia was directly condensed onto the mixture at -78 °C. In order to guarantee the permanent absence of moisture and air, the tube was sealed under ammonia atmosphere. Before NMR measurements on these

solutions were performed, the fresh samples were stored at low temperature until the initial blue color turned to deeply red.

Solvation of Zintl phases in liquid ammonia

Under completely inert conditions (Glovebox), the respective solid material (Rb_4Sn_4 : 25 mg, 0.031 mmol; $\text{K}_6\text{Rb}_6\text{Si}_{17}$: 20 mg, 0.016 mmol) was transferred into an NMR tube. The dissolution of Rb_4Sn_4 in liquid ammonia was carried out in the presence of [2.2.2]-cryptand (18 mg, 0.048 mmol) and the dissolution of $\text{K}_6\text{Rb}_6\text{Si}_{17}$ in the presence of [2.2.2]-cryptand (6 mg, 0.016 mmol) and a small amount of RbNH_2 . Anhydrous liquid ammonia was directly condensed onto the respective sample at -78°C . In order to guarantee permanently the absence of moisture and air, the tube was sealed under ammonia atmosphere.

5.3.2 Phase Determination and NMR data

General considerations

The FT-Raman spectra were recorded at room temperature under inert conditions from powdered samples sealed in pyrex tubes ($\varnothing = 0.7\text{--}1.0\text{ mm}$) using a Raman module coupled to a Varian FTS 7000e spectrometer (Nd:YAG-laser, $\lambda = 1064\text{ nm}$). Data were processed with OriginPro 7.5 and Microsoft Excel 2007. X-ray powder diffraction data were collected on a transmission powder diffraction system (STADI P, Fa. Stoe Cie, Darmstadt, Cu- $\text{K}\alpha$ radiation with $\lambda = 1.540598\text{ \AA}$). Capillaries were charged with the respective powdered samples and air-proof sealed. Data were processed with WinXPow (STOE & Cie 2000 Darmstadt, WinXPow, Vol. [1.08]). Solid state ^{29}Si MAS-NMR spectra were recorded with a 400 MHz spectrometer using a standard Bruker pulse program (hpdec.av), 128 number of scans, $\text{TD} = 16\text{ k}$, a MAS-frequency of 12 k and a relaxation delay of 180 s. Data were processed with the Bruker software TOPSPIN 2.1 using $\text{SI} = 16\text{ k}$. The chemical shifts are reported in ppm relative to SiMe_4 .

Solid phase characterization

Rb_4Sn_4 . The Raman spectrum of Rb_4Sn_4 shows the characteristic frequencies of Sn_4^{4-} at 133.1 cm^{-1} and 184.2 cm^{-1} (Figure 5.3)^[23]. Furthermore, the solution and refinement of the experimental powder diffraction data yielded a tetragonal body centered cell of the space group $\text{I4}_1/\text{acd}$ with cell parameters which fit the values published for Rb_4Sn_4 (Figure 5.4)^[24–26]. Consequently, we assume that Rb_4Sn_4 is a phase pure solid and

contains Sn_4^{4-} as the exclusive anionic moiety, since no indication for the presence of Sn_9^{4-} was found by either Raman spectroscopy or X-ray diffraction.

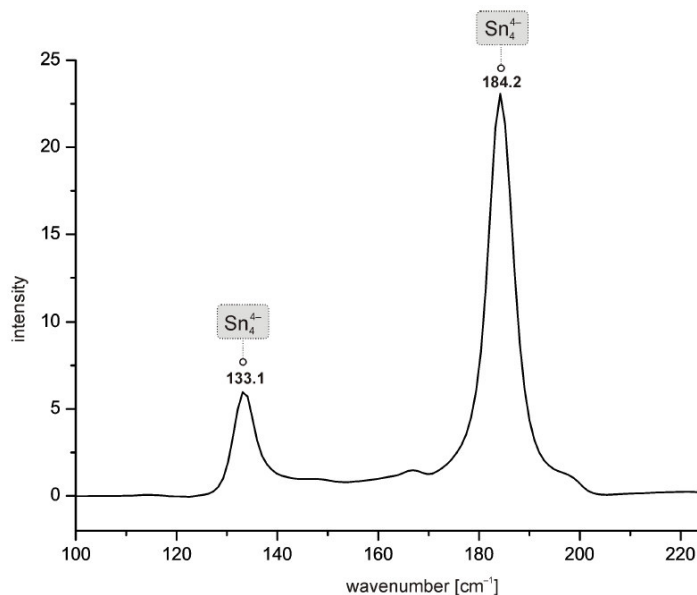


Figure 5.3: The Raman spectrum shows the characteristic vibrations of Rb_4Sn_4 .

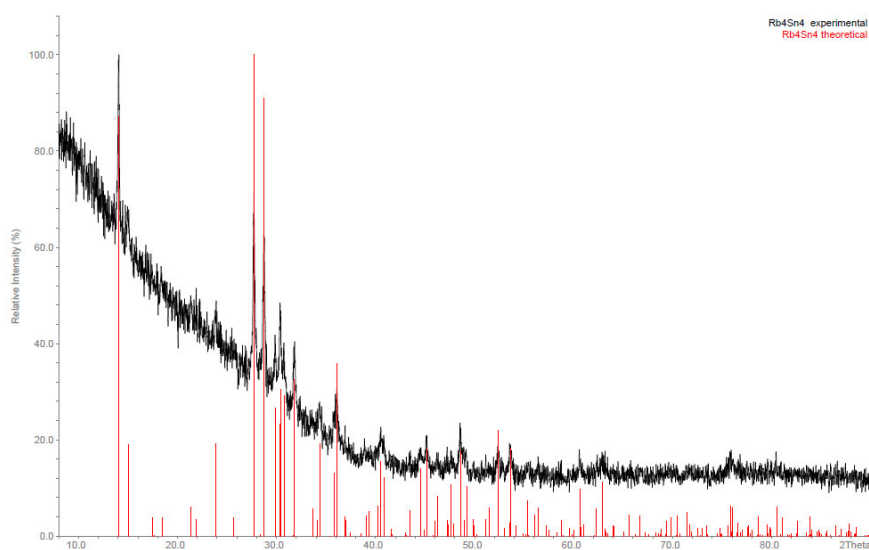


Figure 5.4: Comparison of experimental (black) and theoretical (red) diffraction pattern of Rb_4Sn_4 . The latter was calculated from single crystal data as there are no recorded powder data available.

$\text{K}_6\text{Rb}_6\text{Si}_{17}$. The starting material of the nominal composition $\text{K}_6\text{Rb}_6\text{Si}_{17}$ can be considered as a mixture of $(\text{K,Rb})_4\text{Si}_4$, $(\text{K,Rb})_{12}\text{Si}_{17}$ and amorphous material of unknown composition. The Raman spectrum shows the frequencies of Si_4^{4-} (286.2 cm^{-1} , 355.9 cm^{-1} and 479.3 cm^{-1}) and Si_9^{4-} (391.6 cm^{-1}) (Figure 5.5)^[26]. The experimental diffraction patterns presented in Figure 5.6a and Figure 5.6c show only the peaks of $(\text{K}_2\text{Rb}_2)\text{Si}_4$ and Si. The expected reflections of $\text{A}_{12}\text{Si}_{17}$ (with $\text{A} = \text{K, Rb}$) (Figure 5.6b) are missing, the material is presumably of very poor crystallinity. So, Raman spectroscopy,

powder diffraction and MAS-NMR experiments (see main article Figure 5.2b) confirmed the presence of Si_4^{4-} in the solid starting material, while the presence of Si_9^{4-} could only be proven by Raman spectroscopy.

1.2 Phase Determination and NMR data 6

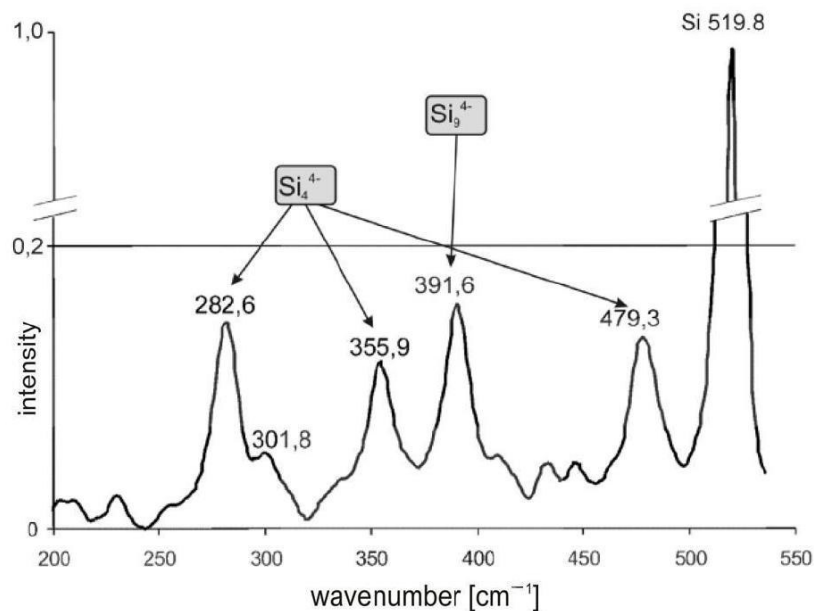


Figure 5.5: The Raman spectrum shows the characteristic frequencies of, both Si_4^{4-} and Si_9^{4-} clusters.

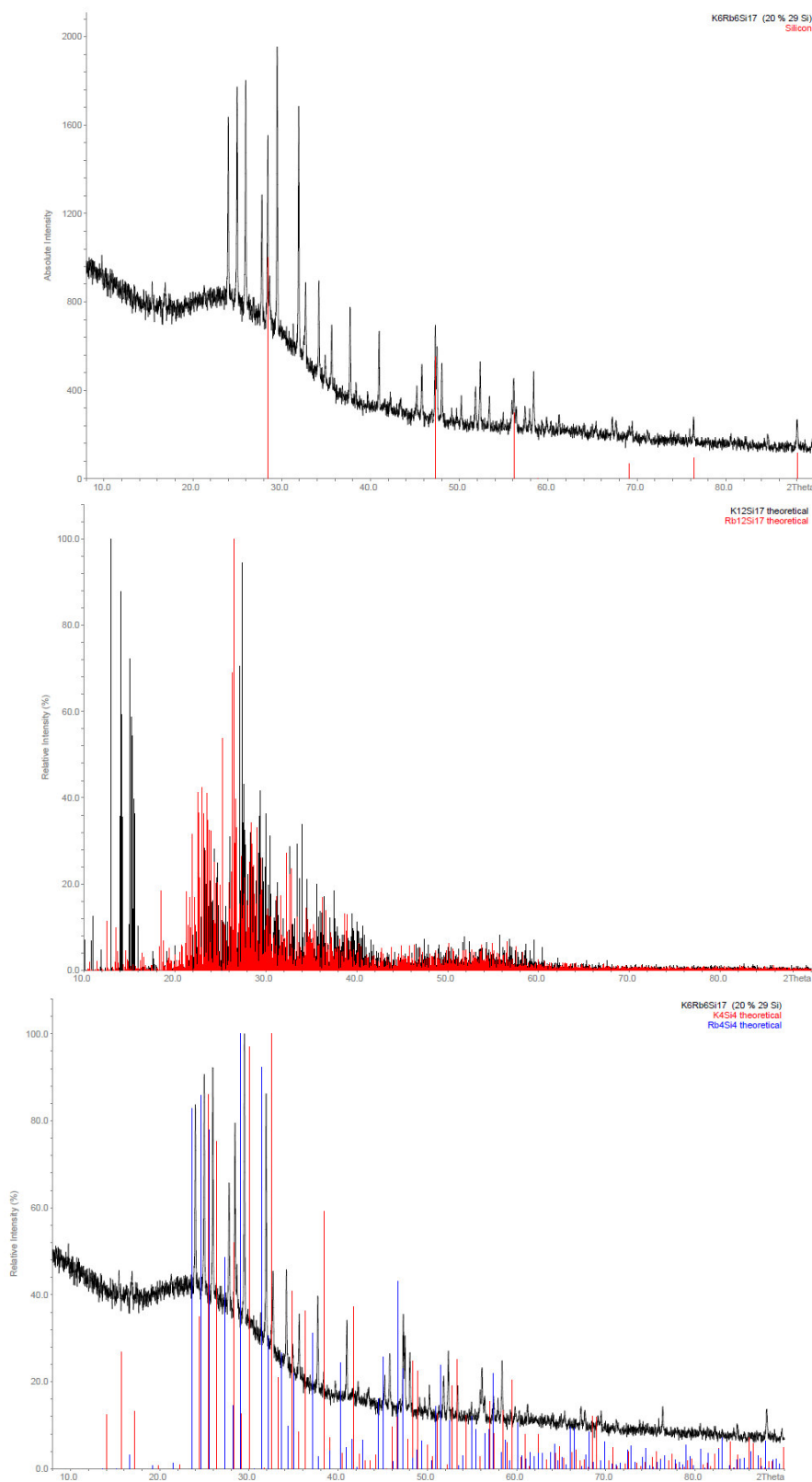


Figure 5.6: (a) Comparison of the experimental diffraction pattern of $K_6Rb_6Si_{17}$ (black) and unreacted silicon (red). (b) Theoretical diffraction patterns of $K_{12}Si_{17}$ (black) and $Rb_{12}Si_{17}$ (red). (c) Comparison of the experimental diffraction pattern of $K_6Rb_6Si_{17}$ (black) and the theoretical diffraction patterns of K_4Si_4 (red) and Rb_4Si_4 (blue).

Data collecting and processing

The NMR spectra were recorded on a Bruker Avance 600 spectrometer equipped with a 5 mm broadband triple resonance Z-gradient probe. The temperatures for all measurements were controlled by a Bruker BVTE 3900 temperature unit. ^{119}Sn measurements were carried out with a standard Bruker pulse program (zg) using 70k number of scans, 2 dummy scans, TD = 8k with a relaxation delay of 0.3 s. Data were processed with the Bruker software TOPSPIN 3.1 using the processing parameters SI = 16 k, WDW = EM and LB = 50 Hz. The chemical shifts are reported in ppm relative to SnMe_4 . ^{29}Si measurements were carried out with a standard Bruker pulse program (zg30) using 3k number of scans, 8 dummy scans, TD = 8k with a relaxation delay of 5 s. Data were processed with the Bruker software TOPSPIN 3.1 using the processing parameters SI = 16k, WDW = EM and LB = 1 Hz. The chemical shifts are reported in ppm relative to SiMe_4 . All signal to noise ratios were determined by using the Bruker analysis tool for S/N calculations.

Signal assignment

The more abundant ^{119}Sn was used as observe nucleus and the ^{117}Sn - ^{119}Sn scalar coupling for signal assignment. Therefore, the coupling patterns for all possible cluster sizes (4, 5 and 9) were calculated from the statistical distribution of both NMR active nuclei over the respective polyanion (see Table 5.1). Based on these calculations and for a better visualization, theoretical NMR spectra were simulated for these patterns and compared to the experimental ones.

Table 5.1: Theoretical coupling pattern.

Possible Clusters	Theoretical coupling
E_4^{4-}	0.047:0.324:1.000:0.324:0.047
E_5^{2-}	0.011:0.170:1.000:0.170:0.011
E_9^{4-}	0.006:0.128:1.000:0.128:0.006

Additional NMR spectra (see Figures 5.7, 5.8, 5.9 and 5.10).

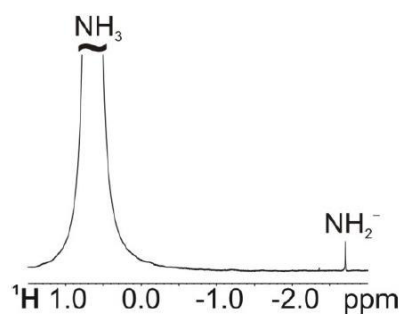


Figure 5.7: ^1H spectrum of pure RbNH_2 at 195K in liquid ammonia serves as reference for further signal assignment.

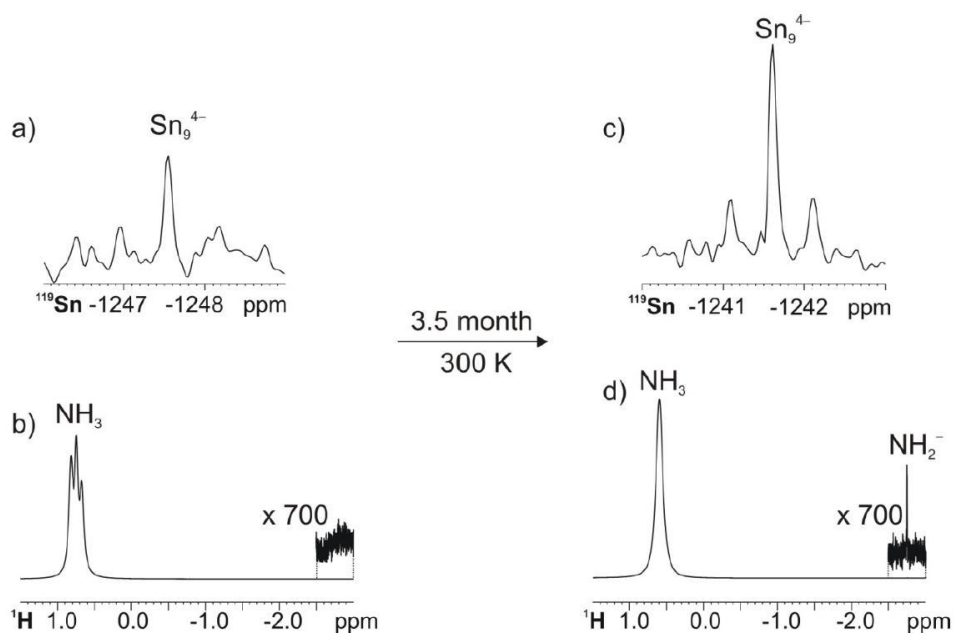


Figure 5.8: Solvation of Rb_4Sn_4 in liquid ammonia. The ^{119}Sn spectrum recorded from the freshly prepared sample at 195K (a) shows a small Sn_9^{4-} signal at -1247.5 ppm. The corresponding proton spectrum (b) shows a triplet for liquid ammonia and no detectable amount of NH_2^- (assigned by comparison with the reference spectrum of NH_2^- in liquid ammonia shown in Figure 5.7). Upon storing the sample at room temperature for 3.5 month, the signal grows significantly, which is visible in the ^{119}Sn spectrum (c) recorded at 300 K. Probably, the chemical shift offset of 6 ppm is due to a temperature effect. The signal growth of Sn_9^{4-} is accompanied by (d) the evolution of NH_2^- , which is detectable alongside of NH_3 . Simultaneously, the coupling pattern of ammonia breaks down. Presumably, this effect is due to chemical exchange with the amide.

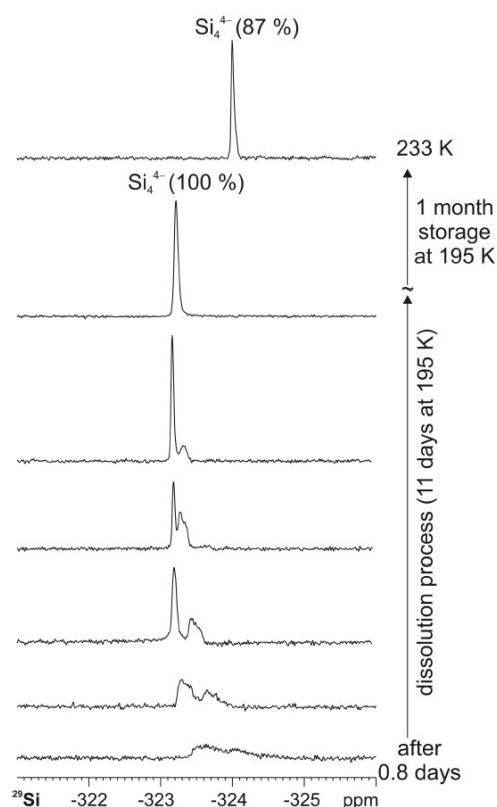


Figure 5.9: ^{29}Si spectra recorded at 195 K from the solvation of $\text{K}_6\text{Rb}_6\text{Si}_{17}$ (20 % enriched in ^{29}Si) and [2.2.2]-cryptand in liquid ammonia. The spectra clearly show the solvation process of the solid state material. In the beginning, this process is characterized by a 1.6 ppm extended signal, which results in one narrow line after 10 days. Due to the unexpected stability, this signal is also detectable at 233 K with an upfield shift of 0.9 ppm, which agrees with the greater cation mobility at elevated temperatures.

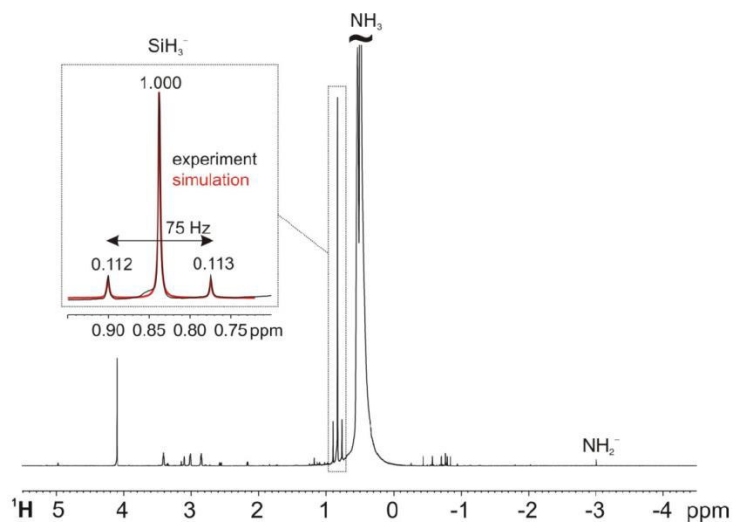


Figure 5.10: After one year storage of the solvation sample of $\text{K}_6\text{Rb}_6\text{Si}_{17}$ in liquid ammonia at 195 K and in the absence of stabilizing [2.2.2]-cryptand, the ^1H spectrum shows a variety of degradation products. The signals for SiH_3^- and NH_2^- could be unambiguously assigned in comparison to the simulated signal of SiH_3^- including the 20% ^{29}Si labeling and a reference spectrum of NH_2^- in liquid ammonia (see Figure 5.7).

5.4 Additional Findings

5.4.1 Reaction of Sn_4^{4-} in Liquid Ammonia:

The formation of $\text{Rb}_6[(\eta^2\text{-Sn}_4)\text{Zn}(\eta^3\text{-Sn}_4)] \cdot 5\text{NH}_3^{**}$

I performed the NMR spectroscopic investigations. The synthesis and the characterization of the solids as well as the sample preparation were carried out by Franziska Fendt and Stefanie Gärtner.

******Franziska Fendt, Carina Koch, Stefanie Gärtner and Nikolaus Korber,
Dalton Trans. **2013**, 42, 15548-15550.

DOI: 10.1039/c3dt51932e

Reproduced by permission of The Royal Society of Chemistry.

Abstract

The reaction of Rb_4Sn_4 with ZnPh_2 in liquid ammonia in presence of [2.2.2]-cryptand yielded crystals of $\text{Rb}_6[(\eta^2\text{-Sn}_4)\text{Zn}(\eta^3\text{-Sn}_4)] \cdot 5\text{NH}_3$, which could be characterized by single crystal X-ray diffraction. This is the first example of a successful solution reaction of the highly charged tetrahedral Sn_4^{4-} anions. The homoleptic $[\text{E}_4\text{ZnE}_4]^{6-}$ complex (E = tetrel element) was previously known only for E = Ge and Si/Ge.

Introduction

Homoatomic polyanions of group 14 or 15 are a very fascinating class of compounds as they can be considered as molecular, discrete building blocks of the main group elements.^[1] These polyanions are known from solid state materials, where the term *Zintl* phases holds true.^[27] Some of the *Zintl* phases are soluble in appropriate solvents like ethylenediamine or liquid ammonia and undergo versatile chemical transformations with different (post-) transition metal complexes as well as main group element compounds. These investigations have been limited to the well investigated E_9^{4-} (E=Si-Pb) anions and a large number of reaction products can be found in the literature.^[1] In contrast, only very little is known about the solution behavior of the more highly reduced tetrahedral species E_4^{4-} , which exist in the binary *Zintl* phases A_4E_4 and $\text{A}_{12}\text{E}_{17}$.^[24–31] Only very few compounds are reported for derivatives of these anions. By reacting $\text{K}_6\text{Rb}_6\text{Si}_{17}$ or $\text{K}_{14}\text{ZnGe}_{16}$, respectively, with MesCu in liquid ammonia compounds including the $[(\text{MesCu})_2\text{E}_4]^{4-}$ (E=Si^[10] or Ge^[32]) anion could be crystallized. The use of mixed $\text{K}_{12}(\text{Si,Ge})_{17}$ precursor materials reacted with diphenylzinc resulted in the formation of $\text{K}_6\text{ZnSi}_{4.1(1)}\text{Ge}_{3.9(1)} \cdot 11\text{NH}_3$.^[33] The lack of similar results for the heavier homologues tin and lead is conspicuous. A possible explanation could be that the potential precursor materials A_4E_4 were supposed to be insoluble until very recently.^[32]

Results and Discussion

In preliminary investigations we were able to show that Rb_4Sn_4 is soluble in anhydrous liquid ammonia, which is the best solvent for these very air and moisture sensitive compounds.^[34] However, ^{119}Sn NMR experiments on ammonia solutions of Rb_4Sn_4 demonstrated that the use of pure liquid ammonia, without any further additives, exclusively yields Sn_9^{4-} clusters by fast rearrangement of the tetrahedral species in solution. Fortunately, the tetrahydride anions can be stabilized in solution by the use of [2.2.2]-cryptand. We now employed the thus acquired knowledge to investigate the

chemical reactions of Sn_4^{4-} anions towards post-transition metal compounds. As a first result, we here present the formation of $\text{Rb}_6[(\eta^2\text{-Sn}_4)\text{Zn}(\eta^3\text{-Sn}_4)] \cdot 5\text{NH}_3$ (**1**) by reacting Rb_4Sn_4 with diphenylzinc in liquid ammonia in presence of [2.2.2]-cryptand. The anionic moiety is represented by a $[(\text{Sn}_4)_2\text{Zn}]^{6-}$ (**1a**) unit, where a Zn^{2+} cation is coordinated by two Sn_4^{4-} anions (Figure 5.11).

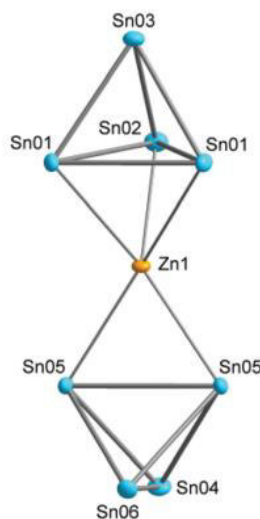


Figure 5.11: Representation of the homoleptic complex **1a**. Anisotropic displacement ellipsoids are shown with 50% probability level.

The coordination of a post-transition metal (M) by two group 14 tetrahedra (E_4) to form dimers ($\text{M}=\text{Zn}$, $\text{E}=\text{Ge}$ or Si/Ge),^[32,33,35] one-dimensional strands ($\text{M}=\text{Au}$, $\text{E}=\text{Sn}$ or Pb)^[36,37] or oligomers ($\text{M}=\text{Cd}$, $\text{E}=\text{Pb}$)^[38] is a well-known structural characteristic. A size effect seems to play a major role, as similar anionic moieties are reported for mixed alkali metal silicides and germanides, where the two tetrahedra are bridged by the smaller alkali metal.^[39–44] Concerning zinc, such compounds including the structural characteristic $[\text{E}_4\text{ZnE}_4]^{6-}$ are exclusively known for $\text{E}=\text{Ge}$ in solid state^[32,35] or obtained by reaction in solution for $\text{E}=\text{Si/Ge}$ (mixed)^[33]. The tetrahedra show a versatile coordination behavior towards the central atom by using two triangular faces, two edges or the combination of one triangular face and one edge giving coordination numbers of four to six for the Zn^{2+} cation (Table 5.2). It has to be noted, that in the here presented compound the junction of a (post-) transition metal and Sn_4^{4-} in general succeeded for the first time, and concerning zinc no comparable material is known in solid state or from solution experiments. With respect to the interaction of tin *Zintl* clusters and zinc, *closo*- $[\text{Sn}_9\text{ZnR}]^{3-}$ ($\text{R} = \text{Ph}$, *Mes*, *ⁱPr*) containing compounds are the only reported materials.^[45,46]

Table 5.2: Zn^{2+} linked group 14 tetrahedra show different coordination numbers of Zn^{2+} .

Compound	Anion	CN(Zn^{2+})
$\text{Cs}_6\text{Ge}_8\text{Zn}^{14}$	$[(\eta^3\text{-Ge}_4)\text{-Zn}(\eta^3\text{-Ge}_4)]^{6-}$	6
$\text{A}_{14}\text{ZnGe}_{16}$ (A=K, Rb) ¹¹	$[(\eta^2\text{-Ge}_4)\text{-Zn}(\eta^3\text{-Ge}_4)]^{6-}$	5
$\text{K}_6\text{Zn}(\text{Si,Ge})_8 \cdot 11\text{NH}_3$ ¹²	$[(\eta^2\text{-(Si,Ge)}_4)\text{-Zn}(\eta^2\text{-(Si,Ge)}_4)]^{6-}$	4
$\text{Rb}_6\text{ZnSn}_8 \cdot 5\text{NH}_3$	$[(\eta^2\text{-Sn}_4)\text{-Zn}(\eta^3\text{-Sn}_4)]^{6-}$	5

The asymmetric unit of **1** consists of six tin atoms, one Zn atom, six Rb cations and four ammonia molecules. Several of the atoms are located on special position $4i$ of space group $I2/m$ (four tin atoms, the Zn atom, five Rb cations and three nitrogen atoms). The Rb atom on the general position shows a site occupancy factor of 0.5, so that the electron count is balanced and gives a charge of -6 for the **1a** unit, in agreement with the formulation as Sn_4^{4-} and Zn^{2+} ions. In this anionic moiety, two Sn_4^{4-} tetrahedra coordinate to the Zn^{2+} cation and form a homoleptic complex. One triangular face of the first tetrahedron coordinates the Zn atom, additionally one edge of the second tetrahedron coordinates in an η^2 -like fashion, which gives a total coordination number of five for the Zn atom. The same coordination number is observed in the related germanium compound $\text{A}_{14}\text{ZnGe}_{16}$. The Sn-Sn bond lengths of the triangular face respectively edge which are capped by Zn^{2+} are significantly elongated compared to uncoordinated Sn_4^{4-} anions in solvate structures. The remaining Sn-Sn distances show the expected values for this class of compounds.^[9] The Sn-Zn distances lie between 2.7553(8) Å and 2.8062(6) Å and therefore are very close to the values of the $[\text{Sn}_9\text{ZnR}]^{3-}$ compounds ($d_{\text{Av}}(\text{Sn-Zn})=2.78$ Å).^[45,46] Figure 5.11 shows **1a**, the according distances are given in Table 5.3.

Table 5.3: Selected bond lengths for **1a**.

Bond ^a	Distance [Å]
Sn01–Sn01	3.0139(6)
Sn01–Sn02	3.0439(5)
Sn01–Sn03	2.8822(5)
Sn02–Sn03	2.8737(6)
Sn04–Sn05	2.8974(5)
Sn04–Sn06	2.9324(6)
Sn05–Sn05	3.0628(6)
Sn05–Sn06	2.9014(5)
Zn1–Sn01	2.8062(6)
Zn1–Sn02	2.7553(8)
Zn1–Sn05	2.7875(6)

As the asymmetric unit consists of six tin atoms, four of which are located on special positions, each tetrahedron only shows four instead of six unique distances. The coordination sphere of the anion is completed by 16 Rb^+ cations at Rb-Sn distances between 3.685(7) Å and 4.3798(3) Å which interconnect the **1a** anions to form a three dimensional network of cations and anions. The coordination sphere of the Rb atoms is

saturated by two to three ammonia molecules at distances between 2.90(4) Å and 4.036(7) Å. Considering the Rb-ammonia network within the given distances, one dimensional strands along the crystallographic *b*-axis can be described, which are interconnected due to the $\text{Rb}^+ - \text{Sn}_4^{4-}$ interaction giving a three dimensional network of cations, anions and ammonia molecules.

According to our stoichiometric approach of $\text{Rb}_4\text{Sn}_4 : \text{ZnPh}_2 : [\text{2.2.2}]\text{-crypt}$ of 1:1:1 one would expect unreacted Ph_2Zn , benzene and $[\text{2.2.2}]\text{-cryptand}$ to remain in solution. In contrast, the results of ^{13}C and $^1\text{H}, ^{13}\text{C}$ HSQC NMR investigations only gave rise to the presence of benzene and cryptand. Careful examination of the reaction precipitate showed the presence of further crystals, very similar in shape and colour to those of **1**. Single crystal X-ray determination showed the compound to be a zincate with the composition $[(\text{Rb@crypt})\text{ZnPh}_3 \cdot \text{NH}_3]$ (**2**), which contains the well-known zincate anion $[\text{ZnPh}_3]^-$.^[47] This allows for the remaining phenyl substituents as well as the excessive ZnPh_2 . The requirement of excess Ph_2Zn needs to be proven. Despite much effort, no ^{119}Sn signal could be detected so far, which might indicate low concentrations of **1** in solution. Similar observations were previously reported by other groups.^[45]

Conclusion

We present here the first successful chemical transformation of the highly charged tin Zintl anion Sn_4^{4-} by using the binary solid state material Rb_4Sn_4 , $[\text{2.2.2}]\text{-cryptand}$ and diphenylzinc in liquid ammonia solution. The presence of this anion in solution could be proven only very recently; the here shown possibility of reacting them opens doors to a versatile solution chemistry of tetrahedral tin *Zintl* anions Sn_4^{4-} .

Supplementary Information

Experimental procedure. All manipulations were performed under argon atmosphere using standard Schlenk and Glovebox techniques. Liquid ammonia was dried over elemental potassium prior to use. Diphenylzinc, ZnPh_2 , and [2.2.2]-cryptand (systematic name: 4,7,13,16,21,24-Hexaoxa-1,10-diazabicyclo[8.8.8]heccacosane) were commercially purchased from Sigma Aldrich and used without further drying.

50 mg Rb_4Sn_4 (0.06 mmol) were dissolved in approximately 5 mL liquid ammonia together with 13 mg ZnPh_2 (0.06 mmol) (further information concerning synthesis and characterization see chapter 5.3.1 or the Supporting Information of the previously published article ^[34]). The solution immediately turned deeply red after the addition of liquid ammonia and was stored at 236 K for about 6 months until crystallization. Crystals of $\text{Rb}_6[(\eta^2\text{-Sn}_4)\text{Zn}(\eta^3\text{-Sn}_4)] \cdot 5\text{NH}_3$ (**1**) (major product) and $(\text{Rb}@[2.2.2]\text{-crypt})\text{ZnPh}_3 \cdot \text{NH}_3$ (**2**) were obtained.

Crystal structure determination. Thermally unstable, air- and moisture- sensitive crystals of **1** and **2** suitable for X-ray structure analysis were isolated and directly transferred from the mother liquor into a perfluorether oil at 213 K. The crystals were mounted onto an Agilent SuperMova diffractometer and analytical absorption correction respectively multiscan absorption correction was applied. Data collection was carried out at 123 K by using graphite-monochromated Mo-K- α radiation ($\lambda=0.71073\text{\AA}$). The data reductions were performed with the CrysAlis program package (CrysAlisPro, Agilent Technologies, Version 1.171.36.28 (release 01-02-2013 CrysAlis171 .NET)). The structures of **1** and **2** were determined with the SIR92^[48,49] or OLEX2^[50] program packages and refined anisotropically with SHELXL-97^[51] against $|F^2|$ for all non-hydrogen atoms.

The crystal of **1** showed non-merohedral twinning. Due to only few overlapping reflections (200) the reflections from the main domain (indexing of 75%) allowed the solution of the structure. Hydrogen atoms of one ammonia molecule could be located in the difference fourier maps, for 2 ammonia molecules, the hydrogen atoms were placed in geometrically reasonable positions. For one disordered ammonia molecule constructed positions did not seem reasonable. Rb4 showed disordering, which allowed the introduction of split positions. Rb5 is located on a general position but a s.o.f. of 0.5 was fixed (after a careful examination by using a second free variable which refined to a value

of 0.5) and allowed the electroneutral formulation of **1**. The selected X-ray data and refinement parameters for **1** are shown in Table 5.4. Atomic coordinates and displacement parameters are listed in Table 5.6 to Table 5.8.

Table 5.4: Selected X-ray data collection and refinement parameters for $\text{Rb}_6\text{Sn}_8\text{Zn} \cdot 5\text{NH}_3$ (Deposition number CSD 426039).

FW/g mol ⁻¹	1613.08
Space group, <i>Z</i>	<i>I</i> 2/ <i>m</i> (No.12)*, 4
<i>a</i> /Å	19.7142(3)
<i>b</i> /Å	7.82480(10)
<i>c</i> /Å	21.0029(3)
β /°	105.632(2)
<i>V</i> /Å ³	3120.06(8)
ρ_{calc} /g cm ⁻³	3.434
Radiation, λ /Å	MoK α , 0.71073
<i>T</i> /K	123.15
μ /cm ⁻¹	16.339
Reflections collected	26678
Independent reflections	3416
<i>R</i> _{int}	0.0347
<i>R</i> ₁ / <i>w R</i> ₂ , <i>I</i> ≥ 2σ ₁	0.0198/0.0509
<i>R</i> ₁ / <i>w R</i> ₂ , all data	0.0228/0.0520

For the crystal structure of **2**, the hydrogenatoms of the cryptand molecule and ZnPh_3 were placed using HFIX 23 or HFIX 43, respectively. The hydrogen atoms of the ammonia molecule could be located in the fourier difference maps and were refined isotropically. For further information on structure determination see Table 5.5.

Table 5.5: Selected X-ray data collection and refinement parameters for $(\text{Rb}@[2.2.2]\text{-crypt})\text{ZnPh}_3 \cdot \text{NH}_3$ (Deposition number CCDC 939282).

FW/g mol ⁻¹	775.66
Space group, <i>Z</i>	<i>P</i> 2 ₁ / <i>c</i> , 4
<i>a</i> /Å	15.12530(10)
<i>b</i> /Å	13.62330(10)
<i>c</i> /Å	18.76700(10)
β /°	99.3590(10)
<i>V</i> /Å ³	3815.59(4)
ρ_{calc} /g cm ⁻³	1.350
Radiation, λ /Å	MoK α , 0.71073
<i>T</i> /K	123.15
μ /cm ⁻¹	1.956
Reflections collected	23861
Independent reflections	6967
<i>R</i> _{int}	0.0188
<i>R</i> ₁ / <i>w R</i> ₂ , <i>I</i> ≥ 2σ ₁	0.0225/0.0516
<i>R</i> ₁ / <i>w R</i> ₂ , all data	0.0263/0.0533

Table 5.6: Atomic Coordinates and Isotropic Displacement Parameters for $\text{Rb}_6\text{Sn}_8\text{Zn} \cdot \text{NH}_3$.

Atom	x [Å]	y [Å]	z [Å]	s.o.f	Ueq[Å ²]
Sn04	0.66397(2)	0.00000	0.14159(2)	1	0.0172(1)
Sn02	0.48552(2)	-0.50000	0.23844(2)	1	0.0168(1)
Sn03	0.36543(2)	-0.50000	0.29134(2)	1	0.0161(1)
Sn01	0.48594(1)	0.30741(4)	0.36446(1)	1	0.0145(1)
Sn05	0.72250(1)	0.30429(4)	0.38612(1)	1	0.0139(1)
Sn06	0.81540(2)	-0.50000	0.49156(2)	1	0.0151(1)
Zn1	0.60008(3)	-0.50000	0.34796(3)	1	0.0116(2)
N03	0.4012(5)	0.00000	0.4868(4)	1	0.059(3)
N02	0.2300(2)	-0.2542(6)	0.3639(2)	1	0.0237(12)
N01	0.4388(3)	0.00000	0.1866(3)	1	0.0291(19)
N4A	0.6062(7)	-0.50000	0.0217(14)	0.50(10)	0.020(6)
N4B	0.5976(7)	-0.50000	0.0575(12)	0.50(10)	0.017(5)
Rb01	0.58652(3)	0.00000	0.28525(3)	1	0.0150(2)
Rb02	0.33234(3)	0.00000	0.32606(4)	1	0.0235(2)
Rb03	0.67859(3)	-0.50000	0.20650(3)	1	0.0173(2)
Rb4B	0.773(2)	0.00000	0.5320(10)	0.52(16)	0.043(4)
Rb5	0.48785(4)	-0.23123(12)	0.07888(5)	0.500	0.0195(3)
Rb6	0.37206(4)	-0.50000	0.47736(4)	1	0.0406(3)
Rb4A	0.7508(10)	0.00000	0.5247(5)	0.48(16)	0.0251(15)

Table 5.7: Atomic Coordinates of Hydrogen Atoms and Isotropic Displacement Parameters for $\text{Rb}_6\text{Sn}_8\text{Zn} \cdot \text{NH}_3$.

Atom	x [Å]	y [Å]	z [Å]	s.o.f	Ueq[Å ²]
H03A	0.43400	-0.05380	0.47040	0.5	0.0740
H4AA	0.60340	0.05590	0.47690	0.5	0.0740
H03B	0.41490	-0.10960	0.49730	0.5	0.0740
H02A	0.25210	-0.31840	0.34200	1	0.05(2)
H4AB	0.79820	0.33620	0.61620	1	0.040(17)
H02B	0.19410	-0.21310	0.33010	1	0.06(2)
H01B	0.44040	-0.01230	0.23020	0.5	0.0740
H01A	0.43290	-0.10440	0.16690	0.5	0.0740
H01C	0.40120	-0.06790	0.16690	0.5	0.0740

Table 5.8: Atomic Coordinates and Anisotropic Displacement Parameters for $\text{Rb}_6\text{Sn}_8\text{Zn} \cdot \text{NH}_3$.

Atom	U ₁₁ [Å ²]	U ₂₂ [Å ²]	U ₃₃ [Å ²]	U ₂₃ [Å ²]	U ₁₃ [Å ²]	U ₁₂ [Å ²]
Sn04	0.0123(2)	0.0243(3)	0.0172(2)	0.0000	0.0078(2)	0.0000
Sn02	0.0165(2)	0.0236(2)	0.0110(2)	0.0000	0.0051(2)	0.0000
Sn03	0.0102(2)	0.0195(2)	0.0176(2)	0.0000	0.0020(2)	0.0000
Sn01	0.0138(2)	0.0107(2)	0.0196(2)	0.0036(1)	0.0055(1)	0.0002(1)
Sn05	0.0124(1)	0.0092(2)	0.0189(2)	-0.0014(1)	0.0024(1)	-0.0006(1)
Sn06	0.0155(2)	0.0173(2)	0.0107(2)	0.0000	0.0007(2)	0.0000
Zn1	0.0073(3)	0.0154(4)	0.0124(3)	0.0000	0.0034(3)	0.0000
N03	0.071(6)	0.045(5)	0.044(5)	0.0000	-0.012(4)	0.0000
N02	0.028(2)	0.022(2)	0.023(2)	0.0038(19)	0.0102(19)	-0.0008(19)
N01	0.018(3)	0.036(4)	0.029(3)	0.0000	-0.001(3)	0.0000
N4A	0.020(6)	0.021(7)	0.022(14)	0.0000	0.011(6)	0.0000
N4B	0.024(6)	0.019(6)	0.013(11)	0.0000	0.013(6)	0.0000
Rb01	0.0144(3)	0.0145(3)	0.0169(3)	0.0000	0.0058(2)	0.0000
Rb02	0.0181(3)	0.0151(3)	0.0386(4)	0.0000	0.0097(3)	0.0000
Rb03	0.0210(3)	0.0165(3)	0.0161(3)	0.0000	0.0080(2)	0.0000
Rb4B	0.0890(10)	0.0177(12)	0.037(3)	0.0000	0.042(5)	0.0000
Rb5	0.0136(4)	0.0178(4)	0.0239(5)	0.0027(4)	-0.0003(3)	0.0007(3)
Rb6	0.0200(4)	0.0881(7)	0.0151(3)	0.0000	0.0072(3)	0.0000
Rb4A	0.049(4)	0.0127(12)	0.0221(19)	0.0000	0.024(2)	0.0000

NMR-Data collection and processing. NMR spectra were recorded on a Bruker Avance 600 (600.13 MHz) spectrometer with a 5 mm broadband triple resonance Z-gradient (53.5 G cm⁻¹). The temperature was controlled by a Bruker BVTE 3000 unit. NMR data were processed with the Bruker TOPSPIN 3.2 program.

For ZnPh₂ four signals would be expected in ¹³C NMR-experiments (148.1, 137.7, 127.8, 127.6 ppm).ⁱ These could be neither detected in 1D-¹³C spectrum nor in the ¹H, ¹³C HSQC spectrum. We only observed signals at 7.17 ppm and 128.33 ppm, which fit the literature known values for benzene (Figure 5.12).ⁱⁱ The remaining ¹³C signals can be assigned to the [2.2.2]-cryptand molecule.

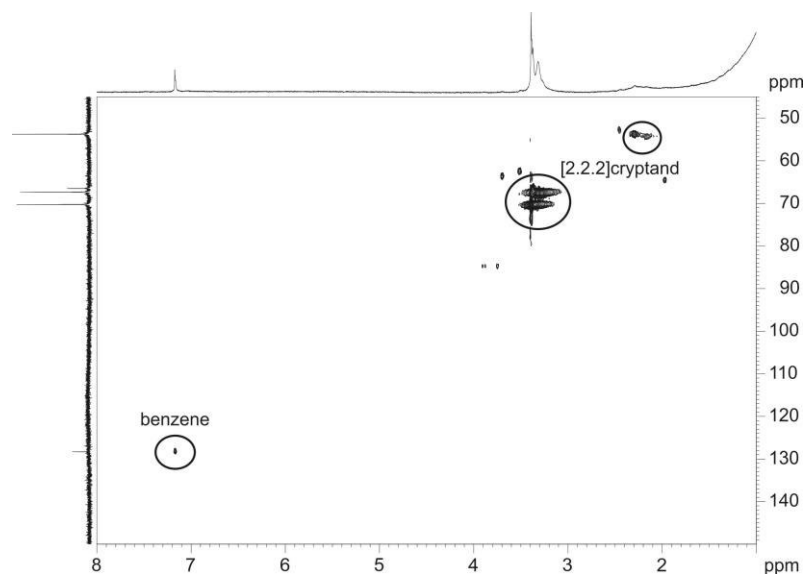


Figure 5.12: ¹H, ¹³C HSQC spectrum of Rb₄Sn₄ + [2.2.2]-cryptant + ZnPh₂ in liquid NH₃ at 233 K, shows the signal for benzene, but none for ZnPh₂ are detected in this solution.

ⁱ These data have been obtained by own measurements of ZnPh₂ CD₂Cl₂.

ⁱⁱ Predicted NMR data calculated using Advanced Chemistry Development, Inc. (ADC/Labs) Software V11.01 (© 1994-2013 ADC/Labs).

5.5 References

- [1] S. Scharfe, F. Kraus, S. Stegmaier, A. Schier, T. F. Fässler, *Angew. Chem. Int. Ed.* **2011**, *50*, 3630–3670.
- [2] A. M. Guloy, R. Ramlau, Z. Tang, W. Schnelle, M. Baitinger, Y. Grin, *Nature* **2006**, *443*, 320–323.
- [3] N. Chandrasekharan, S. C. Sevov, *J. Electrochem. Soc.* **2010**, *157*.
- [4] M. Baudler, K. Glinka, *Chem. Rev.* **1993**, *93*, 1623–1667.
- [5] R. W. Rudolph, W. L. Wilson, R. C. Taylor, *J. Am. Chem. Soc.* **1981**, *103*, 2480–2481.
- [6] W. L. Wilson, R. W. Rudolph, L. L. Lohr, R. C. Taylor, P. Pyykko, *Inorg. Chem.* **1986**, *25*, 1535–1541.
- [7] R. W. Rudolph, W. L. Wilson, F. Parker, R. C. Taylor, D. C. Young, *J. Am. Chem. Soc.* **1978**, *100*, 4629–4630.
- [8] F. S. Kocak, D. O. Downing, P. Zavalij, Y.-F. Lam, A. N. Vedernikov, B. Eichhorn, *J. Am. Chem. Soc.* **2012**, *134*, 9733–97410.
- [9] K. Wiesler, K. Brandl, A. Fleischmann, N. Korber, *Z. Anorg. Allg. Chem.* **2009**, *635*, 508–512.
- [10] M. Waibel, F. Kraus, S. Scharfe, B. Wahl, T. F. Fässler, *Angew. Chem. Int. Ed.* **2010**, *49*, 6611–6615.
- [11] M. Ichinohe, M. Toyoshima, R. Kinjo, A. Sekiguchi, *J. Am. Chem. Soc.* **2003**, *125*, 13328–13329.
- [12] J. M. Goicoechea, S. C. Sevov, *Inorg. Chem.* **2005**, *44*, 2654–2658.
- [13] J. M. Goicoechea, S. C. Sevov, *J. Am. Chem. Soc.* **2004**, *126*, 6860–6861.
- [14] S. Joseph, C. Suchentrunk, N. Korber, *Z. Naturforsch. B* **2010**, *65*, 1059–1065.
- [15] S. Joseph, C. Suchentrunk, F. Kraus, N. Korber, *Eur. J. Inorg. Chem.* **2009**, 4641–4647.
- [16] S. Joseph, M. Hamberger, F. Mutzbauer, O. Härtl, M. Meier, N. Korber, *Angew. Chem.* **2009**, *121*, 8926–8929.
- [17] K. Abersfelder, A. J. P. White, R. J. F. Berger, H. S. Rzepa, D. Scheschkewitz, *Angew. Chem. Int. Ed.* **2011**, *50*, 7936–7939.

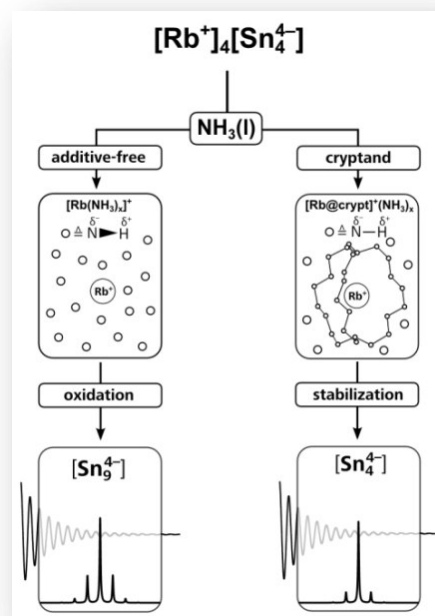
-
- [18] J. D. Corbett, P. A. Edwards, *J. Chem. Soc. Chem. Commun.* **1975**, 984–985.
- [19] F. Teixidor, M. L. Luetkens, R. W. Rudolph, *J. Am. Chem. Soc.* **1983**, *105*, 149–150.
- [20] L. A. Stearns, J. Gryko, J. Diefenbacher, G. K. Ramachandran, P. F. McMillan, *J. Solid State Chem.* **2003**, *173*, 251–258.
- [21] T. Goebel, A. Ormeci, O. Pecher, F. Haarmann, *Z. Anorg. Allg. Chem.* **2012**, *638*, 1437–1445.
- [22] F. Fehér, M. Krancher, M. Fehér, *Z. Anorg. Allg. Chem.* **1991**, *606*, 7–16.
- [23] M. Somer, U. Aydemir, M. Baitinger, H. G. von Schnering, *Z. Anorg. Allg. Chem.* **2006**, *632*, 1281–1286.
- [24] H. G. von Schnering, M. Baitinger, Y. Grin, R. Kniep, *Z. Krist. NCS* **1999**, *214*, 457–458.
- [25] H. G. von Schnering, Y. Grin, M. Baitinger, R. Kniep, *Z. Krist. NCS* **1999**, *214*, 453.
- [26] C. Hoch, M. Wendorff, C. Röhr, *J. Alloy. Comp.* **2003**, *361*, 206–221.
- [27] S. Gärtner, N. Korber, in *Zintl Inons Princ. Recent Dev.* (Ed.: T.F. Fässler), Springer-Verlag, Berlin Heidelberg, Germany, **2011**, pp. 25–56.
- [28] H. G. von Schnering, M. Schwarz, J.-H. Chang, K. Peters, E.-M. Peters, R. Nesper, *Z. Krist. NCS* **2005**, *220*, 525–527.
- [29] T. Goebel, Y. Prots, F. Haarmann, *Z. Krist. NCS* **2008**, *223*, 187–188.
- [30] H. G. von Schnering, J. Llanos, J.-H. Chang, K. Peters, E.-M. Peters, R. Nesper, *Z. Krist. NCS* **2005**, *220*, 324–326.
- [31] R. E. Marsh, D. P. Shoemaker, *Acta Crystallogr.* **1953**, 197–205.
- [32] S. Stegmaier, M. Waibel, A. Henze, L. A. Jantke, A. J. Karttunen, T. F. Fässler, *J. Am. Chem. Soc.* **2012**, *134*, 14450–14460.
- [33] M. Waibel, T. Henneberger, L.-A. Jantke, T. F. Fässler, *Chem. Commun.* **2012**, *48*, 8676–8678.
- [34] M. Neumeier, F. Fendt, S. Gärtner, C. Koch, T. Gärtner, N. Korber, R. M. Gschwind, *Angew. Chem. Int. Ed.* **2013**, *52*, 4483–4486.
- [35] V. Queneau, S. C. Sevov, *J. Am. Chem. Soc.* **1997**, *119*, 8109–8110.
- [36] U. Zachwieja, M. Wlodarski, *Z. Anorg. Allg. Chem.* **2004**, *630*, 993–997.
-

- [37] U. Zachwieja, J. Müller, J. Wlodarski, *Z. Anorg. Allg. Chem.* **1998**, 624, 853–858.
- [38] E. Todorov, S. C. Sevov, *Angew. Chem. Int. Ed.* **1999**, 38, 1775–1777.
- [39] M. Schwarz, PhD Thesis, Universität Stuttgart, **1987**.
- [40] H. G. von Schnering, M. Schwarz, R. Nesper, *Angew. Chem. Int. Ed.* **1986**, 98, 558.
- [41] T. Goebel, F. Haarmann, *Z. Krist. Suppl.* **2009**, 29, 132.
- [42] T. Goebel, F. Haarmann, *Z. Anorg. Allg. Chem.* **2008**, 634, 2040.
- [43] T. Goebel, Y. Prots, A. Ormeci, O. Pecher, F. Haarmann, *Z. Anorg. Allg. Chem.* **2011**, 637, 1982–1991.
- [44] T. Goebel, P. Jeglic, F. Haarmann, *Z. Krist. Suppl.* **2008**, 28, 18–20.
- [45] B. B. Zhou, M. S. Denning, C. Jones, J. M. Goicoechea, *Dalt. Trans. (Cambridge, Engl. 2003)2* **2009**, 1571–1578.
- [46] J. M. Goicoechea, S. C. Sevov, *Organometallics* **2006**, 25, 4530–4536.
- [47] M. Krieger, G. Geiseler, K. Harms, J. Merle, W. Massa, K. Dehnicke, *Z. Anorg. Allg. Chem.* **1998**, 624, 1387–1388.
- [48] L. J. Farrugia, *J. Appl. Cryst.* **1999**, 32, 837.
- [49] P. Sluis, A. L. van der & Spek, *Acta Crystallogr.* **1990**, A46, 194–201.
- [50] O. V. Dolomanov, L. J. Bourhis, R. J. Gildea, J. A. K. Howard, H. Puschmann, *J. Appl. Cryst.* **2009**, 42, 339–341.
- [51] G. Sheldrick, SHELX97 - Programs for Solution and Refinement of Crystal Structures, Universität Göttingen, **1997**.

6 Investigations on the Solvation and Transformation Chemistry of Zintl Anions in Liquid Ammonia

Full Paper

*“Stability and Conversion of Tin Zintl Anions in Liquid Ammonia Investigated by NMR Spectroscopy”**



The NMR spectroscopic investigations were performed in close collaboration with Maria Neumeier. The synthesis and characterization of the solids as well as the sample preparation were carried out by Franziska Fendt (homoatomic stannides) and Ute Friedrich (heteroatomic stannides).

*Franziska Fendt^[+], Carina Koch^[+], Maria Neumeier, Stefanie Gärtner, Nikolaus Korber and Ruth M. Gschwind,

Chem. Eur. J. **2015**, submitted for publication.

Unpublished work © 2015 American Chemical Society

[+] These authors contributed equally to this work.

In Additional Findings:

*“Synthesis of heteroatomic Zintl anions in liquid ammonia – the new highly charged [Sn₄Bi₄]⁴⁻ and fully ordered [Sn₂Bi₂]²⁻”***

**Ute Friedrich, Maria Neumeier, Carina Koch and Nikolaus Korber,
Chem. Commun. **2012**, 48, 10544-10546.

6.1 Abstract

Homoatomic polyanions of post-transition main group metals, namely Zintl anions, are precasted in analogues Zintl phases and can be reacted in solution to form new materials. Despite comprehensible reaction approaches, the formed products cannot be planned in advance, as hitherto undetected and therefore disregarded side reactions are taking place. The results and interpretation of the reactions of Zintl anions are so far based mainly on crystal structures, which only allow for the characterization of the product that features the lowest solubility. Here, we present the results of our investigations concerning the stability of the highly charged tin Zintl anions in liquid ammonia which are not exclusively based on solution effects but also on the oxidation property of the solvent. This allows for a deeper understanding of the ongoing processes in solution and opens doors to the directed synthesis of transition metal complexes of Sn_4^{4-} , here shown by its reactivity towards MesCu .

6.2 Manuscript

6.2.1 Introduction

Zintl phases can be seen as representatives for metalides, hence metals in negative oxidation states, which are formed by reacting a group 14, 15 or 16 element with an alkali or alkaline earth metal at high temperatures by solid state methods. Some of these phases are soluble in liquid ammonia or ethylenediamine and allow for chemical transformations in solution.^[1] Concerning soluble alkali metal Zintl materials including homoatomic polyanions of group 14 elements, convenient precursor materials are restricted to a minor number of solid state phases following the compositions A_4E_4 , A_4E_9 and $\text{A}_{12}\text{E}_{17}$ (A = alkali metal; E = group 14 element). In A_4E_4 with a formal charge (C_f) of -1 per atom, small tetrahedral E_4^{4-} anions are present, which are (valence-)isoelectronic to white phosphorus. A_4E_9 materials contain the mono-capped square-antiprismatic shaped E_9^{4-} clusters ($C_f = -0.444$), whereas Zintl phases following the formula $\text{A}_{12}\text{E}_{17}$ include both kinds of cluster anions in the ratio of $\text{E}_4^{4-}:\text{E}_9^{4-}$ equals 2:1. Aside from the dissolution of Zintl phases prepared by common solid state methods, the desired homoatomic polyanions can also be prepared by directly reducing the pure element by solvated electrons derived from alkali metals dissolved in liquid ammonia. This preparation method is applicable for group 14 (Sn, Pb) and group 15 (P-Bi) elements and represents the oldest method to generate homoatomic polyanions in solution.^[2] The number of

compounds which have been crystallized from pure stannide solutions prepared either by dissolution or direct reduction experiments is rather small, until today only $A_4Sn_4 \cdot 2NH_3$ ($A=Rb, Cs$),^[3] $Na_4Sn_4 \cdot 13NH_3$,^[4] $Na_4Sn_9 \cdot 7en$ ^[5] and $[Li(NH_3)_4]_4Sn_9 \cdot NH_3$ ^[6] are known. In contrast to that, the number of compounds containing additional chelating ligands like [2.2.2]-cryptand or 18-crown-6 significantly exceeds the number of solvates of the pure binary compounds, which was attributed to an enhanced solubility and better crystallization induced by the ligands.^[7,8] Regarding transformation reactions of Zintl anions with (post-) transition metal complexes, there are a variety of crystallographically characterized cluster compounds ranging from oxidatively coupled species over exo- and endohedral variants up to intermetalloid clusters like e.g. $[Ge_9-Ge_9]^{6-}$,^[9] $[Ge_9-Zn(C_6H_5)]^{3-}$,^[10] $[Pt_2@Sn_{17}]^{4-}$,^[11] $[Si_9-\{Ni(CO)_2\}_2-Si_9]^{8-}$,^[12] $[Si_4(CuMes)_2]^{4-}$ ^[13] or $[Cu@Sn_9]^{3-}$ ^[14]. $[Si_4(CuMes)_2]^{4-}$ and $[Cu@Sn_9]^{3-}$ were obtained from liquid ammonia solutions of $K_6Rb_6Si_{17}$ or K_4Sn_9 and mesitylcopper(I).

Following the lead of Corbett *et al.*, who showed the effect of cryptands on the solubility of Zintl phases,^[7] these additives are commonly used during chemical transformations in solution, but a directed and controlled reaction between transition metal complexes and group 14 Zintl anions is very difficult as obviously additional processes are taking place in solution. This is due to the numerous reaction possibilities of this class of materials, where the Zintl anion may act as a ligand towards the transition metal atom forming complexes like e.g. $[Sn_9Cr(CO)_3]^{4-}$.^[15] Alternatively, the insertion of the metal atom into the deltahedral cluster is possible and endohedrally filled anions like $[Cu@E_9]^{3-}$ ($E= Sn, Pb$) are formed.^[13] Additionally, even non-deltahedral intermetalloids like $[M@Ge_{10}]^{3-}$ ($M=Co, Fe$) can be observed.^[16–18]

For a targeted synthesis, at first it is important to know which conditions are necessary to stabilize the favored kind of cluster in solution, followed by the targeted reaction. The high charge of the cluster anions imposes special demands on the applied solvent: The salt-like nature of the precursor phases implies a very polar solvent, whereas easily abstractable protons lead to the oxidation of the clusters. Apart from that, slightest traces of water seriously harm the delicate systems. Consequently, the most common solvents in this field are ethylenediamine and liquid ammonia as they can be dried by free electrons generated from alkali metals, which naturally represent the strongest possible base.

Recently, NMR studies of Eichhorn *et al.* have shown that in ethylenediamine Sn_9^{4-} clusters can be protonated yielding HSn_9^{3-} in the presence of stoichiometric amounts of

[2.2.2]-cryptand.^[19] We have observed analogous oxidation processes in cryptand-free solutions of $\text{K}_6\text{Rb}_6\text{Si}_{17}$ in liquid ammonia, the latter was identified as the proton source for the protonation of the highly reduced Si_4^{4-} anions leading to monosilanide SiH_3^- and amide as the stable reaction products.^[20] In contrast, the addition of [2.2.2]-cryptand allowed for the detection of Si_4^{4-} anions in solution.

In this paper we show that besides the long known enhancement of solubility by [2.2.2]-cryptand, also the influence on the oxidizing properties of the ammonia plays a crucial role for the stabilization of highly charged polyanions of tin in liquid ammonia solutions. Furthermore, this knowledge was used for the investigation of the reaction of the latter towards mesitylcopper(I) in dependence of the addition of [2.2.2]-cryptand.

6.2.2 Results and Discussion

NMR Analytics. The best analytical method for tracing and analyzing reactions in solution is NMR-spectroscopy. Recently, we showed that it gains deeper insights into the dissolution processes of silicide and stannide Zintl phases in liquid ammonia.^[20] For a better understanding of the solution behavior of this class of compounds we chose stannides as a model system because the scalar coupling of the two NMR active isotopes ^{119}Sn and ^{117}Sn allows for an unambiguous assignment of the cluster size in well resolved spectra. Figure 6.1 shows the simulated spectra for a four (a) and a nine atomic cluster (b) assuming fluctuation and considering the natural abundance of the isotopes. It is obvious that the intensity distribution of the signal pattern is characteristic for both clusters (for detailed information see the Supporting Information).

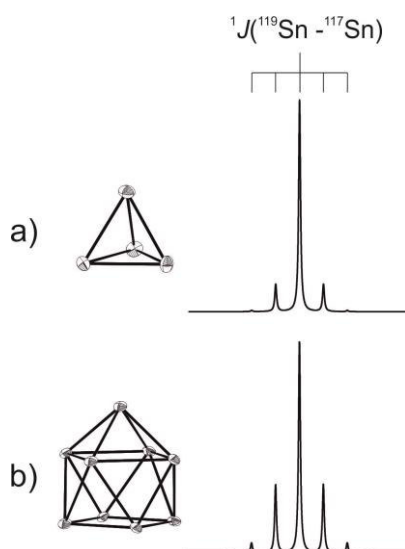


Figure 6.1: Simulated ^{119}Sn spectra of fluctuating a) four and b) nine atomic clusters, based on the scalar coupling of ^{119}Sn with ^{117}Sn . The respective intensity distribution of the isotope pattern allows an assignment of the cluster size to the obtained signals.

Dissolution of Rb_4Sn_4 . In our previous studies we concentrated on the tetrahedral Sn_4^{4-} cluster.^[20] We now show the influence of [2.2.2]-cryptand on the nine atomic clusters, which are always present as a minor component in solution. The dissolution experiments were performed with the single phase solid state material Rb_4Sn_4 , which was unambiguously characterized by powder diffraction and Raman spectroscopy (see the Supporting Information). Hence, any observed cage anion other than Sn_4^{4-} indicates a reaction product of the latter in liquid ammonia solutions.

Previously, we reported on the stabilization of the tetrahedral anion Sn_4^{4-} in solution in the presence of [2.2.2]-cryptand (Figure 6.2b, right).^[20] A singlet ^{119}Sn NMR signal has been detected at -1825 ppm accompanied by ^{117}Sn satellites due to ^{119}Sn , ^{117}Sn -coupling ($^1J_{^{119}\text{Sn},^{117}\text{Sn}} = 1425$ Hz) and was assigned the four-atom cage. In addition to that, nonastannide anions are constantly observed as a side product (Figure 6.2b, left), proving the ongoing oxidation of the tetrastannide-tetraanions.

Concerning the nonastannide anion, interestingly two separated signals for $\text{Rb}_x\text{Sn}_9^{(4-x)-}$ showed up at -1288 ppm ($^1J_{^{119}\text{Sn},^{117}\text{Sn}} = 266$ Hz) and -1302 ppm ($\Delta\nu_{1/2} = 357$ Hz) (Figure 6.2b, left). By taking the substoichiometric amount (0.4 : 1) of [2.2.2]-cryptand in relation to Rb_4Sn_4 into account, the presence of different $\text{Rb}_x\text{Sn}_9^{(4-x)-}$ species is conceivable as the ion-pairing of the nonastannide anion is influenced by [2.2.2]-cryptand and this of course affects the chemical shifts of the signals significantly. Based on the latter, we assume that the Sn_9 species referring to the broad unresolved signal at -1302 ppm shows less or even no direct Rb-Sn contacts. It has to be noted, that we present here the first detection of different nonastannide clusters within one NMR spectrum, which strongly supports a certain rigidity of ion-pairing with well-defined coordination situations for $\text{Rb}_x\text{Sn}_9^{(4-x)-}$ at low temperatures. Eichhorn *et al.* proposed the presence of different species (including protonated clusters) during their NMR investigations of ethylenediamine solutions of K_4Sn_9 in dependence of [2.2.2]-cryptand. We did not obtain any evidence of protonated tin species in liquid ammonia in the ^1H NMR spectra, which emphasizes the lower acidity of liquid ammonia compared to ethylenediamine. This probably is also the reason for silicides to form stable solutions of the highest reduced nine-atom clusters (Si_9^{4-}) only when liquid ammonia is used as solvent.^[21,22]

In ammonia stannide solutions without any additives, only one signal of the nonastannide anion is observed (-1242 ppm; $^1J_{^{119}\text{Sn},^{117}\text{Sn}} = 233$ Hz) (Figure 6.2a) with a downfield shift of 60 ppm compared to the broad signal in [2.2.2]-cryptand containing

solutions, which suggests more direct Rb-Sn contacts. Our proceeding investigations did not give any evidence for a fast crystallization of Sn_4^{4-} being the reason for it being undetectable in these solutions, as no crystals of $\text{Rb}_4\text{Sn}_4 \cdot 2\text{NH}_3$ or comparable phases could be obtained.

The observation of Sn_9^{4-} as the only detectable species in additive-free solutions is a clear indication for the fast oxidation of the Sn_4^{4-} anions since the formation of amide has been monitored simultaneously.^[20] Taking our recent results in silicide solution studies into account, which indicate that ammonia is not an innocent solvent, it became obvious that direct Rb-NH₃ contacts need to be suppressed for the stabilization of highly charged anions by using [2.2.2]-cryptand as a chelating reagent. In our here proposed model, the polarization of the N-H-bonds by direct Rb-NH₃ contacts in additive-free solutions finally leads to an increased acidity of the ammonia molecules in the first coordination sphere of the cations. This results in fast oxidation (maybe subsequent to protonation) of Sn_4^{4-} to Sn_9^{4-} . The addition of [2.2.2]-cryptand inhibits these direct Rb-NH₃ contacts, as the cation is located in the cavity of the cryptate. The cryptate in turn then serves as the counter ion for the highly charged Sn_4^{4-} anions in solution.

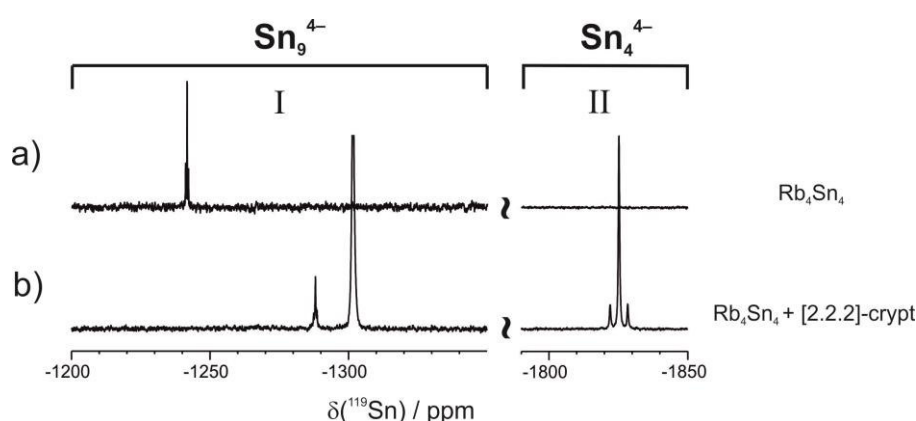


Figure 6.2: ^{119}Sn NMR spectra (224 MHz) of Rb_4Sn_4 dissolved in liquid ammonia a) without [2.2.2]-cryptand (293 K) and b) with a substoichiometric amount of [2.2.2]-cryptand (233K). By suppressing Rb-NH₃ contacts with a chelating additive the oxidation process is influenced and therefore the stabilization of the highly charged cluster Sn_4^{4-} in solution is possible.

Dissolution of Rb_4Sn_9 . A further dissolution study of Rb_4Sn_9 (nominal composition, see the Supporting Information) without [2.2.2]-cryptand yielded, as expected, Sn_9^{4-} as the only detected stannide species in solution. Time-dependent investigations showed a very broad signal ($\Delta\nu_{1/2} = 770$ Hz) which sharpened within one day and resulted in a well resolved signal at -1246 ppm ($^1J_{^{119}\text{Sn},^{117}\text{Sn}} = 263$ Hz) within 17 days. The superposition of the experimental spectrum and the simulated coupling pattern of a nine atomic cluster confirms the assignment (Figure 6.3).

Recently, we reported the dissolution of Rb_4Sn_4 traced by NMR,^[20] and obviously Rb_4Sn_9 shows a similar dissolution behavior. In both cases, the initial broad signal corresponds to an overlap of several signals due to Sn_9 or Sn_4 species with slightly different Rb^+ coordination spheres. These results represent the first experimental evidence of dissolution processes of Zintl phases monitored by NMR spectroscopy and demonstrate a transient existence of bigger aggregates in solution.

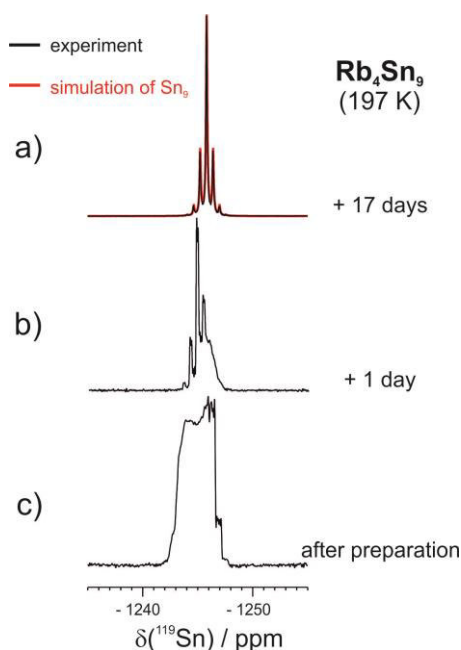


Figure 6.3: ^{119}Sn spectra of the time-resolved dissolution process of Rb_4Sn_9 in liquid ammonia (197 K; 224 MHz), directly after the preparation of the sample (below), after one day (middle) and after 17 days with the superposition of a simulated spectrum of a nine atomic cluster (above).

Direct reduction experiments of Sn with alkali metals (Na-Cs) and the comparison with the solvation of binary Zintl phases. Former crystallization studies of direct reduction experiments using elemental tin and alkali metals in liquid ammonia resulted in the formation of homoatomic polyanions like Sn_9^{4-} in $[\text{Li}(\text{NH}_3)_4]_4\text{Sn}_9 \cdot \text{NH}_3$ ^[6] or Sn_4^{4-} in $\text{A}_4\text{Sn}_4 \cdot 2\text{NH}_3$ ($\text{A}=\text{Rb}, \text{Cs}$).^[3] Therefore, further NMR investigations focused on this alternative access to Zintl ions in solution. Recently, we reported on the ^{119}Sn NMR signal of Sn_4^{4-} at -1725 ppm ($^1J_{119\text{Sn},117\text{Sn}} = 1466$ Hz) generated by the direct reduction of tin with rubidium.^[20] We now extended our studies towards Na, K and Cs (table 1). The determined $^1J_{119\text{Sn},117\text{Sn}}$ coupling constants of 267 Hz (Sn_9^{4-}) and 1466 Hz (Sn_4^{4-}) indicate different binding models for the cluster types: Sn_9^{4-} is considered to be a fluctuating cluster with $2e3z$ bonds^[23] and therefore an averaged singlet signal with a small coupling constant is observed, whereas the large coupling constant of Sn_4^{4-} implies classical $2e2z$ bonds as represented in $(\text{Ph}_2\text{Sn}-\text{SnPh}_2)^{2-}$ ($^1J_{119\text{Sn},117\text{Sn}} = 1950$ Hz).^[24]

Table 6.1: $\delta(^{119}\text{Sn})$ values [ppm] and corresponding coupling constants $^1J_{^{119}\text{Sn},^{117}\text{Sn}}$ [Hz] for Sn_9^{4-} and Sn_4^{4-} detected by direct reduction or dissolution of solids.

	Sn_9^{4-}		Sn_4^{4-}			Sn_9^{4-}		Sn_4^{4-}	
	$\delta(^{119}\text{Sn})$	$^1J_{^{119}\text{Sn},^{117}\text{Sn}}$	$\delta(^{119}\text{Sn})$	$^1J_{^{119}\text{Sn},^{117}\text{Sn}}$		$\delta(^{119}\text{Sn})$	$^1J_{^{119}\text{Sn},^{117}\text{Sn}}$	$\delta(^{119}\text{Sn})$	$^1J_{^{119}\text{Sn},^{117}\text{Sn}}$
Direct Reduction					Dissolution of solids				
Na ^[a]	-1298	n.d.	-1969	n.d.	Rb ₄ Sn ₄ ^[b]	-1242	233	-	-
K ^[a]	-1270	261	-	-	Rb ₄ Sn ₄ + crypt ^[c]	-1302	n.d.	-1825	1423
Rb ^[a]	-1243	267	-1727	-1466	Rb ₄ Sn ₉ ^[a]	-1246	263	-	-
Cs ^[a]	-1157	297	-	-					

[a] 195 K. [b] 293 K. [c] 233 K.

Using sodium as reducing metal, the most highfield shifted signal of Sn_4^{4-} has been observed at -1969 ppm (see the Supporting Information). The upfield shift of 233 ppm compared to the Sn_4^{4-} resonance in the presence of rubidium describes a similar trend compared to Rudolph's work dealing with nonastannide clusters in ethylenediamine solutions,^[25] who also reported on a highfield shift of Sn_9^{4-} for smaller, less polarizable counter cations. In fact, the deviation of the chemical shift of 233 ppm in the case of Sn_4^{4-} is notable, whereas for Sn_9^{4-} anions an upfield shift of only 55 ppm (with Rb or Na as reducing reagents) has been observed (Figure 6.4 and Figure 6.11).^[25]

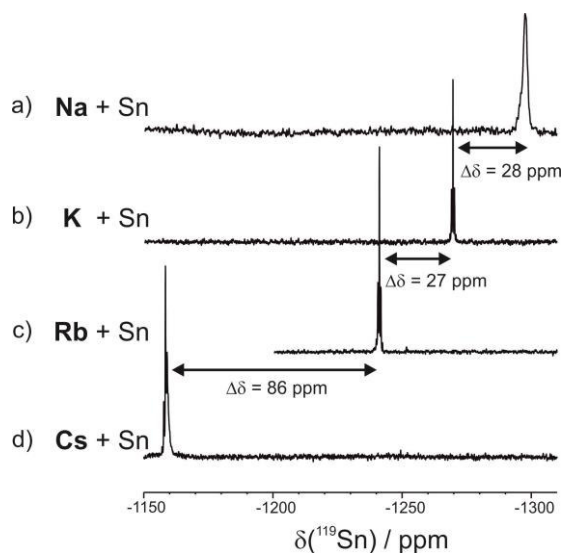


Figure 6.4: Direct reduction of Sn with an alkali metal (Na, K, Rb, Cs) in liquid ammonia leads to Sn_9^{4-} as well as Sn_4^{4-} (see Figure 6.11). The ^{119}Sn spectra (195 K; 224 MHz) of Sn_9^{4-} show a chemical shift deviation of approximately $\Delta\nu_{1/2} = 150$ ppm, depending on the alkali metal used.

The higher charge per atom ratio in Sn_4^{4-} ($C_f = -1$) compared to Sn_9^{4-} ($C_f = -0.444$) implies a stronger cation-anion interaction resulting in an expanded ^{119}Sn resonance

range, which depends on the nature of the cation: The ^{119}Sn resonances of both, Sn_4^{4-} and Sn_9^{4-} , are shifted significantly upfield when smaller alkali metals are present. Concerning the nonastannide anions, the complexation of the smaller alkali metals by ammonia molecules leads to extremely stable ammine complexes $[\text{A}(\text{NH}_3)_x]^+$ ($\text{A} = \text{Li}, \text{Na}, \text{K}$, $x = 4-6$),^[26] which prevent direct A-Sn contacts and therefore increase the local charge density of the tin atoms causing more upfield shifted signals. Interestingly, the Sn_9^{4-} resonances obtained from the direct reduction of tin with sodium and the dissolution of Rb_4Sn_4 in the presence of [2.2.2]-cryptand displayed almost the same chemical shifts and line shapes (see Figure 6.10), most likely due to almost complete anion-cation separation in both experiments. Apparently, even in additive-free stannide solutions which contain sodium instead of rubidium, direct A-Sn contacts are absent. This supports the idea of discrete $[\text{Na}(\text{NH}_3)_5]^+$ complexes in solution prohibiting direct contacts from the cation to the stannide anion, which results in nearly identical chemical shift and line shape of the ^{119}Sn signals for Sn_9^{4-} solutions with $[\text{Rb@crypt}]^+$ or $[\text{Na}(\text{NH}_3)_5]^+$ counter cation complexes.

Concerning Sn_4^{4-} , additive-free solutions of Rb_4Sn_4 never yielded Sn_4^{4-} in ammoniate structures due to the enhanced acidity of ammonia and the therefore rapid oxidation of Sn_4^{4-} to Sn_9^{4-} by protons. Discrete $[\text{Na}(\text{NH}_3)_5]^+$ complexes should be even more acidic due to the smaller and harder cation sodium, but the crystallization of the ammoniate $\text{Na}_4\text{Sn}_4 \cdot 13\text{NH}_3$ ^[4] obtained from cryptand-free solvation experiments of Na_4Sn_4 suggests that the low solubility of some sodium Zintl compound ammoniates allows crystallization in advance of oxidation. This hypothesis was supported during our NMR study, as during the direct reduction experiment using sodium, crystallization in the NMR tube prevented further investigation of the sample. The detection of Sn_4^{4-} in direct reduction experiments of tin and rubidium is attributed to a kinetic effect, as during the reaction an excess of electrons is provided which of course stabilizes the higher reduced species in solution.

In conclusion, the direct reduction experiments for the first time allowed for the detection of Sn_9^{4-} species in dependence of the counter cation in liquid ammonia. Thereby, the homoleptic ammine complexes of sodium $[\text{Na}(\text{NH}_3)_5]^+$ show similar effects on the corresponding ^{119}Sn NMR signal as $[\text{Rb@crypt}]^+$ complexes, which suggests isolated cationic and anionic moieties. The detection of Sn_4^{4-} was possible for sodium and rubidium, and in the case of sodium the fast crystallization of an ammoniate was observed.

Conversion of Rb_4Sn_4 with organometallic reagents. The dissolution of Rb_4Sn_4 and diphenylzinc together with [2.2.2]-cryptand as a stabilizing reagent for Sn_4^{4-} in liquid ammonia recently succeeded in the formation of a dimeric Sn_4^{4-} cluster unit bridged by a Zn^{2+} cation. This was found to be the first experimental evidence of an effective chemical conversion of Sn_4^{4-} in solution.^[27] As MesCu is known to react with $\text{K}_6\text{Rb}_6\text{Si}_{17}$ yielding the substituted Si_4^{4-} anion, $[\text{Si}_4(\text{CuMes})_2]^{4-}$,^[13] we performed NMR-monitored dissolution experiments of Rb_4Sn_4 and MesCu with and without [2.2.2]-cryptand, in order to investigate the reaction behavior.

The addition of [2.2.2]-cryptand to stannide solutions of Rb_4Sn_4 and MesCu resulted in a new ^{119}Sn signal at -1609 ppm ($^1J_{119\text{Sn},117\text{Sn}} = 1272$ Hz) with a well resolved isotope pattern corresponding to a four atomic Sn-species by means of simulations (Figure 6.5a). Its intense downfield shift of 203 ppm compared to the naked Sn_4^{4-} cluster indicates a reduced effective charge density of the tin atoms. According to this reasoning, distinctive Cu-Sn-interactions in a “Cu- Sn_4^{4-} ”-like species analogous to $[\text{Si}_4(\text{CuMes})_2]^{4-}$ seems possible. In addition to the new signal, different Sn_9^{x-} species and Sn_4^{4-} (-1812 ppm, $^1J_{119\text{Sn},117\text{Sn}} = 1397$ Hz) are observed.

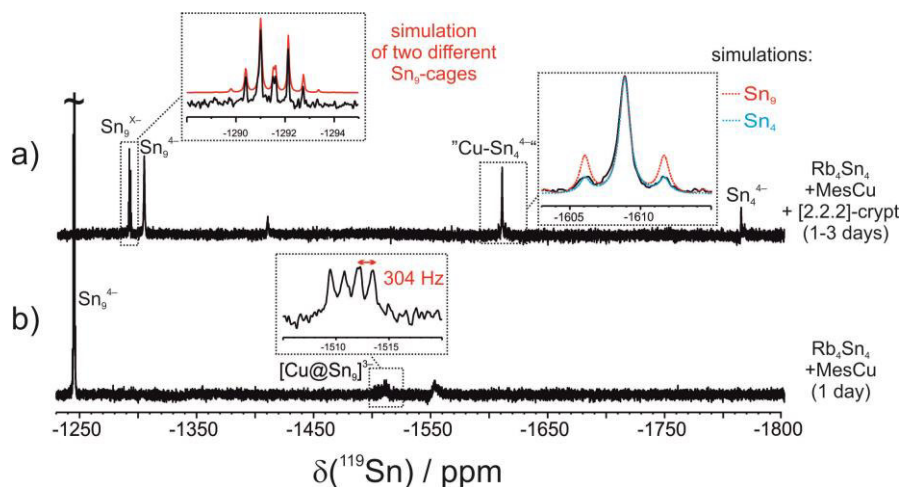


Figure 6.5: ^{119}Sn spectra of the conversion of Rb_4Sn_4 with MesCu in liquid ammonia (233 K; 224 MHz) a) with and b) without [2.2.2]-cryptand. Various Sn-Cu-species are emerging.

In comparison, the ^{119}Sn spectrum of the cryptand-free sample of Rb_4Sn_4 and MesCu shows two further signals with extremely weak intensities besides Sn_9^{4-} (-1245 ppm) (Figure 6.5b). In fact, the quartet signal at -1511 ppm ($^1J_{119\text{Sn},63/65\text{Cu}} = 304$ Hz) can be assigned to the literature known complex $[\text{Cu}@\text{Sn}_9]^{3-}$ ^[14] but the broad ($\Delta\nu_{1/2} = 880$ Hz) upfield shifted signal at -1551 ppm does not allow any assignment due to its low signal-to-noise-ratio. However, it seems that Sn_9 species are the main products of this reaction, induced by the fast oxidation of Sn_4^{4-} in the absence of [2.2.2]-cryptand. Again, [2.2.2]-

cryptand is essential for the stabilization of Sn_4^{4-} and the subsequent formation of a “Cu- Sn_4 ”-species. In contrast, the endohedral $[\text{Cu}@\text{Sn}_9]^{3-}$ is only present when large quantities of Sn_9^{4-} are provided in solution. This knowledge about the influence of [2.2.2]-cryptand on reaction products should facilitate the directed synthesis of transition metal compounds of Zintl anions.

Corresponding crystallization approaches have not yielded crystals of a “Cu- Sn_4 ”-species until today, but referring to the results of Fässler et al., who reported on the use of 18-crown-6 during the crystallization of compounds containing $[(\text{MesCu})_2(\eta_3\text{-Si}_4)]^{4-}$ and $[(\text{MesCu})_2(\eta_3\text{-Ge}_4)]^{4-}$,^[13,28] the additional use of this additive might allow for the crystallization of the heavier homologue containing Sn_4 tetrahedra. The here presented signal of the Cu- Sn_4 species represents the first evidence of such a compound, of which a crystal structure is still missing.

6.2.3 Conclusion

In summary, the here presented NMR spectroscopic investigations on tin Zintl anions in liquid ammonia solutions provide deeper insights into the dissolution, degradation and transformation processes of Zintl anions in solution. The two known preparation methods of Zintl anions, dissolution of solids and direct reduction, were examined carefully and the stabilizing effect of [2.2.2]-cryptand for the highly charged Sn_4^{4-} was taken into account. It could be shown that the role of [2.2.2]-cryptand needs to be revisited, as it not only enhances the solubility of the Zintl phases but also suppresses direct contacts of the alkali metal to the non-innocent solvent liquid ammonia. This results in a reduced oxidation of Sn_4^{4-} to Sn_9^{4-} . Hence stabilization of the highly charged Sn_4^{4-} can be realized by suppressing the cation- NH_3 contacts with a chelating additive. Furthermore, we were able to convert Sn_4^{4-} anions with MesCu to form a “Cu- Sn_4 ”-species in solution. Further work is planned to support this hypothesis by crystal structures. To boil it down to the briefest conclusion, the choice of the cation as well as the use of chelating additives are essential for the resulting anionic species in solution and this needs to be carefully reviewed in advance of planned experiments. These results are the basis for further extended investigations on Zintl anions of the remaining group 14 elements and are a further step down the road to new targeted synthesis of materials including homoatomic polyanions. Furthermore, it has to be seen if these effects are also trend-setting for other low-valent metal compounds like e.g. metallates of the transition metals.

6.3 Supporting Information

6.3.1 Solid State Phases

General Considerations

All manipulations mentioned below were performed in a purified argon atmosphere (glove box) by using glass vessels or NMR tubes dried at least three times in vacuo. Mesitylcopper(I), elemental tin, [2.2.2]-cryptand and 18-crown-6 were purchased from Sigma-Aldrich. The latter was sublimated before using. Elemental sodium and potassium were obtained from a commercial source and purified by liquation. Elemental rubidium and cesium were synthesized by the reduction of RbCl or CsCl and purified by distillation due to Hackspill^[29]. To remove residual moisture traces, the commercially acquired gaseous ammonia (Linde AG, purity 3.8) was condensed onto elemental sodium and stored for at least two to three days.

Syntheses

Rb₄Sn₄ and Rb₄Sn₉ were synthesized by gradually heating (60°C/h) stoichiometric amounts of elemental rubidium and elemental tin (see Table 6.2) in Duran glass ampoules to 450°C and held at this temperature for 20h. Afterwards, the reaction mixtures were annealed to room temperature (60°C/h). Due to their sensitivity towards moisture and air the solid state phases were handled and stored under argon atmosphere.

Table 6.2: Weigh-in quantities of the elements for the preparation of Rb₄Sn₄ and Rb₄Sn₉.

	m(Rb)	m(Sn)
Rb₄Sn₄	0.64 g (7.5 mmol)	0.78 g (6.6 mmol)
Rb₄Sn₉	0.40 g (4.7 mmol)	1.09 g (9.2 mmol)

Characterization

The FT-Raman spectra were recorded at room temperature under inert conditions from powdered samples sealed in pyrex tubes ($\varnothing = 1.0$ mm) using a DRX SmartRaman spectrometer (Thermo Scientific, DRX laser with $\lambda = 780$ nm, CCD detector). X-ray powder diffraction data were collected on a transmission powder diffraction system (STADI P, Fa. Stoe Cie, Darmstadt, Cu- K_α radiation with $\lambda = 1.540598$ Å). Capillaries were loaded with the respective powdered samples and air-proof sealed. Data were processed with STOE WinXPOW 1.08 and visualized with GNU PLOT 4.6.

Rb₄Sn₄. Raman measurements of Rb₄Sn₄ showed the characteristic vibrational frequencies of Sn₄^{4−} at 74 cm^{−1}, 108 cm^{−1}, 134 cm^{−1} and 185 cm^{−1} (see Figure 6.6)^[30]. The solution and refinement of the experimental powder diffraction data yielded a tetragonal body centered cell of the space group *I*41/*acd* with cell parameters which fit the values published for Rb₄Sn₄ (see Figure 6.7)^[31]. Since no indication for the presence of Sn₉^{4−} was found by either Raman spectroscopy or X-ray diffraction we assume that Rb₄Sn₄ is a phase pure solid and contains Sn₄^{4−} as the single anionic moiety.

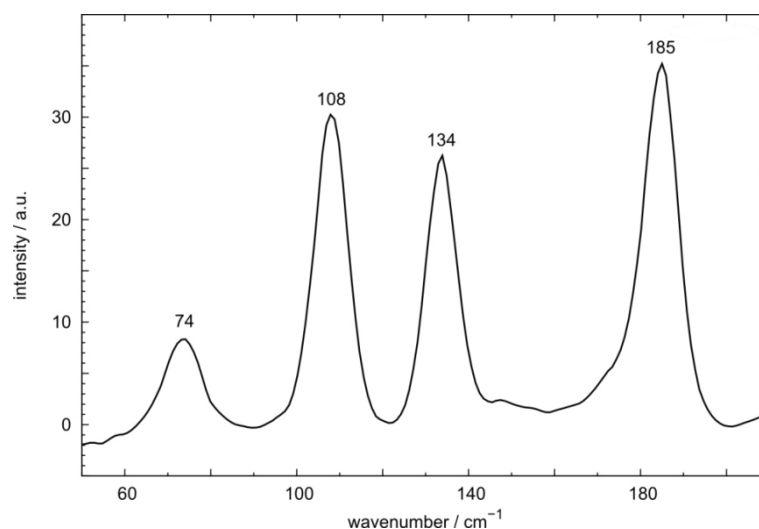


Figure 6.6: Experimental raman spectrum of Rb₄Sn₄.

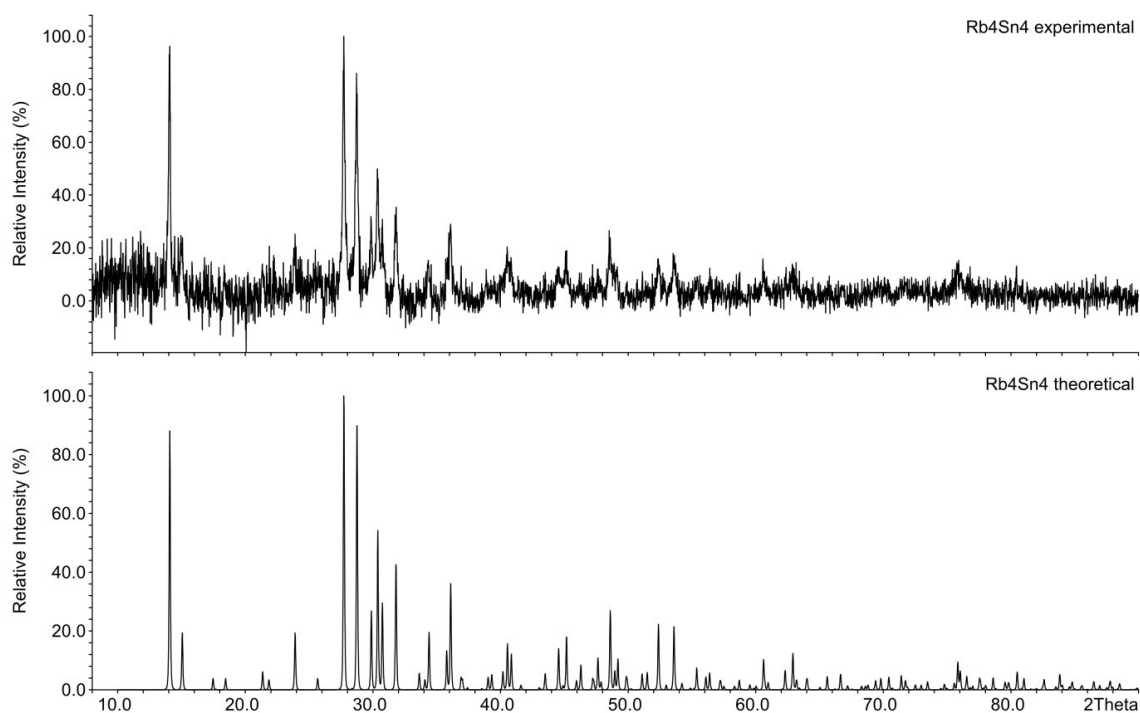


Figure 6.7: Comparison of experimental and theoretical calculated powder pattern of Rb_4Sn_4 .

Rb_4Sn_9 . The Raman spectrum of Rb_4Sn_9 showed the characteristic vibrational frequencies of Sn_9^{4-} at 104 cm^{-1} and 149 cm^{-1} (see Figure 6.8).^[32] As the crystallinity of the sample was extremely low, therefore powder diffraction measurements haven't been successful.

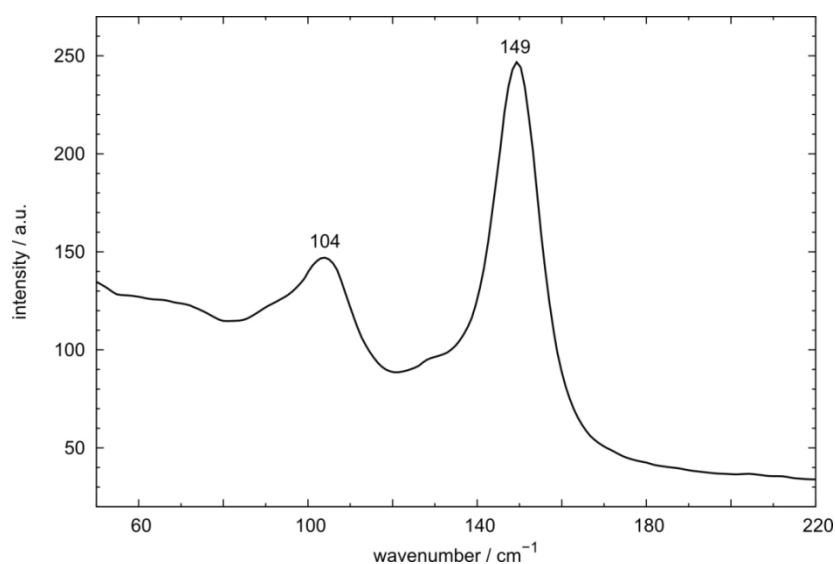


Figure 6.8: Experimental Raman spectrum of Rb_4Sn_9 .

6.3.2 Sample Preparation

Solvation

Under inert conditions an NMR tube was charged with the respective educts (see Tables 6.3-6.4) afterwards liquid ammonia was condensed onto the mixtures whereupon the solutions turned red-brown.

Table 6.3: Weigh-in quantities of additive-free and additive-containing Rb_4Sn_4 and Rb_4Sn_9 solvation experiments.

	m(Rb_4Sn_4)	m(Rb_4Sn_9)	m(crypt)	m(MesCu)	stoichiometric ratio
a	35 mg	–	–	–	–
b	25 mg	–	18 mg	–	1:1.6
c	25 mg	–	–	5.6 mg	1:1
d	15 mg	–	10.4 mg	3.4 mg	1:1:1.5
e	–	20 mg	–	–	–

Direct Reduction

All direct reduction experiments were directly performed in heavy walled NMR tubes. Under inert conditions tin and the particular alkali metal were placed in a NMR tube (see Table 6.4) and subsequently anhydrous liquid ammonia was condensed onto the mixture. Avoiding air and moisture impurities, the tubes were melt off and then stored at 230 K until the initial blue color of the solution turned red-brown. Afterwards NMR measurements were carried out.

Table 6.4: Weigh-in quantities of direct reduction experiments.

Alkali metal (A)	m(A)	m(Sn)	stoichiometric ratio
Na	11 mg	60 mg	1:1
K	18 mg	60 mg	1:1
Rb	39 mg	60 mg	1:1
Cs	61 mg	60 mg	1:1

6.3.3 NMR Data

Data Collection and Processing

The NMR spectra were recorded on a Bruker Avance 600 spectrometer (600.13 and 223.79 MHz for ^1H and ^{119}Sn , respectively) equipped with a 5mm broadband triple resonance z-gradient probe. The temperatures for all measurements were controlled by a Bruker BVTE 3900 temperature unit. ^{119}Sn measurements were carried out with a standard Bruker pulse program (zg and zgig) using 70k number of scans, 2 dummy scans, TD = 8k with a relaxation delay of 0.3 s. Data were processed with the Bruker software TOPSPIN 3.2 using the processing parameters SI = 16 k and WDW = EM. The chemical shifts are reported in ppm relative to SnMe_4 used as external standard.

Signal Assignment

The more abundant ^{119}Sn was used as observe nucleus and the ^{117}Sn - ^{119}Sn scalar coupling for signal assignment. Therefore, the coupling patterns for four and nine atomic cluster sizes were calculated from the statistical distribution of both NMR active nuclei over the respective polyanion (signal intensity distribution for Sn_4 : 0.006 : 0.0128 : 1.000 : 0.128 : 0.006 and Sn_9 : 0.047 : 0.324 : 1.000 : 0.324 : 0.047). Based on these calculations and for a better visualization, theoretical NMR spectra were simulated with Bruker's TOPSPIN 3.2 software tool DAISY and compared to the experimental ones.

Further NMR Spectra

Sn_9^{4-} : Comparison of Direct Reduction and Solvation. Figure 6.10 shows the signals of nine atomic tin clusters, received either by direct reduction experiments or by solvation experiments of Rb_4Sn_4 with [2.2.2]-cryptand. The chemical shift values and the line width of the two observed clusters are similar and therefore an equal electronic environment is proposed. Meaning that in both cases the alkali metal cations are kept away from the cluster, which therefore isn't influenced by any ionic contact. For Na^+ very stable ammine complexes are postulated and the Rb^+ atoms are chelated by [2.2.2]-cryptand.

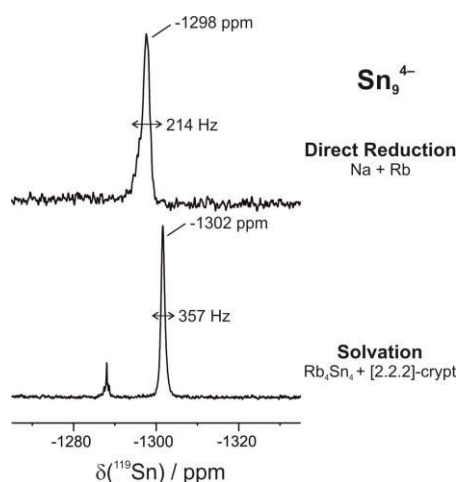


Figure 6.10: ^{119}Sn spectra of the Sn_9^{4-} cluster received by direct reduction 195 K (above) and solvation with Rb_4Sn_4 and [2.2.2]-cryptand at 233 K (below).

Sn_4^{4-} by Direct Reduction. Figure 6.11 shows the signal of the highly charged Sn_4^{4-} which is obtained by direct reduction experiments using Na or Rb as alkali metal. For Na the chemical shift is $\delta(\text{ppm}) = -1969$ ppm with $\Delta\nu_{1/2} = 428$ Hz and for Rb $\delta(\text{ppm}) = -1727$ ppm with $^1J_{119\text{Sn}117\text{Sn}} = 1466$ Hz. The higher upfield shift in the spectra using Na is explained by stronger ammine complexes, so the charge of the cluster is less compensated by contact with the alkali cation and therefore the nuclei is more shielded.

In spectra using K or Cs for direct reduction it was not yet possible to obtain any signal of the four atomic cluster. This might be explained by lower concentration of Sn_4^{4-} in solution due to a faster crystallization of those complexes or by a faster oxidation process to Sn_9^{4-} .

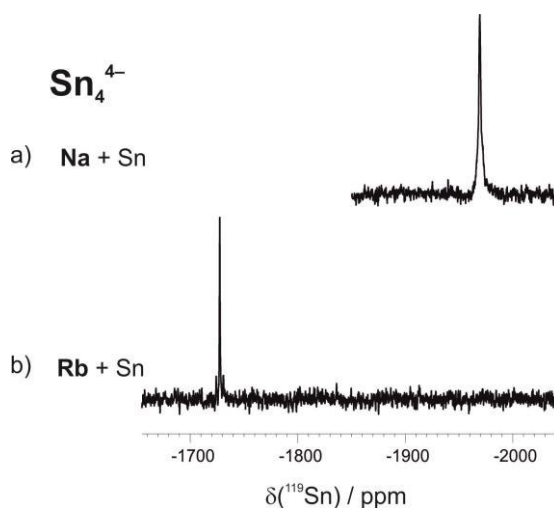
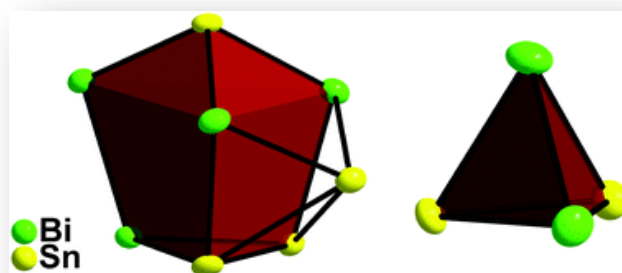


Figure 6.11: ^{119}Sn spectra of samples containing Sn_4^{4-} species received by direct reduction experiments (195 K).

6.4 Additional Findings

6.4.1 Zintl Synthesis of Heteroatomic Zintl Anions in Liquid Ammonia – the New Highly Charged $[\text{Sn}_4\text{Bi}_4]^{4-}$ and Fully Ordered $[\text{Sn}_2\text{Bi}_2]^{2-}$



**The NMR spectroscopic investigations were performed in close collaboration with Maria Neumeier. The synthesis and characterization of the ternary phases as well as the sample preparation and theoretical calculations were performed by Ute Friedrich.

Ute Friedrich, Maria Neumeier, Carina Koch and Nikolaus Korber,
Chem. Commun. **2012**, 48, 10544-10546.

DOI: 10.1039/c2cc35380f

Reproduced by permission of The Royal Society of Chemistry.

Abstract

The new Zintl anion $[\text{Sn}_4\text{Bi}_4]^{4-}$, synthesized by dissolving CsSnBi in liquid ammonia, forms a monocapped nortricyclane-like cage. Its electron localization function (ELF) analysis shows evidence for 3-centre bonding. The analogous reaction with KSnBi results in a crystallographically fully ordered tetrahedral $[\text{Sn}_2\text{Bi}_2]^{2-}$ ion.

Introduction

Since the discovery by Joannis in 1891^[2,33] and the development of Eduard Zintl's well-known potentiometric analysis,^[34–36] the chemistry of main group metal polyanions, often called Zintl anions, has flourished, greatly facilitated by the introduction of cryptands as alkali metal cation ligands by J. Corbett.^[1,37] Next to the better known homoatomic Zintl anions, heteroatomic polyanions have also been investigated by the same methods. Reported molecular species include $[\text{Sb}_2\text{Ge}_7]^{2-}$, $[(\text{SbGe}_8-(\text{Ge}_8\text{Sb}))]^{4-}$,^[38] $[\text{In}_4\text{Bi}_5]^{3-}$, $[\text{InBi}_3]^{2-}$, $[\text{GaBi}_3]^{2-}$,^[39] $[\text{TiSn}_8]^{3-}$ and $[\text{TiSn}_9]^{3-}$.^[40] The tetrahedral cages $[\text{Ti}_2\text{Te}_2]^{2-}$,^[41] $[\text{Pb}_2\text{Sb}_2]^{2-}$,^[42] or $[\text{Sn}_2\text{Bi}_2]^{2-}$,^[43] which have the same number of valence electrons as the phosphorus molecule P_4 , have also been among the early examples. The isostructural anion $[\text{Sn}_2\text{Sb}_2]^{2-}$ was obtained by Dehnen *et al.* in 2009.^[44] In 2011 the same group reported the structural characterisation of $[\text{Sn}_7\text{Bi}_2]^{2-}$ as one product of the reaction between $[\text{K}([2.2.2]\text{-crypt})]_2[\text{Sn}_2\text{Bi}_2]_{\text{en}}$ and ZnPh_2 .^[45] Unfortunately, all of the crystal structures of tin–bismuth anions reported to date show severe disorder, which does not allow the Sn and Bi positions to be distinguished.

In this communication we report the preparation of $[\text{K}(18\text{-crown-6})]_2[\text{Sn}_2\text{Bi}_2] \cdot 2\text{NH}_3$ (**1**) and $[\text{Cs}(18\text{-crown-6})]_4[\text{Sn}_4\text{Bi}_4] \cdot 12\text{NH}_3$ (**2**), in which fully ordered anions could be characterised. The starting materials of nominal compositions KSnBi and CsSnBi , respectively, were prepared at the comparatively low temperature of 723 K using glass ampoules. Each solid state material was dissolved in liquid ammonia together with an equimolar amount of 18-crown-6. After storage at 237 K, reddish-brown crystals of **1** (Table 6.5) and black crystals of **2** (Table 6.5) could be isolated from solution. Both crystalline compounds reveal the usual pronounced thermal instability of ammoniates.

Results and discussion

The anion $[\text{Sn}_2\text{Bi}_2]^{2-}$ of compound **1** is anchored in the crystal structure by contact with two K^+ cations, as depicted in Figure 6.12. Disorder of the anion, which has been reported for $[\text{K}([2.2.2]\text{-crypt})]_2[\text{Sn}_2\text{Bi}_2]_{\text{en}}$ ^[43] or $[\text{K}(18\text{-crown-6})]_2[\text{Sn}_2\text{Bi}_2]$,^[46] is

prevented by the use of 18-crown-6 as a sequestering agent on the one hand and by the low temperatures during the crystallisation process on the other. Goicoechea and Sevov demonstrated that the use of 18-crown-6 as a sequestering agent can successfully prevent disorder during the investigation of the Zintl ion Si_9^{2-} .^[47] This anion, which is fully ordered in $[\text{K}(18\text{-crown-6})]_2\text{Si}_9\text{py}$, shows great disorder in its cryptate compound $[\text{K}([2.2.2]\text{-crypt})]_2\text{Si}_9$.

The absence of disorder allowed the bond lengths within this anion to be determined for the first time (Table 6.6). As expected, the largest distance of 3.0316(6) Å in the tetrahedral anion can be found between the two bismuth atoms, whereas the two tin atoms are closest to each other with a distance of 2.8700(8) Å. The bond lengths between bismuth and tin atoms range from 2.9815(10) Å to 2.9923(8) Å. The total average bond length for the tetrahedron is calculated to be 2.9749 Å, which is in accordance with the value of 2.957 Å found by Critchlow and Corbett^[43] and 2.949 Å reported by Dehnen and co-workers^[46] for the disordered anions.

Table 6.5: Crystallographic data of **1** and **2**.

	Compound 1	Compound 2
Formula	$\text{C}_{24}\text{H}_{54}\text{Bi}_2\text{K}_2\text{N}_2\text{O}_{12}\text{Sn}_2$	$\text{C}_{48}\text{H}_{132}\text{Bi}_4\text{Cs}_4\text{N}_{12}\text{O}_{24}\text{Sn}_4$
Formula weight/ g mol^{-1}	1296.23	3103.98
Crystal system	Orthorhombic	Triclinic
Space group, Z	$P2_12_12_1$, 4	$P\bar{1}$, 2
$a/\text{\AA}$	10.4079(7)	15.5211(2)
$b/\text{\AA}$	14.4988(10)	16.7664(2)
$c/\text{\AA}$	27.679(2)	21.7756(2)
$\alpha/^\circ$	90	72.442(1)
$\beta/^\circ$	90	87.793(1)
$\gamma/^\circ$	90	62.570(1)
$V/\text{\AA}^3$	4176.8(5)	4761.4(1)
Radiation, λ	Mo-K α , 0.71073	Mo-K α , 0.71073
T/K	123(1)	123(1)
μ/mm^{-1}	9.831	9.964
R_{int}	0.0958	0.0783
R_1 (all data)	0.0445	0.0612
wR_2 (all data)	0.0887	0.0931
S	0.944	1.047

The electron spray mass spectrum of a fresh solution of KSnBi in ethylenediamine–dimethylformamide shows no signal for the $[\text{Sn}_2\text{Bi}_2]^-$ fragment. Instead, mainly nine-atom species $\text{Sn}_{9-x}\text{Bi}_x^-$ ($x = 0\text{--}3$) are present in solution, which seem to be the more stable cages. The ^{119}Sn NMR spectrum of the crude reaction mixture shows a singlet at

–1746 ppm ($^1J_{119\text{Sn}117\text{Sn}} = 1532$ Hz), which can be assigned to $[\text{Sn}_2\text{Bi}_2]^{2-}$. The upfield shift with respect to the values of –1575 ppm ($^1J_{119\text{Sn}117\text{Sn}} = 1638$ Hz) found by Wilson *et al.*^[25] and of –1650 ppm reported by Lips and Dehnen^[45] is due to the presence of 18-crown-6 in solution. Studies on the influence of cryptands on the chemical shift show an increasing upfield shift with an increasing amount of sequestering agent.^[19] In addition, nine-atom species such as Sn_9^{4-} (–1267 ppm) and $\text{Sn}_6\text{Bi}_3^{2-}$ (–1244 ppm) could be identified (for more details see the Supporting Information).

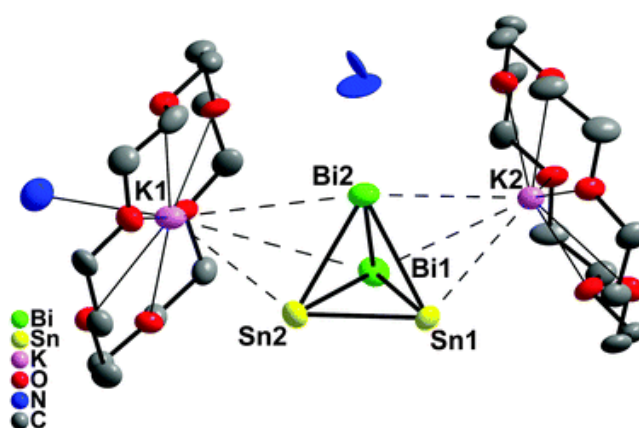


Figure 6.12: Coordination of $[\text{Sn}_2\text{Bi}_2]^{2-}$ by $[\text{K}(18\text{-crown-6})]^+$ in **1**. Anisotropic displacement ellipsoids at the 50% probability level, hydrogen atoms neglected.

Table 6.6: 2 Bond lengths of $[\text{Sn}_2\text{Bi}_2]^{2-}$ in **1**.

Atoms	d/Å	Atoms	d/Å
Bi1–Bi2	3.0316(6)	Bi2–Sn2	2.9857(9)
Bi1–Sn1	2.9923(8)	Bi2–Sn1	2.9880(8)
Bi1–Sn2	2.9815(10)	Bi2–Sn2	2.8700(8)

The use of caesium as the alkali metal in the solid precursor material resulted in the formation of **2** upon dissolution in liquid ammonia. The central structural unit of **2** is a novel eight-atom tin–bismuth species (Figure 6.13 and 6.14). The triangular base of the nortricyclane-like cage consists of two tin atoms and one bismuth atom, three bismuth atoms connect the base to the apical tin atom. The single resulting symmetrical quadrangular face (Sn1–Sn4–Bi4–Bi3) is capped by a tin atom, in such a way that an approximate mirror plane bisecting the anion is observed. The height h of the cage, as defined by Von Schnering and Hönlé,^[48] is calculated to be 4.2230 Å, the angles are $\gamma(\text{Sn3–Bi2–Bi1}) = 97.614(12)^\circ$, $\delta(\text{Sn3–Bi3–Sn1}) = 103.007(14)^\circ$ and $\varepsilon(\text{Sn3–Bi4–Sn4}) = 103.414(14)^\circ$. The isostructural clusters $[\text{E}_7\text{Ti}]^{2-}$ (E = P, As) were characterised by Goicoechea *et al.* in 2011.^[49] These were synthesized by a metathesis reaction between

ethylenediamine solutions of K_3E_7 ($E = P, As$) and $TlCl$. A well resolved crystal structure of $[TlAs_7]^{2-}$ was obtained exclusively by use of 18-crown-6 as a sequestering agent.

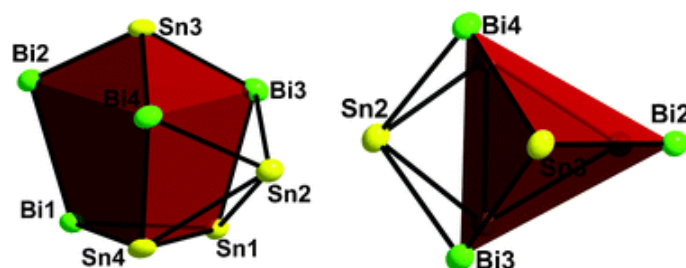


Figure 6.13: Structure of $[Sn_4Bi_4]^{4-}$. Left: side-view. Right: top-view.

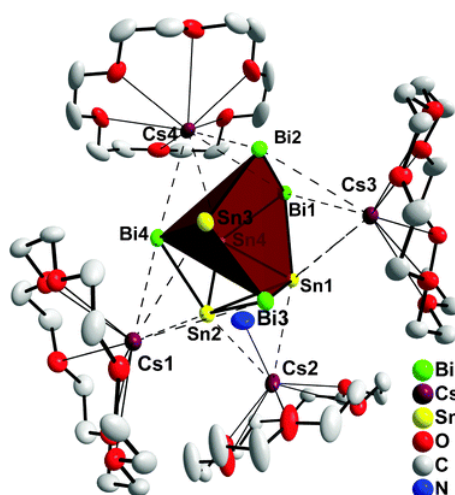


Figure 6.14: Interactions between $[Sn_4Bi_4]^{2-}$ and $[Cs(18\text{-crown-}6)]^+$ counteranions in **2**. Anisotropic displacement ellipsoids pictured at the 50% probability level, hydrogen atoms neglected.

Considering the nortricyclane cage of **2**, its distribution of tin and bismuth atoms is in accordance with the minimum structure previously calculated by Dehnen *et al.*,^[50] which demonstrates the predictive power of quantum chemical calculations even for these heavy atom clusters. However, a closed-shell Sn_3Bi_4 cage of this configuration would have an overall charge of -6 (one formal charge per threefold-bonded tin atom, one formal charge per twofold-bonded bismuth atom), which is an unusually high charge for ions observed in solution. The formal coordination of the $[Sn_3Bi_4]^{6-}$ ion by a Sn^{2+} cation reduces the charge, but leads to a cluster in which the four remaining negative charges cannot be assigned to four specific atoms any more. The electron distribution closest to a traditional Lewis formula would have one formal charge at Sn3 and Bi2 each and the remaining two charges indeterminately distributed between Sn1, Sn2 and Sn4. Electron localization

function calculations (ELF)^{i[51–54]} on $[\text{Sn}_4\text{Bi}_4]^{4-}$ support this view of the chemical bonding in the cage anion. Disynaptic basins can be found between the bismuth and tin atoms as well as between Bi1 and Bi2. Each basin is populated by 1.42 to 1.73 electrons. One trisynaptic basin is located in the middle of the triangular face Sn1–Sn2–Sn4 with a population of 1.52 electrons (Figure 6.15). This basin complies with a 3-centre-bond and explains the elongated tin–tin bonds for this face that are observed in the crystal structure (Table 6.7). Each monosynaptic valence basin is populated by 2.10 to 2.27 electrons for all tin atoms and Bi2. For Bi1, Bi3 and Bi4 a population of 2.82 to 3.01 electrons can be found. The higher electron density in the valence basins of bismuth atoms is in accordance with results of Eisenstein *et al.*^[55] Their theoretical calculations on $[\text{Sn}_2\text{Bi}_2]^{2-}$ proved that more charge is located on bismuth atoms ($-0.58e$) than on tin atoms ($-0.42e$).

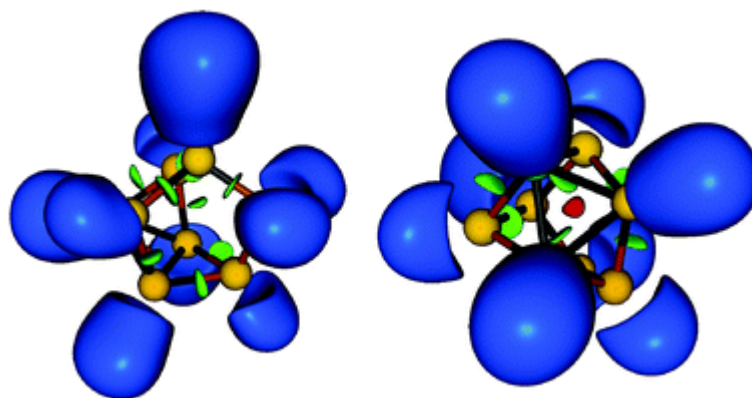


Figure 6.15: ELF representation of $[\text{Sn}_4\text{Bi}_4]^{4-}$, $Z = 0.66$; monosynaptic valence basins, blue; monosynaptic core basins, yellow; disynaptic valence basins, green; trisynaptic valence basins, red.

Table 6.7: Bond lengths of $[\text{Sn}_4\text{Bi}_4]^{4-}$ in **2**.

Atoms	d/Å	Atoms	d/Å
Bi1–Sn1	2.9594(5)	Bi4–Sn4	2.9495(5)
Bi1–Sn4	2.9717(5)	Bi4–Sn3	2.9826(5)
Bi1–Bi2	3.0307(3)	Bi4–Sn2	2.9886(5)
Bi2–Sn3	2.8647(5)	Sn1–Sn2	3.0932(6)
Bi3–Sn1	2.9542(5)	Sn1–Sn4	3.1363(6)
Bi3–Sn3	2.9799(5)	Sn2–Sn4	3.0515(7)
Bi3–Sn2	3.0173(5)		

The electron spray mass spectrum of a fresh solution of CsSnBi in ethylenediamine–dimethylformamide shows neither the $[\text{Sn}_2\text{Bi}_2]^-$ nor the $[\text{Sn}_4\text{Bi}_4]^-$ fragment. Again different nine-atom clusters are dominant in the spectrum, as was found for KSnBi. The

ⁱ M. Kohout, Radebeul, 2011, DGRid, version 4.6.

highly unstable solution of CsSnBi can be stabilized by the addition of small amounts of 18-crown-6. In this case the ESI mass spectrum reveals the formation of smaller fragments such as the $[\text{Sn}_2\text{Bi}_2]^-$ anion. ^{119}Sn NMR experiments on the crude reaction mixture confirm the presence of $[\text{Sn}_2\text{Bi}_2]^{2-}$ and several nine atom species. The singlet at -1699 ppm with a coupling constant of $J_{(119\text{Sn}117\text{Sn})} = 1525$ Hz (47 ppm upfield shift with respect to the KSnBi sample) is assigned to $[\text{Sn}_2\text{Bi}_2]^{2-}$. Further signals at -1185 ppm and -1162 ppm are attributed to Sn_9^{4-} and Sn_6Bi_3^- . Thus, $[\text{Sn}_4\text{Bi}_4]^{4-}$ clearly exists in the solid compound **2**, but its existence in solution has remained elusive up to now.

Conclusion

The preparation and structural analysis of **2** show that it is possible to obtain new Sn–Bi clusters by dissolving ternary alkali metal–tin–bismuth solid state materials in liquid ammonia. The crystallization at low temperatures and the use of crown ethers as sequestering agents contribute to the prevention of disorder in the anions. An unusual bonding situation is encountered in $[\text{Sn}_4\text{Bi}_4]^{4-}$, which is currently the subject of further investigation.

6.4.2 Supporting Information

Experimental details

All manipulations were performed under argon atmosphere using standard Schlenk or glovebox techniques. Liquid ammonia was dried over elemental potassium for at least 24 h. 18-crown-6 was dried in vacuum and sublimated prior to use.

For the starting materials KSnBi and CsSnBi equimolar amounts of the corresponding elements were weighed into glass ampoules, which were evacuated and sealed. The ampoules were heated to 723 K and kept at this temperature for 24 h. The cooling process was performed with a rate of 150 K/h to room temperature. 367 mg KSnBi or 461 mg CsSnBi, respectively, were dissolved in approximately 15 ml of liquid ammonia together with 132 mg (0.5 mmol) 18-crown-6. Both solutions showed a reddish-brown colour immediately after the addition of liquid ammonia and were stored at 237 K until crystallisation. $[\text{K}(18\text{-crown-6})_2[\text{Sn}_2\text{Bi}_2]\cdot 2\text{NH}_3]$ (**1**) forms in about 20 % and $[\text{Cs}(18\text{-crown-6})_4[\text{Sn}_4\text{Bi}_4]\cdot 12\text{NH}_3]$ (**2**) in about 10 % crystalline yield.

¹¹⁹Sn NMR-spectroscopy

NMR spectroscopy was done on a Bruker Avance 600 spectrometer equipped with a 5 mm broadband triple resonance Z-gradient probe. The temperatures for all measurements were controlled by a Bruker BVTE 3900 temperature unit. ¹¹⁹Sn measurements were carried out with a standard Bruker pulse program using 55k number of scans for solutions of KSnBi or 80k number of scans for solutions of CsSnBi, 2 dummy scans, TD=8k and a relaxation delay of 0.3 s. Data were processed with the software Bruker TOPSPIN 2.1 using the processing parameters SI=16k, WDW=EM and LB=50 Hz. The chemical shifts are reported in ppm and are externally referenced to SnMe₄. For the measurements the original reaction solutions (solid state material + 18-crown-6 in liquid ammonia) were used.

In the spectrum of KSnBi (Figure 6.16, top) the singlet at -1746 ppm with $^1J_{119\text{Sn}117\text{Sn}} = 1532$ Hz is assigned to $[\text{Sn}_2\text{Bi}_2]^{2-}$. The upfield shift compared to the value of -1575 ppm with $^1J_{119\text{Sn}117\text{Sn}} = 1638$ Hz found by Wilson *et al.*^[25] or of -1650 ppm reported by Dehnen *et al.*^[45] is due to the presence of 18-crown-6 in solution^[19] and the use of liquid ammonia as solvent instead of ethylenediamine. For the same reasons the signal at -1267 ppm with $^1J_{119\text{Sn}117\text{Sn}} = 263$ Hz, which is assigned to Sn_9^{4-} , is shifted about 60 ppm upfield with respect to the value found by Wilson *et al.* (-1210 ppm, $^1J_{119\text{Sn}117\text{Sn}} = 263$ Hz).^[25] The signal at -1244 ppm with $^1J_{119\text{Sn}117\text{Sn}} = 615$ Hz shows the best accordance with the simulated pattern of $[\text{Sn}_6\text{Bi}_3]^-$. The weak signal at -1192 ppm is supposed to be another substituted Sn_9^{4-} species, but this cannot be proven. According to their chemical shifts, the singlets at -1011 ppm and -1004 ppm should belong to species with a lower formal negative charge per tin atom and might therefore belong to Sn_{10}^{2-} , which can be detected by ESI-MS in solution. But this is speculative due to the lack of further indicators.

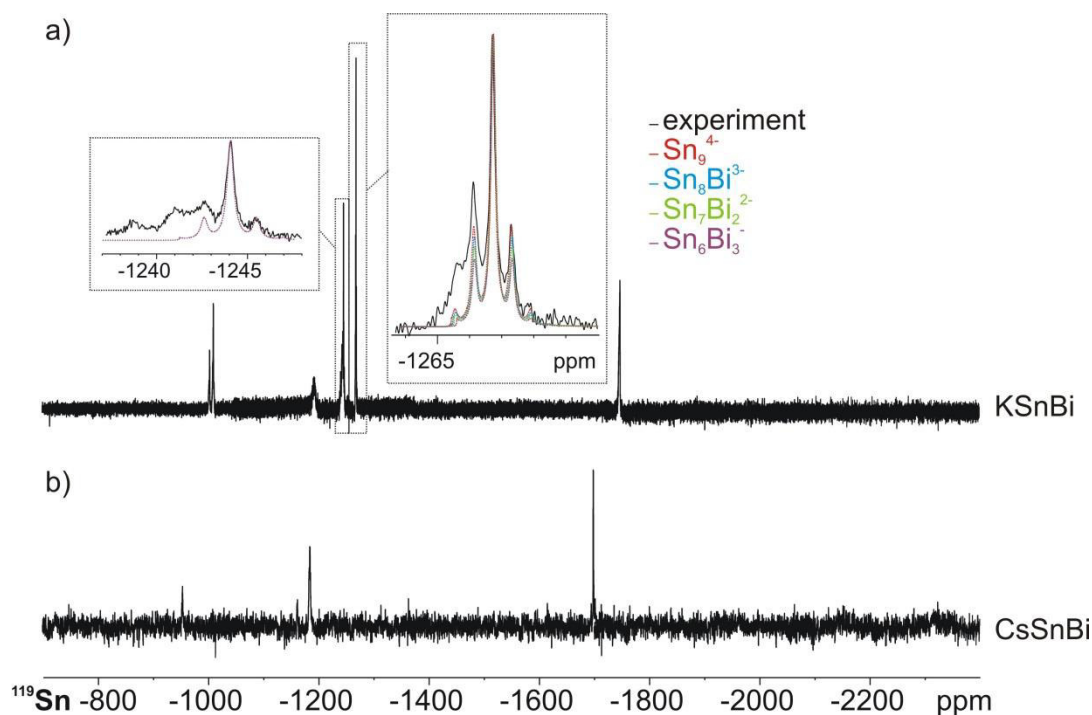


Figure 6.16: Experimental (black) and simulated (coloured) ^{119}Sn NMR spectrum of KSnBi in liquid ammonia (top), experimental ^{119}Sn NMR spectrum of CsSnBi (bottom).

For CsSnBi (Figure 6.16, bottom) four signals at -954 ppm, -1162 ppm, -1185 ppm and -1699 ppm ($^1J_{119\text{Sn}117\text{Sn}} = 1525$ Hz) can be detected. Due to the influence of the cation these signals are shifted to lower field in contrast to the KSnBi sample. Table 6.8 gives an overview over the signals detected in both samples and the assigned species.

Table 6.8: ^{119}Sn NMR signals common in KSnBi and CsSnBi solutions.

Species	$\delta(\text{KSnBi}) / \text{ppm}$	$\delta(\text{CsSnBi}) / \text{ppm}$
$[\text{Sn}_2\text{Bi}_2]^{2-}$	-1746	-1699
Sn_9^{4-}	-1267	-1185
$[\text{Sn}_6\text{Bi}_3]^-$	-1244	-1162
unidentified	-1011	-954

6.5 References

- [1] S. Scharfe, F. Kraus, S. Stegmaier, A. Schier, T. F. Fässler, *Angew. Chem. Int. Ed.* **2011**, *50*, 3630–3670.
- [2] A. Joannis, *C. R. Hebd. Seances Adac. Sci.* **1891**, *113*, 795.
- [3] K. Wiesler, K. Brandl, A. Fleischmann, N. Korber, *Z. Anorg. Allg. Chem.* **2009**, *635*, 508–512.
- [4] M. Waibel, T. F. Fässler, *Z. Naturforsch.* **2013**, *68b*, 732–734.
- [5] L. Diel, K. Khodadadeh, D. Kummer, J. Strähle, *Chem. Ber.* **1976**, *109*, 3404–3418.
- [6] A. Fleischmann, N. Korber, *Dalt. Trans.* **2001**, 383–385.
- [7] J. D. Corbett, D. G. Adolphson, D. J. Merryman, P. A. Edwards, F. J. Armatis, *J. Am. Chem. Soc.* **1975**, *97*, 6267–6268.
- [8] J. D. Corbett, P. A. Edwards, *Chem. Commun.* **1975**, 984–985.
- [9] L. Xu, S. C. Sevov, *J. Am. Chem. Soc.* **1999**, *121*, 9245–9246.
- [10] J. M. Goicoechea, S. C. Sevov, *Organometallics* **2006**, *25*, 4530–4536.
- [11] B. Kesanli, J. E. Halsig, P. Zavalij, J. C. Fettingner, Y.-F. Lam, B. Eichhorn, *J. Am. Chem. Soc.* **2007**, *129*, 4567–4575.
- [12] S. Joseph, M. Hamberger, F. Mutzbauer, O. Härtl, M. Meier, N. Korber, *Angew. Chem.* **2009**, *121*, 8926–8929.
- [13] M. Waibel, F. Kraus, S. Scharfe, B. Wahl, T. F. Fässler, *Angew. Chem. Int. Ed.* **2010**, *49*, 6611–6615.
- [14] S. Scharfe, T. F. Fässler, S. Stegmaier, S. D. Hoffmann, K. Ruhland, *Chem. Eur. J.* **2008**, *14*, 4479–4483.
- [15] B. Kesanli, J. C. Fettingner, B. Eichhorn, *Chem. Eur. J.* **2001**, *7*, 5277–5285.
- [16] J.-Q. Wang, S. Stegmaier, T. F. Fässler, *Angew. Chem. Int. Ed.* **2009**, *48*, 1998–2002.
- [17] B. Zhou, M. S. Denning, D. L. Kays, J. M. Goicoechea, *J. Am. Chem. Soc.* **2009**, *131*, 2802–2803.

- [18] S. Gärtner, N. Korber, in *Main-Gr. Elem. Compr. Inorg. Chem. II (Second Ed.* (Eds.: K. Poeppelemeier, R. J.), Elsevier Ltd., Amsterdam Oxford Waltham, **2013**, pp. 251–267.
- [19] F. S. Kocak, D. O. Downing, P. Zavalij, Y.-F. Lam, A. N. Vedernikov, B. Eichhorn, *J. Am. Chem. Soc.* **2012**, *134*, 9733–97410.
- [20] M. Neumeier, F. Fendt, S. Gärtner, C. Koch, T. Gärtner, N. Korber, R. M. Gschwind, *Angew. Chem. Int. Ed.* **2013**, *52*, 4483–4486.
- [21] S. Joseph, C. Suchentrunk, F. Kraus, N. Korber, *Eur. J. Inorg. Chem.* **2009**, 4641–4647.
- [22] S. Joseph, C. Suchentrunk, N. Korber, *Z. Naturforsch.* **2010**, *65b*, 1059–1065.
- [23] J. Rosdahl, T. F. Fässler, L. Kloo, *Eur. J. Inorg. Chem.* **2005**, 2888–2894.
- [24] M. Trummer, PhD Thesis, ETH Zürich, Switzerland, **2011**.
- [25] W. L. Wilson, R. W. Rudolph, L. L. Lohr, R. C. Taylor, P. Pyykko, *Inorg. Chem.* **1986**, *25*, 1535–1541.
- [26] G. Jander, H. Spandau, C. C. Addison, *Anorganische Und Allgemeine Chemie in Flüssigem Ammoniak, Teilband I*, Friedr. Vieweg & Sohn, Braunschweig, **1966**.
- [27] F. Fendt, C. Koch, S. Gärtner, N. Korber, *Dalt. Trans.* **2013**, *42*, 15548–15550.
- [28] S. Stegmaier, M. Waibel, A. Henze, L. A. Jantke, A. J. Karttunen, T. F. Fässler, *J. Am. Chem. Soc.* **2012**, *134*, 14450–14460.
- [29] G. Brauer, *Handbuch Der Präparativen Anorganischen Chemie*, 3. Aufl., Ferdinand Enke Verlag, Stuttgart, **1975**.
- [30] M. Somer, U. Aydemir, M. Baitinger, H. G. von Schnering, *Z. Anorg. Allg. Chem.* **2006**, *632*, 1281–1286.
- [31] W. Klemm, I. F. Hewaidy, E. Busmann, *Z. Anorg. Allg. Chem.* **1964**, *328*, 283–293.
- [32] H. G. von Schnering, M. Baitinger, U. Bolle, W. Carrillo-Cabrera, J. Curda, Y. Grin, F. Heinemann, J. Llanos, K. Peters, A. Schmeding, et al., *Z. Anorg. Allg. Chem.* **1997**, *623*, 1037–1039.
- [33] A. Joannis, *C. R. Hebd. Seances Adac. Sci.* **1892**, *114*, 585.
- [34] A. Schneider, *Z. Elektrochem.* **1941**, *47*, 291.
- [35] C. Wagner, *Angew. Chem.* **1941**, *54*, 525–527.
- [36] W. Klemm, *Z. Anorg. Allg. Chem.* **1941**, *247*, 1–21.

-
- [37] J. D. Corbett, *Chem. Rev.* **1985**, 85, 383–397.
- [38] M. M. Gillett-Kunnath, A. G. Oliver, S. C. Sevov, *J. Am. Chem. Soc.* **2011**, 133, 6560–6562.
- [39] L. Xu, S. C. Sevov, *Inorg. Chem.* **2000**, 39, 5383–5389.
- [40] R. C. Burns, J. D. Corbett, *J. Am. Chem. Soc.* **1982**, 104, 2804–2810.
- [41] R. C. Burns, J. D. Corbett, *J. Am. Chem. Soc.* **1981**, 103, 2627–2632.
- [42] S. C. Critchlow, J. D. Corbett, *Inorg. Chem.* **1985**, 24, 979–981.
- [43] S. C. Critchlow, J. D. Corbett, *Inorg. Chem.* **1982**, 21, 3286–3290.
- [44] F. Lips, I. Schellenberg, R. Pöttgen, S. Dehnen, *Chem. Eur. J.* **2009**, 15.
- [45] F. Lips, S. Dehnen, *Angew. Chem.* **2009**, 121, 6557–6560.
- [46] F. Lips, M. Raupach, W. Massa, S. Dehnen, *Z. Anorg. Allg. Chem.* **2011**, 637, 859–863.
- [47] J. M. Goicoechea, S. C. Sevov, *Inorg. Chem.* **2005**, 44, 2654–2658.
- [48] H. G. von Schnering, W. Höhle, *Chem. Rev.* **1988**, 88, 243–273.
- [49] C. M. Knapp, J. S. Large, N. H. Rees, J. M. Goicoechea, *Dalt. Trans.* **2011**, 40, 735–745.
- [50] F. Lips, R. Clérac, S. Dehnen, *Angew. Chem.* **2011**, 123, 991–995.
- [51] A. D. Becke, K. E. Edgecombe, *J. Chem. Phys.* **1990**, 92, 5397.
- [52] A. Savin, A. D. Becke, J. Flad, R. Nesper, H. Preuss, H. G. von Schnering, *Angew. Chem. Int. Ed. Engl.* **1991**, 30, 409–412.
- [53] A. Savin, R. Nesper, S. Wengert, T. F. Fässler, *Angew. Chem. Int. Ed. Engl.* **1997**, 36, 1808–1832.
- [54] T. F. Fässler, A. Savin, *Chem. Unserer Zeit* **1997**, 31, 110–120.
- [55] R. J. Cave, E. R. Davidson, P. Sautet, E. Canadell, O. Eisenstein, *J. Am. Chem. Soc.* **1989**, 111, 8105–8111.
- [56] U. Friedrich, M. Neumeier, C. Koch, N. Korber, *Chem. Commun.* **2012**, 48, 10544–10546.
-

7 NMR Spectroscopic Investigations on the Solvation of Alkali Salts (^{87}Rb , ^{23}Na , ^7Li) in Liquid Ammonia

Parts of the here presented investigations were performed as bachelor thesis of Jakob Asenbauer in 2014.
I performed the NMR spectroscopic investigations, while the sample preparation was done by Jakob Asenbauer. The sample preparation in liquid ammonia was done by Franziska Fendt.

Carina Koch, Franziska Fendt, Jakob Asenbauer, Ruth M. Gschwind

To be published.

7.1 Abstract

The stabilization of Zintl anions in solution was until recently very challenging. But the latest investigations showed that it is possible to stabilize highly charged polyanions by the addition of [2.2.2]-cryptand. Furthermore, it was shown that also the used alkali metal has an influence on the stabilization. Therefore, the investigations were extended to the perspective of the alkali salt. Here, the NMR spectroscopic studies of rubidium salts in liquid ammonia showed that it is possible to stabilize contact ion pairs and solvent-separated ion pairs side by side in solution. Thereby, the amount of the contact ion pair is decreased by increasing size of the halide. After the addition of chelating cryptand, it was possible to detect even three species in solution. Moreover, the investigations were extended to sodium and lithium salts and were performed in further organic solvents. This first NMR spectroscopic investigation on alkali salts in liquid ammonia will help to understand the role of the alkali metal for the stabilization of highly charged cluster atoms and will improve targeted reactions of homoatomic polyanions in liquid ammonia for the formation of new materials.

7.2 Introduction

The chemistry of main group metal polyanions, also known as Zintl anions, is of high importance in the field of inorganic chemistry, since they can be manipulated in solution and are the basis of a lot of reaction products which can be found in the literature.^[1] However, the access to targeted synthesis and controlled transformation reactions is so far not feasible, as the solvation, transformation and degradation processes in solution are not completely understood. Zintl phases in solution are either received by the solvation of the solid phase (e.g. Rb_4Sn_4 or $\text{Rb}_{12}\text{Sn}_{17}$) or by the direct reduction of tin with an alkali metal (see chapter 5 and 6 of this thesis).^[2] Very recently, our investigations on highly charged polyanions showed, that the protons of the liquid ammonia are responsible for their oxidation (e.g. Sn_4^{4-} to Sn_9^{4-}).^[3] Moreover, we were able to elucidate that the contacts between the alkali metal and the solvent molecules lead to a polarization of the ammonia and thus the oxidation can be inhibited by the addition of a cryptand (see chapter 6 of this thesis). This means, that besides the known enhancement of the solubility of Zintl phases in solution,^[4] the cryptand also has a crucial role on the oxidizing properties, and can therefore be used to stabilize the highly charged anions (Sn_4^{4-} and Si_4^{4-}).^[3]

After recognizing that the alkali metal is not innocent for the stabilization of the Zintl anions in solution, the investigation was focused on the rubidium ion. Thereby, the NMR spectroscopy offers a direct insight in the solution and is the analytical method of choice to elucidate the ion-ion, ion-solvent and ion-ligand interactions, as a slight variation of the chemical environment is observable by a shift of the signal. So far, no NMR spectroscopic investigations on alkali salts in liquid ammonia are known. The here presented NMR investigations are focused on rubidium salts, to get a comparison to our former studies of stannides where rubidium was used as alkali metal. Moreover, very less is known about the formation of rubidium ammoniates, while a lot of very stable ammoniates of sodium and lithium can be found in the literature.^[5] Therefore also these alkali metals were investigated by NMR spectroscopy. Unfortunately, owing to the frequency range of the used probe head it was so far not possible to perform investigations on the potassium and cesium salts.

Herein, we present the first NMR spectroscopic investigation of alkali salts in liquid ammonia by simple rubidium salts (RbX ; $\text{X} = \text{F}, \text{Cl}, \text{Br}$) and examine their behavior at various temperatures and the influence of chelating additives. Additionally, further organic solvents, which are known for the dissolution of Zintl phases are applied and the examination was also extended to sodium and lithium salts.

7.3 Results and Discussion

7.3.1 RbX ($\text{X} = \text{F}, \text{Cl}, \text{Br}$) in Liquid Ammonia at Various Temperatures

Recently, the investigations on the solvation and transformation processes of Zintl phases showed that the protons of the liquid ammonia are responsible for the oxidation processes,^[3] and that the oxidation behavior can be reduced by suppressing the cation- NH_3 interactions by a cryptand (see chapter 6 of this thesis), which leads to the stabilization of the highly charged polyanions. For that reason, the perspective of the alkali metal in these systems is of great interest, for the controlling of solvation processes in solution. Therefore, beside the ^{87}Rb NMR spectra of rubidium stannides (see the Supporting Information, Figure 7.9), for the elucidation of the interactions between the Rb^+ ion and the liquid ammonia simple rubidium salts (RbX ; $\text{X} = \text{F}, \text{Cl}, \text{Br}$) were investigated at various temperatures.

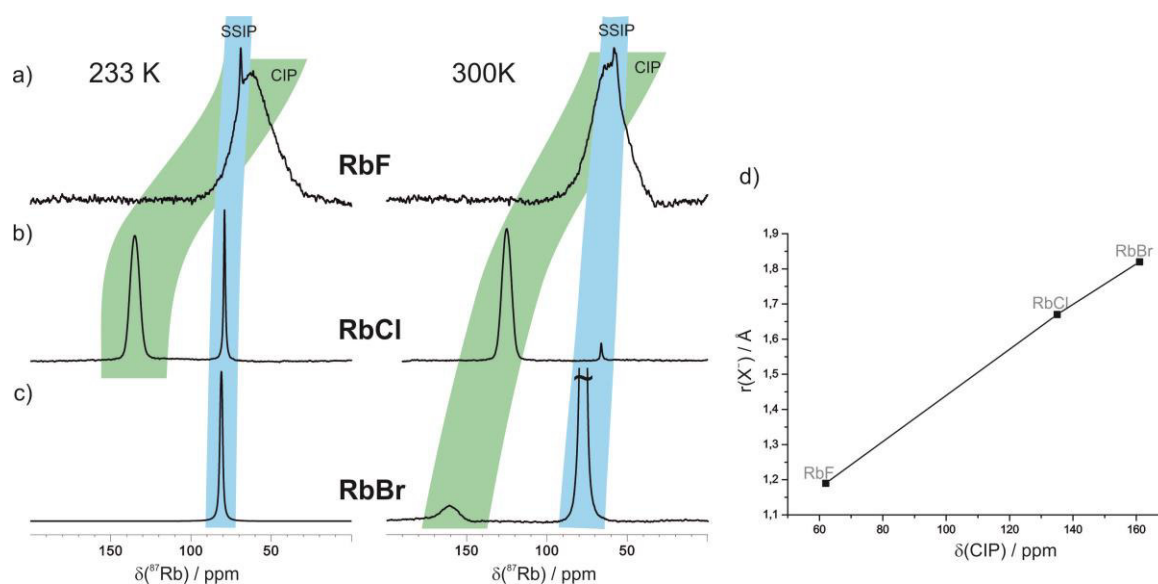


Figure 7.1: ^{87}Rb spectra of different rubidium salts a) RbF, b) RbCl and c) RbBr; at 233 K (left) and 300 K (right) in liquid ammonia. d) Plot of the chemical shift values of the CIP at 300 K against the ionic radius of the halides (F $^-$ to Br $^-$).^[6]

The ^{87}Rb NMR spectra of various rubidium salts (RbX; X = F, Cl, Br) in liquid ammonia at 233 and 300 K are shown in Figure 7.1. The spectrum of RbCl at 233 K showed two signals at 135 ppm ($\Delta\nu_{1/2} = 1297$ Hz) and 79 ppm ($\Delta\nu_{1/2} = 195$ Hz) (Figure 7.1b, left). For RbF, also two overlapping signals were observed, at 69 ppm ($\Delta\nu_{1/2} = \sim 540$ Hz) and 62 ppm ($\Delta\nu_{1/2} = \sim 4500$ Hz) (Figure 7.1a, left). The sample of RbBr in liquid ammonia at 233 K (Figure 7.1c, left) showed only one signal at 81 ppm ($\Delta\nu_{1/2} = 482$ Hz). The appearance of two separated signals for RbCl in liquid ammonia was not expected, but can be explained by two solvation forms of the Rb $^+$ ions that are very stable and show a slow exchange on the NMR timescale. The more upfield shifted, narrow signal is assigned to the solvent-separated ion pair (SSIP) Rb $^+(\text{NH}_3)_x$, where the Rb $^+$ ions have no contact to the Cl $^-$ ions. This assumption is supported by the spectra of RbF and RbBr (Figure 7.1, a and c). In those spectra, signals with narrow line widths were occurring with approximately the same chemical shift values compared to the upfield shifted one of RbCl. These signals are assigned to a SSIP, as owing to the unaffected chemical shift value the Rb $^+$ ion seems not to be influenced of the halide and must therefore be separated from it. The solvents molecules have a shielding effect on the Rb $^+$ ion as the signals is arising more upfield shifted as it would be expected for an isolated cation. For example the signal of a carbon cation ((CH $_3$) $_3\text{C}^+$) is known to arise at 330 ppm which is a tremendously downfield shifted in comparison to common ^{13}C chemical shift values.^[7] The broad signal is therefore assigned to the contact ion pair (CIP) Rb $^+\text{Cl}^-$, as

here the less deshielding influence of the halide is observable by a downfield shift of the signal from F^- to Br^- . This downfield shift can be explained by an exchange of the solvent molecules by a halide to form a CIP like $Rb^+X^-(NH_3)_y$. So for a greater radius of the halide, more solvent molecules are released from the coordination sphere of the Rb^+ ion which leads to a deshielding effect accompanied by a downfield shift. By plotting the ionic radius of the halides (F^- , Cl^- and Br^-) and the chemical shift values of their CIP against each other, a linear correlation is found (see Figure 7.1d), which supports this assumption. Moreover it is obvious, that the F^- ion shows a similar deshielding effect on the Rb^+ ion as the solvent molecules so both show similar donor properties. But besides the size of the halide and the amount of released ammonia molecules, two further explanations can be made for the different deshielding effect of the halides. There is also the direct interaction of the halide with the Rb^+ ion, which would in general lead to the opposing shift, as in comparison fluorine alkanes are known to arise more downfield shifted than bromine alkanes. Then, there is also the disturbance of the ammonia hydrogen-bonded network, which should also be taken into account. Overall, all of these influences are occurring in solution, but their particular amount of the deshielding cannot be determined by 1D NMR spectroscopic methods. However, a trend for the different halides is observable and theoretical calculations on this issue are planned.

Considering the varying ratios of CIP to SSIP for the different rubidium salts, it is obvious that with RbF the amount of SSIP is lower than for $RbBr$. This can be explained by the enthalpy of formation, which is decreasing in the order of $RbBr$ to RbF ($\Delta H_{f,RbF} = -558$ kJ/mol; $\Delta H_{f,RbCl} = -435$ kJ/mol, $\Delta H_{f,RbBr} = -395$ kJ/mol)^[6] and therefore provides an energetically more favored bond cleavage of the rubidium halide bond for $RbBr$ than for RbF .

The examination of the same samples at 233 K and 300 K (Figure 7.1, left and right) show that at higher temperatures the amount of CIPs is increasing, for $RbCl$ from 78 % to 97 % and for $RbBr$ from 0 % to 6 %. For RbF no statement can be made as the signals of the CIP and the SSIP are overlapping, but it can be estimated that the signal of the CIP is increasing at higher temperatures, as well. This temperature effect can be explained by an entropy increase at higher temperatures if the CIP is formed, as more ammonia molecules are released than halide molecules are bound the Rb^+ ion. While at lower temperatures the effect of the energy release by the building of SSIP is more pronounced. However, for $RbCl$ at 195 K an opposite effect was observed (see Table 7.1 and the Supporting

Information, Figure 7.7). An explanation for this effect is so far not found, but the measurement of RbF and RbBr at 195 K will show whether this trend can be observed also for other rubidium salts.

Table 7.1: The chemical shifts ($\delta(^{87}\text{Rb})$), line widths ($\Delta\nu_{1/2}$) and amounts of CIP and SSIP occurring in spectra with RbX ($\text{X} = \text{F}, \text{Cl}, \text{Br}$) in liquid ammonia, at different temperatures and the ionic radius of the halides (F^- , Cl^- , Br^-).

	CIP : SSIP	CIP		SSIP		$r(\text{X}^-)$
		$\delta(^{87}\text{Rb})$ [ppm]	$\Delta\nu_{1/2}$ [Hz]	$\delta(^{87}\text{Rb})$ [ppm]	$\Delta\nu_{1/2}$ [Hz]	
RbF						1.19
233 K	96 % : 4 %	62	$\sim 4500^*$	69	$\sim 540^*$	
300 K	n.d.	62	$\sim 4500^*$	58	n.d.	
RbCl						1.62
195 K	87 % : 13 %	127	1285	71	242	
233 K	78 % : 22 %	135	1343	79	245	
300 K	97 % : 3 %	125	1166	66	$\sim 100^*$	
RbBr						1.82
233 K	0 % : 100 %	-	-	81	185	
300 K	6 % : 94 %	161	$\sim 1700^*$	77	135	

* These values were determined manually.

The ^{87}Rb NMR spectra of various rubidium salts showed that contact ion pairs (CIP) and solvent-separated ion pairs (SSIP) can be stabilized side by side in liquid ammonia. Their ratio is on the one hand dependent on the associated halide, since at 233 K for RbF the major part of the Rb^+ ions is occurring in form of a CIP, while for RbBr no CIP was observed. But on the other hand also temperature-dependent, as at higher temperatures the amount of CIPs is increasing. For RbCl the two signals are baseline separated at all considered temperatures, while for RbF the signals are overlapping and for RbBr at 233 K solely the signal of SSIP is observed. Thus, for further investigations RbCl will be used as model system.

7.3.2 Influence of Additives on the Solvation of RbCl in Liquid Ammonia

The solubility enhancement of Zintl phases by addition of [2.2.2]-cryptand is literature known.^[4] In addition, very recently we were able to show that [2.2.2]-cryptand can be applied for the stabilization of highly charged polyanions of tin and silicon in liquid ammonia.^[3] Moreover, the reason for this stabilizing effect was examined in a further investigation (see chapter 6 of this thesis), where it was shown that the shielding of the rubidium ion by [2.2.2]-cryptand suppresses the contacts between the alkali cation and the solvent molecules, which leads to a reduced oxidation property of the protons of the ammonia and therefore the oxidation of Sn_4^{4-} to Sn_9^{4-} is inhibited. For this reason, we investigated also the influence of additives on the alkali cation in liquid ammonia.

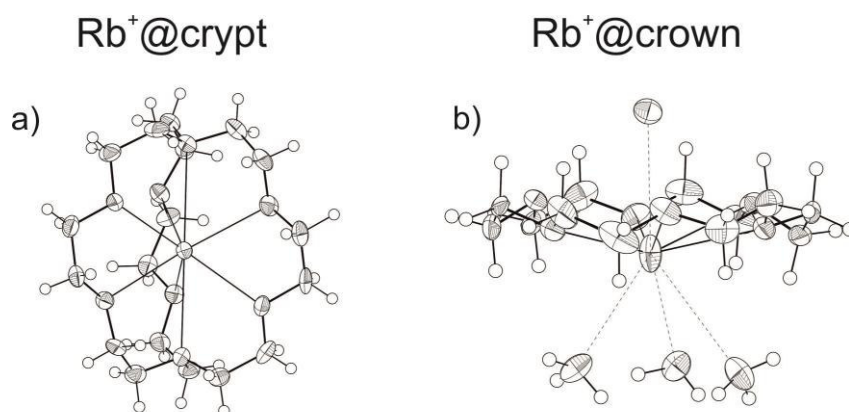


Figure 7.2: Schematic representation of a Rb^+ ion captured by the used additives: a) $\text{Rb}^+@[\text{2.2.2}]\text{-crypt}$, the Rb^+ ion is completely shielded from the solvent, b) $\text{Rb}^+@18\text{-crown-6}$, additional interactions with the solvent molecules can be formed.ⁱ

These investigations were performed with RbCl, as this alkali salt shows two baseline separated signals for the CIP and the SSIP at various temperatures in liquid ammonia (see Figure 7.1b and the Supporting Information Figure 7.6). As chelating additives [2.2.2]-cryptand and 18-crown-6 were applied as they show good chelating properties to Rb^+ ions^[6] and both of them have been used in our former studies of Zintl phases. With [2.2.2]-cryptand the Rb^+ ion is completely shielded from the solvent molecules and therefore no direct cation-ammonia interaction is possible (see Figure 7.2a), while 18-crown-6 partially enables this interaction on free coordination sites (see Figure 7.2b), which should lead to different electronic properties on the Rb^+ ion and therefore the change of the additive should be visible in the ^{87}Rb NMR spectrum. For the formation of further species besides the chelated ion an amount of 0.5 equivalents of additive to RbCl

ⁱ The graphics were made by Franziska Fendt, using Olex2.

was used. To prevent potential exchange processes, also an excess of additive was given to the solution.

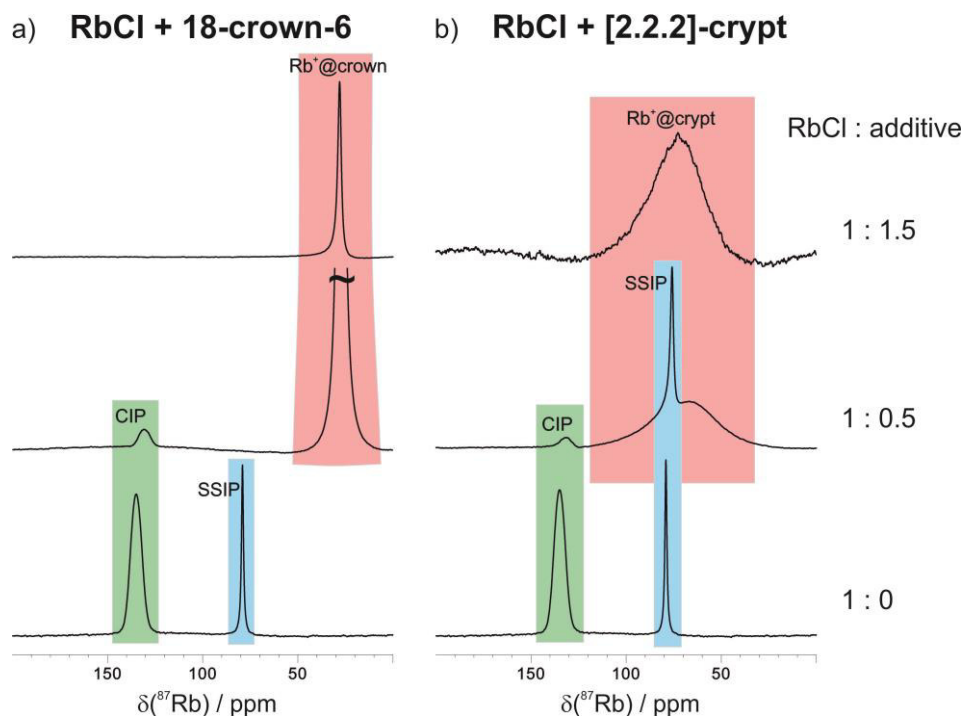


Figure 7.3: ^{87}Rb NMR spectra of RbCl with a) 18-crown-6 and b) [2.2.2]-cryptand, at 233 K in liquid ammonia; using 1.5 eq (above), 0.5 eq (middle) and no additive (below).

In the ^{87}Rb NMR spectrum of RbCl with 0.5 equivalents of [2.2.2]-cryptand (Figure 7.3b, middle) three species were observable, the CIP at 131 ppm (1400 Hz), the SSIP at 79 ppm (520 Hz) and $\text{Rb}^+\text{@crypt}$ at 67 ppm (6800 Hz) with amounts of 3 % : 17 % : 80 % (determined by simulation). At 300 K the determination of the ratios of SSIP and $\text{Rb}^+\text{@crypt}$ was not possible, as owing to their line broadening, the signals were almost completely overlapping, while at 195 K only the signals of CIP and SSIP were observable (see the Supporting Information Figure 7.7a and c). Using 0.5 equivalents of 18-crown-6, two signals arose, one of CIP at 132 ppm ($\Delta\nu_{1/2} = 1400$ Hz) and one of $\text{Rb}^+\text{@crown}$ at 27 ppm ($\Delta\nu_{1/2} = 740$ Hz) with a ratio of 4 % : 96 % (Figure 7.3a, middle). At 300 K the same signals were observable, but the amount of CIP is slightly decreasing (2 % : 98 %), while the line widths were changing ($\Delta\nu_{1/2} = 1500$ and 380 Hz, respectively) (data not shown). By using an excess of the additives, as expected, in both cases only one broad signal was observable, for $\text{Rb}^+\text{@crypt}$ at 59 ppm (3100 Hz) and $\text{Rb}^+\text{@crown}$ 28 ppm (360 Hz), respectively (Figure 7.3, above).

The observation of three separated signals in the spectrum with [2.2.2]-cryptand, shows that the chemical exchange rate of CIP, SSIP and $\text{Rb}^+\text{@crypt}$ is slow on the NMR

timescale. The high ratio of 80 % of Rb^+ ions which are bound to 0.5 equivalents of [2.2.2]-cryptand, seems to be puzzling, but can be explained by the partial solvation of the rubidium salt, thus the residue contains the remaining Rb^+ ions. These well-separated signals were only observed at 233 K, at 195 K and 300 K the signals were not well-resolved (see the Supporting Information, Figure 7.7). With an excess of [2.2.2]-cryptand all Rb^+ ions are bound to the cryptand, as it would be expected.

For RbCl with 0.5 equivalents 18-crown-6, no separated signal for the SSIP arose. It is assumed that the signal assigned as $\text{Rb}^+@crown$ represents an averaged signal of $\text{Rb}^+@crown$ and SSIP. If the same ratio of CIP to SSIP like in the spectra without additive is assumed, the shift of the averaged signal in comparison to the signal of $\text{Rb}^+@crown$ would be 0.5 ppm which is within the experimental error and would therefore not be resolved. The solubility enhancement of the rubidium salt by an additive is responsible for this ratio of CIP to $\text{Rb}^+@crown$ of 4 % to 96 % (or if the SSIP is estimated to be 1 % of 4 % : 1 % : 95 %). The spectrum at 300 K shows a slightly decreasing amount of CIP, which is puzzling, as this is opposing to the results for RbCl at 233 and 300 K described above (see the Supporting Information, Figure 7.6).

The upfield shift of the Rb^+ ions (CIP: $\delta(^{87}\text{Rb}) = 135$ ppm, SSIP: $\delta(^{87}\text{Rb}) = 79$ ppm, $\text{Rb}^+@crypt$: $\delta(^{87}\text{Rb}) = 73$ ppm, $\text{Rb}^+@crown$: $\delta(^{87}\text{Rb}) = 28$ ppm) shows that the electron density on the Rb^+ ion is increasing in this order. Hence, the additives lead to a stronger shielding than the solvent molecules. In case of 18-crown-6 the combined shielding of the crown ether compared with the contacts of the solvent molecules leads to a stronger shielding compared to [2.2.2]-cryptand which results in a strong upfield shift. This is supported by investigations in other solvents and examinations of sodium salts (see below, Figure 7.4 and 7.5).

Furthermore, it is notable, that the CIP of RbF ($\delta(^{87}\text{Rb}) = 62$ ppm, Figure 7.1a) shows a chemical shift value like $\text{Rb}^+@crypt$ ($\delta(^{87}\text{Rb}) = 68$ ppm). This means that the Rb^+ ions experience in both cases a similar electronic environment, which leads to the suggestion, that the addition of the costly cryptand for the stabilization of highly charged stannides might be circumvented, by addition of NaF or LiF . However, in this case potential counter ion interactions of Na^+ or Li^+ ions, respectively, must be taken into account, which is not required for the neutral [2.2.2]-cryptand. The investigation of this approach will be part of future work.

The addition of chelating additives to RbCl in liquid ammonia showed for a substoichiometric amount of [2.2.2]-cryptand three separated signals. Besides the CIP and the SSIP also the signal of $\text{Rb}^+@crypt$ arises and shows that these three species are stable and in slow chemical exchange. For 0.5 eq of 18-crown-6 only two signals have been observed, for CIP and $\text{Rb}^+@crown$. If an excess of the additive is applied, in both cases exclusively the signal for the chelated Rb^+ ion occurs, which shows for 18-crown-6 the most upfield shifted signal compared to the other solvated species.

7.3.3 RbCl in Organic Solvents and Enhancement of Solvation by Chelating Additives

Supplementary to the studies in liquid ammonia, the solvation of alkali salts in organic solvents was investigated. Owing to the above described results, RbCl was applied with the chelating additives 18-crown-6 and [2.2.2]-cryptand, as model system for the alkali metals. Besides ethylenediamine and liquid ammonia, commonly used solvents for investigations on Zintl ions are pyridine, tetrahydrofuran and acetonitrile, thus these solvents have been chosen for further investigations.

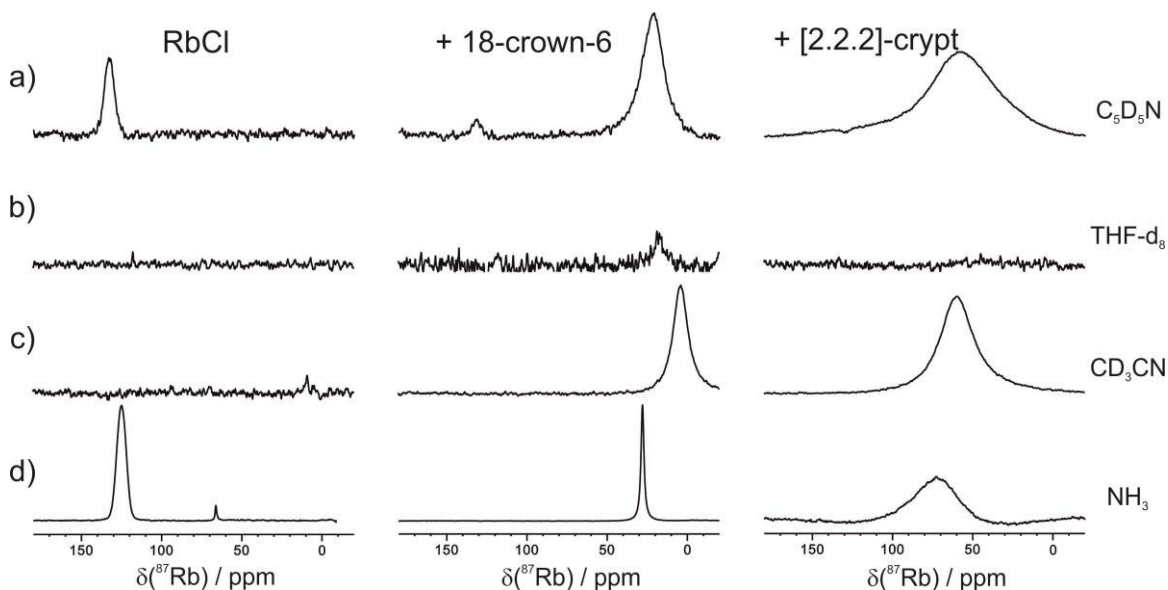


Figure 7.4: ^{87}Rb NMR spectra of a) RbCl , and RbCl with additives (1.0-1.5 eq): b) with 18-crown-6 and c) [2.2.2]-cryptand in different solvents ($\text{C}_5\text{D}_5\text{N}$, THF-d_8 , CD_3CN and NH_3) at 300 K.

Without additives, RbCl was soluble in pyridine (see Figure 7.4a, right), compared to liquid ammonia, only one signal for a CIP at 133 ppm arose, but none for a SSIP. In case 18-crown-6 or [2.2.2]-cryptand was added to this solution besides the signal of the chelated Rb^+ ion (at 22 ppm and 63 ppm, respectively) a small signal for CIP was observed (134 ppm), which hints at a slightly substoichiometric amount of the additive in

solution. RbCl was not soluble at 300 K in acetonitrile and tetrahydrofuran. However, with chelating additives, the solubility was enhanced for RbCl in acetonitrile, showing the signals of the chelated Rb^+ ions at 4 ppm and 60 ppm, respectively (Figure 7.4c). For tetrahydrofuran the solubility of RbCl was only slightly increased by the addition of 18-crown-6 and a very small signal at 17 ppm $\text{Rb}^+@ \text{crown}$ arose (Figure 7.4b), while with [2.2.2]-cryptand no signal was observed.

By comparing the ^{87}Rb NMR spectra of RbCl with additives in different solvents the interaction between the Rb^+ ion and the solvent is visible. Thereby the spectra of pyridine are leaved aside, owing to the feature of pyridine to act as a shift reagent. With 18-crown-6 the chemical shift values from pyridine to acetonitrile are upfield shifted (22 ppm in $\text{C}_5\text{D}_5\text{N}$, 18 ppm in NH_3 , 17 ppm in THF-d_8 , 4 ppm in CD_3CN). As already mentioned, the Rb^+ ions are not completely shielded by the crown ether, therefore, free coordination sites are occupied by the solvent molecules (see Figure 7.2). Here, also the ring current of pyridine and the magnetic shielding anisotropy of acetonitrile must be taken into account. Furthermore, it is obvious, that the line widths of the signals are strongly deviating, especially the one of NH_3 is narrower. If [2.2.2]-cryptand is added to RbCl, as expected, the deviation of the chemical shift values is not so pronounced, as the Rb^+ ion is completely shielded from the solvent by the cryptand, and therefore the solvent shows less influence on the Rb^+ ion.

The solvation of RbCl in organic solvents showed, that RbCl is soluble in pyridine without chelating additives, as a CIP. In acetonitrile, the solvation is only observable by the addition of additives, which are strongly enhancing the solubility. In comparison, tetrahydrofuran, showed only slightly increased solvation by 18-crown-6. The signals observed in the spectra of RbCl with additives, all showed one signal for the Rb^+ ion, which is chelated by the additive. Owing to the free coordination sites in 18-crown-6 a stronger solvent-dependence was observed than for [2.2.2]-cryptand. Further examinations with substoichiometric amounts of the additives will show, whether it is also possible to stabilize more than one species in pyridine or acetonitrile, as it was observed in liquid ammonia. Since pyridine dissolves RbCl without additives and shows similar signals and interactions compared to those in liquid ammonia, it will be preferentially used in further investigations on other alkali salts.

7.3.4 Investigations on Alkali Salts of ^{23}Na and ^7Li

After the observation of two species in the ^{87}Rb NMR spectra for RbCl in liquid ammonia, the investigations were expanded on further alkali metals. ^{23}Na and ^7Li were investigated, because it is supposed, that they are forming stable ammine complexes in liquid ammonia like it is known from the solid phase.^[5] Moreover, it is possible to prepare highly charged Zintl ions by direct reduction of tin with sodium.^[2,3] Thus, the stabilization of Na^+ or Li^+ ions in liquid ammonia without additives by the formation of highly stable homoleptic ammine complexes, might also stabilize the highly charged Zintl anions (like Sn_4^{4-}), as these ammine complexes are so strong, that the polarization of the ammonia and thus the oxidation potential of the protons is inhibited. This access would be cheaper, because the use of expensive additives would then no longer be necessary for the stabilization of Zintl ions in solution. Getting an insight of the occurring interactions in those solutions is therefore of high importance.

As solvents for these studies, besides liquid ammonia, which is the standard solvent for our investigations on Zintl ions, pyridine was chosen, as it showed with rubidium the best agreeing results to liquid ammonia. Unfortunately, the solubility of NaCl was low in pyridine, and no signal was observed in the ^{23}Na NMR spectra. Therefore, the investigations were performed in acetonitrile. As sodium salts NaCl and NaBr were chosen, as the interaction with the halide might have an influence on the chemical shift value of the CIP, an unambiguous assignment of CIPs and SSIPs is possible. At 233 K NaBr was not soluble therefore, the sample was warmed up to 300 K and investigated at this temperature, while NaCl was so far only investigated at 233 K. This must be taken into account for the interpretation of the spectra. In liquid ammonia LiCl was swelling during the solvation process and was covering the spectrometer coil, so no results are so far received from these samples. But as it was soluble in pyridine, it was feasible to investigate the influence of 12-crown-4 on the Li^+ ion.

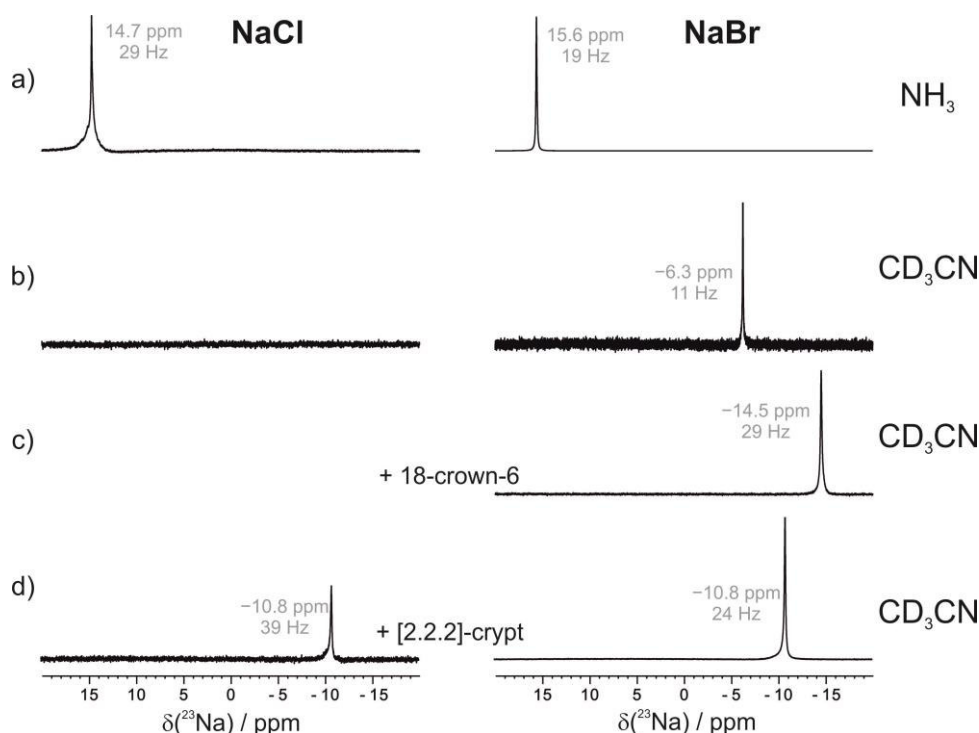
NaCl and NaBr in NH₃ and CD₃CN

Figure 7.5: ^{23}Na spectra of NaCl (left) and NaBr (right), in a) NH_3 , b)-d) in CD_3CN , b) without additive, c) with 18-crown-6, d) with [2.2.2]-cryptand, at 300 K (and NaCl in NH_3 at 233 K).

The samples in liquid ammonia show for both sodium salts only one signal, NaCl at 14.7 ppm and NaBr at 15.6 ppm (Figure 7.5a). For the investigations in acetonitrile, only for NaBr a upfield shifted signal is observed at -6.3 ppm, while the solubility of NaCl is too low in acetonitrile and thus no signal is observed (Figure 7.5b, above). After the addition of [2.2.2]-cryptand to the samples in acetonitrile, both show one signal at -10.8 ppm (Figure 7.5b, below), while for NaBr with 18-crown-6 a more upfield shifted signal at -14.5 ppm arises (Figure 7.5b, middle).

After the observation of two separated signals for a CIP and a SSIP of rubidium salts in liquid ammonia, the arising of only one signal for the Na^+ ion was not expected, as the ammine complexes formed with Na^+ ions are known to be highly stable. Since the signals of NaCl and NaBr show a deviation in the chemical shifts of $\Delta\delta(^{23}\text{Na}) = 0.9$ ppm (which is not irrelevant for the chemical shift range of ^{23}Na from 20 to -65 ppm), there are two plausible explanations. Either the shift is occurring owing to the different temperatures of the experiment, or it can be explained by an averaged signal, as the Na^+ ions are exchanging so fast on the NMR timescale, that only the averaged signal of the CIP and the SSIP is observable. The trend of an upfield shift for the signal of NaBr is therefore in agreement with the results of rubidium, where, the SSIP shows approximately the same

chemical shift values and the values of the CIP is upfield shifted from RbF to RbBr at 300 K (for RbF to RbCl : $\Delta\delta(^{87}\text{Rb}) = 34$ ppm, and for RbCl to RbBr : $\Delta\delta(^{87}\text{Rb}) = 64$ ppm). However, the line widths (NaCl : 29 Hz and NaBr : 19 Hz, respectively) are slightly broader than the one for NaBr (11 Hz) in acetonitrile which might hint to an exchange. But so far, these points are speculative and the assignment of the signals will need more experimental evidence, e.g., the addition of chelating additives in a substoichiometric amount could show several species, as it was observed with RbCl or the temperature can be decreased to separate the averaged signals.

The investigations in acetonitrile showed, that the addition of [2.2.2]-cryptand to NaCl enhanced the solubility. Moreover, exactly the same chemical shift value is observed for $\text{Na}^+@crypt$ in the spectra of NaCl and NaBr , which arises upfield shifted to the one of NaBr in acetonitrile. The signal for $\text{Na}^+@crown$ in the spectrum of NaBr with 18-crown-6 arises even more upfield shifted, which is in agreement with the results received for RbCl with chelating additives. Also here, the application of substoichiometric amounts of additives might show further signals in the spectra. Furthermore, the strong upfield shift of the signal of NaBr in acetonitrile in comparison to the one in liquid ammonia could be a hint for a SSIP in acetonitrile. However, the magnetic shielding anisotropy of acetonitrile must be taken into account for this comparison and therefore no assignment to a CIP and a SSIP can be made so far.

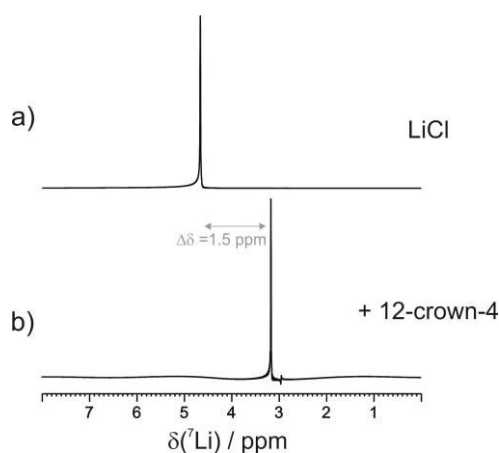
LiCl in pyridine and the influence of 12-crown-4

Figure 7.6: ^7Li NMR spectra of a) LiCl and b) with 12-crown-4 in $\text{C}_5\text{D}_5\text{N}$ at 300 K.

The ^7Li NMR spectrum of LiCl in pyridine shows one signal at 4.7 ppm (Figure 7.6a). As already mentioned for sodium, here the observation of only one signal was not expected, owing to the highly stable ammine complexes. If a stoichiometric amount of 12-crown-4 is given to this solution, the signal for $\text{Li}^+\text{@crown}$ arises upfield shifted at 3.2 ppm. This upfield shift is in agreement with the experiments of RbCl and NaBr shown above. However, further experiments with variations of the halide of the lithium salt, cryptand as chelating additive and investigations in liquid ammonia will enable the assignment of the occurring species of Li^+ ions in solution.

In conclusion, in spectra of sodium and lithium salts contrary to rubidium salts the CIP and the SSIP were not observed simultaneously in solution, but only one signal arose. So far, it was not possible to assign this signal to a CIP or a SSIP, or to elucidate if it is an averaged signal of both. For sodium salts a great upfield shift between the signal observed in liquid ammonia and acetonitrile showed a high solvent-dependence. The investigations on sodium and lithium salts with chelating additives supported the observations of RbCl, for an upfield shift of the signal for $\text{A}^+\text{@crown}$ (A = alkali metal) compared to the signal without additives. The signal for $\text{A}^+\text{@crypt}$ arose in both cases between these signals.

Part of further investigations will be the intensive try to solve the sodium and lithium salts in liquid ammonia, as the studies in this solvent are of great importance for investigations on the solvation processes of highly charged Zintl anions. Furthermore, the variation of the solvent and the application of further alkali salts will help elucidate the solvated species which are occurring in solution. The focus on the salts of potassium and cesium will be part of future work, as well.

7.4 Conclusion

In summary, the investigations on rubidium salts in liquid ammonia showed that the simultaneous observation of CIPs and SSIPs is possible in ^{87}Rb NMR spectra. Thereby, the ratio of the CIP to the SSIP is temperature-dependent and also dependent on the halide of the rubidium salt. At higher temperatures and with smaller halides an increasing amount of the CIP is observed. By applying a substoichiometric amount of [2.2.2]-cryptand even three signals were detected, showing additionally the signal of $\text{Rb}^+@crypt$, which is the only occurring signal with an excess of the chelating additive. Besides liquid ammonia, the solvation behavior was also investigated in further organic solvents. Here RbCl showed only one signal and an enhance solubility after the addition of a chelating additive. With 18-crown-6 a solvent-dependence is observable, while with [2.2.2]-cryptand the interaction with the solvent is less pronounced.

Furthermore, first investigations on sodium salts in liquid ammonia showed only one signal. The assignment of the observed signal to a CIP, a SSIP or an averaged signal of both was so far not possible. However, the effects of chelating additives on the cations of sodium and lithium salts are in agreement with those observed for RbCl . For a detailed understanding, further investigations with unsaturated solutions of the alkali salts in liquid ammonia, substoichiometric amounts of chelating additives and different alkali salts, besides a variation of the temperature are necessary for a deeper understanding of these systems.

These investigations on interactions and solvation behaviors of alkali salts will improve the understanding of the role of the alkali metal for the stabilization of Zintl anions in solution and will enable targeted synthesis and transformations of those cluster species. NMR spectroscopic investigations on the salts of ^{39}K and ^{133}Cs , as well as theoretical calculations are part of future work.

7.5 Supporting Information

7.5.1 Further ^{87}Rb NMR Spectra

RbCl in liquid ammonia at various temperatures

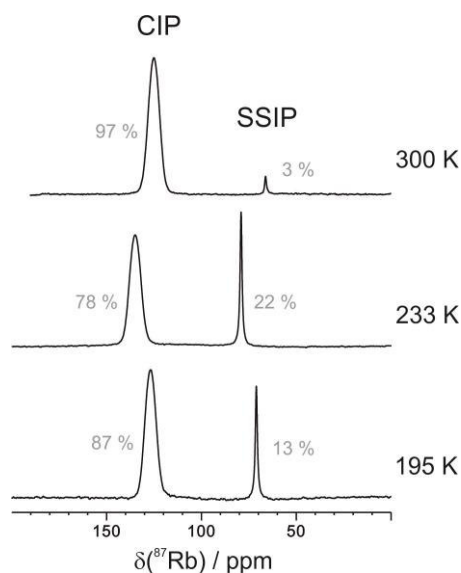


Figure 7.7: Comparison of ^{87}Rb NMR spectra of RbCl in liquid ammonia at different temperatures of 300, 233 and 195 K. On the left the signal for the CIP (contact ion pair) arises, on the right the one for a SSIP (solvent-separated ion pair). The integral distribution (in gray) is dependent on the temperature.

For RbCl at different temperatures, an increasing amount of CIP is detected, if the sample is heated from 233 to 300 K (Figure 7.7). Furthermore, the building of this ratio is reversible, which was investigated by a subsequent cooling of the sample to 233 K. However, for RbCl at 195 K an opposing effect was observed. Here, the amount of CIP is increasing in comparison to 233 K (Figure 7.7). This effect is contrary to the above given postulations and cannot be explained so far.

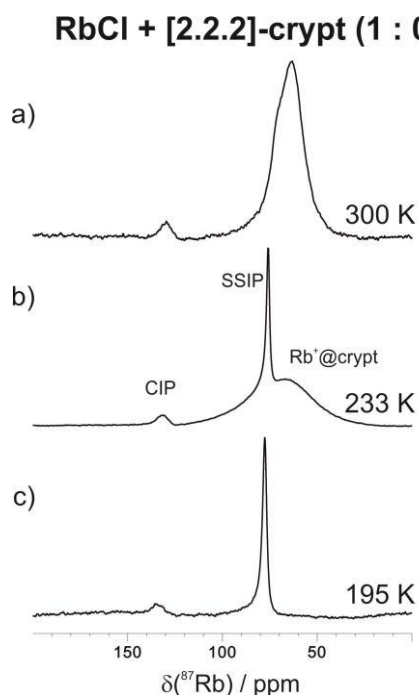
RbCl with [2.2.2]-cryptand at various temperatures

Figure 7.8: ^{87}Rb NMR spectra, of RbCl with [2.2.2]-crypt (1:0.5), at a) 300 K, b) 233 K and c) 195 K, in liquid ammonia.

The spectrum of RbCl with a 0.5 equivalents of [2.2.2]-cryptand shows three species in solution at 233 K. At 300 K the signals of SSIP and $\text{Rb}^+\text{@crypt}$ are hugely overlapping and only the shoulder on the left side of the signal is a hint for the presence of SSIP in this solution. At 195 K it seems like the signal of $\text{Rb}^+\text{@crypt}$ becomes so broad, that it is no longer observable in the spectrum. The line width of the signal at 78 ppm matches exactly with the one for the SSIP at 233 K, therefore, an averaged signal of SSIP and $\text{Rb}^+\text{@crypt}$ is excluded, as it would result in a much broader line width and a slight upfield shift. The signals of CIP and SSIP arise at 134 ppm ($\Delta\nu_{1/2} = 1400$ Hz) and 78 ppm ($\Delta\nu_{1/2} = 520$ Hz), respectively, with an amount of 11 % : 89 % (the amount of Rb^+ ions bound in $\text{Rb}^+\text{@crypt}$ are not taken into account).

For the sample of RbCl with 18-crown-6 (1 : 0.5) at 300 K, also two species occur (data not shown). The amount of CIP is slightly decreasing in comparison to the spectrum at 233 K (2 % : 98 %, CIP : (SSIP + $\text{Rb}^+\text{@crown}$)), while the line width of the CIP is increasing ($\Delta\nu_{1/2} = 1500$ Hz) and the one for the averaged signal is decreasing ($\Delta\nu_{1/2} = 380$ Hz).

Table 7.2: Values of the ratios, chemical shifts and line widths of CIP, SSIP and Rb^+ @additive of RbCl , and RbCl with the additives 18-crown-6 or [2.2.2]-crypt, respectively, in an amount of 0.5 eq or 1.5 eq in liquid ammonia at 233 K.

	CIP:SSIP: Rb^+ @additive	CIP		SSIP		Rb^+ @additive	
		$\delta(^{87}\text{Rb})$ [ppm]	$\Delta\nu_{1/2}$ [Hz]	$\delta(^{87}\text{Rb})$ [ppm]	$\Delta\nu_{1/2}$ [Hz]	$\delta(^{87}\text{Rb})$ [ppm]	$\Delta\nu_{1/2}$ [Hz]
RbCl	78 % : 22 % : -	135	1343	79	245	-	-
+ 18-crown-6							
(0.5 eq)	4 % : 0 % : 96 %	132	1038	n.d.	n.d.	27	621
(1.5 eq)	0 % : 0 % : 100 %	n.d.	n.d.	n.d.	n.d.	28	331
+ [2.2.2]-crypt							
(0.5 eq)	3 % : 17 % : 80 %	135	~1400*	76	~520*	67	~7200*
(1.5 eq)	0 % : 0 % : 100 %	n.d.	n.d.	n.d.	n.d.	73	6011

* These values were determined manually by simulations.

Solvation of RbCl with additives in various organic solvents

Table 7.3: Values of the chemical shifts and line widths of CIP of RbCl and of SSIP of RbCl with the additives 18-crown-6 or [2.2.2]-crypt, respectively, in $\text{C}_5\text{D}_5\text{N}$, CD_3CN and THF-d_8 at 300 K in comparison to those in liquid ammonia at 233 K.

	NH_3		$\text{C}_5\text{D}_5\text{N}$		CD_3CN		THF-d_8	
	$\delta(^{87}\text{Rb})$ [ppm]	$\Delta\nu_{1/2}$ [Hz]	$\delta(^{87}\text{Rb})$ [ppm]	$\Delta\nu_{1/2}$ [Hz]	$\delta(^{87}\text{Rb})$ [ppm]	$\Delta\nu_{1/2}$ [Hz]	$\delta(^{87}\text{Rb})$ [ppm]	$\Delta\nu_{1/2}$ [Hz]
CIP(Rb^+Cl^-)	135	1343	133	1100	n.d.	n.d.	n.d.	n.d.
Rb^+@crown	27	331	22	2544	4	1765	17	n.d.
Rb^+@crypt	73	6011	63	~8500*	60	~4400*	n.d.	n.d.

* These values were determined manually.

The chemical shift values and the line width of the CIP observed for RbCl without additives and the Rb^+ @crown or Rb^+ @crypt are shown in Table 7.3. RbCl is besides in liquid ammonia only soluble in pyridine, but not in acetonitrile or tetrahydrofuran. In tetrahydrofuran, with 18-crown-6 a very small signal was observable, while for RbCl without additive or with [2.2.2]-cryptand no signal could be observed.

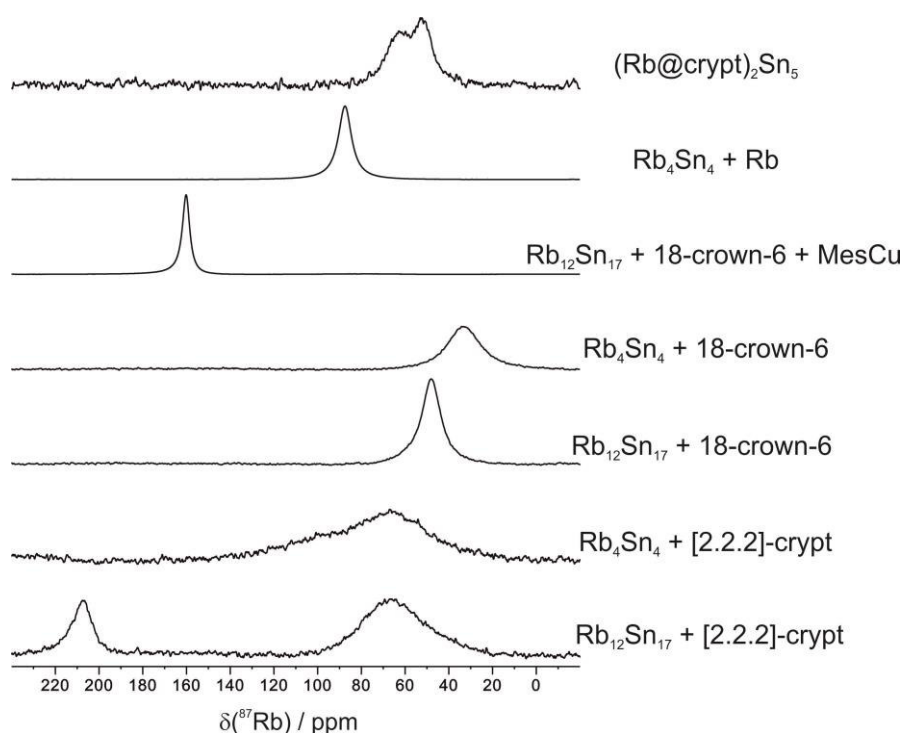
^{87}Rb NMR spectra of investigations on rubidium stannides

Figure 7.9: ^{87}Rb NMR spectra of various investigations of rubidium stannides in liquid ammonia at 233 K.

Figure 7.9 shows the ^{87}Rb NMR spectra of various rubidium stannides with additives or additive and MesCu or without additive and elementary rubidium in liquid ammonia. An unambiguous assignment of the occurring species is so far not possible and further investigations are necessary, for example the ^{87}Rb NMR spectra of Rb_4Sn_4 and $\text{Rb}_{12}\text{Sn}_{17}$ without additives are required as reference. Notable is the spectrum of $\text{Rb}_4\text{Sn}_4 + \text{Rb}$ as only one signal occurs and the observation of two signals in the spectrum of $\text{Rb}_{12}\text{Sn}_{17} + \text{crypt}$, here the substoichiometric amount of cryptand leads to two signals as it was observed with RbCl . The CIP at ppm is very upfield shifted, owing to the contacts with the highly charged Zintl anions but does not fit in the straight line of the plot in Figure 7.1d. The signal of $\text{Rb}^+@crypt$ is again in dependent from the counterions, while the signals for the $\text{Rb}^+@crown$ shows a downfield shift with $\text{Rb}_{12}\text{Sn}_{17}$ in comparison to the signal with Rb_4Sn_4 . So far it is puzzling, why the MesCu leads to a downfield shift of the signal. In general, in all the spectra in Figure 7.9 the signal for SSIP (81-69 ppm) is not occurring.

7.5.2 Experimental Part

Sample preparation

General considerations. To remove residual moisture traces, the commercially acquired gaseous ammonia (Linde AG, purity 3.8) was condensed onto elemental sodium and stored for at least two to three days. [2.2.2]-cryptand and 18-crown-6 were purchased from Sigma-Aldrich. 18-crown-6 was sublimated before using. RbCl, RbBr, and RbF were purchased from ABCR and dried at 300 °C under vacuum. Following chemicals were commercially available and used without any further purification: NaCl (100 %, VWR Chemicals), LiCl (Sigma Aldrich, 12-crown-4 (Merck), C₅D₅N (99 %, Sigma Aldrich), THF-d₈ (99.5 %, Euriso-Top), CD₃CN (99.98 %, Deutero).

Samples in liquid ammonia. All sample preparations in liquid ammonia were performed in a purified argon atmosphere (glove box) by using heavy walled NMR tubes. Under inert conditions an NMR tube was charged with the respective reagents (see Table 7.4) afterwards liquid ammonia was condensed onto the mixtures. To avoid air and moisture impurities, the tubes were melt off.

Table 7.4: Weigh-in quantities of various alkali salts (AX), additive-free or additive-containing, solved in liquid ammonia and the measuring temperature (T).

	m(AX)	m(18-crown-6)	m(2.2.2-crypt)	stoichiometric ratio	T [K]
RbCl	20 mg	–	–	–	233, 300, 195
RbCl	5 mg	16 mg	–	1:1.5	233, 300
RbCl	10 mg	10 mg	–	1:0.5	233, 300
RbCl	5 mg	–	23 mg	1:1.5	233, 300
RbCl	10 mg	–	15 mg	1:0.5	233, 300, 195
RbBr	25 mg	–	–	–	233, 300, 233
RbF	28 mg	–	–	–	233, 300
NaCl	20 mg	–	–	–	–
NaCl	<20 mg	–	–	–	233
NaBr	70 mg	–	–	–	300
LiCl	30 mg	–	–	–	–

Samples in C₅D₅N, CD₃CN and THF-d₈. The reagents were given directly to an NMR tube, according to Table 7.5-7.7, and solved in 0.4 mL of the respective solvent. In case, the solubility was low, the NMR tubes were treated 15 minutes in an ultrasonic bath at 25-50 °C.

Table 7.5: Weigh-in quantities of various alkali salts (AX), additive-free or additive-containing, solved in 0.4 mL $\text{C}_5\text{D}_5\text{N}$ and the measuring temperature (T).

	m(AX)	m(18-crown-6)	m(2.2.2-crypt)	stoichiometric ratio	T [K]
RbCl	13.1 mg	–	–	–	300
RbCl	13.3 mg	28.0 mg	–	1:1	300
RbCl	13.2 mg	–	38.2 mg	1:1	300
LiCl	18.5 mg	–	–	–	300
LiCl	3.3 mg	20 mg	–	1:1	300
LiCl	3.0 mg	–	25.6 mg	1:1	300
NaCl	24.9 mg	–	–	–	300

Table 7.6: Weigh-in quantities of various alkali salts (AX), additive-free or additive-containing, solved in 0.4 mL CD_3CN and the measuring temperature (T).

	m(AX)	m(18-crown-6)	m(2.2.2-crypt)	stoichiometric ratio	T [K]
RbCl	7.1 mg	–	–	–	300
RbCl	7.1 mg	15.6 mg	–	1:1	300
RbCl	7.1 mg	–	22.5 mg	1:1	300
NaCl	1.2 mg	–	–	–	300
NaCl	1.2 mg	–	8.7 mg	1:1	300
NaBr	2.3 mg	–	–	–	300
NaBr	2.3 mg	3.0	–	1:0.5	300
NaBr	2.3 mg	–	5.8 mg	1:1	300

Table 7.7: Weigh-in quantities of RbCl, additive-free or additive-containing, solved in 0.4 mL THF-d_8 and the measuring temperature (T).

	m(AX)	m(18-crown-6)	m(2.2.2-crypt)	stoichiometric ratio	T [K]
RbCl	7.1 mg	–	–	–	300
RbCl	7.1 mg	15.7 mg	–	1:1	300
RbCl	7.1 mg	–	22.1 mg	1:1	300

7.5.3 NMR Data Collection and Processing

The NMR spectra were recorded on a Bruker Avance III HD 600 spectrometer (600.13 MHz for ^1H ; 196.37 MHz for ^{87}Rb ; 158.75 MHz for ^{23}Na ; 233.33 MHz for ^7Li) equipped with a 5 mm double resonance broad band Prodigy (BBO) z-gradient probe or a 5 mm broadband triple resonance z-gradient probe. The temperatures for all measurements were controlled by a Bruker VTU temperature unit. ^{87}Rb , ^{23}Na and ^7Li measurements were carried out with a standard Bruker pulse program zg.

For ^{87}Rb with $P_1(^{87}\text{Rb}) = 19.4 \mu\text{s}$, $\text{PLW}(^{87}\text{Rb}) = 70 \text{ W}$ / $\text{PLdB} = -18.45 \text{ dBW}$ using 100-10k number of scans, 0 dummy scans, $\text{TD} = 16\text{k}$ with a relaxation delay of 0.03 s. The Ξ value of RbCl, used as external standard (300 K, 1 M D_2O), was applied.

For ^{23}Na with $P1(^{23}\text{Na}) = 12.5\ \mu\text{s}$, $PLW(^{23}\text{Na}) = 80\ \text{W}$ / $PLdB = -19.03\ \text{dBW}$ using 50-1k number of scans, 0 dummy scans, $TD = 16\text{k}$ with a relaxation delay of 0.3 s. The Ξ value of NaCl, used as external standard (300 K, 1 M D_2O), was applied.

For ^7Li with $P1(^7\text{Li}) = 24.0\ \mu\text{s}$, $PLW(^7\text{Li}) = 70\ \text{W}$ / $PLdB = -18.45\ \text{dBW}$ using 64 number of scans, 0 dummy scans, $TD = 16\text{k}$ with a relaxation delay of 5.0 s. The Ξ value of LiCl, used as external standard (300 K, 1 M D_2O), was applied.

Data were processed with the Bruker software TOPSPIN 3.2 using the processing parameters $SI = 32\ \text{k}$ and $WDW = \text{EM}$ (1-100 Hz). Theoretical NMR spectra were simulated with Bruker's TOPSPIN 3.2 software tool DAISY.

7.6 References

- [1] S. Scharfe, F. Kraus, S. Stegmaier, A. Schier, T. F. Fässler, *Angew. Chem. Int. Ed.* **2011**, 50, 3630–3670.
- [2] A. Joannis, *C. R. Hebd. Seances Acad. Sci.* **1891**, 113, 795.
- [3] M. Neumeier, F. Fendt, S. Gärtner, C. Koch, T. Gärtner, N. Korber, R. M. Gschwind, *Angew. Chem. Int. Ed.* **2013**, 52, 4483–4486.
- [4] J. D. Corbett, D. G. Adolphson, D. J. Merryman, P. A. Edwards, F. J. Armatris, *J. Am. Chem. Soc.* **1975**, 97, 6267–6268.
- [5] S. A. Baer, F. Kraus, *Z. Naturforsch.* **2010**, 65b, 1177–1184.
- [6] A. F. Holleman, E. Wiberg, *Lehrbuch Der Anorganischen Chemie*, De Gruyter & Co., Berlin, **1995**.
- [7] M. Hesse, H. Meier, B. Zeeh, *Spektroskopische Methoden in Der Organischen Chemie*, Georg Thieme Verlag, Stuttgart - New York, **1984**.

8 Summary and Outlook

The copper-catalyzed asymmetric conjugated 1,4-addition reaction of organozinc reagents to α,β -unsaturated compounds is a very effective and widely used method for the enantioselective carbon-carbon bond formation. By the use of phosphoramidite ligands it is possible to reach *ee*-values and conversion up to > 99 %. Furthermore, this outstanding reaction provides lower costs in comparison to other transition-metal catalyzed reactions and compatibility to many functional groups. Despite the great success of this reaction, the structural and mechanistic insight has been very limited so far. But for the optimization of the existing reactions and the development of new targeted catalysts it is of high importance to identify the occurring structures in solution.

It took almost a decade to elucidate the dimeric precatalyst structure of the copper complex which shows a trigonal/tetrahedral coordination on copper. The next step of the catalytic cycle, the transfer of the organic moiety from an organozinc reagent to the copper complex is postulated as a transmetalation step. Owing to the low amount of the transmetalation intermediate in solution, their detection with standard 1D NMR spectra was not possible. Therefore, a new method by using HMBC spectra as spectroscopic filter was applied. Hence, only those species which are showing a coupling between ^1H and ^{31}P are detected, while all other signals are eliminated. But besides scalar couplings also relaxation interferences between chemical shift anisotropy and dipolar interactions can cause a signal in HMBC spectra. To distinguish those signals from signals of scalar coupling a special set of 1D $^1\text{H}, ^{31}\text{P}$ HMBC spectra was applied. By using ZnEt_2 this led to the first direct experimental detection of a transmetalation intermediate in a copper catalyzed asymmetric synthesis. The determination of the structures was possible by using mixtures of enantiomeric and enantiopure ligands. Two types of transmetalation intermediates were identified, monomeric complexes with one ligand and a dimeric complex which showed the trigonal/tetrahedral coordination on the copper atoms as it was observed for the precatalyst. On basis of theoretical studies by Woodward *et al.* and further NMR spectroscopic experiments the dimeric transmetalation intermediate is assumed to be the catalytic active species. The retention of the dimeric structure upon transmetalation explains the best results with a copper salt to ligand ratio of 2:1 in empirically optimized reactions. This special NMR spectroscopic approach to identify species below the detection limit of ^1H spectra can be applied also to further classes of catalysts.

Further investigations with ZnMe_2 did not provide a transmetalated species so far. Therefore, the more reactive organometallic reagent MeLi was used for the formation of a transmetalation intermediate bearing a methyl group. With the help of chelating crown ether it was possible to elucidate that the lithium ion is not involved in the structure of the transmetalation intermediate. This access was not possible for the zinc reagents as no chelating additive with a higher affinity for the complexation of zinc prior to copper is known. Furthermore, it was shown that a precoordination of α,β -unsaturated substrates by the precatalyst does not take place, which led to the assumption that the order of addition is not important for the outcome of the reaction, in contrast this is well-known for reactions of organoaluminium reagents in tetrahydrofuran where the order of addition must be considered.

The mechanistic study on a copper complex in a photoredox reaction with an LED-illumination device led to the observation that the complex does not release one ligand in the first step of the reaction. This examination is the basis for future investigations.

The NMR spectroscopy is a widely used method for the structure elucidation in the field of inorganic chemistry. However, for some heteronuclear spins the total frequency range exhibits many tens of kilohertz. Therefore, the group of Prof. Dr. Burkhard Luy developed a broadband pulse, named xyBEBOP pulse, which provides an excitation over a bandwidth of 1000 kHz. After the implementation of this pulse to our spectrometer validation studies in comparison to a 90° hard pulse on real samples of Zintl anions were performed, providing high reliability for integrals, coupling constants and line widths. Especially the precise reproduction of coupling constants was not expected because of the phase profile of the xyBEBOP pulse but will help for assignments of e.g. the cluster sizes of Zintl anions in solution.

The fascinating chemistry of Zintl anions dates back only a few decades. Since their discovery the number of crystal structures of these binary alloys of group 14 and 15 is strongly increasing. However, the solvation, transformation and degradation processes in solution are so far not completely understood. But this knowledge is necessary for using these polyanions for targeted synthesis of new materials.

With the help of heteronuclear NMR spectroscopy it was possible for the first time to detect the long-time elusive highly charged silicide Si_4^{4-} and stannide Sn_4^{4-} by utilizing the stability effect of [2.2.2]-cryptand. Furthermore the first experimental proof for the longstanding assumption that the protons of liquid ammonia are acting as oxidizing agent

on the Zintl anions was given by the detection of NH_2^- . As degradation product of the silicides SiH_3^- was observed.

The extensive studies of the two known preparation methods of Zintl anions, dissolution of solids and direct reduction, revealed that the stabilizing effect of [2.2.2]-cryptand does not only arise from an enhanced solubility, but also from the suppressed contacts of the alkali metal and liquid ammonia, which reduces the oxidation properties of the solvent. Based on these results, further investigations on the detection of ^{207}Pb -polyanions and the transformation reaction of stannides with ^{195}Pt complexes have already begun. Here, the use of the xyBEBOP pulse is of high importance owing to the strongly extended chemical shift range of these heteronuclei.

The investigations on Zintl anions showed that the contacts between the alkali metal cations and ammonia enhanced the oxidation property of the solvent. Therefore the first NMR spectroscopic study on alkali metals in liquid ammonia was performed. Here, it was shown that the exchange of the rubidium ions between contact ion pairs and solvent-separated ion pairs is slow on the NMR timescale, which led to two separated signals in the ^{87}Rb NMR spectrum. This was not the case for sodium and lithium salts, although very stable ammine complexes are known for these alkali metals from crystal structures. The use of [2.2.2]-cryptand showed an almost complete shielding of the rubidium ion, while an interaction with the solvent was observable, if the alkali metals were chelated by a crown ether. Future work on NMR spectroscopic investigations of ^{39}K and ^{133}Cs salts is planned, as well as theoretical calculations. The aim of these investigations is an improved knowledge of the role of the alkali metal for the stabilization of Zintl anions in solution.

9 Zusammenfassung

Die Kupfer-katalysierte asymmetrisch konjugierte 1,4-Additionsreaktion mit Organozinkreagenzien an α,β -ungesättigte Verbindungen ist eine sehr effektive und weitverbreitete Methode zur enantioselektiven C-C-Bindungsknüpfung. Durch die Verwendung von Phosphoramidit-Liganden ist es möglich *ee*-Werte und Ausbeuten bis zu > 99 % zu erlangen. Darüber hinaus bietet diese herausragende Reaktion geringere Kosten im Vergleich zu anderen Übergangsmetall-katalysierten Reaktionen und Kompatibilität mit vielen funktionellen Gruppen. Trotz des großen Erfolges dieser Reaktion, sind die Erkenntnisse über die Strukturen und den Mechanismus bisher sehr begrenzt. Jedoch ist für die Optimierung von existierenden Reaktionen und für die Entwicklung neuer, gezielt entwickelter Katalysatoren die Identifizierung der in Lösung auftretenden Strukturen von enormer Bedeutung.

Es dauerte fast ein Jahrzehnt bis die dimere Präkatalysatorstruktur des Kupferkomplexes mit einer trigonal-tetraedrischen Koordination an Kupfer, aufgeklärt wurde. Im nächsten Schritt des Katalysezyklus wird die Übertragung eines organischen Rests vom Organozinkreagenz auf den Kupferkomplex als Transmetallierungsschritt postuliert. Aufgrund des geringen Anteils an Transmetallierungsintermediaten in Lösung war ihre Detektion mit üblichen 1D NMR-Spektren nicht möglich. Deshalb wurde eine neue Methode angewendet, bei der HMBC-Spektren als spektroskopischer Filter verwendet wurden. Somit wurden nur diejenigen Spezies, die eine skalare Kopplung zwischen ^1H und ^{31}P aufwiesen, detektiert, während alle anderen Signale eliminiert wurden. Allerdings können neben skalaren Kopplungen auch Relaxationsinterferenzen zwischen anisotropen chemischen Verschiebungen und dipolaren Wechselwirkungen ein Signal im HMBC-Spektrum hervorrufen. Um diese Signale von Signalen skalarer Kopplung zu unterscheiden wurde ein spezieller Satz an 1D $^1\text{H}, ^{31}\text{P}$ HMBC Spektren verwendet, welche mit ZnEt_2 zur ersten direkten experimentellen Detektion eines Transmetallierungsintermediates in der Kupfer-katalysierten asymmetrischen Synthese führten. Die Strukturbestimmung wurde durch die Verwendung von enantiomeren und enantiomerenreinen Ligandmischungen ermöglicht. Zwei Arten von Transmetallierungsintermediaten wurden dabei identifiziert, monomere Komplexe mit einem Liganden und dimere Komplexe, welche die trigonal-tetraedrische Koordination an den Kupferatomen zeigten, wie es bereits für den Präkatalysator beobachtet wurde. Aufgrund der theoretischen Studien von Woodward *et al.* und weiterer NMR-spektroskopischer

Experimente wird das dimere Transmetallierungsintermediat als katalytisch aktive Spezies vermutet. Die Beibehaltung der dimeren Struktur während der Transmetallierung erklärt das beste Ergebnis bei der Verwendung des Verhältnisses von Kupfersalz zu Ligand von 2 : 1, welches in empirisch optimierten Reaktionen gefunden wurde. Dieser spezielle NMR-spektroskopische Zugang zur Identifizierung von Spezies unterhalb des Detektionslimits von ^1H Spektren kann auch für weitere Katalysen angewendet werden.

Weitere Untersuchungen mit ZnMe_2 zeigten bisher keine transmetallierte Spezies. Deshalb wurde das reaktivere organometallische Reagenz MeLi für die Bildung eines Transmetallierungsintermediates, welches eine Methylgruppe trägt, verwendet. Mit Hilfe von chelatisierendem Kronenether war es möglich aufzuklären, dass das Lithiumion nicht in die Struktur des Transmetallierungsintermediates eingebunden ist. Dieser Zugang war mit Zinkreagenzien nicht möglich, da kein chelatisierendes Additiv bekannt ist, welches eine höhere Komplexierungsaffinität für Zink im Vergleich zu Kupfer aufweist. Weiterhin konnte gezeigt werden, dass die präkoordination von α,β -ungesättigten Substraten durch den Präkatalysator nicht stattfindet, was zur Vermutung führte, dass die Zugabereihenfolge für das Ergebnis der Reaktion keine Rolle spielt, im Gegensatz zu Reaktionen mit Organoaluminiumreagenzien in Tetrahydrofuran wo die Zugabereihenfolge beachtet werden muss.

Die mechanistischen Studien zu einem Kupferkomplex in Photoredoxreaktionen mit einer LED-Beleuchtungseinheit führten zu der Beobachtung, dass der Komplex im ersten Schritt der Reaktion keinen Liganden abspaltet. Diese Analyse legte den Grundstein für künftige Untersuchungen.

Die NMR-Spektroskopie ist eine weitverbreitete Methode zur Strukturuntersuchung auf dem Gebiet der anorganischen Chemie. Jedoch umfasst der Frequenzbereich mancher Heterokernspins mehrere zehntausend Hertz. Aus diesem Grund wurde ein Breitbandpuls, genannt xyBEBOP Puls, von der Gruppe von Prof. Dr. Burkhard Luy entwickelt, welcher eine Breitbandanregung von 1000 kHz bietet. Nach der Implementierung dieses Pulses an unserem Spektrometer wurden Validierungsstudien im Vergleich zu einem 90° Hartpuls an Proben von Zintlanionen durchgeführt, welche eine hohe Verlässlichkeit für Integrale, Kopplungskonstanten und Linienbreiten zeigte. Besonders die präzise Reproduktion der Kopplungskonstanten wurde aufgrund des Phasenprofils des xyBEBOP Pulses nicht vermutet, jedoch wird dies helfen z.B. Clustergrößen von Zintlanionen in Lösung zuzuweisen.

Die faszinierende Chemie der Zintl-anionen geht erst auf einige Jahrzehnte zurück. Seit ihrer Entdeckung ist die Anzahl an Kristallstrukturen dieser binären Legierungen der Gruppe 14 und 15 stark angestiegen. Jedoch sind die Solvations-, Umsetzungs- und Abbauprozesse bisher noch nicht vollständig verstanden. Allerdings ist dieses Verständnis nötig um diese Polyanionen für die gezielte Synthese neuer Materialien zu verwenden.

Mit Hilfe von Heterokern-NMR-Spektroskopie war es zum ersten Mal möglich das für lange Zeit schwer fassbare, hochgeladene Silizid Si_4^{4-} und Stannid Sn_4^{4-} durch die Verwendung des stabilisierenden Effekts von [2.2.2]-Kryptand zu detektieren. Des Weiteren wurde der erste experimentelle Beweis für die seit langem vermutete Annahme gefunden, dass die Protonen des flüssigen Ammoniaks als Oxidationsmittel für die Zintl-anionen agieren aufgrund der Detektion von NH_2^- . Als Abbauprodukt für die Silicide wurde SiH_3^- beobachtet.

Die intensiven Untersuchungen der zwei bekannten Präparationsmethoden von Zintl-anionen, die Auflösung von Festkörpern und die direkte Reduktion, zeigten, dass der Stabilisierungseffekt von [2.2.2]-Kryptand nicht nur aufgrund der erhöhten Löslichkeit auftritt, sondern auch durch die Unterdrückung der Kontakte zwischen Alkalimetall und dem flüssigen Ammoniak, was die Oxidationseigenschaften des Lösungsmittels reduziert. Auf Basis dieser Ergebnisse wurden weitere Untersuchungen zur Detektion von ^{207}Pb -Polyanionen und der Umsetzungsreaktion von Stanniden mit ^{195}Pt -Komplexen bereits begonnen. Aufgrund des stark verbreiterten chemischen Verschiebungsbereichs dieser Heterokerne wird hierbei die Verwendung des xyBEBOP Pulses von großer Bedeutung sein.

Die Untersuchungen von Zintl-anionen zeigten, dass die Kontakte zwischen dem Alkalimetallkation und Ammoniak die Oxidationseigenschaften des Lösungsmittels erhöhen. Deshalb wurde die erste NMR-spektroskopische Untersuchung von Alkalimetallen in flüssigem Ammoniak durchgeführt. Hierbei wurde gezeigt, dass der Austausch von Rubidiumionen zwischen dem Kontaktionenpaar und dem Solvens-separiertem Ionenpaar langsam auf der NMR Zeitskala ist, was zu zwei separierten Signalen im ^{87}Rb NMR-Spektrum führte. Für Natrium- und Lithiumsalze war das nicht der Fall, obwohl für diese Alkalimetalle sehr stabile Ammoniakate von Kristallstrukturen bekannt sind. Die Verwendung von [2.2.2]-Kryptand zeigte eine annähernd komplette Abschirmung des Rubidiumions, während die Wechselwirkungen mit dem Lösungsmittel bei der Chelatisierung des Alkalimetalls mit Kronenether sichtbar wurden. NMR-spektroskopische Untersuchungen von ^{39}K und ^{133}Cs , sowie theoretische Studien sind für

weitere Arbeiten geplant. Das Ziel dieser Untersuchungen ist ein verbessertes Verständnis der Rolle des Alkalimetalls bei der Stabilisierung von Zintlanionen in Lösung.

10 Appendix

10.1 Curriculum Vitae

Carina Koch

born on 11th June 1986, Kempten (Allgäu)



EDUCATION

- 12/2011 - 05/2015 PhD thesis, AK Gschwind, Universität Regensburg, Germany
Focus: NMR-spectroscopic elucidation of mechanistic steps of copper catalyzed reactions and structure elucidation of Zintl anions.
- 10/2009 - 09/2011 MSc Chemistry, Universität Regensburg, Germany
Title of master thesis: "NMR-spectroscopic studies of mechanistic key steps in the Cu-catalyzed conjugated 1,4-addition reaction with dimethylzinc"
- 10/2006 - 09/2009 BSc Chemistry, Universität Regensburg, Germany
Titel of bachelor thesis: "Recognition of biological substrates with CEAA appended Zn-Biscyclene-Complexes"
- 09/1996 - 06/2006 Allgäu-Gymnasium, Kempten (Allgäu), Germany
Higher Education Entrance Qualification
Advanced courses: Chemistry, German

EXPERIENCE

- 12/2011 - 05/2015 Teaching assistant in laboratory courses for chemists, biologists and teachers, supervisor for bachelor and master students

COOPERATIONS

Prof. Dr. N. Korber, University of Regensburg
Prof. Dr. O. Reiser, University of Regensburg
Prof. Dr. B. Luy, Karlsruhe Institute of Technology

10.2 Publications and Conferences

Publications*

„Elusive Transmetalation Intermediate in Copper-Catalyzed Conjugate Additions: Direct NMR Detection of an Ethyl Group Attached to a Binuclear Phosphoramidite Copper Complex”, F. von Rekowski, C. Koch, R. M. Gschwind, *J. Am. Chem. Soc.* **2014**, 136, 11389-11395.

DOI: 10.1021/ja504577t

“NMR Spectroscopic Aspects”, F. von Rekowski, C. Koch, R. M. Gschwind in Copper-Catalyzed Asymmetric Synthesis, A. Alexakis, N. Krause, S. Woodward (Eds.), Wiley-VCH, 1st edition – **2014**.

„Reaction of Sn_4^{4-} in Liquid Ammonia: the Formation of $\text{Rb}_6[(\eta^2\text{-Sn}_4)\text{Zn}(\eta^3\text{-Sn}_4)]\cdot 5\text{NH}_3$ ”, F. Fendt, C. Koch, S. Gärtner, N. Korber, *Dalton Trans.* **2013**, 42, 15548-15550.

DOI: 10.1039/C3DT1932E

„Detection of the Elusive Highly Charged Zintl Ions Si_4^{4-} and Sn_4^{4-} in Liquid Ammonia by NMR Spectroscopy”, M. Neumeier, F. Fendt, S. Gärtner, C. Koch, T. Gärtner, N. Korber, R.M. Gschwind, *Angew. Chem. Int. Ed.* **2013**, 52, 4483-4486.

DOI: 10.1002/ange.201209578

„Synthesis of heteroatomic Zintl anions in liquid ammonia – the new highly charged $[\text{Sn}_4\text{Bi}_4]^{4-}$ and fully ordered $[\text{Sn}_2\text{Bi}_2]^{2-}$ “, U. Friedrich, M. Neumeier, C. Koch, N. Korber, *Chem. Commun.* **2012**, 48, 10544-10546.

DOI: 10.1039/C2CC35380F

Luminescent Hybrids Combining a Metal Complex and a Crown Ether – Receptors for Peptidic Ammonium Phosphates“, A. Späth, C. Koch, B. König, *Eur. J. Inorg. Chem.* **2010**, 19, 2926-2935.

DOI: 10.1002/ejic.201000239

* Permission for partial or full reuse of articles in this PhD-thesis granted by Rightslink.

International and National Conferences

TALKS

CCROS-Workshop, 21-22th June 2012, Basel.

SMASH, 7-10th September 2014, Atlanta.

Christmas Colloquium, 17th December 2014, Regensburg.

POSTERS

Iron Symposium, 4-5th June 2012, Regensburg.

ICOMC, 2-7th September 2012, Lisbon.

EUROMAR, 30th June – 5th July 2013, Crete.

FGMR Discussion Meeting, 9-12th September 2013, Frauenchiemsee.

SMASH, 7-10th September 2014, Atlanta.

FURTHER VISITED CONFERENCES

BRUKER NMR Benutzertagung, 6-7th November 2012, Ettlingen.

GDCh-NMR-Diskussionstagung, 14-15th January 2013, Erlangen.

Hemdsärmelkolloquium, 7-9th March 2013, Freiburg.

